

# **Early Eocene paleosols on King George Island, Maritime Antarctica as a paleoenvironmental proxy**

## **Dissertation**

der Mathematisch-Naturwissenschaftlichen Fakultät

der Eberhard Karls Universität Tübingen

zur Erlangung des Grades eines

Doktors der Naturwissenschaften

(Dr. rer. nat.)

vorgelegt von

M.Sc. Diogo Noses Spinola

aus Belo Horizonte, Brasilien

Tübingen

2017

Gedruckt mit Genehmigung der Mathematisch-Naturwissenschaftlichen Fakultät der  
Eberhard Karls Universität Tübingen.

Tag der mündlichen Qualifikation:

07/02/2018

Dekan:

Prof. Dr. Wolfgang Rosenstiel

1. Berichterstatter:

Dr. Peter Kühn

2. Berichterstatter:

Prof. Dr. Thomas Scholten

This page intentionally left blank.

## Table of Contents

|   |             |
|---|-------------|
| <b>List of Tables</b> .....   | <b>ii</b>   |
| <b>List of Figures</b> .....  | <b>iii</b>  |
| <b>Abbreviations</b> .....  | <b>iv</b>   |
| <b>Abstract</b> .....   | <b>v</b>    |
| <b>Zusammenfassung</b> .....  | <b>vi</b>   |
| <b>List of publications and personal contribution</b> .....   | <b>viii</b> |
| <b>Share in publications</b> .....  | <b>viii</b> |
| <b>1. Introduction</b> .....  | <b>9</b>    |
| 1.1. Paleoenvironmental proxies .....   | 10          |
| 1.2. Paleosols on King George Island .....  | 12          |
| 1.3. Objectives and hypotheses .....  | 12          |
| <b>2. Methodology</b> .....   | <b>14</b>   |
| 2.1. Study area .....   | 14          |
| 2.2. Laboratory methods.....  | 16          |
| 2.2.1. Micromorphology .....  | 16          |
| 2.2.2. Scanning Electron Microscopy (SEM) equipped with Energy-Dispersive X-Ray Spectroscopy (EDS)..... | 17          |
| 2.2.3. Geochemistry.....  | 17          |
| 2.2.4. Particle size distribution .....   | 17          |
| 2.2.5. X-ray diffraction and differential X-ray diffraction .....                                       | 17          |
| 2.2.6. Mineralogy of iron oxides .....  | 18          |
| 2.2.7. <sup>40</sup> Ar/ <sup>39</sup> Ar dating.....   | 19          |
| 2.2.8. Diffuse Reflectance Spectroscopy (DRS) .....   | 20          |
| 2.2.9. Magnetic susceptibility .....  | 21          |
| <b>3. Results and Discussion</b> .....  | <b>22</b>   |
| 3.1. Pedogenic and diagenetic features of the paleosols and their paleoenvironmental significance. .... | 22          |
| 3.2. Origin of clay minerals in the paleosols. ....   | 32          |
| 3.3. Evidence of diagenetic reddening of the paleosols.....   | 37          |
| <b>4. Summary and outlook</b> .....   | <b>47</b>   |
| <b>5. References</b> .....  | <b>50</b>   |
| <b>Manuscript 1</b> .....   | <b>61</b>   |
| <b>Manuscript 2</b> .....   | <b>107</b>  |
| <b>Manuscript 3</b> .....   | <b>151</b>  |
| <b>Scientific publications and conference contributions</b> .....                                       | <b>195</b>  |
| <b>Acknowledgments</b> .....  | <b>196</b>  |

## List of Tables

|   |    |
|---|----|
| <b>Table 1.</b> Selected main macromorphological properties.....  | 24 |
| <b>Table 2.</b> Selected main micromorphological characteristics. ....  | 25 |
| <b>Table 3.</b> Selected chemical characteristics: chemical index of alteration minus K (CIA-K); ratio of crystalline pedogenic iron oxides; amounts of carbonate (CaCO <sub>3</sub> ) and total organic carbon (TOC). .... | 30 |
| <b>Table 4.</b> Alteration types distribution through the paleosols horizons. ....  | 32 |
| <b>Table 5.</b> Munsell colours taken in field and converted DR spectra in Munsell and L*a*b* colours .....   | 38 |
| <b>Table 6.</b> Hematite properties calculated from XRD. Full width at half maximum (FWHM) and crystallite size. ....   | 42 |
| <b>Table 7.</b> Selective and sequential extraction of iron oxides. ....  | 44 |

## List of Figures

|  |    |
|--|----|
| <b>Figure 1.</b> Carbon dioxide levels and Cenozoic climate change.....  | 9  |
| <b>Figure 2.</b> Location of the sampling site at the King George Island.....  | 11 |
| <b>Figure 3.</b> Schematic field section with the location of the profiles..   | 15 |
| <b>Figure 4.</b> Location of the sampling site at the King George Island and photographs<br>of the profiles with field colours.....            | 16 |
| <b>Figure 5.</b> Bioturbation voids.....   | 26 |
| <b>Figure 6.</b> Bioturbation voids.....   | 26 |
| <b>Figure 7.</b> Groundmass and pedogenic features .....   | 27 |
| <b>Figure 8.</b> Mineral weathering examples.....  | 28 |
| <b>Figure 9.</b> Plant residues, under PPL.....  | 29 |
| <b>Figure 10.</b> Types of zeolite crystallization in the horizons in contact with the lava<br>flow, under XPL.....                            | 30 |
| <b>Figure 11.</b> Depth function of the CIA-K values.....  | 31 |
| <b>Figure 12.</b> Alterations types occurring in the groundmass of paleosols and in rock<br>fragments under Plane Polarized Light (PPL).....   | 33 |
| <b>Figure 13.</b> Petrographic and SEM images of selected alterations.....   | 34 |
| <b>Figure 14.</b> XRD patterns of clay samples from selected horizons.....   | 35 |
| <b>Figure 15.</b> Degree of crystallinity of smectitic and interstratified components of the<br>paleosol samples and the parent material ..... | 36 |
| <b>Figure 16.</b> Types of iron oxide distribution in the paleosols.....   | 39 |
| <b>Figure 17.</b> The second-derivative curves of K–M function for selected samples.....   | 42 |
| <b>Figure 18.</b> X-ray patterns of a representative sample .....  | 43 |
| <b>Figure 19.</b> Depth function of mineral magnetic susceptibility parameters.....  | 45 |

## Abbreviations

|                 |  |
|-----------------|--|
| Al <sub>o</sub> | Aluminium extracted by acid ammonium oxalate                 |
| CIA-K           | Chemical index of alteration minus K                         |
| CIE             | International Commission on Illumination                     |
| CLICIT          | Cadmium-Lined in-Core Irradiation Tube                       |
| CNPq            | National Counsel of Technological and Scientific Development |
| DRS             | Diffuse reflectance spectroscopy                             |
| EDS             | Energy dispersive X-ray spectroscopy                         |
| FC3             | Fish Canyon tuff sanidine                                    |
| Fe <sub>d</sub> | Iron extracted by dithionite-citrate-bicarbonate             |
| Fe <sub>o</sub> | Iron extracted by acid ammonium oxalate                      |
| Fe <sub>t</sub> | Iron extracted by XRD  |
| FWHM            | Full width at half maximum                                   |
| I/S             | Interstratified illite-smectite                              |
| KGI             | King George Island   |
| K-M             | Kubelka-Munk remission function                              |
| LD              | Lithic discontinuity   |
| LM              | Lower Member   |
| PPL             | Plane polarized light  |
| SEM             | Scanning electron microscope                                 |
| Si <sub>o</sub> | Silica extracted by acid ammonium oxalate                    |
| SP              | Superparamagnetic  |
| TC              | Total carbon   |
| TIC             | Total inorganic carbon                                       |
| TOC             | Total organic carbon   |
| TRIGA           | Training, Research, Isotopes, General Atomics)               |
| UM              | Upper Member   |
| XPL             | Crossed polarized light                                      |
| XRD             | X-ray diffraction  |
| XRF             | X-ray fluorescence   |

## Abstract

The Eocene epoch was one of the most important greenhouse periods during the Cenozoic era. Antarctica's landscape was completely different during the Eocene: there was a predominance of green rainforests rather than glaciers and ice caps. Most evidences for this warm period were found mostly in Southern Ocean sediments and a few from terrestrial settings. King George Island (KGI), South Shetlands Islands, Maritime Antarctica are one of the key sites, where terrestrial evidence from the Eocene are archived. Although the presence of paleosols are known, no detailed paleopedological studies have been conducted so far. This gap in paleopedological research on Eocene paleosols in Antarctica will be narrowed with this study.

The main objective was to use the properties of three paleosols on KGI as proxies for the paleoenvironmental reconstruction of the early Eocene. To achieve this objective, a set of different methodologies (i.e. macro- and micromorphology, X-ray fluorescence, X-ray diffraction, diffuse reflectance spectroscopy, magnetic susceptibility and  $^{40}\text{Ar}/^{39}\text{Ar}$  dating) were used with a focus on those properties that have paleo-environmental significance (mainly morphological and micromorphological features, mineralogy of clays and iron oxides). These properties were related to macromorphological and micromorphological features, and mineralogy of clays and iron oxides of the paleosols.

The macromorphological and micromorphological properties were used to attribute a pedogenic origin of the paleosols. A gradual change in soil properties and features with depth, such as colour, structure, bioturbation, iron mottles/nodules made it possible to distinguish soil horizons. Consequently, a pedogenic origin for the paleosols was confirmed. In addition, the results demonstrated that pedogenesis as well as pre-weathering and diagenesis played a role for the formation of the properties of these paleosols. The clay mineralogy showed mainly smectites inherited from the parent material being later modified by pedogenesis. The reddish colour of the paleosols was mainly caused by hematite that was rather formed by dehydration of ferrihydrite during post-burial diagenesis than by pedogenesis.

The results indicated that the weakly/moderately developed paleosols were formed under a cool and humid paleoenvironment. Although pre-weathering and diagenesis had played a role in developing properties of the paleosols, the paleoenvironmental significance is still preserved in these paleosols (soil memory). The, the paleosols on KGI are an important proxy to better understand the greenhouse period of the Eocene.

## Zusammenfassung

Das Eozän war eine der bedeutendsten Warmperioden im Känozoikum. Die Umwelt der Antarktis war im Eozän anders als heute: es gab vorherrschend grüne Regenwälder statt Gletscher und Eiskappen. Die meisten Nachweise für die warm Epoche des Eozäns wurden vor allem in Tiefseesedimenten der Ozeane auf der Südhalbkugel und terrestrischen Standorten wie auf King George Island (KGI), den Süd-Shetland-Inseln und die der Maritime Antarktis gefunden. Obwohl das Vorkommen von Paläoböden an einigen Standorten in der Antarktis seit vielen Jahren bekannt ist, wurden an diesen bisher keine detaillierten paläopedologischen Studien durchgeführt. Diese Lücke der paläopedologischen Forschung in der Antarktis wird mit dieser Arbeit verkleinert.

Das Hauptziel dieser Arbeit war es, anhand einer paläopedologischen Analyse von drei früheozänen Paläoböden auf KGI und unter Nutzung der Paläoböden als Proxies die Paläoumwelt zu rekonstruieren. Um dieses Ziel zu erreichen, wurden eine Reihe unterschiedlicher Methoden (d.h. Makro- und Mikromorphologie, Röntgenfluoreszenzanalyse, Röntgendiffraktometrie, diffuse Reflexionsspektroskopie, magnetische Suszeptibilität und  $^{40}\text{Ar}/^{39}\text{Ar}$  Datierung) mit einem Fokus auf jene Eigenschaften verwendet, die eine große Bedeutung zur Beurteilung der Pedogenese haben (hauptsächlich morphologische und mikromorphologische Merkmale sowie Ton- und Eisenoxidmineralogie). Diese Eigenschaften wurden mit makro- und mikromorphologischen Merkmalen sowie Ergebnissen aus der Ton- und Eisenoxidmineralogie verbunden.

Die makro- und mikromorphologischen Eigenschaften wurden verwendet, um einen pedogenen Ursprung der Paläoböden zuzuordnen. Eine allmähliche Veränderung der Tiefenfunktion der Bodeneigenschaften wie Farbe, Struktur, Bioturbationsmerkmale, Eisen-Mangan Konkretionen ermöglichten die Unterscheidung von Bodenhorizonten. Folglich wurde ein pedogener Ursprung für die Paläoböden bestätigt. Darüber hinaus zeigten die Ergebnisse, dass sowohl die Pedogenese als auch die Verwitterung und die Diagenese bei der Bestimmung der Eigenschaften tertiärer Paläoböden eine große Rolle spielten. Die tonmineralogische Analyse zeigte, dass die Tonminerale hauptsächlich vom Ausgangssubstrat vererbt waren und die Smektite später durch Pedogenese modifiziert worden sind. Die rötliche Farbe der Paläoböden wurde hauptsächlich durch Hämatit verursacht, der mit großer Wahrscheinlichkeit nicht pedogenetisch entstanden ist, sondern vielmehr durch die Dehydratation von

Ferrihydrit während der Diagenese gebildet wurde, die nach weiterer Überdeckung mit Sedimenten einsetzte.

Die Ergebnisse zeigten, dass sich die schwach entwickelten Paläoböden in einer kühlfeuchten Paläoumgebung gebildet haben. Obwohl die Vorwitterung und die Diagenese bei der Entwicklung der Eigenschaften der Paläoböden eine Rolle gespielt haben, blieben die Merkmale der Paläoumwelt im Archiv bzw. im Gedächtnis (soil memory) der Paläoböden erhalten. Daher sind die Paläoböden auf KGI ein wichtiger Proxy, um die Treibhausperiode des Eozäns besser zu verstehen.

## List of publications and personal contribution

### Published papers

(1) Spinola, D.N., Portes, R. de C., Srivastava, P., Torrent, J., Barrón, V., Kühn, P., 2017. Diagenetic reddening of Early Eocene paleosols on King George Island, Antarctica. *Geoderma* 315, 149–159. doi:10.1016/j.geoderma.2017.11.010

(2) Spinola, D.N., Pi-Puig, T., Solleiro-Rebolledo, E., Egli, M., Sudo, M., Sedov, S., Kühn, P., 2017. Origin of clay minerals in Early Eocene volcanic paleosols on King George Island, Maritime Antarctica. *Sci. Rep.* 7, 6368. doi:10.1038/s41598-017-06617-x

(3) Spinola, D.N., Portes, R. C., Schaefer, C.E.G.R., Solleiro-Rebolledo, E., Pi-Puig, T., Kühn, P., 2017. Eocene paleosols on King George Island, Maritime Antarctica: Macromorphology, micromorphology and mineralogy. *Catena*. doi:10.1016/j.catena.2017.01.004

### Share in publications

| Publication n° | Published | N° of authors | Authorship position | Scientific ideas of candidate | Data generation by candidate | Analysis and interpretation by candidate | Paper writing by candidate |
|----------------|-----------|---------------|---------------------|-------------------------------|------------------------------|--|----------------------------|
| 1              | Yes       | 6             | 1                   | 80                            | 70                           | 80                                       | 80                         |
| 2              | Yes       | 7             | 1                   | 90                            | 70                           | 70                                       | 80                         |
| 3              | Yes       | 6             | 1                   | 90                            | 60                           | 70                                       | 90                         |

## 1. Introduction

The importance of the Antarctica for world climate patterns is largely recognized because it is the largest continent on Earth and is covered by a massive ice cap almost 4 km thick in some areas (Francis et al., 2007). Nevertheless, the Cenozoic climate history of Antarctica (last 65 Ma) is punctuated by periods with less or no ice sheets. These are the so-called “greenhouse” periods during which Antarctica was dominated by rainforests rather than ice (Barrett, 2008; Francis et al., 2009, 2007).

The Eocene (56–34 Ma) was the most significant greenhouse period of the Cenozoic era. The Antarctic landscape was completely different, with a predominance of a lush rainforest without ice caps, despite the polar darkness (Askin, 1991; Birkenmajer and Zastawniak, 1989; Francis and Poole, 2002; Hunt and Poole, 2003; Mozer, 2012; Poole et al., 2001; Pross et al., 2012). The high concentration of CO<sub>2</sub> is the most accepted hypothesis for such a warm paleoclimate (Fig.1) (DeConto and Pollard, 2003; Pagani et al., 2005; Pearson et al., 2009; Zachos et al., 2001).

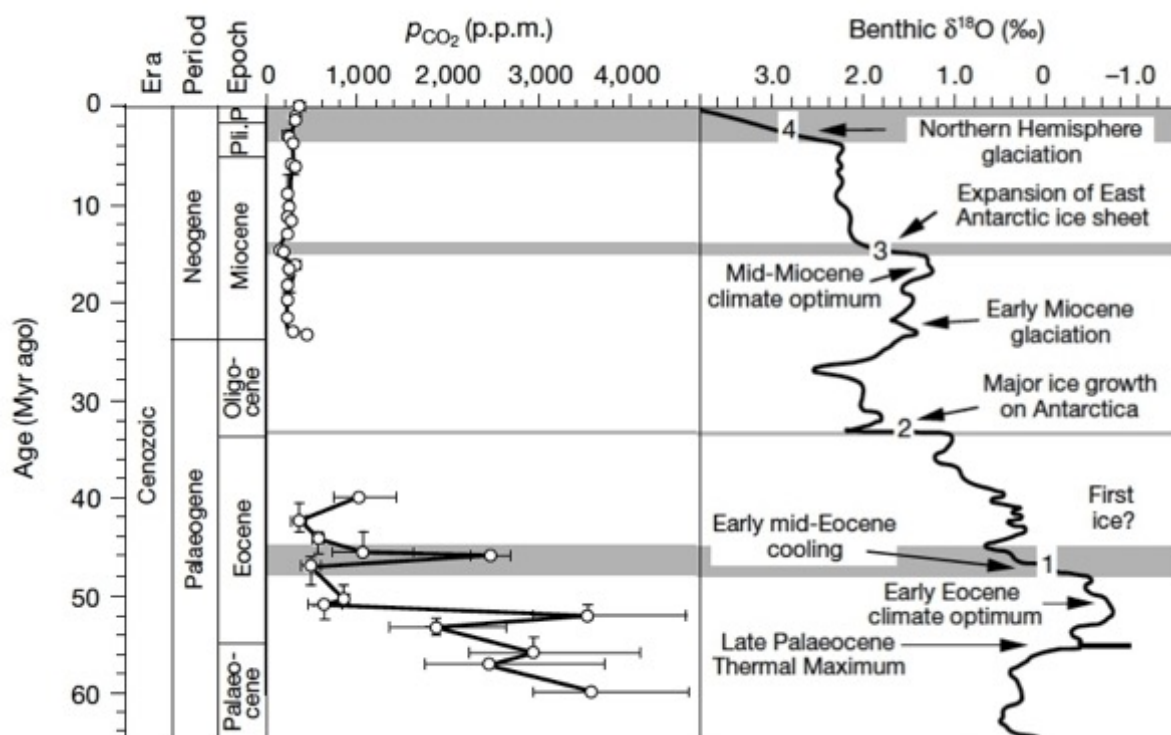


**Figure 1.** Carbon dioxide levels and Cenozoic climate change. The trend towards more positive  $\delta^{18}\text{O}$  results from a combination of deep-sea cooling and global ice volume increases. Four major steps (numbered 1 to 4) in  $\delta^{18}\text{O}$  are indicated. Modified from (Pearson and Palmer, 2000).

There are different conclusions about the paleoclimate patterns during the Eocene, such as paleotemperature and paleoprecipitation. These conclusions vary according

to the location of the studied site (e.g. maritime or continental, west or east Antarctica) and the proxy adopted. Nonetheless, the Eocene paleoclimate is roughly divided into three major paleoclimatic units (Dingle and Lavelle, 2000, 1998a; Francis et al., 2009): 1) Early-Middle Eocene – warm to cool temperate humid, dominated by forests in a frost-free environment with a cooling trend towards the Middle Eocene; 2) Late Eocene – continuous cooling trend with a decline on vegetation species variety and abundance, but still ice-free; 3) Eocene-Oligocene transition – the onset of glaciation, with appearance of the ice sheets in comparable size with the modern ones.

### **1.1. Paleoenvironmental proxies**

The Antarctic paleoclimate has been studied by several different proxies, such as sedimentology (Ehrmann et al., 1992; Mackensen and Ehrmann, 1992; Robert and Kennett, 1997), marine microfossils (Elliot et al., 1994; Stickley et al., 2004), palaeontology (Feldmann and Woodburne, 1988; Mansilla et al., 2013, 2012; Reguero et al., 2002), ocean isotope geochemistry (Coxall et al., 2005; Zachos et al., 2001, 1996), paleoflora/palynomorphs (Askin, 1991; Francis and Poole, 2002; Griener et al., 2013; Poole et al., 2005, 2003, 2001; Pross et al., 2012), and computer modelling (DeConto and Pollard, 2003; Huber et al., 2004). Most of these studies were carried out in ocean sediment samples from the surrounding oceans, because Antarctica is almost totally covered by ice. There are just a few sites where terrestrial records of Eocene are still preserved. KGI, South Shetlands Island, Maritime Antarctica is one of these sites where terrestrial records of the Eocene can be found (Fig. 2).

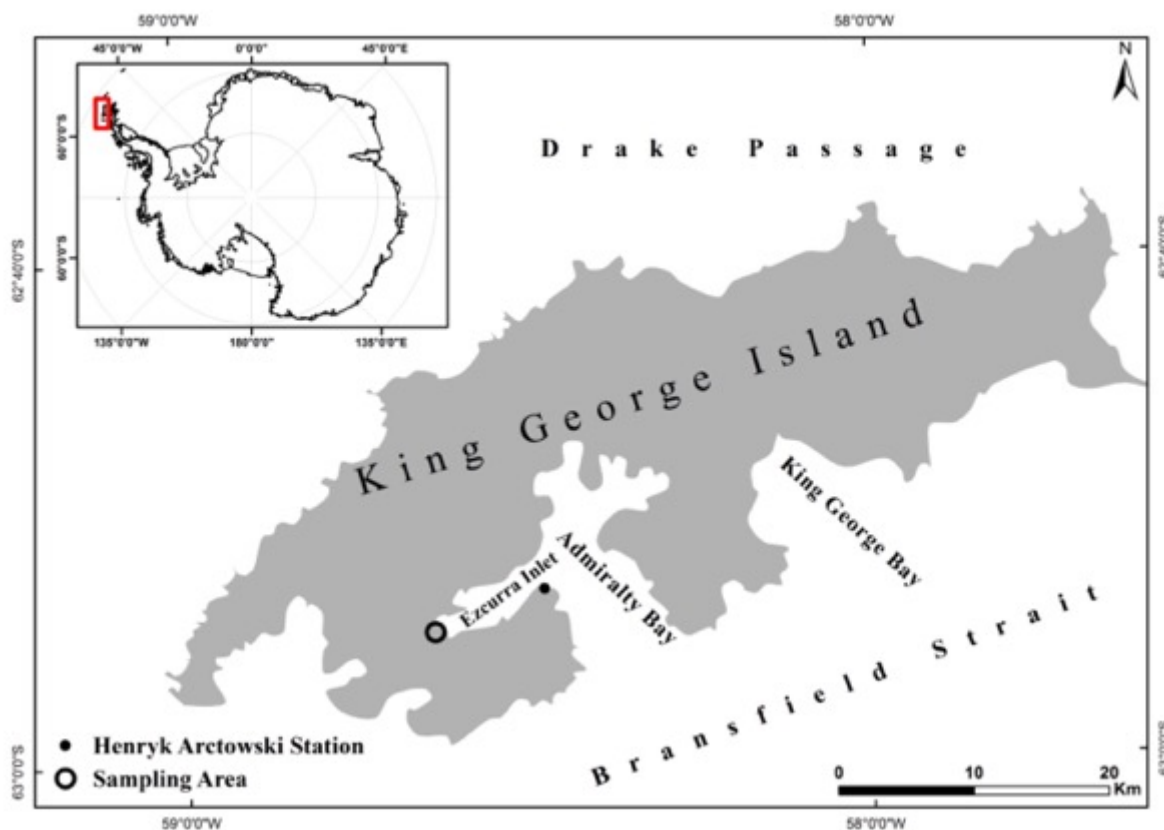


**Figure 2.** Location of the sampling site at the King George Island.

Previous paleobotanical research carried out on KGI showed a landscape dominated by rainforest trees, typical of cool, humid environments. The best modern analogue for such paleoenvironment is the Valdivian rainforest on Southern Chile (Birkenmajer and Zastawniak, 1989; Francis and Poole, 2002; Hunt and Poole, 2003; Mozer, 2012; Poole et al., 2003, 2001). The Valdivian rainforest climate is heterogeneous because of its large extension (34 million hectares), ranging from 36°S and to 47°S latitude (Veblen and Alaback, 1996). Nevertheless, the paleoclimate studies usually link Antarctica's paleoclimate with the cooler and wetter regions of the Valdivian forest with estimated paleotemperature between 5°C–15°C and precipitation more than 1000mm without a large dry season (Francis et al., 2009). Beyond the similar fossil flora assemblage, the Valdivian forest is formed in an actively volcanic landscape, like KGI. Such an environment in the modern Valdivian rainforest is usually dominated by Andosols (IREN, 1978).

## 1.2. Paleosols on King George Island

In KGI, the eruption of basalt flows occurred episodically, and during the intervals of flows, the landscape was sufficiently stable for paleosol development. However, there is very little information about the paleosols on KGI, with only one publication from the 90's (Birkenmajer and Łydka, 1990). This study indicated a warm, humid paleoclimate, because the paleosols were composed of smectite and kaolinite. Although no further detailed research about these paleosols has been conducted so far, other studies have recognized weathered paleosurfaces, usually between two basalt flows (Birkenmajer et al., 2005; Canile, 2010; Mozer, 2012). Therefore, there is a gap in the study of paleosols on KGI.

## 1.3. Objectives and hypotheses

Considering the potential of paleosols as a paleoenvironmental archive and the relevance of the Eocene for the understanding of Antarctica's climate history, the main objective was to reconstruct the paleoenvironment of KGI using paleosols as a proxy. To achieve this objective, this thesis was divided into three manuscripts. The manuscripts were designed to achieve specific objectives related to the paleosols characteristics.

**Objective 1:** To identify the main pedogenic properties and features that would define the intrabasaltic red layers as a paleosol ([Manuscript 1](#)).

Recognition of paleosols in certain situations is complicated, and it is crucial to differentiate between paleosols and another geological phenomenon. In the present study, the paleosols occurred as reddish layers (50 cm–100 cm thick) between basalt flows. Red layers occurring between basalt flows are very often defined as baked zone, sediments, and altered pyroclasts. Therefore, a proper identification of these red layers as a paleosols or not is essential to provide paleoenvironmental information.

### **Hypotheses:**

- a) The Eocene red layers in KGI are paleosols formed during periods of lower or no volcanic activity.
- b) These paleosols are suitable proxies for paleoenvironmental reconstruction.

**Objective 2:** To determine the origin of the clay minerals in KGI paleosols ([Manuscript 2](#))

These paleosols had a reasonable amount of clays (>15%) and mostly composed of smectite. In volcanic soils, the predominance of smectite is related more with warm temperate climates with long dry seasons (e.g. the Mediterranean). However, as demonstrated in Section 1, the paleoclimate was likely humid, without a long dry season. For this reason, the predominance of smectite would indicate a contradictory finding. On the other hand, smectite is not always formed during pedogenesis. In volcanic parent materials, smectite can be formed by hydrothermal alteration of the tephra. Afterwards, the smectite is progressively released into the soil during the weathering and soil formation. Thus, the understanding of smectite origin is essential to avoid paleoenvironmental misinterpretations.

**Hypothesis:** The smectite on KGI paleosols were inherited from the parent material, because the paleosols were weak/moderated developed under a cool, humid climate, which is not conducive for smectite formation.

**Objective 3:** To investigate if the early Eocene paleosols on King George Island, Maritime Antarctica have acquired their reddish colour during the paleopedogenesis, by burial diagenesis and/or by heating of a covering lava flow ([Manuscript 3](#)).

These paleosols present strong reddish colours that are in apparent disagreement with their weakly/moderated pedogenic development. Furthermore, they were formed on a basaltic tephra under a cool, humid paleoclimate prone to ferrihydrite formation rather than hematite. In addition, these paleosols were covered by a lava flow, which could be another pathway for reddening. Therefore, the understanding of the origin of the red colour of the paleosols can provide a clue about their paleoenvironment and/or indicate diagenetic processes.

**Hypotheses:**

- a) The red colours of the KGI paleosols are the result of burial reddening, because these paleosols were weakly/moderated developed under a cool, humid climate, not prone to hematite formation.
- b) The horizons in contact with the lava flow were not affected by heating because they are not redder than the deeper horizons.

## **2. Methodology**

### **2.1. Study area**

The samples were collected on King George Island, South Shetland Islands, Maritime Antarctica. The specific outcrop is located in the Cytadela area of the Ezcurra Inlet in the Admiralty Bay (62° 11.057'S - 58° 35.209'W) (Fig. 3). The deposits in the outcrop stratigraphically belongs to the Point Thomas Formation, Ezcurra Inlet Group, which comprises a 500 m thick Paleogene (Eocene-Oligocene) volcanic succession (Birkenmajer, 1980a; Birkenmajer and Zastawniak, 1989). This formation was deposited during the Arctowski interglacial period (ca 50 to ca 32 Ma), a climostratigraphic unit introduced by Birkenmajer (1988).

Two informal units of the Point Thomas Formation are recognized at the Cytadela, the Lower Member (LM) and Upper Member (UM) (Birkenmajer, 1980a). The LM is a 20–40 m thick regular high - Al flow basalt with a thickness of 1–6 m alternating with pyroclastic deposits. The LM corresponds to the Early Eocene humid temperate climate, similar to the present-day Chilean Valdivian rainforest (Mozer, 2012) (Fig. 3). The UM comprises 150–450 m of irregular, lenticular basalt lavas alternating with feldspathic tuff, interbedded with coarse vent breccia and plant-bearing tuff.

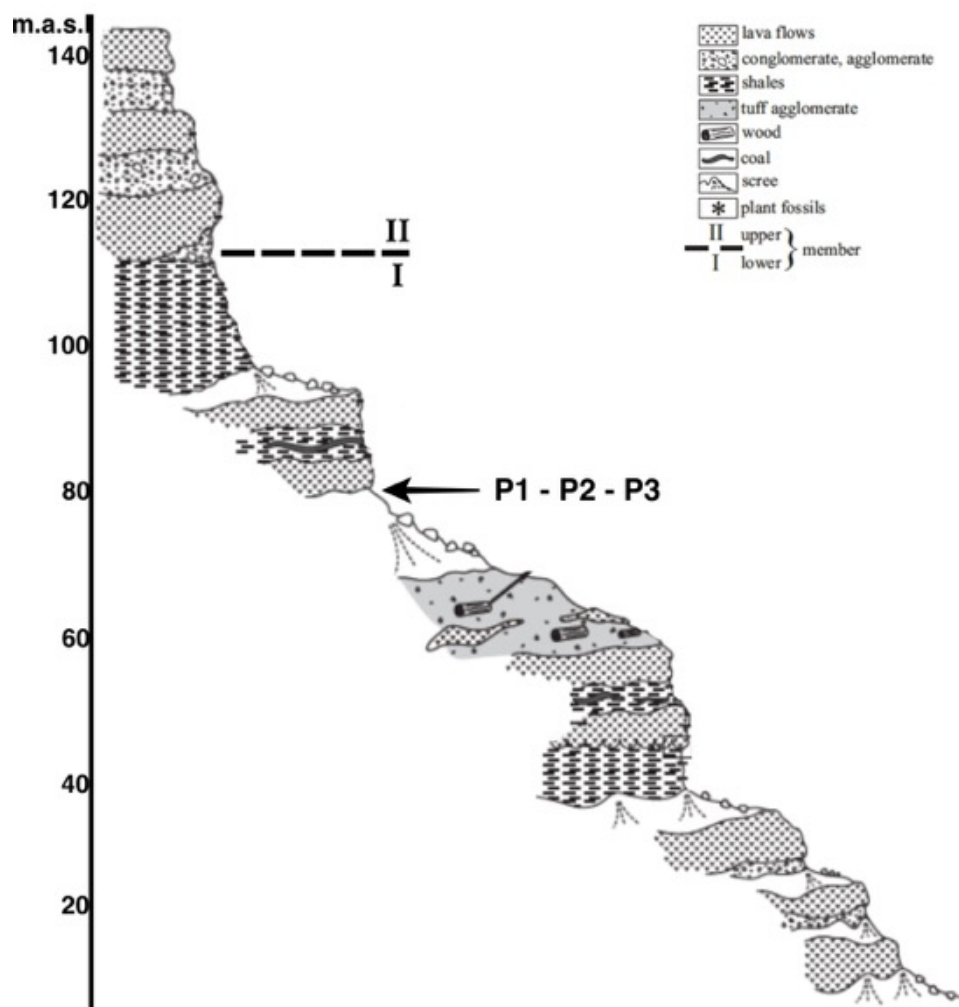


**Figure 3.** Schematic field section with the location of the profiles. Modified from Mozer, 2012. Samples were taken from a red layer covered by the 6th basalt flow basalt flow (from bottom to top) in the LM of the schematic field section made by (Mozer, 2012). Three profiles (P1, P2 and P3) were chosen (Fig.4), which are located with a distance of 60 m between the P1 and P2 and of 90 m between P2 and P3.

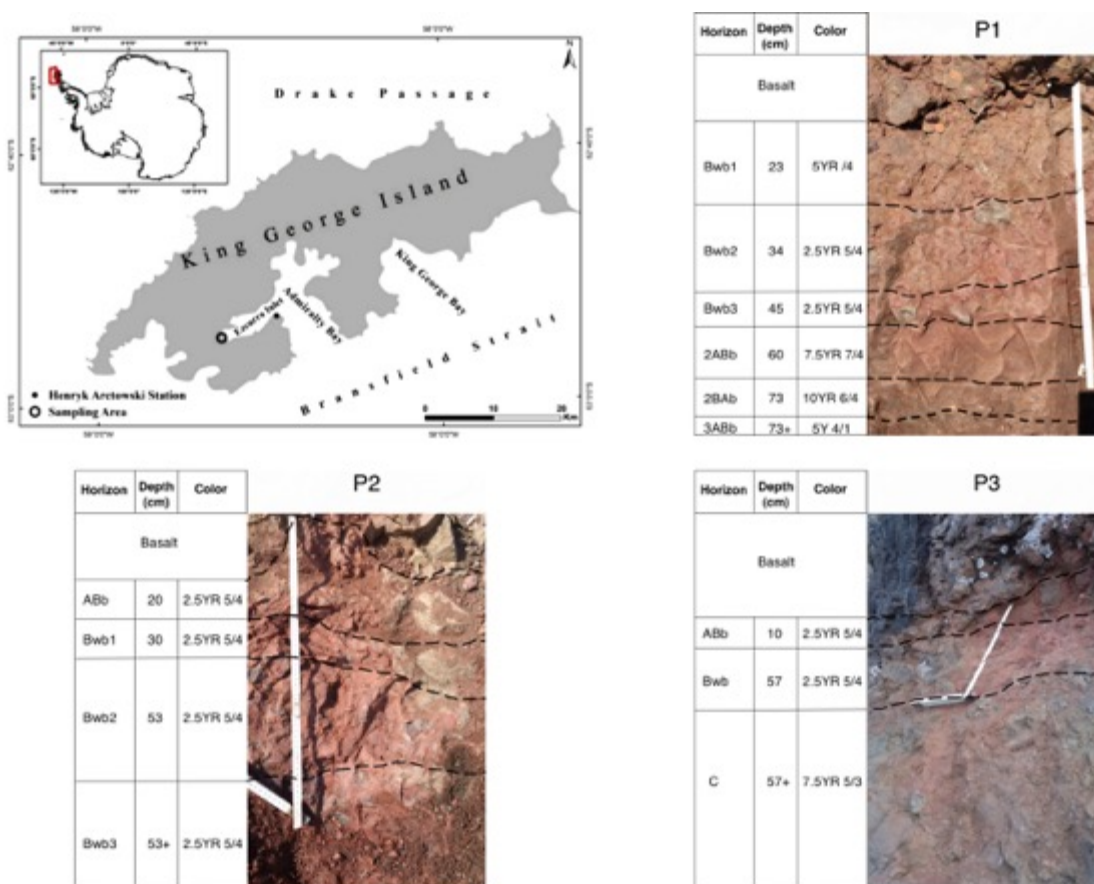


**Figure 4.** Location of the sampling site at the King George Island and photographs of the profiles with field colours.

After removing overlying debris, the profile face was excavated ~20 cm to provide a fresh surface for describing and sampling. The profiles were described following FAO (2006) with a particular focus on horizon boundaries, colour (Munsell soil colour charts), structure (size and type), visual estimation of rock fragments and presence of plant fossils. A total of 13 bulk samples from red layers were sampled.

## 2.2. Laboratory methods

### 2.2.1. Micromorphology ([Manuscript 1](#), [Manuscript 2](#) and [Manuscript 3](#))

For micromorphological analysis, 12 undisturbed and oriented samples were taken from the paleosols horizons and six samples from the overlying and underlying basalts.

The undisturbed samples were not impregnated with resin because of sufficient induration of the material. The samples were sliced into 9 x 6 cm thin sections. Afterwards, they were analysed and photographed using a polarizing microscope (Zeiss Axio Imager.A2m, Software AxioVision 4.7.2) with plane polarized light (PPL),

crossed polarized light (XPL) and oblique incident light (OIL). Description followed (Delvigne, 1998) and (Stoops, 2003).

### **2.2.2. Scanning Electron Microscopy (SEM) equipped with Energy-Dispersive X-Ray Spectroscopy (EDS) ([Manuscript 2](#))**

Textures and microchemistry of selected samples were determined using a Hitachi TM3030 Plus Scanning electron microscope (SEM) coupled with a Bruker Quantax 70 X-ray microanalysis detector (EDS) on polished uncoated thin sections at the Institute of Mineralogy and Geodynamics, University of Tübingen.

### **2.2.3. Geochemistry ([Manuscript 1](#))**

The bulk samples (ratio Li-metaborate to soil 1:5) were ground with an agate mill for 10 minutes and the major elements were measured with a wavelength dispersive XRF device (PANalytical PW 2400). Information about the standard errors of the calibration for the major elements is provided in the supplementary data of Manuscript 1.

The Chemical Index of Alteration minus K (CIA - K) was used (Maynard, 1992) (calculated in molar portions). The K is excluded in this equation to avoid any possible effect of K-metasomatism (Maynard, 1992).

$$\text{CIA-K} = [\text{Al}_2\text{O}_3 / (\text{Al}_2\text{O}_3 + \text{CaO}^* + \text{Na}_2\text{O})] \times 100 \quad (1)$$

where CaO\* is the amount of silicate-bound CaO. For that, we calculated the CaCO<sub>3</sub> bound Ca from the carbonate content and subtracted that from CaO.

Total carbon (TC) content was measured on ground samples with an Elementar Analyser (DIN ISO 10694, 1995) and the total inorganic carbon (TIC) content was determined gas volumetrically (DIN ISO 10693, 1995).

### **2.2.4. Particle size distribution ([Manuscript 1](#) and [Manuscript 2](#))**

Particle size distribution analysis was performed by a combined sieving and pipette method (NRCS, 1996).

### **2.2.5. X-ray diffraction and differential X-ray diffraction ([Manuscript 1](#), [Manuscript 2](#) and [Manuscript 3](#))**

The clay fraction (<2µm) of all horizons and the coarse fraction (>2mm) of selected horizons. The coarse fraction is the rocks fragments (pyroclastic material) forming the paleosol parent material.

The clay fraction was separated in distilled water according to Stoke's law and was

prepared using two different methods:

Air-dried oriented preparations were obtained by pipetting some drops of the suspensions onto a glass slide, which was then dried at 30°C for a few hours (Moore and Reynolds Jr, 1997).

Ethylene glycol solvation of the slides was achieved by exposing them to ethylene glycol vapor at 70°C for a minimum of 12 hours.

Randomly oriented samples, to measure the 060 reflections that allowed the distinction between dioctahedral and trioctahedral clay minerals, were prepared using a back-loading procedure (Moore and Reynolds Jr, 1997).

Measurements were made using an Empyrean diffractometer operating with an accelerating voltage of 45V and a filament current of 30mA, using CuK $\alpha$  radiation, nickel filter and PixCELL 3D detector.

Oriented samples were examined by XRD in the air-dried form, saturated with ethylene glycol (EG) and after heating (550°C). The preparations were measured over a 2 $\theta$  angle range of 2-70° (air-dried) and 2-30° (glycolated and heated) with a step size of 0.04° (2 $\theta$ ) and 40s of scan step time. For randomly samples the peaks were resolved from the background by small step scan (0.002° 2 $\theta$ ) and long count time (100s) measurements.

Profile fitting was calculated from oriented samples using simple peak weighting factors. For area estimation, we used Fityk (Wojdyr, 2010), a software for data processing and nonlinear curve fitting, simple background subtraction and easy placement of peaks and changing of peak parameters. The smectite peak was evaluated by peak fitting that is based on a pseudo-Voigt function.

The decomposition of peaks using profile fitting allows the identification of clay assemblage and provides information of peak position and full width at half maximum intensity (FWHM). For the FWHM measurement, instrumental broadening effects were calibrated via a LaB6 standard (NIST 660a).

#### **2.2.6. Mineralogy of iron oxides** ([Manuscript 1](#) and [Manuscript 3](#))

The following extractions were made sequentially.

First, the nanocrystalline Fe (Fe<sub>o</sub>) compounds were extracted by shaking 2.5 g of soil 100 mL 0.2M acid ammonium oxalate (pH3) for 4 h in the dark (Schwertmann, 1964).

With the residuum of this treatment we carried out the selective dissolution of maghemite ( $\gamma$  -  $\text{Fe}_2\text{O}_3$ ) using  $\text{H}_2\text{SO}_4$  using a concentration of 1M during 1h at 75°C (Schwertmann and Fechter, 1984). The remaining residues were extracted with dithionite-citrate-bicarbonate (DCB) solution, dissolving the well-crystallized iron forms (Mehra and Jackson, 1960).

The proportion of crystalline pedogenic iron against the total amount of iron was determined using  $\text{Fe}_d/\text{Fe}_t \cdot 100$  ratio, where  $\text{Fe}_t$  is the total  $\text{Fe}_2\text{O}_3$ , measured by X-ray fluorescence (XRF).

The mineralogical composition of the bulk samples was achieved by X-ray diffraction (XRD) of randomly oriented specimens using an EMPYREAN diffractometer with Ni filter, a CuK $\alpha$  radiation at 40 kV and 30 mA. The samples were scanned from 5° to 70° (2 $\theta$ ), with counting for 40s every 0.03° (2 $\theta$ ) in an aluminium rotating sample-holder. Same XRD procedures for randomly oriented samples were repeated after removal of free-iron by DCB, producing a differential X-ray diffraction (Schulze, 1981).

#### **2.2.7. $^{40}\text{Ar}/^{39}\text{Ar}$ dating ([Manuscript 2](#))**

The groundmass samples with 250-500  $\mu\text{m}$  size were prepared by crushing the fresh part of the rock, sieving, washing and the removal of phenocrysts with a magnetic separator and by handpicking. Finally, the samples were soaked in 1N HCl for a few minutes to remove secondary minerals on their surface.

Neutron activation of the groundmass was performed at the Oregon State TRIGA Reactor (OSTR) in the University of Oregon, USA. The samples were irradiated by the fast neutrons in the CLICIT facility, in which a Cd tube with 0.51 mm thickness is equipped. Samples were wrapped by commercial Al foils, then were loaded into the 99.999% pure Al sample container together with the neutron-flux monitoring mineral, Fish Canyon Tuff sanidine (FC3), prepared by Geological Survey of Japan (27.5 Ma; (Ishizuka, 1998; Uto et al., 1997) crystals of  $\text{K}_2\text{SO}_4$  and  $\text{CaF}_2$  for correction of interference by the Ar isotopes produced from K and Ca in the samples. They all had been irradiated for 4 hours with the fast neutron flux of  $2.5 \times 10^{13}$  n/cm $^2$ /s. After cooling of samples, they were sent back to Potsdam then their Ar isotopes were analysed at the  $^{40}\text{Ar}/^{39}\text{Ar}$  geochronology laboratory in the University of Potsdam (Halama et al., 2014; Wilke et al., 2010).

The Ar isotopic analytical system consists of, (1) a New Wave Gantry Dual Wave laser

ablation system with a 50W CO<sub>2</sub> laser (wavelength 10.6 micrometre) for heating samples and extracting gases, (2) an ultra-high vacuum purification line equipped with SAES getters and the cold trap held at the frozen temperature of ethanol, and (3) a high-sensitivity Micromass 5400 noble gas mass spectrometer equipped with an electron multiplier conducting the pulse-counting analysis. All groundmass samples of about 13 mg each were firstly loaded into the sample chamber. Then the sample chamber and the purification line were baked for 24 hours at 100 and 200°C. The groundmass samples were firstly preheated and pumped with 1.2% output (0.6W), then were analysed by stepwise heating for two minutes with 10-15 steps with a continuous CO<sub>2</sub> laser beam with 1.5 mm diameter. The obtained Ar isotope ratios by the analysis are corrected for blank, mass discrimination, interferences and decay corrections following Uto et al. (1997), and then the plateau age, total gas age, normal and inverse isochron ages are calculated for each sample. Decay constants and atmospheric Ar isotope ratios follow Steiger and Jäger (1977) and the calculation of isochron ages follows York (1969). Plateau ages were determined by the criteria of Fleck et al. (1977). Finally concluded ages for each sample were obtained by the comparison among plateau age, normal and inverse isochron ages from plateau steps or all steps and total gas age with considering if the initial <sup>40</sup>Ar/<sup>36</sup>Ar ratios obtained by isochrons were valid. See section Supplementary data of [Manuscript 2](#) for supplementary tables and figures.

### **2.2.8. Diffuse Reflectance Spectroscopy (DRS) ([Manuscript 3](#))**

The detection of goethite and hematite were performed by DRS after Torrent et al. (2007). DR spectra were recorded at a scan rate of 30 nm min<sup>-1</sup> from 380 to 770 nm in 0.5 nm steps using a Varian Cary 5000 UV-Vis-NIR spectrophotometer equipped a diffuse reflectance attachment.

The samples were heated in different temperatures in a muffle furnace for 2 hours at 300°C, 400°C, 500°C, 600°C, 700°C, 800°C and measured after each heating interval.

The second derivative of the Kubelka–Munk (K–M) remission function within the 380–710 nm range were calculated by using a cubic spline procedure based on segments of 30 data points. The intensities of spectral bands at ~415 nm and ~535 nm are proportional to the concentration of goethite and hematite, respectively (Scheinost et al., 1998). With this technique, it is possible to detect goethite and hematite concentrations of less than 0.1%, which is more than one order of magnitude smaller

than the detection limit of ordinary X-ray diffraction (Torrent and Barrón, 2002).

The spectra measurements were converted into tristimulus values (X, Y, Z) according to the CIE colour system (Commission Internationale de L'Eclairage, 1978). Afterwards, the X, Y, Z values were converted to Munsell hue (H), value (V), and chroma (C) and to L\* a\* b\* colour systems (Wyszecki and Stiles, 1982). The L\*-axis represents "lightness-darkness", the a\*-axis "redness-greenness", and the b\*-axis "yellowness-blueness".

### **2.2.9. Magnetic susceptibility ([Manuscript 3](#))**

The magnetic susceptibility,  $\chi$ , of fine earth fraction was measured at both low (470 Hz = Lf) and high (4700 Hz = Hf) frequencies, using a Bartington MS- 2 magnetic susceptibility meter (Bartington Instruments, Witney, UK) equipped with an MS-2B sensor. The absolute frequency-dependent susceptibility,  $\chi_{fd}$ , was defined as  $\chi_{lf} - \chi_{hf}$ . The per cent frequency-dependent susceptibility,  $\chi_{fd}\%$ , was defined as  $(\chi_{fd} / \chi_{lf}) \times 100$ . Values of  $\chi_{fd}\% < 5\%$  are typical for samples in which non-SP grains dominate the assemblage or where extremely fine grains (<0.005  $\mu\text{m}$ ) dominate the superparamagnetic (SP) fraction. Samples dominated by SP grains (e.g. maghemite) have  $\chi_{fd}\%$  between 10-14% and  $\chi_{fd}$  can be used semi-quantitatively to estimate their total concentration in soils (Dearing, 1999).

### **3. Results and Discussion**

#### **3.1. Pedogenic and diagenetic features of the paleosols and their paleoenvironmental significance (Manuscript 1).**

This study was conducted in order to define whether the red layers are paleosols and to interpret the paleoenvironmental signal they may have. Another objective was to identify the diagenetic features, which are those formed after the burial of the paleosol. The identification of such features is important to make reliable paleoenvironmental interpretations because diagenesis can disturb the paleoenvironmental signal of paleosols.

The three profiles had their morphology analysed in field followed by micromorphological, geochemical and mineralogical analysis. The main morphological features were colour, structure and how they change in depth. The profiles are reddish-brown with gradual colour changes with depth. They have predominantly strong blocky (more angular) and platy structure with variable size with depth. With the exception of P1, rock fragments became more abundant and larger with depth (Table 1). The combination of diffuse transitions of colour and changes in structure can be taken as main physical properties indicating pedogenesis (Retallack, 1988). The differences noticed in structure, either shape or size of peds across the horizons of the investigated profiles, can be considered as ample features of pedogenesis (Fenwick, 1985).

The reddish colours called the attention because red soils are predominantly found in tropical regions and on land surfaces hundreds of thousands to millions of years old (Blodgett et al., 1993). This was not the case because the red layers were weakly-moderately weathered as detected by micromorphology and geochemistry. Therefore, the red colours were considered partially the results of diagenesis. On the other hand, the role of pedogenic processes is demonstrated by the diffuse transition of the colours between the horizons, a common behaviour in soils (Fenwick, 1985; Retallack, 1988).

The  $Fe_d - Fe_o / Fe_t$  ratio also supports the combination of pedogenesis with post-burial reddening (Table 3). The reddish horizons, which have similar colours, display varied  $Fe_d - Fe_o / Fe_t$  ratios. The Bwb1 horizon in P2 for example, with the highest ratio of 18, has a similar colour compared with the other horizons (hue 2.5YR). This indicates that the iron released during pedogenesis was different among the horizons but they

caused almost the same colours. On the other hand, the yellowish horizons 2ABb and 2BAb in P1 have values of 10, which is not much different compared to the reddish horizons. This suggests that the burial reddening did not, or only partly, affect these horizons. Following this rationale, P1-3ABb is gray (5Y 4/1) and have measurable crystalline iron (=5). It means that this horizon was not affected by post-burial reddening. Hence, the paleo pedogenesis also played an important role forming a yellowish/gray colour in these horizons.

Among the micromorphological features, the occurrence of channels, passage features and unaccommodated voids were the most important because they point to biological activity in all profiles (Stoops, 2003). The planar voids, channels (Fig. 5a, b) and vughs are the predominant void types (Table 2). Accommodated to partially accommodated planar voids are most common but unaccommodated planar voids were also observed (Fig. 6). Passage features are present in all horizons, except in P2 (the ABb horizon) and P3 (the Bwb horizon). Although bioturbation can also occur in e.g. marine/lake sediments (Buurman, 1975), the presence of channels is a useful feature to differentiate paleosols from other materials (Singer, 1970). Moreover, neither sedimentary structures nor features were found, ruling out such a marine or lacustrine paleoenvironment.

**Table 1.** Selected main macromorphological properties (after FAO, 2006).

| Profile   | Horizon | Depth<br>[cm] | Horizon boundaries<br>(distinctness - topography) | Structure <sup>1</sup> |           | Colour (Munsell) |                    | Rock fragments     | Plant fossil | Particle size %  |                           |                               | Textural class  |
|-----------|---------|---------------|---|------------------------|-----------|------------------|--------------------|--------------------|--------------|------------------|---------------------------|-------------------------------|-----------------|
|           |         |               |   | Type                   | Size      | Dry              | Name               |                    |              | Clay (<2 $\mu$ ) | Silt (2 $\mu$ -63 $\mu$ ) | Sand (63 $\mu$ - 2000 $\mu$ ) |                 |
| <b>P1</b> | Bwb1    | 0 - 23        | clear - wavy                                      | sb +pl                 | very fine | 5YR 5/4          | Dull reddish brown | many               |              | 15               | 18                        | 67                            | Sandy loam      |
|           | Bwb2    | 23 - 34       | gradual – smooth                                  | sb+pl                  | fine/thin | 2.5YR 5/4        | Dull reddish brown | common             |              | 15               | 19                        | 66                            | Sandy loam      |
|           | Bwb3    | 34 - 45       | abrupt- smooth                                    | ab                     | fine      | 2.5YR 5/4        | Dull reddish brown | common             |              | 14               | 19                        | 67                            | Sandy loam      |
|           | 2ABb    | 45 - 60       | clear - smooth                                    | ab                     | fine      | 7.5YR 7/4        | Dull orange        | none               |              | 17               | 21                        | 62                            | Sandy loam      |
|           | 2BAb    | 60 - 73       | abrupt - smooth                                   | ab+pl                  | coarse    | 10YR 6/4         | Dull yellow orange | none               |              | 20               | 22                        | 58                            | Sandy clay loam |
|           | 3ABb    | 73+           |   |                        | pl+ab     | medium           | 5Y 4/1             | Gray               | none         | x                | 20                        | 15                            | 65              |
| <b>P2</b> | ABb     | 0 - 20        | abrupt - smooth                                   | sb                     | medium    | 2.5YR 5/4        | Dull reddish brown | few                |              | 19               | 17                        | 64                            | Sandy clay loam |
|           | Bwb1    | 20 - 30       | gradual - smooth                                  | ab+pl                  | coarse    | 2.5YR 2/4        | Reddish            | few                |              | 15               | 19                        | 66                            | Sandy loam      |
|           | Bwb2    | 30 - 53       | diffuse - irregular                               | ab+pl                  | medium    | 2.5YR 5/4        | Dull reddish brown | common             |              | 15               | 18                        | 67                            | Sandy loam      |
|           | Bwb3    | 53+           |   |                        | ab+sb     | medium           | 2.5YR 5/4          | Dull reddish brown | many         |                  | 15                        | 13                            | 72              |
| <b>P3</b> | ABb     | 0 - 10        | diffuse   | sb+pl                  | fine/thin | 2.5YR 5/4        | Dull reddish brown | common             |              | 12               | 15                        | 73                            | Sandy loam      |
|           | Bwb     | 10 - 57       | gradual   | sb+pl                  | medium    | 2.5YR 5/4        | Dull reddish brown | common             |              | 14               | 20                        | 66                            | Sandy loam      |
|           | C       | 57+           |   | sb+pl                  | coarse    | 7.5YR 5/3        | Dull               | many               |              | 11               | 10                        | 79                            | Sandy loam      |

<sup>1</sup>**Structure type:** ab= angular blocky., sb= subangular blocky., pl= platy. **Size:** vf= very fine/thin., fi= fine/thin., me=medium., co= coarse/thick

**Table 2.** Selected main micromorphological characteristics.

| Profile   | Horizon | Depth<br>[cm] | Pedality |    |    | Voids |     |     |    |    |    | Accomodation |      |                | Microstructure | Micromass |        |     |          |     | Plant residue | Pedofeatures |    |           | Zeolite |  |
|-----------|---------|---------------|----------|----|----|-------|-----|-----|----|----|----|--------------|------|----------------|----------------|-----------|--------|-----|----------|-----|---------------|--------------|----|-----------|---------|--|
|           |         |               | sp       | mp | wp | spv   | cmv | cxp | ch | cm | ve | vu           | a    | pa             |                | un        | Colour |     | b-fabric |     |               | cc           | pf | Fe/Mn nod |         |  |
|           |         |               |          |    |    |       |     |     |    |    |    |              |      |                |                |           | ppl    | oil | u        | ssp |               | gs           |    |           |         |  |
| <b>P1</b> | Bwb1    | 0 - 23        | x        |    |    | x     |     | x   | x  |    | x  | x            | x    | sb, (gr-cr)    | br, rd, lb, bl | rd        | x      |     |          |     |               | x            | x  |           | x       |  |
|           | Bwb2    | 23 - 34       |          |    | x  |       |     |     |    | x  |    | x            | (sb) | br, rd, lb, bl | rd             | x         |        |     |          |     |               |              | x  |           |         |  |
|           | Bwb3    | 34 - 45       |          | x  |    |       |     | x   |    |    |    | x            | x    | sb, (gr)       | br, rd, lb, bl | rd        | x      |     |          |     |               |              | x  |           |         |  |
|           | 2ABb    | 45 - 60       |          |    | x  |       |     | x   |    |    |    | x            |      | (sb)           | lb, br, rd     | lb, br    | x      | (x) | (x)      |     | x             |              | x  | x         |         |  |
|           | 2BAb    | 60 - 73       |          | x  |    |       |     |     |    | x  |    | x            |      | (gr)           | lb, br, rd     | lb, br    | x      | (x) | (x)      |     | x             |              | x  | x         |         |  |
| 3ABb      | 73+     |               |          |    |    |       |     |     |    |    |    |              |      | gr, lb, br     | ol, lb         | x         | (x)    | (x) |          |     |               | x            | x  |           |         |  |
| <b>P2</b> | ABb     | 0 - 20        |          | x  |    | x     | x   | x   | x  |    | x  | x            | x    | sb, gr         | br, lb, rd, bl | rd        | x      |     |          |     | x             |              |    | x         | x       |  |
|           | Bwb1    | 20 - 30       |          | x  |    |       |     | x   |    |    | x  | x            | x    | sb, (gr-cr)    | br, lb, rd, bl | rd        | x      |     |          |     |               |              | x  | x         |         |  |
|           | Bwb2    | 30 - 53       |          |    | x  |       |     | x   |    | x  | x  | x            |      | (sb)           | br, lb, rd, bl | rd        | x      |     |          |     |               |              | x  | x         |         |  |
|           | Bwb3    | 53+           |          |    | x  |       |     | x   |    |    | x  | x            |      | (sb)           | br, lb, rd, bl | rd        | x      |     |          |     |               |              | x  | x         |         |  |
| <b>P3</b> | ABb     | 0 - 10        |          | x  |    |       |     | x   |    |    | x  | x            | x    | sb             | br, lb, rd, bl | rd        | x      |     | (x)      |     | x             |              | x  | (x)       | x       |  |
|           | Bwb     | 10 - 57       |          |    | x  |       |     | x   |    |    | x  | x            | x    | sb, (gr-cr)    | br, lb, rd, bl | rd        | x      |     |          |     |               |              |    |           |         |  |

The micromorphological property is shown by the presence (cross) or absence (no cross).

The brackets are used when the property is weakly expressed

**Pedality:** sp=strongly developed pedality., mp=moderately developed., wp=weakly developed

**Voids:** spv= simple packing voids., cmv= compound packing voids., cxp= complex packing voids., ch= channels., cm= chamber., ve= vesicles., vu= vughs

**Accomodation of planar voids:** a= accommodated., pa= partially accommodated., un= unaccommodated

**Microstructure:** sb= subangular., gr= granular., cr= crumb

**Colour:** PPL (Plane Polarized Light); OIL (Oblique Incident Light): rd= red., br= brown., bl= black., lb= light brown., ol= olive, gr= grey

**b-fabric:** u= undifferentiated., ssp= stipple speckled., gs= granostriated

**Pedofeatures:** cc = clay coatings, pf= passage features, Fe/Mn nod = iron/manganese nodules

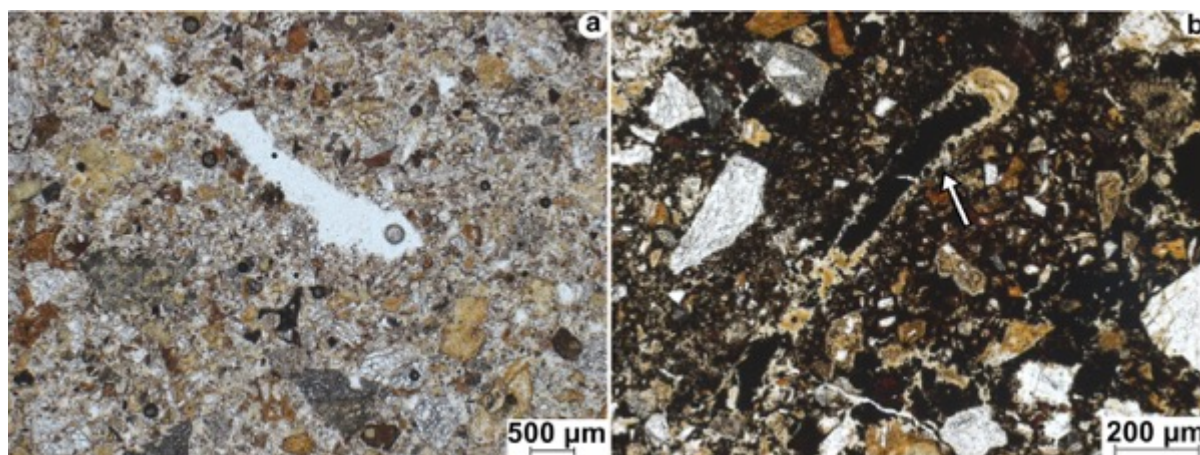


**Figure 5.** Bioturbation voids: a) P1-ABb, 60cm: a channel; b) P1-2BAb, 73cm: a channel (white arrow) filled by Fe/Mn oxide.

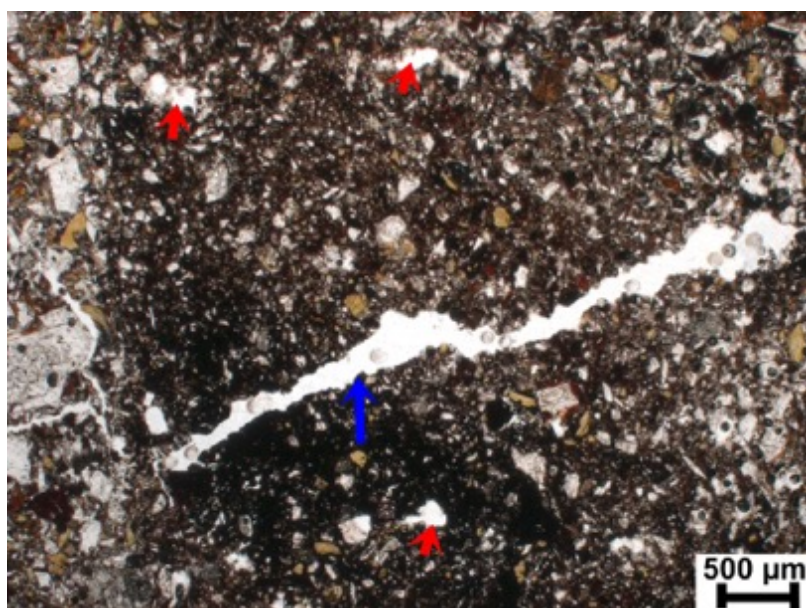


**Figure 6.** Bioturbation voids. P2-Bwb1, 30cm: unaccommodated void (blue arrow) and several channels around (red arrows). Note the void is crossing a moderately impregnated area by Fe/Mn oxides.

Angular, subangular blocky, platy and, less common granular and crumb microstructures are most prominent in all profiles. However, they are not well developed because pedality or planes of weakness are poorly or moderately expressed. These kinds of structure are related to pedo/bioturbation. Even though the undifferentiated b-fabric was predominant, the presence of weakly expressed granostriated and stipple-speckled b-fabrics also corroborate to pedoturbation process (i.e. swelling and shrinking processes) (Fig. 7a, b). Furthermore, the XRD data confirmed the dominance of smectite, which could be the responsible for the swelling and shrinking processes (Kovda and Mermut, 2010).

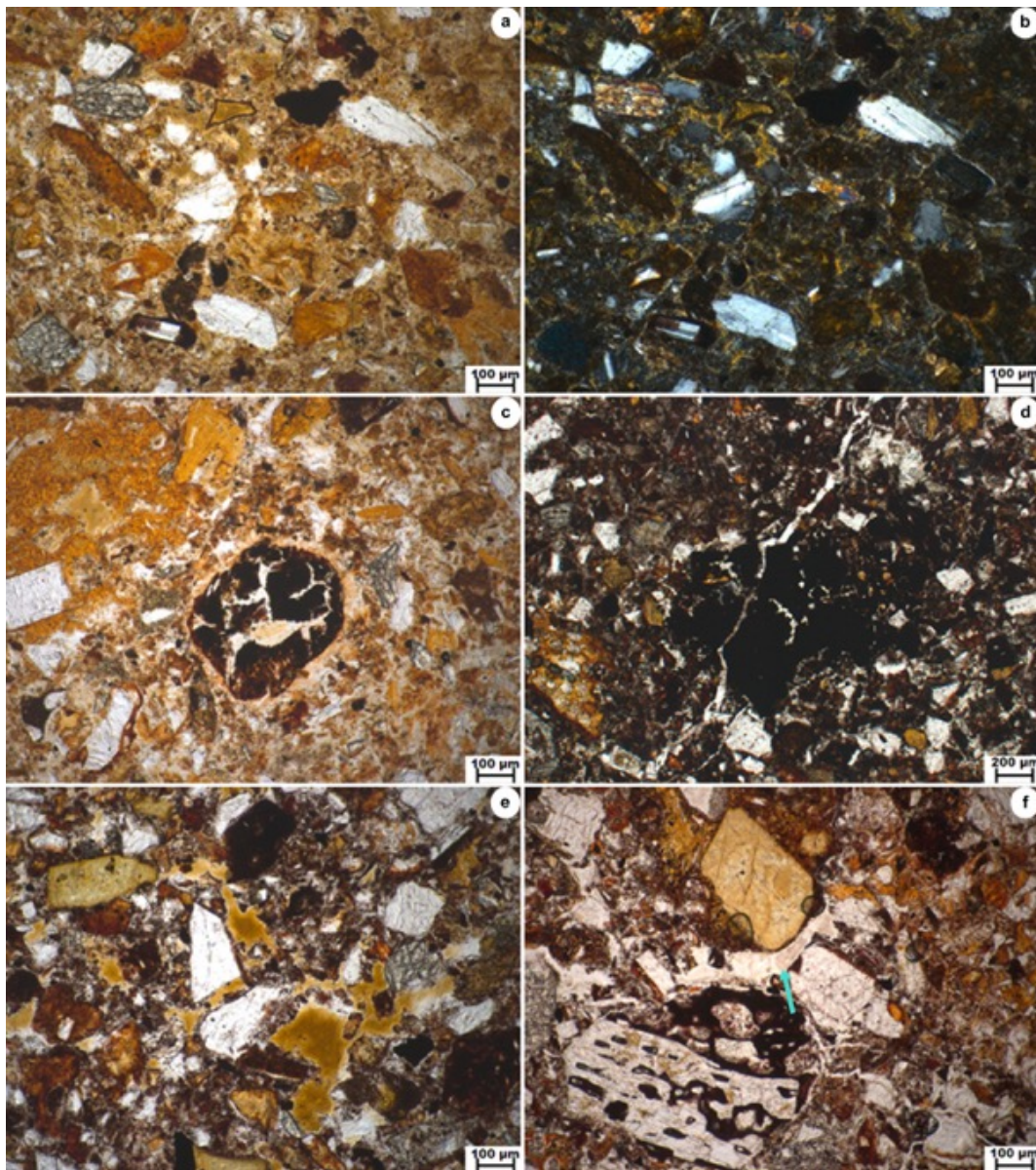


**Figure 7.** Groundmass and pedogenic features: a) P1-2BAb, 70cm: brownish fine mass (PPL); b) granostriated and stipple-speckled b-fabric (XPL); c) P1-2BAb, 70cm: typical disorthic disjointed Mn nodule (PPL); d) P2-Bwb2, 53cm: typical orthic digitate Mn nodule (PPL); e) P1-Bwb3, 45cm: yellowish-orange clay infilling (PPL); f) P2-Bwb2, 53cm: white/grey clay infilling (blue arrow) (PPL).

The differences in weathering degree in depth was an important micromorphological feature, indicating pedogenesis. Overall, the weathering degree was moderate because there were no fresh minerals, except the plagioclases, which exclude a heavy weathering degree (Fig. 8).

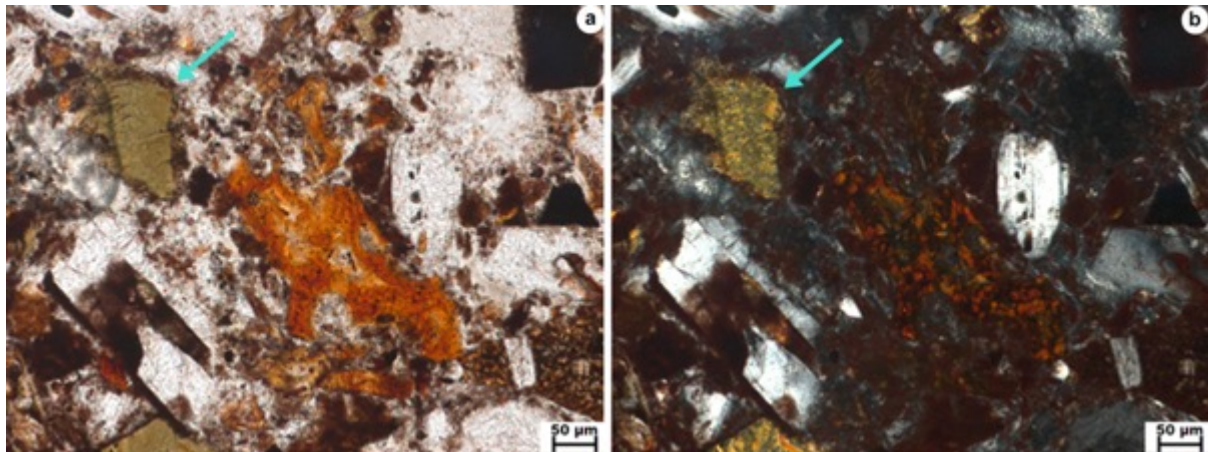


**Figure 8.** Mineral weathering examples. P2-Bwb1, 30cm. a) a yellowish sand-sized clay-body with mosaic-speckled b-fabric (blue arrow), orange glass fragment at the center of the figure (PPL); b) minerals showing speckled b-fabric due to clay neoformation, note the preservation of the shape of both alteromorphs (XPL).

Another pedogenic fingerprint was the Fe/Mn impregnation features and nodules, signalling to wet/dry cycles (Fig. 7c, d). These features were not heavily expressed nor had showed depletion features in the groundmass, suggesting short-periods of waterlogging (Veneman et al., 1976).

The presence of plant residues was one of the most important findings, indicating a former land surface. They were found in all profiles and particularly in the 2ABb, 2BAb and 3ABb horizons of P1. Organ (mainly roots) and tissue residues with reddish and orange/yellowish colours, probably impregnated by iron oxide (Fig. 9a), were found in the 2ABb and 2BAb horizons. Charcoal was found in the 3ABb horizon (Fig. 9b). Plant residues are scarce in P2 and P3 and were found only in A horizons.

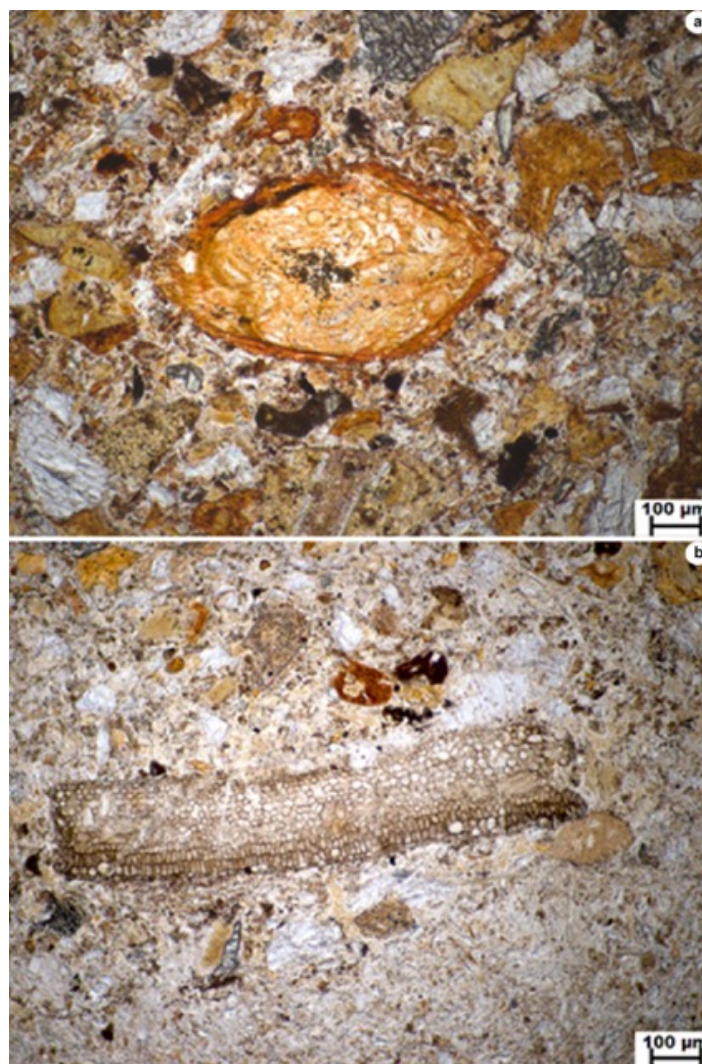


**Figure 9.** Plant residues, under PPL. a) P1-ABb, 60cm: root fragment; b) P1-3ABb, 73+cm: charcoal fragment.

Voids filled with zeolite crystals were detected only in the uppermost horizons of all profiles. This finding corresponds with the field observations; thus, an effect of the covering lava flows has to be considered. Euhedral zeolite crystals occur in the fillings of the uppermost horizons of P1 and P2, whereas anhedral crystals are characteristic for the fillings in the uppermost horizon of P3 (Fig. 10). Even though zeolites can be present in natural soils, their occurrence is very rare (Ming and Boettinger, 2001). Zeolite filling voids of the former surficial horizons are an evidence of circulation of hydrothermal fluids with a temperature range of 40° to 250°C (Kristmannsdottir and Tomasson, 1978). Such feature has been observed in other red layers and paleosols covered by lava flows (García-Romero et al., 2005; Gérard et al., 2007; Parra et al., 1987).



**Figure 10.** Types of zeolite crystallization in the horizons in contact with the lava flow, under XPL. a) P1- Bwb1, 23cm: euhedral zeolite crystals filling a large void; b) P2-ABb, 20cm: euhedral zeolite crystals filling a large void; c) P3-ABb, 10cm: anhedral zeolite crystals filling a large void.

Total organic carbon (TOC) and carbonates are present in negligible concentration in all samples (Table 3). The values are slightly higher in the 2ABb horizon of P1 with 0.3% of TOC and 2.6% of CaCO<sub>3</sub>. This means that the TOC content does not reflect the occurrence of (once) organic material, detected by micromorphology. The source of the CaCO<sub>3</sub> in the 2ABb horizon was not detected in the thin sections. Therefore, their origin could not be traced.

**Table 3.** Selected chemical characteristics: chemical index of alteration minus K (CIA-K); ratio of crystalline pedogenic iron oxides; amounts of carbonate (CaCO<sub>3</sub>) and total organic carbon (TOC).

| Profile | Horizon | Depth<br>[cm] | CIA-K <sup>1</sup> | $(Fe_d - Fe_o) / (Fe_t) * 100^2$ | CaCO <sub>3</sub> | TOC |
|---------|---------|---------------|--------------------|----------------------------------|-------------------|-----|
|         |         |               |                    |                                  | %                 | %   |
| P1      | Bwb1    | 0 - 23        | 50                 | 11                               | 0,2               | 0,0 |
|         | Bwb2    | 23 - 34       | 53                 | 12                               | 0,5               | 0,0 |
|         | Bwb3    | 34 - 45       | 54                 | 15                               | 0,6               | 0,0 |
|         | 2ABb    | 45 - 60       | 54                 | 10                               | 2,6               | 0,3 |
|         | 2BAb    | 60 - 73       | 56                 | 10                               | 0,6               | 0,0 |
|         | 3ABb    | 73+           | 56                 | 5                                | 0,6               | 0,1 |
| P2      | ABb     | 0 - 20        | 52                 | 14                               | 0,0               | 0,0 |
|         | Bwb1    | 20 - 30       | 52                 | 18                               | 0,1               | 0,0 |
|         | Bwb2    | 30 - 53       | 52                 | 14                               | 0,1               | 0,0 |
|         | Bwb3    | 53+           | 52                 | 14                               | 0,2               | 0,0 |
| P3      | ABb     | 0 - 10        | 52                 | 12                               | 0,1               | 0,0 |
|         | Bwb     | 10 - 57       | 53                 | 11                               | 0,3               | 0,0 |
|         | C       | 57+           | 50                 | 8                                | 0,1               | 0,0 |

<sup>1</sup>after Maynard (1992)

<sup>2</sup>after Arduino et al., (1984)

The CIA-K (wt%) values show weak variations with depth in each profile and between the profiles, with an average value of 51 (Table 3, Fig. 11). These values were below

the expected because they are lower than the CIA-K values for modern cryoturbated in King George Island with similar parent material (average CIA-K = 61 in Lee et al., 2004). In addition, the uppermost horizons of the profiles are less weathered than the others below, which is not a normal pedogenic behaviour (except for arid areas).

Although zeolite infillings were only found in the horizons in contact with the uppermost lava flow, it seems likely that a rejuvenation and a geochemical homogenization effect by percolation of hydrothermal fluids after the burial has occurred. Another potential geochemical rejuvenation in volcanic soils, which can disturb the weathering indices, is the upbuilding pedogenesis by an eventual addition of fresh volcanic ash (Lowe, 2000; Lowe and Tonkin, 2010; Sedov et al., 2010). Hence, the CIA-K should be used with caution in such circumstances.

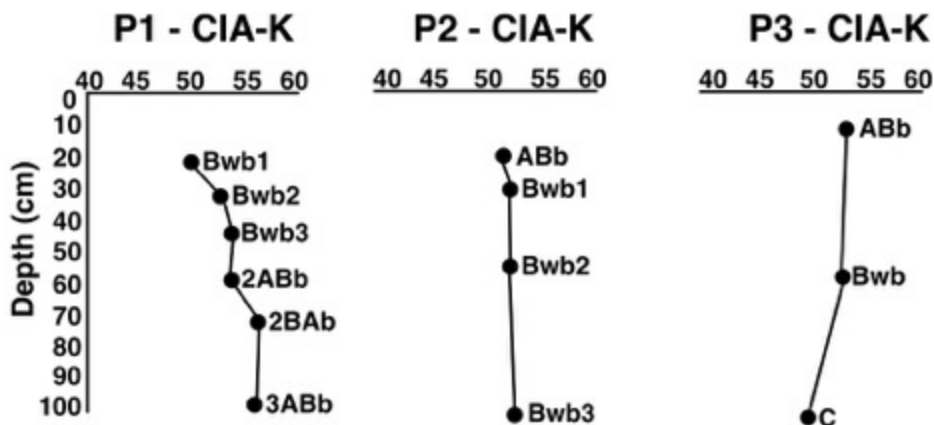


Figure 11. Depth function of the CIA-K values.

Overall, soil forming processes have occurred in all profiles, confirming the hypothesis that these red layers are paleosols. Several features related to soil formation were identified: soil horizons (defined by colour and peds), bioturbation, Fe/Mn nodules, clay neoformation, clay infilling, striated b-fabrics and plant residues. The main diagenetic features were the reddening of oxyhydroxides by dehydration, burial compaction, loss of organic matter and induration.

The paleoenvironment interpretation is in agreement with previous studies (Mozer, 2012; Poole et al., 2003) indicating a humid temperate environment, which are

supported by the abundant presence of pyroclastic material, plant residues, Fe/Mn nodules, moderate weathering, lack of carbonates and presence of some yellowish/gray horizons.

### 3.2. Origin of clay minerals in the paleosols (Manuscript 2).

The main objective of this study was to investigate the origin of smectites in the paleosols by using X-ray diffraction, microscopic and sub-microscopic techniques (SEM-EDS).

In addition to investigate the origin of smectite, the ages of the basalt flows underlying and covering the paleosols were determined in this study by  $^{40}\text{Ar}/^{39}\text{Ar}$ . A late Early Eocene age was confirmed, with ages ranging from 51 to 48 Ma.

Two profiles were studied, P1 and P2. The microscopic analysis revealed six alteration types that occur both in the soil groundmass and in the rock fragments (Table 4, Fig. 12). Three types of alteration show a topotactic reaction or alteromorphism (transformation of a primary mineral to a secondary product with shape preservation) of olivine, plagioclase (partially transformed) and glass to clays (Delvigne, 1998). The absence of olivine and glass in the XRD analysis indicate their complete transformation to secondary products (i.e. alteration of olivine to smectite and less frequently to serpentine). The other three clay types were neoformed and are characterized by a brown, grey and green infillings. Infillings and alteromorphs of olivine were the most frequent alterations types followed by alterations of glass and plagioclase.

**Table 4.** Alteration types distribution through the paleosols horizons.

| Profile | Horizon | Depth<br>(cm) | Alteration type |             |       |                |               |                |
|---------|---------|---------------|-----------------|-------------|-------|----------------|---------------|----------------|
|         |         |               | Transformation  |             |       | Neoformation   |               |                |
|         |         |               | Olivine         | Plagioclase | Glass | Brown infiling | Grey infiling | Green infiling |
| P1      | Bwb1    | 0-23          | x               | x           | x     | x              |               |                |
|         | Bwb2    | 23-34         | x               | x           | x     | x              |               |                |
|         | Bwb3    | 34-45         | x               | x           | x     | x              |               |                |
|         | 2ABb    | 45-60         | x               | x           | x     | x              |               |                |
|         | 2BAb    | 60-73         | x               | x           | x     | x              |               |                |
|         | 3ABb    | 73+           | x               | x           | x     | x              |               |                |
| P2      | ABb     | 0-20          | x               | x           | x     | x              | x             |                |
|         | Bwb1    | 20-30         | x               | x           | x     | (x)            | x             |                |

|      |       |   |   |   |     |   |   |
|------|-------|---|---|---|-----|---|---|
| Bwb2 | 30-53 | x | x | x | (x) | x |   |
| Bwb3 | 53+   | x | x | x | (x) | x | x |

Alteromorphism of primary minerals, such as the plagioclases or olivine, is often used as a proof of deuteritic alterations (Hekinian, 1982). Delvigne et al. (1979), however, demonstrated that either deuteritic alteration or weathering of olivine can produce similar products. Nonetheless, it seems that rock weathering has left the infillings and olivines alteromorphs in the soil groundmass as a residuum (Jongmans et al., 1994). The alteration of plagioclase in the present study was caused by deuteritic alteration. One proof is that the plagioclase phenocrysts within rock fragments are more weathered than the glassy groundmass. As a result of weathering and pedogenic processes the glassy groundmass should have been much more weathered than plagioclases in rock fragments.

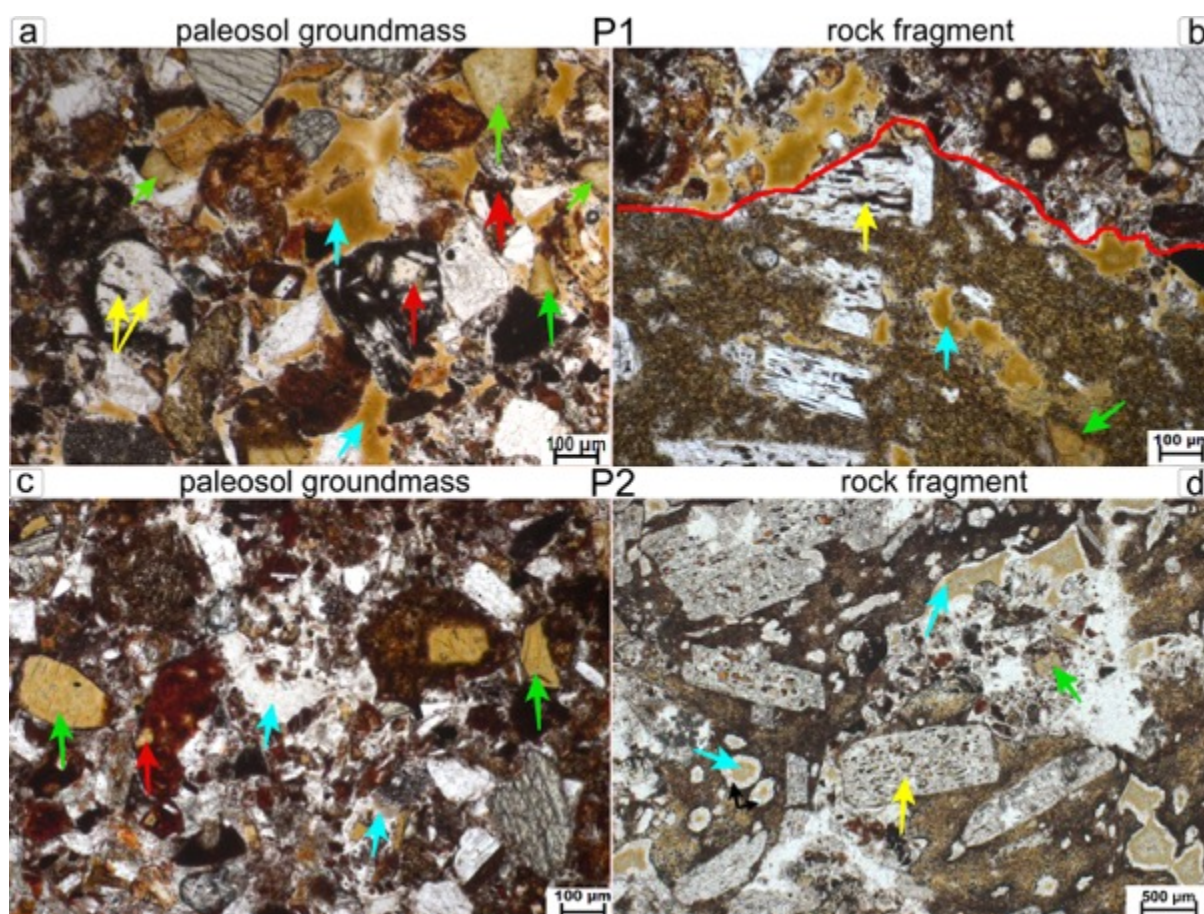


**Figure 12.** Alterations types occurring in the groundmass of paleosols and in rock fragments under Plane Polarized Light (PPL). a-) P1-Bwb2, 23-34cm: brown infillings (blue arrows); clay filling vesicles in glass shards (red arrows); brownish clays of former olivines (green arrows); yellow arrows: alterations of plagioclase b-) P1-Bwb2, 23-34cm: similar alterations occurring inside a rock fragment, the red line defines the limit between rock (below the line) and

paleosol (above the line). c-) P2-Bwb1, 20-30cm: grey infillings are almost transparent under PPL (blue arrows); clay (red arrow) filling vesicles in glass shards; brownish clays in former olivine (green arrows). d-) P2-Bwb1, 20-30cm: same alterations occurring in a rock fragment, note the brown infilling (blue arrow) surrounded by a white rim due to Fe depletion (black arrows); alteration of plagioclase (yellow arrow).

Neoformation of clays occurs generally as infillings. These are a common feature in both profiles. The centre of the infilling has a speckled b-fabric (not well-oriented clay) and the boundaries of the infilling has extinction bands (well-oriented clay). Such behaviour was also detected under SEM (Fig. 13). These infillings are predominantly brown in P1 (Fig. 12a), whereas they are mostly light-grey and nearly transparent in P2 (Fig. 12c) together with brown and green colours. These differences in colour are most probably related to paleodrainage conditions. The colour of the infillings in P1 is brown while in P2 is predominantly grey, with minor brown and green. In P2, the green infilling was only detected in the lowermost horizon (Bwb3), while a brown colour was present in rock fragments upwards in the profile. This suggests that the brown colour was the original colour that turned into green in Bwb3 horizon under more reducing conditions. In addition, the predominant grey colour in the soil groundmass of all horizons indicates Fe depletion, confirmed with EDS (Fig. 13f), suggesting slightly reductive conditions.

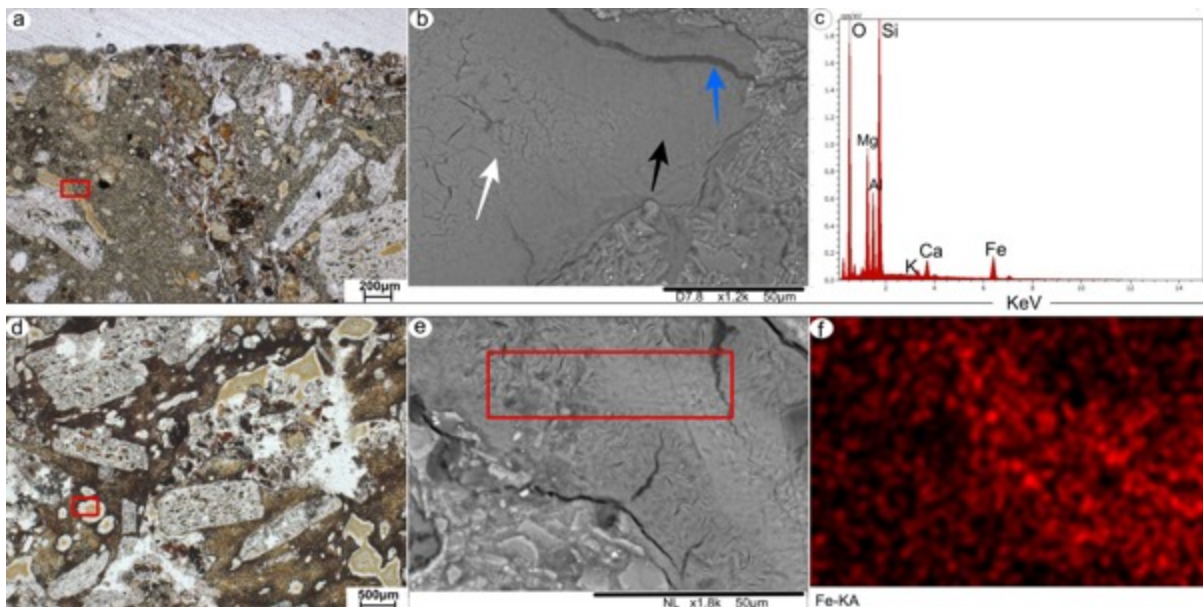


**Figure 13.** Petrographic and SEM images of selected alterations. a-) P1-Bwb3, 34-45cm: brown infilling in a rock fragment (red rectangle). b-) the same infilling analysed with SEM. Note the abundant cracks in the centre of the infilling (white arrow) with smoother boundaries (black arrow) and a large crack next to the contact with the rock (blue arrow). c-) EDS spectrum of the infilling. d-) P2-Bwb1, 20-30cm: brown infilling with a white rim in a rock fragment. e-) the same infilling analysed with SEM. Red rectangle indicate the selected area for elemental mapping f-) distribution of Fe in the infilling. Darker areas (borders) indicate a lower content, whereas brighter red colours (towards the centre of the image) indicate a higher Fe content.

The clay mineralogy of the profiles is generally homogeneous. The clays are composed of smectite having some randomly interstratified components. Smectite was confirmed by a strong  $d_{001}$  reflection at about 1.4 nm under air-dried conditions that shifted to about 1.7 nm after ethylene glycol treatment and collapsed to 1.0 nm after heating at 550°C (Fig. 14). The presence of a shoulder in the  $d_{001}$  peak in some samples indicated a presence of randomly interstratified illite-smectite (I/S), which was better detectable after decomposing the spectra using profile fitting techniques (Wojdyr, 2010) (Fig. 15).

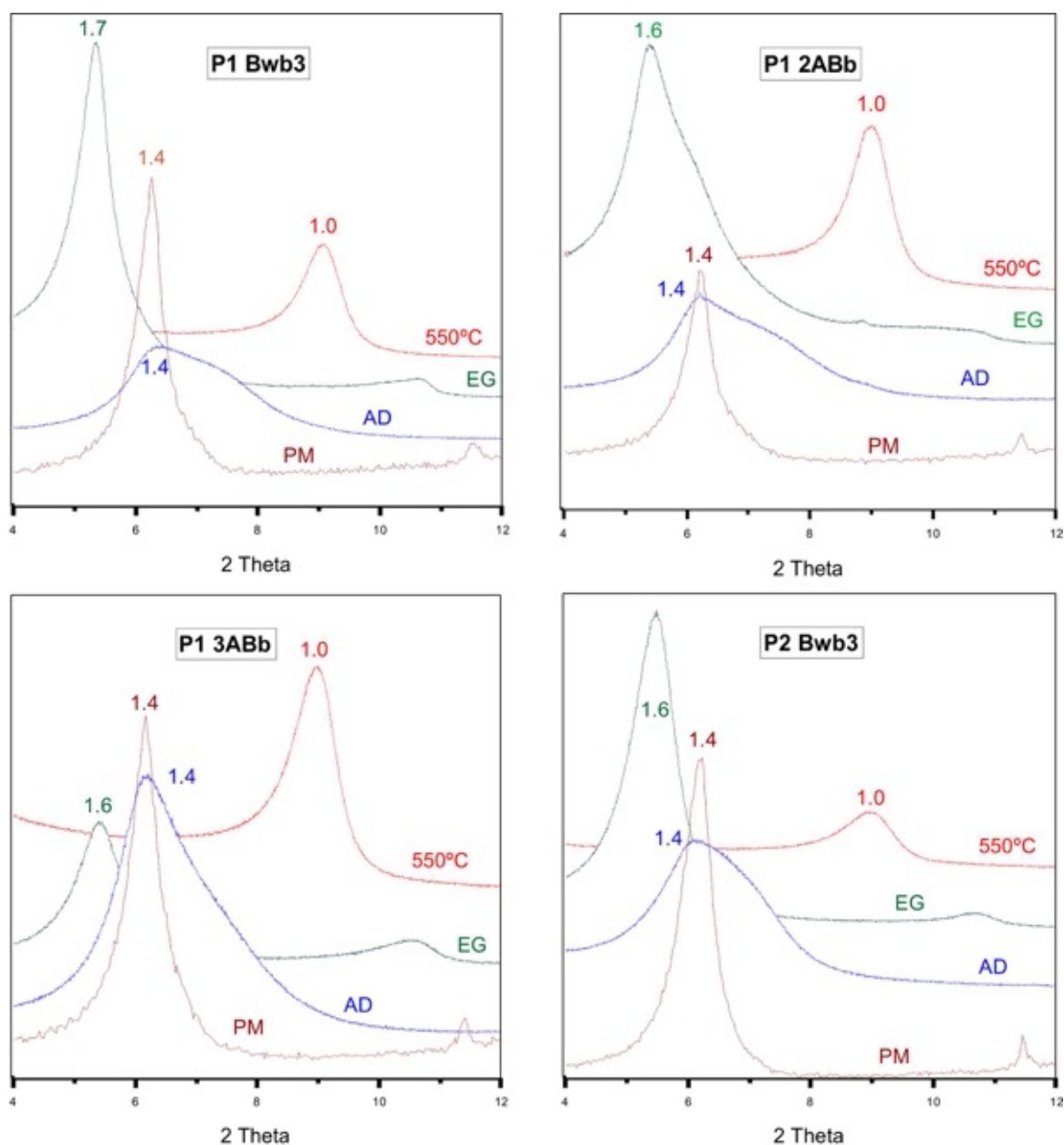


**Figure 14.** XRD patterns of clay samples from selected horizons. The d-spacing are given in nm. AD = Air dried, EG = Ethylene glycol solvation, 550OC = sample heated at 550OC, PM = parent material.

In both profiles, the smectitic component is better crystallized, having sharper peaks and a lower *Full Width at Half Maximum* (FWHM) value than the interstratified component. In the rock samples, the smectites have a higher degree of crystallinity, with sharper peaks (Fig. 14) and lower FWHM values than the smectitic component in the paleosols (Fig. 15).

The degree of crystallinity of the smectitic component is also an important difference between the paleosols and rocks samples. Pedogenic smectites tend to be less crystalline (Velde and Meunier, 2008), producing broader peaks or higher FWHM values, which corresponds to our findings. The smectites of the paleosols were less crystalline (higher FWHM) than those in rocks.

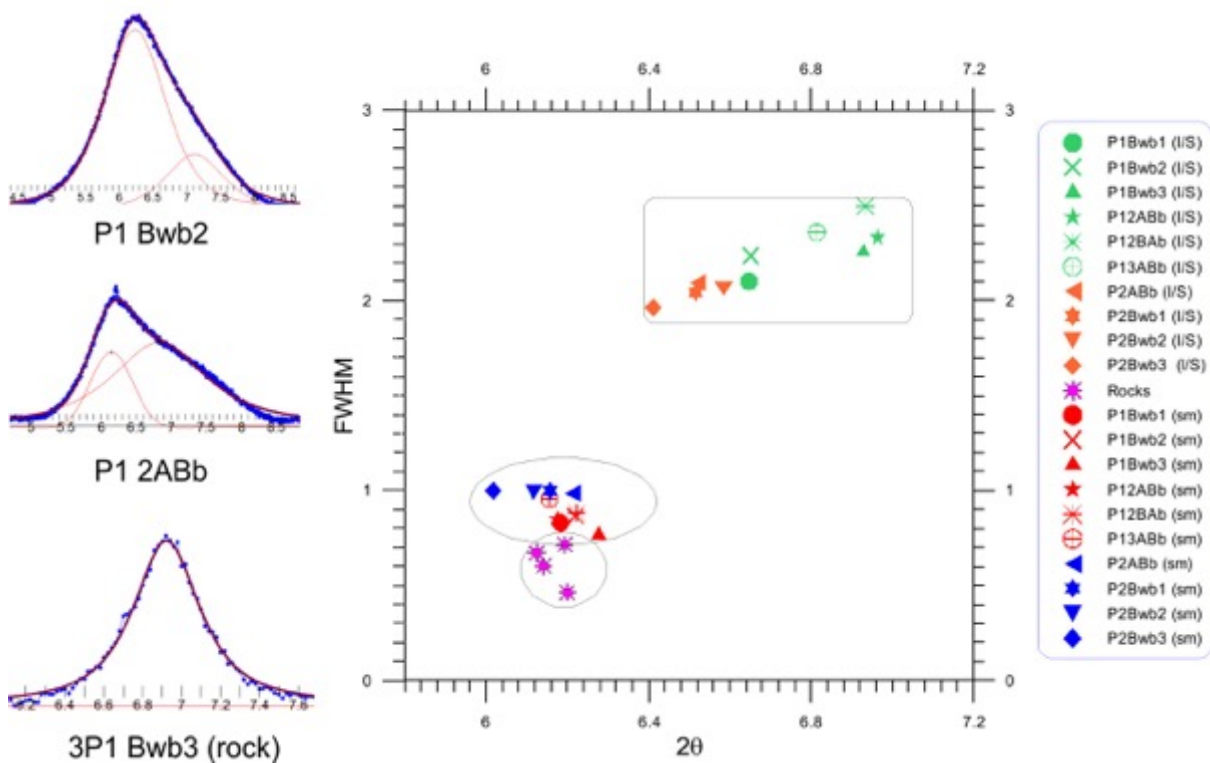


**Figure 15.** Degree of crystallinity of smectitic and interstratified components of the paleosol samples and the parent material. a-) Examples of profile fitting analysis obtained for clay samples of selected horizons; b-) Full width at half maximum (FWHM) of paleosols and rock samples. The lower the FWHM, the better the crystallinity and vice-versa. Smectitic component of P1 and P2 in red and blue, respectively. Interstratified component of P1 and P2 in green and orange, respectively. Smectite of rocks samples in pink. Each symbol represents one horizon. Note the smectitic component is more crystalline than the I/S component. Smectite from the rocks has a higher crystallinity with lower FWHM values.

There is a dominance of dioctahedral smectite over trioctahedral smectite with more than 80% of dioctahedral smectite in all horizons (Table 4). The portions of the dioctahedral and trioctahedral smectites in the rocks samples are similar, but the

dioctahedral component is still higher. These results are in accordance with the common knowledge that dioctahedral smectites are more common in soils because of its higher stability than the trioctahedral types (Borchardt, 1989; Velde and Meunier, 2008; Wilson, 1999). Even in soils formed in Siberia, with limited chemical weathering, Lessovaia et al. (2016) reported an increase in the proportion of dioctahedral smectites in relation to trioctahedral ones from bottom to top soil horizons. Nahon et al. (1982) demonstrated in a study about weathering of olivine-bearing rocks that the formation of smectites started with trioctahedral species being progressively replaced by dioctahedral smectites. Some paleosols between basalts in India also had smectites formed by deuteritic alteration followed by weathering (Craig et al., 2017). Thus, it can be inferred that trioctahedral smectites in the present study were a product of deuteritic alteration of the pyroclastic rocks and were progressively transformed to dioctahedral smectites during weathering in a soil environment.

The morphological similarity between smectites of the paleosols and its parent material suggests inheritance from a deuteritic altered parent material as the origin. Further weathering in a soil paleoenvironment produced the differences discussed above, such as differences in crystallinity, octahedral occupancy, and interstratification. Similar clay composition between parent material and soil was previously described in other volcanic areas such as in Italy (Fiore, 1993; Fiore et al., 1992; Mirabella et al., 2005), Costa Rica (Jongmans et al., 1994) and US (Dudas and Harward, 1975; Pevear et al., 1982). In all these cases, the smectites were proven to be inherited from deuteritic or hydrothermally altered parent material.

Homogeneity in clay assemblage and crystallinity in depth within each profile and between the profiles also support the inheritance origin (Mirabella et al., 2005). A clay assemblage formed by pedogenesis should be more heterogeneous, since each soil horizon gather specific chemical-physical and biological conditions (Churchman and Lowe, 2012; Singer, 1980).

### **3.3. Evidence of diagenetic reddening of the paleosols (Manuscript 3).**

In this study, the iron oxides were studied in order to understand on what extent the predominantly reddish colours of the paleosols were given by paleopedogenesis or diagenetic processes.

In general, there were a predominance of reddish hues with some variation in depth

(Table 5) from typical hematite-rich soils (2.5YR 5/4) to goethite-rich soils (5Y 4/1). Furthermore, most of the samples became yellower after mechanical grinding (L\*a\*b colours) during sample preparation because of the destruction of hematite clusters (Torrent and Schwertmann, 1987).

**Table 5.** Munsell colours taken in field and converted DR spectra in Munsell and L\*a\*b\* colours measured on powder-size samples.

| Profile   | Horizon | Depth (cm) | Munsell colour<br>(natural samples) | Munsell colour<br>(converted from DRS measurements) | L*a*b* |      |      |
|-----------|---------|------------|-------------------------------------|---|--------|------|------|
|           |         |            |                                     |   | L*     | a*   | b*   |
| <b>P1</b> | Bwb1    | 0 – 23     | 5YR 5/4                             | 7.5YR 6/3   | 64.3   | 7.4  | 20   |
|           | Bwb2    | 23 – 34    | 2.5YR 5/4                           | 5YR 6/3   | 64.4   | 10   | 20.2 |
|           | Bwb3    | 34 – 45    | 2.5YR 5/4                           | 5YR 6/4   | 63     | 11.1 | 20.9 |
|           | 2ABb    | 45 – 60    | 7.5YR 7/4                           | 7.5YR 7/4   | 66.9   | 6.6  | 21.8 |
|           | 2BAb    | 60 – 73    | 10YR 6/4                            | 7.5YR 7/4   | 68     | 6.3  | 22.8 |
|           | 3ABb    | 73+        | 5Y 4/1                              | 0.6Y 6/3  | 63.1   | 2.6  | 17.2 |
| <b>P2</b> | ABb     | 0 – 20     | 2.5YR 5/4                           | 5YR 6/4   | 59.7   | 11.6 | 20.5 |
|           | Bwb1    | 20 – 30    | 2.5YR 2/4                           | 5YR 6/4   | 58.8   | 11.5 | 20   |
|           | Bwb2    | 30 – 53    | 2.5YR 5/4                           | 5YR 6/4   | 60.4   | 13.5 | 21.3 |
|           | Bwb3    | 53+        | 2.5YR 5/4                           | 5YR 6/4   | 59.6   | 11   | 18.5 |
| <b>P3</b> | ABb     | 0 – 10     | 2.5YR 5/4                           | 5YR 6/4   | 62.1   | 12.2 | 23.1 |
|           | Bwb1    | 10 – 57    | 2.5YR 5/4                           | 5YR 6/4   | 63     | 11.1 | 22.7 |
|           | C       | 57+        | 7.5YR 5/3                           | 10YR 6/4  | 66.6   | 5    | 20.5 |

The main mode of occurrence of iron oxides observed in thin sections was finely dispersed on the groundmass due to the weathering of the basaltic tephra, coating/replacing primary minerals and as mottles or nodules (Figure 16). The micromorphological observations agree with those made in the field. The micromass colours are homogeneously reddish under OIL, with few gradual changes in depth. The concentrations of iron in mottles and/or small nodules were commonly occurring features. The higher the concentration of iron, either in nodules (Fig. 16c-d-e) or mottles (Fig. 16e-f), the darker were these features under PPL and reddish under OIL.

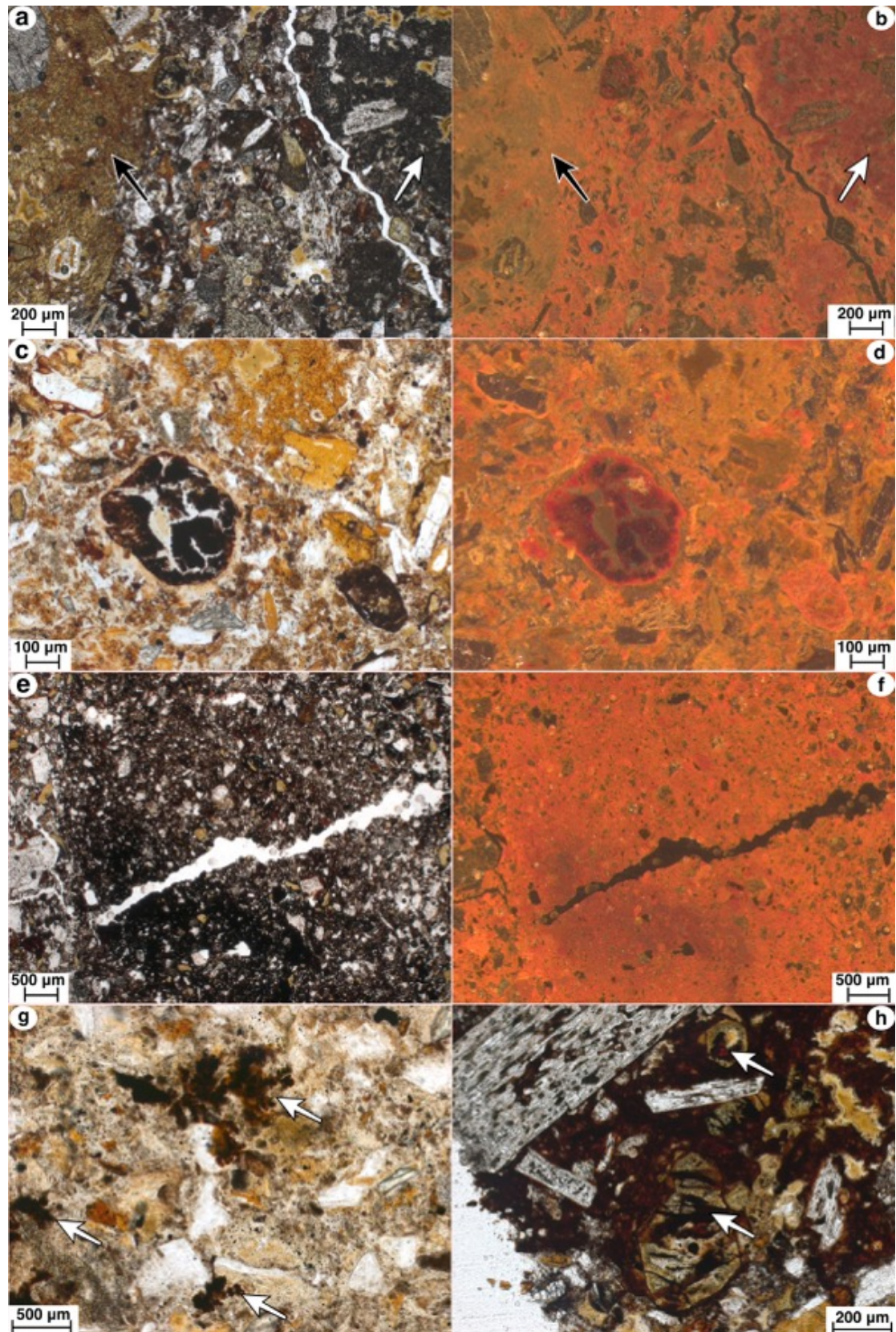


**Figure 16.** Types of iron oxide distribution in the paleosols. Photographs on the left side were taken under Plane Polarizer Light (PPL) and under Oblique Incident Light (OIL) on the right side. a-) P1-Bwb3, 34-45 cm: two different colours of rock fragments reflecting different levels of oxidation. An orange and less oxidized fragment (black arrow) and a darker, more oxidized fragment (white arrow); b-) Same under OIL. Note the strong reddish colours replacing the darker rock fragment (white arrow); c-) P1-2BAb, 60-73 cm: typical disorthic disjoined iron nodule; d-) Same under OIL. Note the strong contrast between the iron concentration in the nodule in comparison with the

surrounding groundmass; e-) P2-Bwb1, 20-30 cm: Different degrees of groundmass impregnation by iron, from strongly impregnated to moderated impregnated. Darker is the impregnation, higher is the iron concentration; f-) Same under OIL. The strongly impregnated area showed darker red colours; g-) P1-3ABb, 73+ cm: dendritic iron nodules (white arrows) in a paler groundmass; h-) P2-Bwb2, 23-34 cm: olivine phenocryst being replaced by an admixture of smectite (brownish colour) and iron oxide (white arrows), photograph taken under PPL.

Figure 17 shows the spectra of the second derivative of the Kubelka–Munk function measured at 25°C and at 800°C for the redder and the less red horizon of each profile. The reason for the heating was to help to discriminate between the most intense absorption band of goethite at ~415 nm and a less intense absorption band of hematite at ~423 nm. The most intense band of hematite occurs at ~535 nm (Scheinost et al., 1998). The absence of goethite was confirmed after heating at 800°C because the permanence of the band at ~425 nm, which can be associated to hematite rather than goethite (~415 nm) (Scheinost et al., 1998). Furthermore, because goethite is unstable upon heating, such band should have disappeared much before 800°C. Some experimental studies have demonstrated that goethite should dehydrate to hematite at about 300°C (Gialanella et al., 2010; Gualtieri and Venturelli, 1999). In Chinese red beds a conversion of goethite to hematite was identified at diagenetic temperatures >150°C (Jiang et al., 2015) and >105°C for Triassic sandstones in Denmark (Weibel, 1999). In reddish pre-Quaternary paleosols, goethite was detected in those not affected by deep-burial or high diagenetic temperatures (Dawit, 2016; Kraus and Hasiotis, 2006; Srivastava et al., 2015; Vacca et al., 2012). Another evidence is the presence of plant residues with preservation of the distinct plant cell structure (Spinola et al., 2017b). Therefore, the conversion of goethite into hematite in buried paleosols or sediments needs a heating source produced by deep-burial.

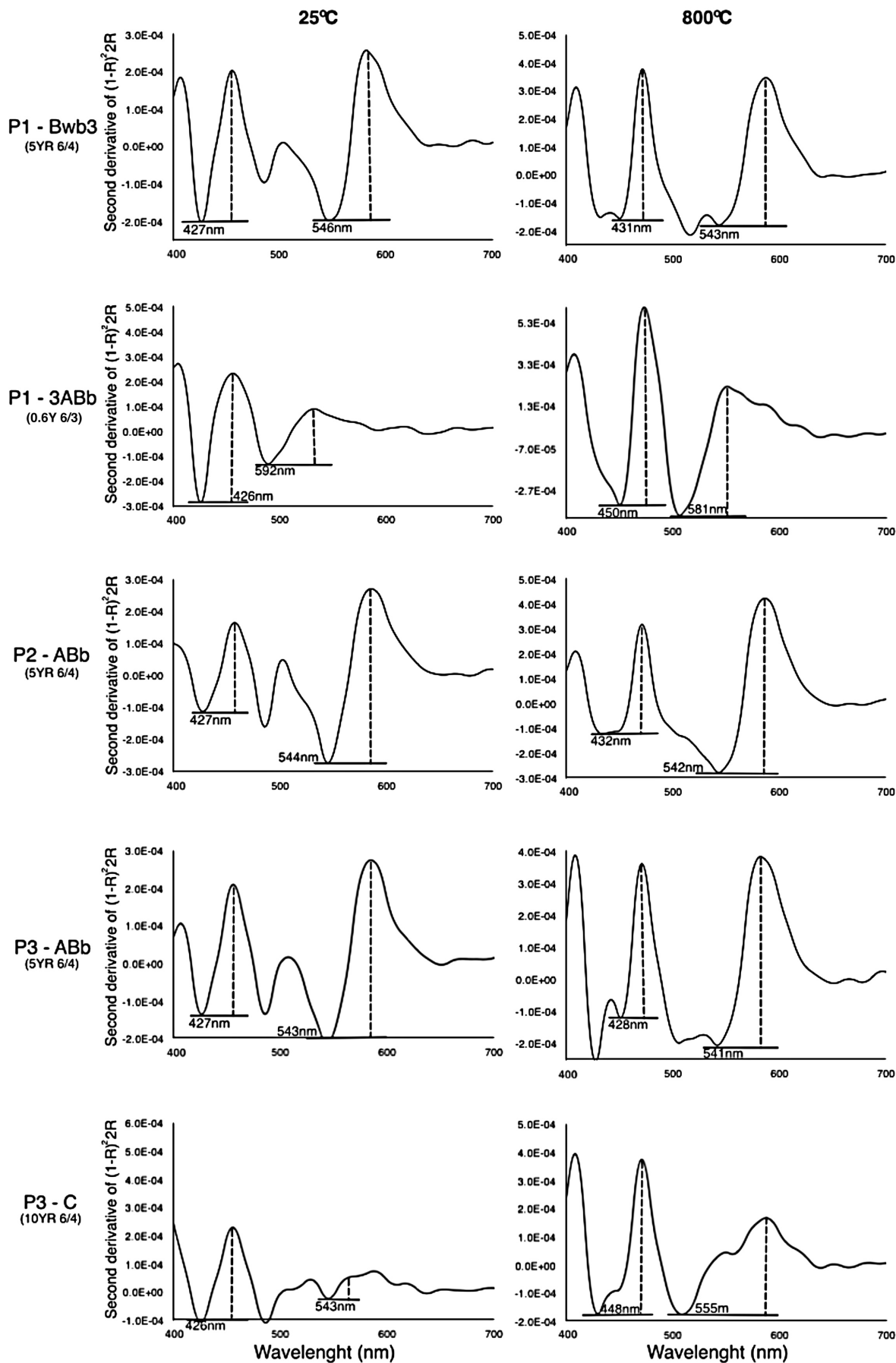


**Figure 17.** The second-derivative curves of K–M function for selected samples. Position (straight line) and amplitude (dashed line) of hematite bands. Measurements taken in air-dried samples at the left side and after heating at 800°C at the right side.

The absence of goethite is supported by the XRD because its most intense peak (110) at 4.18 nm ( $21.2^\circ 2\theta$ ) was not identified in any of the samples. On the other hand, the hematite presented a large crystallite size (between 37 nm and 62 nm). The mean crystallite dimension (MCD) was calculated with the Full Width at Half Maximum (FWHM) values using the Scherrer formula (Table 6). Another evidence of the higher crystallinity of the hematite was the remaining peak (104) at 2.69 nm measured in the DRXD spectra (Fig. 18). Even though its intensity was reduced, the residue of this peak indicated that the Dithionite-Citrate-Bicarbonate (DCB) treatment did not extract all the hematite. No correlation was found between the crystallite size and the  $L^*a^*b^*$  parameters.

**Table 6.** Hematite properties calculated from XRD. Full width at half maximum (FWHM) and crystallite size.

| Profile   | Horizon | Depth (cm) | FWHM (104) | Crystallite size (nm) |
|-----------|---------|------------|------------|-----------------------|
| <b>P1</b> | Bwb1    | 0 – 23     | 0.16       | 58                    |
|           | Bwb2    | 23 – 34    | 0.18       | 50                    |
|           | Bwb3    | 34 – 45    | 0.21       | 41                    |
|           | 2ABb    | 45 – 60    | 0.19       | 47                    |
|           | 2BAb    | 60 – 73    | 0.15       | 62                    |
|           | 3ABb    | 73+        | ND         | ND                    |
| <b>P2</b> | ABb     | 0 – 20     | 0.18       | 50                    |
|           | Bwb1    | 20 – 30    | 0.17       | 53                    |
|           | Bwb2    | 30 – 53    | 0.16       | 58                    |
|           | Bwb3    | 53+        | 0.15       | 62                    |
| <b>P3</b> | ABb     | 0 – 10     | 0.18       | 50                    |
|           | Bwb1    | 10 – 57    | 0.16       | 58                    |
|           | C       | 57+        | 0.23       | 37                    |

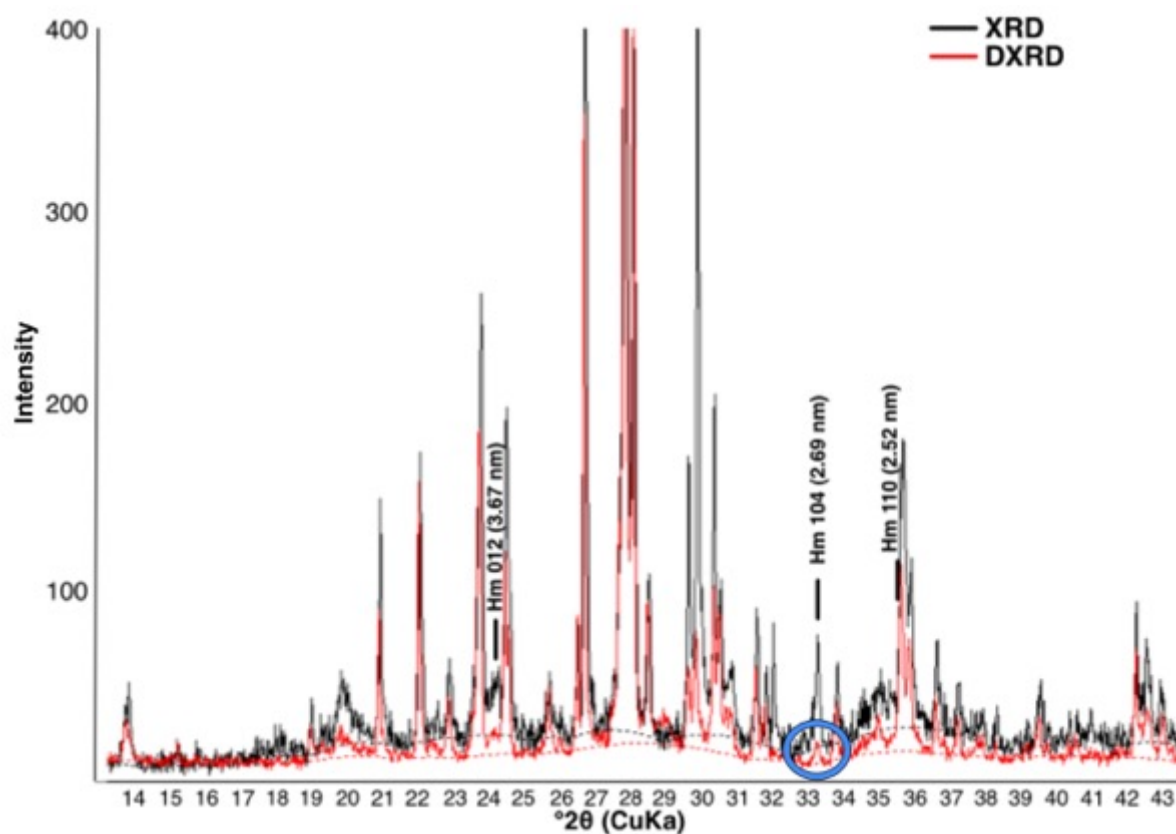


**Figure 18.** X-ray patterns of a representative sample. P1-Bwb1, 0-23 cm. XRD pattern (black) plotted against DCB treated sample (DXRD) (yellow). Note a small remnant peak of hematite peak 104 (blue circle), indicating an incomplete removal of hematite by DCB. Hm = Hematite.

The previous results indicated that the paleosols colours were mostly due to hematite, even in the paleosol horizons with yellower hues. Nevertheless, the higher values of Fe extracted by  $H_2SO_4$  ( $Fe_s$ ) indicated that maghemite was the dominant iron oxide followed by hematite ( $Fe_d$ ) in all samples (Table 7).

**Table 7.** Selective and sequential extraction of iron oxides.

| Profile   | Horizon | Depth<br>(cm) | Fe <sub>s</sub> <sup>1</sup><br>(g/kg <sup>-1</sup> ) | Fe <sub>o</sub> <sup>2</sup><br>(g/kg <sup>-1</sup> ) | Fe <sub>d</sub> <sup>3</sup><br>(g/kg <sup>-1</sup> ) | Fe <sub>t</sub> <sup>4</sup><br>(g/kg <sup>-1</sup> ) | Fe <sub>d</sub> /Fe <sub>t</sub> *100 <sup>5</sup> |
|-----------|---------|---------------|---|---|---|---|--|
| <b>P1</b> | Bwb1    | 0 – 23        | 31  | 1.5   | 15.7  | 80.5  | 19.5   |
|           | Bwb2    | 23 – 34       | 26.7  | 0.9   | 13.5  | 79.3  | 17   |
|           | Bwb3    | 34 – 45       | 29.9  | 1   | 13.3  | 88.7  | 15   |
|           | 2ABb    | 45 – 60       | 32.4  | 0.9   | 10.5  | 79.8  | 13.2   |
|           | 2BAb    | 60 – 73       | 34  | 1   | 12.1  | 83.8  | 14.4   |
|           | 3ABb    | 73+           | 33.9  | 1.7   | 7   | 89.6  | 7.8  |
| <b>P2</b> | ABb     | 0 – 20        | 27.9  | 1   | 21.9  | 107.3   | 20.4   |
|           | Bwb1    | 20 – 30       | 25.1  | 0.8   | 21.7  | 88.3  | 24.6   |
|           | Bwb2    | 30 – 53       | 21.4  | 1.7   | 20.1  | 88.9  | 22.6   |
|           | Bwb3    | 53+           | 22.1  | 1.1   | 18.7  | 83.6  | 22.4   |
| <b>P3</b> | ABb     | 0 – 10        | 28.2  | 1.7   | 14.8  | 84.8  | 17.5   |
|           | Bwb1    | 10 – 57       | 23.9  | 1.5   | 14.7  | 80.7  | 18.2   |
|           | C       | 57+           | 24  | 2.1   | 9.6   | 80.7  | 11.9   |

<sup>1</sup>H<sub>2</sub>SO<sub>4</sub> extraction; <sup>2</sup>Ammonium oxalate extraction; <sup>3</sup>DCB extraction; <sup>4</sup>XRF analysis; <sup>5</sup>Proportion of hematite in relation to total iron (Fe<sub>t</sub>).

The high amounts of maghemite is also expressed by the magnetic susceptibility of the samples (Fig. 19). As a rule, the  $\chi_{fd}$ % of all samples (except P3-3ABb) were higher than 8%. This indicates the predominance of the superparamagnetic (SP) fraction (e.g. maghemite). Furthermore, the relationship between  $\chi_{lf}$  and  $\chi_{fd}$  was high ( $r^2 = 0.83$ ), reinforcing the predominance of the SP minerals over coarse-grained non-SP ferrimagnets (i.e. magnetite).

Although no colour differences were detected in the uppermost horizons of P1 and P2, neoformation and enrichment of ferrimagnetic compounds thermal transformation of other iron oxy-hydroxides at temperatures >250°C in combination with organic matter and lower O<sub>2</sub> supply (Maher, 1986). An enhancement of low-frequency ( $\chi_{lf}$ ) magnetic susceptibility was detected in P1 from 0 to 23 cm (Bwb1 horizon) and in P2 from 0-30 cm. Nevertheless, the frequency-dependent susceptibility,  $\chi_{fd}$  and  $\chi_{fd}$ %, were similar for all horizons. In soils formed in non-mafic parent material (e.g. loess, mudstone), enhancement of  $\chi_{lf}$  occurs simultaneously with  $\chi_{fd}$  and  $\chi_{fd}$ % caused by the neoformation of nano-sized magnetite and/or maghemite (Dearing et al., 1996; Torrent et al., 2006). On the other hand, soils formed from volcanic parent material show an opposite behavior: they have high initial  $\chi_{lf}$  values because of inherited magnetite and lower  $\chi_{fd}$  and  $\chi_{fd}$ %. With the progressive weathering of magnetite and other Fe-bearing minerals, the  $\chi_{lf}$  values decrease and  $\chi_{fd}$  and  $\chi_{fd}$ % increase due to

neof ormation of maghemite (Lu et al., 2008; Preetz et al., 2017; Rivas et al., 2006). Thus, enhanced  $\chi_{lf}$  values with homogeneous  $\chi_{fd}$  and  $\chi_{fd}\%$  in the uppermost horizons of P1 and P2 indicate enrichment in magnetite.

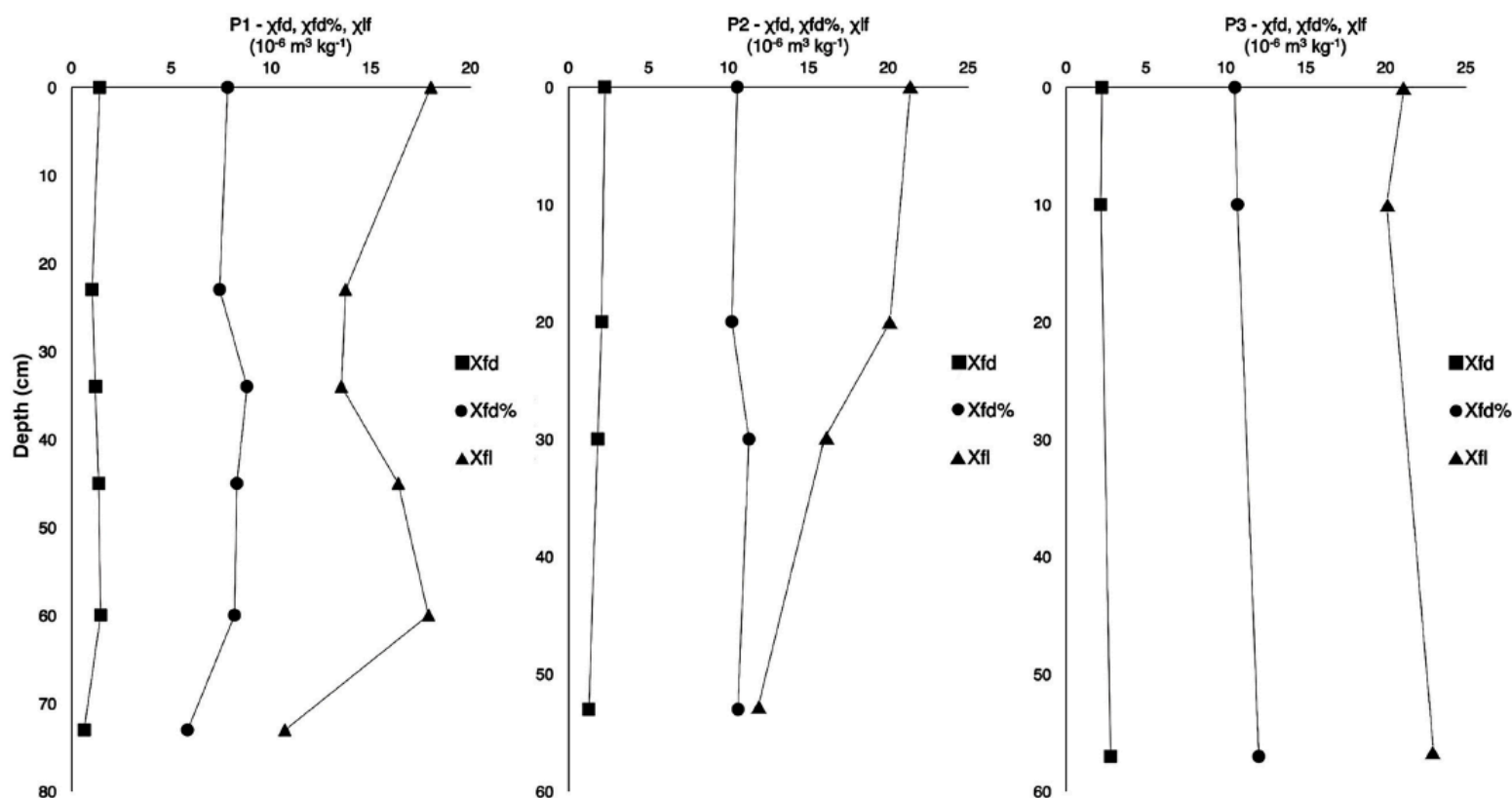


**Figure 19.** Depth function of mineral magnetic susceptibility parameters.

The predominance of maghemite, hematite, and the strong red colours of KGI paleosols is not compatible with their weak to moderate pedogenic development. Therefore, it is unlikely that a predominance of hematite would have been achieved during past pedogenic processes (Retallack, 1991). Weakly to moderately developed volcanic soils are usually brownish/yellowish with ferrihydrite as the main iron hydroxide (Shoji et al., 1993; Ugolini and Dahlgren, 2002). The formation of ferrihydrite in soils depends upon a combination of factors, such as a high rate of  $\text{Fe}^{\text{II}}$  release, presence of silicate, and organic matter. Some of these conditions count for the investigated soils, such as considerably high amounts of  $\text{Fe}_d$ , and widespread iron pigmentation found in thin sections. Although organic matter was not detected because of the burial oxidation (Retallack, 1991), there are still plant residues in the “A” horizons (Spinola et al., 2017b). Nonetheless, ferrihydrite would hardly be preserved in Eocene paleosols because of its metastable nature (Cornell and Schwertmann, 2003).

Both hematite and goethite are common stable end-products of ferrihydrite. Their relative portions are controlled by specific soil chemical conditions: the transformation of ferrihydrite to hematite involves a dehydration step, whereas transformation to goethite involves dissolution and recrystallization. Furthermore, a pH around 7 – 8 will favor hematite (Schwertmann et al., 1999). Although it is not possible to access the pH of the paleosol after burial, some characteristics of these paleosols are indicative of basic pH, such as base-rich parent material (basaltic tephra) and presence of smectite (Spinola et al., 2017a). Hence, we assume that goethite was probably never formed in these paleosols and ferrihydrite was the main iron hydroxide, which later converted to hematite by dehydration after the burial.

#### 4. Summary and outlook

The major objective of this thesis was to reconstruct the paleoenvironment of King George Island, Maritime Antarctica, using paleosols as a proxy. To achieve this objective, the genesis of these paleosols was investigated.

In the first manuscript, the objective was to identify the main pedogenic properties and features of the paleosols. The reasoning is because paleosols between basalt flows are relatively similar to other geological features, such as sediments, zones of thermal contact (bakes zones), or altered pyroclasts. Therefore, a proper characterization of these paleosols was essential to provide reliable paleoenvironmental information.

A combination of field and micromorphological allowed to identify the main pedogenic features of the paleosols. In field, the most important was the variation of colour and structure in depth, which characterize a paleosol horizon. The colours were predominantly reddish but also yellowish and greyish. The structure were mainly angular and subangular blocky.

In the thin sections, the field observations were also present; change in colour and structure horizonwise. Furthermore, some features observed in the thin sections were crucial as a pedogenic fingerprint: pedogenic Fe mottles/nodules, bioturbation features (e.g. channels, passage features, disturbed voids) and *in situ* mineral weathering.

The geochemistry has demonstrated a weak degree of basic cations depletion. However, an additional input of volcanic ash could have played a role on the geochemical rejuvenation. Another important non-pedogenic reason for the geochemical rejuvenation could be the zeolite infillings. Well-formed zeolite crystals were detected in thin sections filling former voids of the horizons in contact with the covering lava flow. Although zeolites were not detected in deeper horizons, its contribution with addition of basic cations could have been possible.

In addition to zeolite crystals, other features occurred probably after the burial (*viz.* diagenetic) such as induration due to compaction, lack of organic matter due to post-burial oxidation and rubification due to dehydration of iron hydroxides to hematite.

An important property of these paleosols were the predominance of smectite in the clay mineralogy. Volcanic soils rich in smectite is more commonly found in semi-arid regions, where there is a marked dry-season, which would contradict the previous

findings of a humid paleoenvironment. For this reason, the origin of the smectites was investigated.

Minor mineralogical changes between the pyroclastic fragments (parent material) and the paleosols and a homogenous distribution of smectites throughout the paleosol horizons were detected by X-ray diffraction and microscopic techniques. These results indicated the smectites were inherited from the parent material, which was altered by hydrothermal fluids before surficial weathering. Nevertheless, the smectites in the paleosols were predominantly dioctahedral and less crystalline in comparison with predominantly trioctahedral and more crystalline in the parent material. These changes in octahedral site occupancy and crystallinity indicates that the smectites were affected by surficial weathering and pedogenesis.

The other important paleosol property was the reddish colour. The strong reddish colours (2.5YR) with variations in depth to yellowish (10YR) and greyish (5Y) were described in the first manuscript as a consequence of pedogenesis and diagenesis. The diagenetic and pedogenic role were detected using micromorphology, Diffuse Reflectance Spectroscopy, X-ray diffraction and mineral magnetic properties. The diagenetic role was confirmed because the dominance of maghemite and hematite as the iron oxides, without goethite. Such iron oxide assemblage is more common in well-developed soils from subtropical-tropical regions rather than in weakly/moderated developed volcanic soils under humid conditions. The ferrihydrite is the main iron oxides under such environmental conditions but it is not sufficiently stable to persist in long-term buried paleosol. Another clue to diagenesis was the large grain size and high crystallinity of hematite that was more similar to diagenetic, like those found in red beds, than to pedogenic hematite.

The pedogenic role was indicated by the content of hematite and the mode of occurrence observed in the thin sections: finely dispersed on the groundmass; coating/replacing primary minerals and as mottles and/or nodules. In addition, hematite clusters were another important property for colours differences. Therefore, these results indicate that the burial reddening took place by dehydration and transformation of ferrihydrite to hematite.

The effect of the covering lava flow was suggested by the enrichment of magnetite in the uppermost horizons of two profiles. Magnetite formation demands the contact of

precursors iron oxy-hydroxides with heating (250°C – 400°C) in combination with organic matter and low O<sub>2</sub> supply, which was the probable conditions during the burial. Nevertheless, the heating had no effect on colours.

The findings of this thesis highlight the importance of combination of methods to understand paleosol genesis. As could be demonstrated, some important paleoenvironmental fingerprints like clay mineralogy, including iron oxides, can be the result of several processes others than pedogenesis. This could lead to misinterpretations of paleoenvironment. A proper study of paleosols should consider pre-weathering (alteration) and post-burial (diagenesis) features. Therefore, a combination of different methods was successfully adopted to understand the genesis of the King George Island paleosols.

The results exposed in the three manuscripts indicated the paleosols of King George Island were weakly/moderated developed formed under a cool humid paleoenvironment. The main pedogenic signatures were the soil horizons, bioturbation, mineral *in situ* weathering, plant fossils. Pre-weathering and diagenesis had disturbed in some extent all pedogenic features as demonstrated by compaction, loss of organic matter, zeolite infillings, clay inheritance and dehydration of iron hydroxides. Despite this, the main objective was achieved.

The further steps for this research will be concentrated on those features that can provide more quantitative results: 1) the isotopic composition of the smectites ( $\delta D$  and  $\delta^{18}O$ ); 2) detailed geochemistry of trace elements and their respective weathering indices; 3) analysis of *n*-alkanes biomarkers, particularly in those horizons with plant residues; 4) paleobotanical analysis of the plant residues and phytoliths.

## 5. References

- Arduino, E., Barberis, E., Carraro, F., Forno, M.G., 1984. Estimating relative ages from Iron-oxide/Total-Iron ratio of soils in the Western Po Valley, Italy. *Geoderma* 33, 39–52.
- Askin, R.A., 1991. Late Cretaceous-Early Tertiary Antarctic outcrop evidence for past vegetation and climates, in: Kennett, J.P., Warnke, D.. (Eds.), *The Antarctic Paleoenvironment: A Perspective on Global Change*. Antarctic Research Series. American Geophysical Union, Washington D.C, pp. 61–73.
- Barrett, P., 2008. A History of Antarctic Cenozoic Glaciation - View from the Margin. *Dev. Earth Environ. Sci.* 8, 33–83. doi:10.1016/S1571-9197(08)00003-7
- Birkenmajer, K., 1988. Tertiary glacial and interglacial deposits, South Shetland Islands, Antarctica: geochronology versus biostratigraphy. *Bull. Polish Acad. Sci. Earth Sci.* 36, 133–145.
- Birkenmajer, K., 1980. Tertiary volcanic-sedimentary succession at Admiralty Bay, King George Island (South Shetland Islands, Antarctica). *Stud. Geol. Pol.* 64, 7–65.
- Birkenmajer, K., Gaździcki, A., Krajewski, K.P., Przybycin, A., Solecki, A., Tatur, A., Yoon, H.I., 2005. First Cenozoic glaciers in West Antarctica. *Polish Polar Res.* 26, 3–12.
- Birkenmajer, K., Łydka, K., 1990. Mineralogical evidence for warm Palaeogene climate from the Ezcurra Inlet Group, King George Island, West Antarctica. *Bull. Polish Acad. Sci. Earth Sci.* 38, 25–38.
- Birkenmajer, K., Zastawniak, E., 1989. Late Cretaceous-early Tertiary floras of King George Island, West Antarctica: their stratigraphic distribution and palaeoclimatic significance. *Geol. Soc. London, Spec. Publ.* 47, 227–240. doi:10.1144/GSL.SP.1989.047.01.17
- Blodgett, R., Crabaugh, J., McBride, E.F., 1993. The colour of red beds: a geologic perspective, in: Bigham, J.H., Ciolkosz, E.. (Eds.), *Soil Colour*. Soil Science Society of America Special Publication, pp. 127–159.
- Borchardt, G., 1989. Smectites, in: Dixon, J., Weed, S.. (Eds.), *Minerals in Soil Environments*. Soil Science Society of America, Madison, Wisconsin, pp. 675–727.
- Buurman, P., 1975. Possibilities of paleopedology. *Sedimentology* 22, 289–298.

- Canile, F.M., 2010. Evidências geológicas de mudanças climáticas (greenhouse-icehouse) na Antártica Ocidental durante a passagem Eoceno-Oligoceno. Universidade Federal de São Paulo.
- Churchman, G.J., Lowe, D., 2012. Alteration, formation, and occurrence of minerals in soils. *Handb. Soil Sci. Prop. Process.* 1, 20–72. doi:10.1201/b11267-24
- Commission Internationale de L'Eclairage, 1978. Recommendations on uniform colour spaces colour difference equations psychometric colour terms, Supplement 2. CIE Publ. 15 (E-1.3.1) 1971/(TC-1.3). Bur. Centrale de la CIE. Paris. Paris.
- Cornell, R.M., Schwertmann, U., 2003. *The Iron Oxides - Structure, properties, reactions, occurrences and uses*, 2nd ed. Wiley-VCH Verlag, Weinheim.
- Coxall, H.K., Wilson, P.A., Pälike, H., Lear, C.H., Backman, J., 2005. Rapid stepwise onset of Antarctic glaciation and deeper calcite compensation in the Pacific Ocean. *Nature* 433, 53–57. doi:10.1038/nature03135
- Craig, P., Chevrier, V., Sayyed, M.R.G., Islam, R., 2017. Spectral analysis of Deccan intrabasaltic bole beds: Implications for the formation and alteration of phyllosilicates on Mars. *Planet. Space Sci.* 135, 55–63. doi:10.1016/j.pss.2016.11.008
- Dawit, E.L., 2016. Paleoclimatic records of Late Triassic paleosols from Central Ethiopia. *Palaeogeogr. Palaeoclimatol. Palaeoecol.* 449, 127–140. doi:10.1016/j.palaeo.2016.02.011
- Dearing, J.A., 1999. Environmental Magnetic Susceptibility Using the Bartington MS2 System. *Interpret. A J. Bible Theol.* 52.
- Dearing, J.A., Hay, K.L., Baban, S.M.J., Huddleston, A.S., Wellington, E.M.H., Loveland, P.J., 1996. Magnetic susceptibility of soil: An evaluation of conflicting theories using a national data set. *Geophys. J. Int.* 127, 728–734. doi:10.1111/j.1365-246X.1996.tb04051.x
- DeConto, R.M., Pollard, D., 2003. Rapid Cenozoic glaciation of Antarctica induced by declining atmospheric CO<sub>2</sub>. *Nature* 421, 245–249. doi:10.1038/nature01290
- Delvigne, J., 1998. *Atlas of Micromorphology of Mineral Alteration and Weathering*, ORSTOM. ed. Mineralogical Association of Canada, Ottawa.
- Delvigne, J., Bisdorf, E.B., Sleeman, J., Stoops, G., 1979. Olivines, their pseudomorphs and secondary products. *Pedologie* 3, 247–309.
- DIN ISO 10693, 1995. Bodenbeschaffenheit Bestimmung des Carbonatgehaltes e

- Volumetrisches Verfahren. Beuth, Berlin.
- DIN ISO 10694, 1995. Bodenbeschaffenheit Bestimmung von organischem Kohlenstoff und Gesamtkohlenstoff nach trockener Verbrennung (Elementaranalyse). Beuth, Berlin.
- Dingle, R.V., Lavelle, M., 2000. Antarctic Peninsula Late Cretaceous-Early Cenozoic paleoenvironments and Gondwana paleogeographies. *J. African Earth Sci.* 31, 91–105. doi:10.1016/S0899-5362(00)00075-0
- Dingle, R. V., Lavelle, M., 1998. Antarctic Peninsular cryosphere: Early Oligocene (c. 30 Ma) initiation and a revised glacial chronology. *J. Geol. Soc. London.* 155, 433–437. doi:10.1144/gsjgs.155.3.0433
- Dudas, M.J., Harward, M.E., 1975. Inherited and detrital 2:1 type phyllosilicates in soils developed from Mazama ash. *Soil Sci. Soc. Am. J.* 39, 571–577. doi:10.2136/sssaj1975.03615995003900030050x
- Ehrmann, W.U., Melles, M., Kuhn, G., Grobe, H., 1992. Significance of clay mineral assemblages in the Antarctic Ocean. *Mar. Geol.* 107, 249–273. doi:10.1016/0025-3227(92)90075-S
- Elliot, D.H., Askin, R.A., Kyte, F.T., Zinsmeister, W.J., 1994. Iridium and dinocysts at the Cretaceous-Tertiary boundary on Seymour Island, Antarctica: implications for the K-T event. *Geology* 22, 675–678. doi:10.1130/0091-7613
- FAO, 2006. Guidelines for soil description, 4th ed. Rome.
- Feldmann, R., Woodburne, M., 1988. Geology and paleontology of Seymour Island, Antarctic Peninsula. Geological Society of America, Memoir 169.
- Fenwick, I., M., 1985. Paleosols: problems of recognition and interpretation, in: Boardman, J. (Ed.), *Soils and Quaternary Landscape Evolution*. John Wiley and Sons, Norwich, p. 391.
- Fiore, S., 1993. The occurrences of smectite and illite in a pyroclastic deposit prior to weathering: implications on the genesis of 2:1 clay minerals in volcanic soils. *Appl. Clay Sci.* 8, 249–259. doi:10.1016/0169-1317(93)90007-N
- Fiore, S., Huertas, F., Linares, J., 1992. Mineralogy and geochemistry of some “so-called” paleosols from Mt. Vulture volcano (southern Italy). *Chem. Geol.* 99, 237–252. doi:10.1016/0009-2541(92)90179-9
- Fleck, R., Sutter, J., Elliot, D., 1977. Interpretation of discordant  $^{40}\text{Ar}/^{39}\text{Ar}$  age-spectra of Mesozoic tholeiites from Antarctica. *Geochim. Cosmochim. Acta* 41, 15–32.

- Francis, J., Poole, I., 2002. Cretaceous and early Tertiary climates of Antarctica: evidence from fossil wood. *Palaeogeogr. Palaeoclimatol. Palaeoecol.* 182, 47–64.
- Francis, J.E., Ashworth, A., Cantrill, D.J., Crame, J.A., Howe, J., Stephens, R., Tosolini, A.-M., Thorn, V., 2007. 100 Million Years of Antarctic Climate Evolution: Evidence from Fossil Plants. *Proc. 10th Int. Symp. Antarct. Earth Sci.* 19–27. doi:10.3133/of2007-1047.kp03
- Francis, J.E., Marensi, S., Levy, R., Hambrey, M., Thorn, V.C., Mohr, B., Brinkhuis, H., Warnaar, J., Zachos, J., Bohaty, S., DeConto, R., 2009. From Greenhouse to Icehouse - The Eocene/Oligocene in Antarctica. *Dev. Earth Environ. Sci.* 8, 309–368. doi:10.1016/S1571-9197(08)00008-6
- García-Romero, E., Vegas, J., Baldonado, J.L., Marfil, R., 2005. Clay minerals as alteration products in basaltic volcanoclastic deposits of La Palma (Canary Islands, Spain). *Sediment. Geol.* 174, 237–253. doi:10.1016/j.sedgeo.2004.12.007
- Gérard, M., Caquineau, S., Pinheiro, J., Stoops, G., 2007. Weathering and allophane neoformation in soils developed on volcanic ash in the Azores. *Eur. J. Soil Sci.* 58, 496–515. doi:10.1111/j.1365-2389.2007.00910.x
- Gialanella, S., Girardi, F., Ischia, G., Lonardelli, I., Mattarelli, M., Montagna, M., 2010. On the goethite to hematite phase transformation. *J. Therm. Anal. Calorim.* 102, 867–873. doi:10.1007/s10973-010-0756-2
- Griener, K.W., Nelson, D.M., Warny, S., 2013. Declining moisture availability on the Antarctic Peninsula during the Late Eocene. *Palaeogeogr. Palaeoclimatol. Palaeoecol.* 383–384, 72–78. doi:10.1016/j.palaeo.2013.05.004
- Gualtieri, A.F., Venturelli, P., 1999. In situ study of the goethite-hematite phase transformation by real time synchrotron powder diffraction. *Am. Mineral.* 84, 895–904. doi:10.2138/am-1999-5-624
- Halama, R., Konrad-Schmolke, M., Sudo, M., Marschall, H., Wiedenbeck, M., 2014. Effects of fluid-rock interaction on  $^{40}\text{Ar}/^{39}\text{Ar}$  geochronology in high-pressure rocks (Sesia-Lanzo Zone, Western Alps). *Geochim. Cosmochim. Acta* 126, 475–494.
- Hekinian, R., 1982. *Petrology of the Ocean Floor*, Elsevier O. ed. Elsevier, Amsterdam-Oxford-New York. doi:10.1016/S0422-9894(08)70937-1
- Huber, M., Brinkhuis, H., Stickley, C.E., Döös, K., Sluijs, A., Warnaar, J.,

- Schellenberg, S.A., Williams, G.L., 2004. Eocene circulation of the Southern Ocean: Was Antarctica kept warm by subtropical waters? *Paleoceanography* 19, 1–12. doi:10.1029/2004PA001014
- Hunt, R.J., Poole, I., 2003. Paleogene West Antarctic climate and vegetation history in light of new data from King George Island. *Geol. Soc. Am. Spec. Pap.* 369, 395–412. doi:10.1130/0-8137-2369-8.395
- IREN, 1978. Estudio de suelos de la provincia de Valdivia.
- Ishizuka, O., 1998. Vertical and horizontal variation of the fast neutron flux in a single irradiation capsule and their significance in the laser-heating  $^{40}\text{Ar}/^{39}\text{Ar}$  analysis: Case study for the hydraulic rabbit facility of the JMTR reactor, Japan. *Geochem. J.* 32, 243–252.
- Jiang, L., Chen, G., Grapes, R., Peng, Z., 2015. Journal of Asian Earth Sciences Thermal origin of continental red beds in SE China : An experiment study. *J. Asian Earth Sci.* 101, 14–19. doi:10.1016/j.jseaes.2015.01.019
- Jongmans, A.G., Nieuwenhuysse, A., Buurman, P., van Doesburg, J.D.J., van Oort, F., Jaunet, A.M., 1994. Inheritance of 2:1 phyllosilicates in Costa Rican Andisols. *Soil Sci. Soc. Am. J.* 58, 494–501. doi:10.2136/sssaj1994.03615995005800020035x
- Jongmans, a. G., Nieuwenhuysse, a., Buurman, P., van Doesburg, J.D.J., van Oort, F., Jaunet, a. M., 1994. Inheritance of 2:1 Phyllosilicates in Costa Rican Andisols. *Soil Sci. Soc. Am. J.* 58, 494. doi:10.2136/sssaj1994.03615995005800020035x
- Kovda, I., Mermut, A.R., 2010. Vertic Features, in: Stoops, G., Marcelino, V., Mees, F. (Eds.), *Interpretation of Micromorphological Features of Soils and Regoliths*. Elsevier, Amsterdam, pp. 109–122. doi:10.1016/B978-0-444-53156-8.00013-1
- Kraus, M.J., Hasiotis, S.T., 2006. Significance of different modes of rhizolith preservation to interpreting paleoenvironmental and paleohydrologic settings: Examples from Paleogene paleosols, Birghorn Basin, Wyoming, U.S.A. *J. Sediment. Res.* 76, 633–646. doi:10.2110/jsr.2006.052
- Kristmannsdottir, H., Tomasson, J., 1978. Zeolite zones in geothermal areas of Iceland, in: Sand, L.B., Mumpton, F.M. (Eds.), *Natural Zeolite Occurrence, Properties and Use*. Pergamon Press, Oxford, pp. 277–284.
- Lee, Y. Il, Lim, H.S., Yoon, H. Il, 2004. Geochemistry of soils of King George Island, South Shetland Islands, West Antarctica: Implications for pedogenesis in cold

- polar regions. *Geochim. Cosmochim. Acta* 68, 4319–4333.  
doi:10.1016/j.gca.2004.01.020
- Lessovaia, S.N., Plötze, M., Inozemzev, S., Goryachkin, S., 2016. Traprock transformation into clayey materials in soil environments of the central Siberian plateau, Russia. *Clays Clay Miner.* 64, 668–676.  
doi:10.1346/CCMN.2016.064042
- Lowe, D.J., 2000. Upbuilding pedogenesis in multisequal tephra- derived soils in the Waikato region, in: Adams, J., Metherell, A. (Eds.), *Soil 200: New Horizons for a New Century*. Australian and New Zealand Second Joint Soils Conference Volume 2: Lincoln University. New Zealand Society of Soil Science, pp. 183–184.
- Lowe, D.J., Tonkin, P.J., 2010. Unravelling upbuilding pedogenesis in tephra and loess sequences in New Zealand using tephrochronology, in: Gilkes, R.J., Prakongkep, N. (Eds.), *Proceedings of the 19th World Congress of Soil Science “Soil Solutions for a Changing World”* (1–6 Aug., 2010, Brisbane), Symposium 1.3.2 Geochronological Techniques and Soil Formation. Brisbane, pp. 34–37.
- Lu, S.G., Xue, Q.F., Zhu, L., Yu, J.Y., 2008. Mineral magnetic properties of a weathering sequence of soils derived from basalt in Eastern China. *Catena* 73, 23–33. doi:10.1016/j.catena.2007.08.004
- Mackensen, A., Ehrmann, W.U., 1992. Middle Eocene through Early Oligocene climate history and paleoceanography in the Southern Ocean: Stable oxygen and carbon isotopes from ODP Sites on Maud Rise and Kerguelen Plateau. *Mar. Geol.* 108, 1–27. doi:10.1016/0025-3227(92)90210-9
- Maher, B., 1986. Characterisation of soils by mineralmagnetic measurements. *Phys. Earth Planet. Inter.* 42, 76–92. doi:10.1016/S0031-9201(86)80010-3
- Mansilla, H.G., De Valais, S., Stinnesbeck, W., Varela, N.A., Leppe, M.A., 2012. New Avian tracks from the lower to middle Eocene at Fossil Hill, King George Island, Antarctica. *Antarct. Sci.* 24, 500–506. doi:10.1017/S0954102012000260
- Mansilla, H.G., Stinnesbeck, W., Varela, N., Leppe, M., 2013. Eocene fossil feather from King George Island, South Shetland Islands, Antarctica. *Antarct. Sci.* 26, 384–388. doi:10.1017/S0954102013000771
- Maynard, J.B., 1992. Chemistry of modern soils as a guide to interpreting Precambrian paleosols. *J. Geol.* 100, 279–289.
- Mehra, O.P., Jackson, M.L., 1960. Iron Oxide Removal from Soils and Clays by a

- Dithionite-Citrate System Buffered with Sodium Bicarbonate. *Clays Clay Miner.* 7, 317–327. doi:10.1346/CCMN.1958.0070122
- Ming, D.W., Boettinger, J.L., 2001. Zeolites in Soil Environments. *Rev. Mineral. Geochemistry* 45, 323–345. doi:10.2138/rmg.2001.45.11
- Mirabella, A., Egli, M., Raimondi, S., Giaccari, D., 2005. Origin of clay minerals in soils on pyroclastic deposits in the Island of Lipari (Italy). *Clays Clay Miner.* 53, 409–421. doi:10.1346/CCMN.2005.0530409
- Moore, D., Reynolds Jr, R., 1997. *X-ray Diffraction and the Identification of Clay Minerals*, 2nd ed. Oxford University.
- Mozer, A., 2012. Pre-glacial sedimentary facies of the Point Thomas Formation (Eocene) at Cytadela, Admiralty Bay, King George Island, West Antarctica. *Polish Polar Res.* 33, 41–62. doi:10.2478/v10183-012-0002-7
- Nahon, D., Colin, F., Tardy, Y., 1982. Formation and distribution of Mg,Fe,Mn-smectites in the first stages of the lateritic weathering of forsterite and tephroite. *Clay Miner.* 17, 339–348. doi:10.1180/claymin.1982.017.3.06
- NRCS, 1996. *Soil Survey Laboratory Methods Manual* 716. doi:10.1021/ol049448l
- Pagani, M., Zachos, J.C., Freeman, K.H., Tripple, B., Bohaty, S., 2005. Marked decline in Atmospheric Carbon Dioxide Concentrations during the Paleocene. *Science* (80-). 309, 600–603. doi:10.1126/science.1110063
- Parra, M., Delmont, P., Dumon, J.C., Ferragne, A., Pons, J.C., 1987. Mineralogy and origin of Tertiary interbasaltic clays from the Faeroe island, Northeastern Atlantic. *Clay Miner.* 22, 63–82.
- Pearson, P.N., Foster, G.L., Wade, B.S., 2009. Atmospheric carbon dioxide through the Eocene–Oligocene climate transition. *Nature* 461, 1110–1113. doi:10.1038/nature08447
- Pearson, P.N., Palmer, M.R., 2000. Atmospheric carbon dioxide concentrations over the past 60 million years. *Nature* 406, 695–699. doi:10.1038/35021000
- Pevear, D., Dethier, D., Frank, D., 1982. Clay minerals in the 1980 deposits from Mount St. Helens. *Clays Clay Miner.* 30, 241–252. doi:10.1346/CCMN.1982.0300401
- Poole, I., Cantrill, D., Utescher, T., 2005. A multi-proxy approach to determine Antarctic terrestrial palaeoclimate during the Late Cretaceous and Early Tertiary. *Palaeogeogr. Palaeoclimatol. Palaeoecol.* 222, 95–121. doi:10.1016/j.palaeo.2005.03.011

- Poole, I., Hunt, R.J., Cantrill, D.J., 2001. A fossil wood flora from King George Island: ecological implications for an Antarctic Eocene vegetation. *Ann. Bot.* 88, 33–54. doi:10.1006/anbo.2001.1425
- Poole, I., Mennega, A.M.W., Cantrill, D.J., 2003. Valdivian ecosystems in the Late Cretaceous and Early Tertiary of Antarctica: Further evidence from myrtaceous and eucryphiaceous fossil wood. *Rev. Palaeobot. Palynol.* 124, 9–27. doi:10.1016/S0034-6667(02)00244-0
- Preetz, H., Igel, J., Hannam, J.A., Stadler, S., 2017. Relationship between magnetic properties and reddening of tropical soils as indicators of weathering. *Geoderma* 303, 143–149. doi:10.1016/j.geoderma.2017.05.007
- Pross, J., Contreras, L., Bijl, P.K., Greenwood, D.R., Bohaty, S.M., Schouten, S., Bendle, J. a, Röhl, U., Tauxe, L., Raine, J.I., Huck, C.E., van de Flierdt, T., Jamieson, S.S.R., Stickley, C.E., van de Schootbrugge, B., Escutia, C., Brinkhuis, H., 2012. Persistent near-tropical warmth on the Antarctic continent during the early Eocene epoch. *Nature* 488, 73–7. doi:10.1038/nature11300
- Reguero, M.A., Marensi, S.A., Santillana, S.N., 2002. Antarctic Peninsula and South America (Patagonia)\nPaleogene terrestrial faunas and environments: biogeographic\nrelationships. *Palaeogeogr. Palaeoclimatol. Palaeoecol.* 2776, 1–22.
- Retallack, G.J., 1991. Untangling the effects of burial alteration and ancient soil formation. *Annu. Rev. Earth Planet. Sci.* 19, 183–206. doi:10.1146/annurev.earth.19.1.183
- Retallack, G.J., 1988. Field recognition of paleosols. *Geol. Soc. Am. Spec. Pap.* 1–20. doi:10.1130/SPE216-p1
- Rivas, J., Ortega, B., Sedov, S., Solleiro, E., Sychera, S., 2006. Rock magnetism and pedogenetic processes in Luvisol profiles: Examples from Central Russia and Central Mexico. *Quat. Int.* 156–157, 212–223. doi:10.1016/j.quaint.2006.05.007
- Robert, C., Kennett, J.P., 1997. Antarctic continental weathering changes during Eocene-Oligocene cryosphere expansion: Clay mineral and oxygen isotope evidence. *Geology* 25, 587–590. doi:10.1130/0091-7613
- Scheinost, A., Chavernas, A., Barrón, V., Torrent, J., 1998. Use and limitations of second-derivative diffuse reflectance spectroscopy in the visible to near-infrared range to identify and quantify Fe oxide minerals in soils. *Clays Clay Miner.* 46,

528–536.

- Schulze, D., 1981. Identification of soil iron oxide minerals by Differential X-ray Diffraction. *Soil Sci. Soc. Am. J.* 45, 437–440.
- Schwertmann, U., 1964. Differenzierung der Eisenoxide des Bodens durch Extraktion mit Ammoniumoxalat-Lösung. *J. Plant Nutr. Soil Sci.* 105, 194–202.
- Schwertmann, U., Fechter, H., 1984. The Influence of aluminum on iron oxides: XI. Aluminum-substituted maghemite in soils and its formation. *Soil Sci. Soc. Am.* 48, 1462–1463. doi:10.2136/sssaj1984.03615995004800060054x
- Schwertmann, U., Friedl, J., Stanjek, H., 1999. From Fe(III) Ions to Ferrihydrite and then to Hematite. *J. Colloid Interface Sci.* 209, 215–223. doi:10.1006/jcis.1998.5899
- Sedov, S., Stoops, G., Shoba, S., 2010. Regoliths and Soils on Volcanic Ash, in: Stoops, G., Marcelino, V., Mees, F. (Ed.), *Interpretation of Micromorphological Features of Soils and Regoliths*. Elsevier, Amsterdam, pp. 275–303. doi:10.1016/B978-0-444-53156-8.00013-1
- Shoji, S., Nanzyo, M., Dahlgren, R.A., 1993. *Volcanic ash soils - Genesis, properties and utilization*, Statewide Agricultural Land Use Baseline 2015. Elsevier Science, Amsterdam.
- Singer, A., 1980. The palaeoclimate interpretation of clay minerals in soil and weathering profiles. *Earth-Science Rev.* 15, 303–326.
- Singer, A., 1970. Edaphoids and paleosols of basaltic origin in The Galilee, Israel. *J. Soil Sci.* 21.
- Spinola, D.N., Pi-Puig, T., Solleiro-Rebolledo, E., Egli, M., Sudo, M., Sedov, S., Kühn, P., 2017a. Origin of clay minerals in Early Eocene volcanic paleosols on King George Island, Maritime Antarctica. *Sci. Rep.* doi:10.1038/s41598-017-06617-x
- Spinola, D.N., Portes, R. de C., Schaefer, C.E.G.R., Solleiro-Rebolledo, E., Pi-Puig, T., Kühn, P., 2017b. Eocene paleosols on King George Island, Maritime Antarctica: Macromorphology, micromorphology and mineralogy. *Catena*. doi:10.1016/j.catena.2017.01.004
- Srivastava, P., Sangode, S.J., Torrent, J., 2015. Mineral magnetic and diffuse reflectance spectroscopy characteristics of the Deccan volcanic bole beds : Implications to genesis and transformations of iron oxides. *Geoderma* 239–240, 317–330. doi:10.1016/j.geoderma.2014.11.010

- Steiger, R., Jäger, E., 1977. Subcommission on geochronology: convention on the use of decay constants in geo- and cosmochronology. *Earth Planet. Sci. Lett.* 36, 359–362.
- Stickley, C.E., Brinkhuis, H., Schellenberg, S.A., Sluijs, A., Röhl, U., Fuller, M., Grauert, M., Huber, M., Warnaar, J., Williams, G.L., 2004. Timing and nature of the deepening of the Tasmanian Gateway. *Paleoceanography* 19, 1–18. doi:10.1029/2004PA001022
- Stoops, G., 2003. Guidelines for Analysis and Description of Soil and Regolith Thin Sections. Soil Science Society of America, Madison, Wisconsin.
- Torrent, J., Barrón, V., 2002. Diffuse reflectance spectroscopy of iron oxides. *Encycl. Surf. Colloid Sci.* 1438–1446.
- Torrent, J., Barrón, V., Liu, Q., 2006. Magnetic enhancement is linked to and precedes hematite formation in aerobic soil. *Geophys. Res. Lett.* 33, 4–7. doi:10.1029/2005GL024818
- Torrent, J., Liu, Q., Bloemendal, J., Barrón, V., 2007. Magnetic enhancement and iron oxides in the Upper Luochuan Loess-Paleosol sequence, Chinese Loess Plateau. *Soil Sci. Soc. Am. J.* 71, 1570–1578. doi:10.2136/sssaj2006.0328
- Torrent, J., Schwertmann, U., 1987. Influence of hematite on the colour of Red Beds. *J. Sediment. Petrol.* 57, 682–686.
- Ugolini, F.C., Dahlgren, R.A., 2002. Soil development in volcanic ash. *Glob. Environ. Res.* 6, 69–81.
- Uto, K., Ishizuka, O., Matsumoto, A., Kamioka, H., Togashi, S., 1997. Laser-heating  $^{40}\text{Ar}/^{39}\text{Ar}$  dating system of the Geological Survey of Japan: System outline and preliminary results. *Bull. Geol. Surv. Japan* 48, 23–46.
- Vacca, A., Ferrara, C., Matteucci, R., Murru, M., 2012. Ferruginous paleosols around the Cretaceous-Paleocene boundary in central-southern Sardinia (Italy) and their potential as pedostratigraphic markers. *Quat. Int.* 265, 179–190. doi:10.1016/j.quaint.2011.07.036
- Veblen, T., Alaback, P., 1996. High-Latitude Rainforests and Associated Ecosystems of the West Coast of the Americas, in: Lawford, R., Fuentes, E., Alaback, P. (Eds.), *High-Latitude Rainforest and Associated Ecosystems of the West Coast of the Americas*. Springer Verlag, New York, pp. 173–213. doi:10.1007/978-1-4612-3970-3
- Velde, B., Meunier, A., 2008. The Origin of Clay Minerals in Soil and Weathered

- Rocks. Springer-Verlag, Berlin Heidelberg.
- Veneman, P.L., Vepraskas, M., Bouma, J., 1976. The physical significance of soil mottling in a Wisconsin toposequence. *Geoderma* 15, 103–118.
- Weibel, R., 1999. Effects of burial on the clay assemblages in the Triassic Skagerrak Formation, Denmark. *Clay Miner.* 34, 619–635.  
doi:10.1180/claymin.1999.034.4.08
- Wilke, F.D., O'Brien, P., Gerdes, A., Timmerman, M., Sudo, M., Khan, M.A., 2010. The multistage exhumation history of the Kaghan Valley UHP series, NW Himalaya, Pakistan from U-Pb and  $^{40}\text{Ar}/^{39}\text{Ar}$  ages. *Eur. J. Mineral.* 22, 703–719.
- Wilson, M.J., 1999. The origin and formation of clay minerals in soils: past, present and future perspectives. *Clay Miner.* 34, 7–25. doi:10.1180/000985599545957
- Wojdyr, M., 2010. Fityk: a general-purpose peak fitting program. *J. Appl. Crystallogr.* 43, 1126–1128. doi:10.1107/S0021889810030499
- Wyszecki, G., Stiles, W., 1982. *Colour science: Concepts and methods, quantitative data and formulae*. Wiley, New York.
- York, D., 1969. Least squares fitting of a straight line with correlated errors. *Earth Planet. Sci. Lett.* 5, 320–324.
- Zachos, J., Pagani, M., Sloan, L., Thomas, E., Billups, K., 2001. Trends, Rhythms, and Aberrations in Global Climate 65 Ma to Present. *Source Sci. New Ser.* 292, 686–693. doi:10.1126/science.1059412
- Zachos, J.C., Quinn, T.M., Salamy, K.A., 1996. High-resolution deep-sea foraminiferal stable isotope records of the Eocene-Oligocene transition. *Paleoceanography*

## **Manuscript 1**

Catena: Volume 152, May 2017, Pages 69-81

10.1016/j.catena.2017.01.004

<https://doi.org/10.1016/j.catena.2017.01.004>

### **Eocene Paleosols on King George Island, Maritime Antarctica: Macromorphology, Micromorphology and Mineralogy**

Diogo Noses Spinola<sup>a</sup>, Raquel de Castro Portes<sup>b</sup>, Carlos Ernesto Gonçalves Reynaud Schaefer<sup>c</sup>, Elizabeth Solleiro-Rebolledo<sup>d</sup>, Theresa Pi-Puig<sup>d</sup>, Peter Kühn<sup>a</sup>

<sup>a</sup> Institute of Geography, University of Tübingen, Germany.

<sup>b</sup> Department of Geography, University of Zürich, Switzerland.

<sup>c</sup> Department of Soil Science, Federal University of Viçosa, Brazil.

<sup>d</sup> Institut of Geology, Nacional Autonomous University of Mexico, Mexico.

### **Abstract**

We investigated the origin of reddish layers between basalt flows in an Early Eocene volcanic succession in King George Island, Maritime Antarctica. Previous studies in the area classified these layers as regolith surfaces, baked zones and paleosols, but the properties of these layers and the reasons for their classification are not clarified. Since the Early Eocene epoch was one of the warmest phases on Earth during the Cenozoic, a proper investigation of these layers is crucial to obtain additional regional information about the paleoenvironment.

The focus of this study is on three profiles located in the Admiralty Bay on King George Island. They were classified as paleosols based on field, micromorphological and mineralogical properties. Main soil forming processes identified by micromorphological analyses were clay neoformation, pedo-/bioturbation and a weak redoximorphosis. The occurrence of plant residues in all profiles was a reliable indicator that these soils formed a land surface during the Early Eocene. Abundant weathered volcanic glass and pyroclasts may indicate andosolization although the main diagnostic features for Andosols, which are the presence of nanocrystalline minerals and organic matter accumulation, were not detected or only in small amounts, respectively. The long-term burial of the paleosol could be a reason for lacking of these diagnostic features. Clay minerals associated with moderately weathered volcanic soils (smectite) were detected in the X-ray diffraction analysis. A pre- dominantly reddish colour of most of the soil horizons is given by hematite, confirmed by the determination of pedogenic oxides. Nevertheless, rubification was not solely a result of pedogenesis but also of reddening of oxyhydroxides by dehydration during diagenesis. Other diagenetic processes were burial compaction, loss of organic matter and induration. In the horizons directly buried by a basalt flow, voids were filled by zeolite crystals, an effect related to lava cooling. Another possible diagenetic effect was the geochemical rejuvenation and homogenization of the profiles. Despite the occurrence of these features, the results are in agreement with previous studies, indicating a humid temperate paleoclimate for King George Island during the Early Eocene.

## 1. Introduction

Sequences of lava flows very often display alternating fine-textured red layers (partly weathered) and basaltic layers (unweathered). These red layers have a potential for paleoenvironmental reconstruction because they may indicate a hiatus in the volcanic activity combined with landscape stability and soil formation (Ghosh et al., 2006; Marques et al., 2014; Pietsch and Kühn, 2012; Sayyed et al., 2014; Sheldon, 2003; Shukla et al., 2014; Singer and Ben-Dor, 1987; Solleiro-Rebolledo et al., 2016)). On the other hand, red layers can also be a product of other geological processes such as hydrothermal alteration (or “fritting”) (Gérard et al., 2006; Graef et al., 1997; Lange et al., 2002a; Müller and Schwaighofer, 1979; Singer, 1970), pyroclast weathering (Emeleus et al., 1996; Widdowson et al., 1997) or sedimentation (Canile, 2010; Srivastava et al., 2012). In the latter cases the red layers do not represent periods of landscape stability and soil formation.

Red layers have been identified in an Early Eocene volcanic succession in King George Island (KGI), South Shetland Islands, Maritime Antarctica (Fig. 1). These layers have been labelled as regolith surfaces (Mozer, 2012), baked zones (Birkenmajer, 1980a) and also as paleosols (Birkenmajer and Łydka, 1990). However, is not clear which properties were crucial for these authors to differentiate either paleosols, regoliths or baked zones. Where these were recognized as paleosols, only clay mineralogy was studied, showing a main composition of kaolinite and smectite (Birkenmajer and Łydka, 1990), despite the importance of paleosols for paleoclimate interpretation (e.g. Kühn et al., 2013; Schatz et al., 2015; Sheldon and Tabor, 2009).

The major importance of detailed studies of these red layers in King George Island is because they were formed during the Early Eocene, which was one of the warmest periods on Earth during the Cenozoic when climatic differences between the equator and the poles were much smaller than today (Bijl et al., 2009; Greenwood and Wing, 1995; Pearson et al., 2009). There is evidence for near-tropical paleoclimate in Antarctica with frost-free winters despite the polar darkness (Dingle and Lavelle, 1998b; Pross et al., 2012). A cool temperate forest similar to the Valdivia Forests, Southern Chile, is often considered the best modern analogue environment in particular for the Antarctica Peninsula (Francis et al., 2009; Hunt and Poole, 2003; Mozer, 2012).

Because no detailed studies of the red layers on KGI have been carried out so far, a

proper genetic interpretation is crucial. For this reason, certain criteria must be adopted to recognize paleosols. The main properties to be identified in the field are the presence of root traces, soil horizons and soil structure (Retallack, 1988). Based on thin section analysis, (Fedoroff et al., 2010) listed the following micromorphological features formed only by in situ pedogenesis: undisturbed biological activity features such as passage features and channels, pedogenic micro- structures, pedogenic b-fabrics and one or more types of undisturbed pedofeatures. Most importantly, however, is the combination of physical properties, micromorphological characteristics and other properties and how they behave in a depth function within a vertical profile (Fenwick.I, 1985).

The hypotheses of this study are: (i) the Eocene red layers in KGI are paleosols formed during periods of lower or no volcanic activity, and (ii) these paleosols are suitable proxies for paleoenvironmental reconstruction.

Our main objective to test the first hypothesis is to identify the main pedogenic properties and features. To test the second hypothesis, the objective is to identify the diagenetic features because they can eventually interfere with the paleoenvironmental record. In this work, we attribute to diagenesis those features formed after the burial of the paleosols, either by effect of the lava flow or due to long-term burial.

## **2. Material and methods**

### **2.1. Site description**

The samples were collected on King George Island, South Shetland Islands, Maritime Antarctica. The specific outcrop is located in the Cytadela area of the Ezcurra Inlet in the Admiralty Bay (62° 11.057'S– 58° 35.209'W) (Fig. 1).

The deposits in the outcrop stratigraphically belong to the Point Thomas Formation, Ezcurra Inlet Group, which comprises a 500 m thick Paleogene (Eocene-Oligocene) volcanic succession (Birkenmajer, 1980b; Birkenmajer and Zastawniak, 1989). This formation was deposited during the Arctowski interglacial period (ca 50 to ca 32 Ma), a climostratigraphic unit introduced by (Birkenmajer, 1988).

Two informal units of the Point Thomas Formation are recognized at the Cytadela, the Lower Member (LM) and Upper Member (UM) (Birkenmajer, 1980a). The LM is a 20–40 m thick regular high-Al flow basalt with a thickness of 1–6 m alternating with pyroclastic deposits. The LM corresponds to the Early Eocene humid temperate

climate, similar to the present-day Chilean Valdivia Forest (Mozer, 2012). The UM comprises 150–450 m of irregular, lenticular basalt lavas alternating with feldspathic tuff, interbedded with coarse vent breccia and plant-bearing tuff.

There is no dating information for the sampled basalts. Accordingly to Mozer (2012) these layers were deposited in the Early Eocene. Radiometric dating (K/Ar) of basalts of Point Thomas Formation on nearby locations gave an oldest age of 49 Ma (Nawrocki et al., 2011) and youngest of 41 Ma (Birkenmajer et al., 2005).

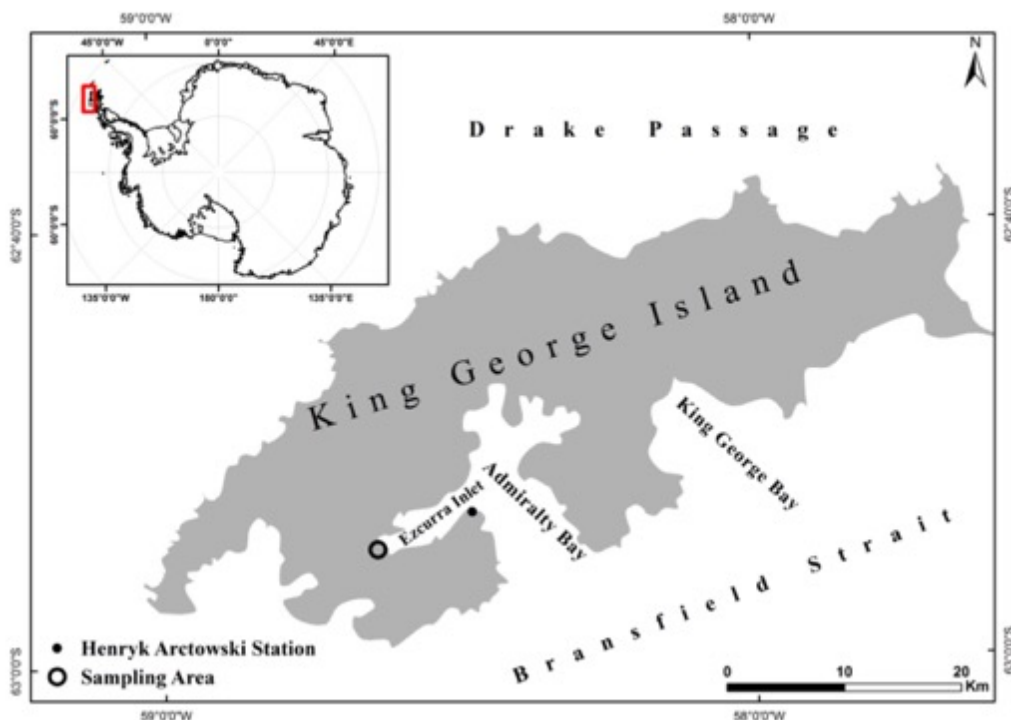


**Figure 1.** Location of the sampling site at the King George Island.

## 2.2. Field and laboratory analyses

Samples were taken from a red layer covered by the 6th basalt flow basalt flow (from bottom to top) in the LM of the schematic field section made by (Mozer, 2012). Three profiles (P1, P2 and P3) were chosen, which are located with a distance of 60 m between the P1 and P2 and of 90 m between P2 and P3 (Fig. 2).

After removing overlying debris, the profile face was excavated ~ 20 cm to provide a fresh surface for describing and sampling. The profiles were described following (FAO, 2006) with a particular focus on horizon boundaries, colour (Munsell soil colour charts), structure (size and type), visual estimation of rock fragments and presence of plant fossils. We sampled each profile with a total of 13 bulk samples from red layers.

For micromorphological analysis, 12 undisturbed and oriented samples were taken from the red layers and six samples from the overlying and underlying basalts. The undisturbed samples were not impregnated with resin because of sufficient induration of the material. The samples were sliced into 9 × 6 cm thin sections. Afterwards, they were analysed and photographed using a polarizing microscope (Zeiss Axio Imager.A2m, Software AxioVision 4.7.2) with plane polarized light (PPL), crossed polarized light (XPL) and oblique incident light (OIL). Description followed Delvigne (1998) and (Stoops, 2003). In order to test for features of soil formation, special attention was given to the type of voids, microstructure and micromass properties, to b-fabrics as well as to some pedogenic features such as passage features, clay coatings, infillings and nodules.

The bulk samples (ratio Li-metaborate to soil 1:5) were ground with an agate mill for 10 min and the major elements were measured with a wavelength dispersive XRF device (PANalytical PW 2400). Information about the standard errors of the calibration for the major elements is provided in the supplementary materials. To verify whether the red layers follow the normal weathering behaviour of surface soils we used the Chemical Index of Alteration minus K (CIA-K) (after Maynard (1992) (calculated in molar portions). The K is excluded in this equation to avoid any possible effect of K-metasomatism (Maynard, 1992).

$$\text{CIA-K} = [\text{Al}_2\text{O}_3 / (\text{Al}_2\text{O}_3 + \text{CaO}^* + \text{Na}_2\text{O})] \times 100 \quad (1)$$

where CaO\* is the amount of silicate-bound CaO. For that, we calculated the CaCO<sub>3</sub> bound Ca from the carbonate content and subtracted that from CaO.

Total carbon (TC) content was measured on ground samples with an Elementar Analyser (DIN ISO 10694, 1995) and the total inorganic carbon (TIC) content was determined gas volumetrically (DIN ISO 10693, 1995). Particle size distribution analysis was performed by a combined sieving and pipette method (NRCS, 1996).

For the X-ray diffraction analysis, the samples were gently disaggregated to avoid artificial grain size reduction of rock components, then was broken into small chips (2 mm) using a porcelain crusher and subsequently dispersed in deionized water. Clay size fraction (<2 μm) was separated in distilled water according to Stoke's law using the most unaggressive method (Moore and Reynolds Jr, 1997).

From the <2 μm fraction, air-dried oriented preparations were obtained by pipetting

some drops of the suspensions onto a glass slide, which was then dried at 30 °C for a few hours (Moore and Reynolds Jr, 1997). Ethylene glycol solvation of the slide was achieved by exposing them to ethylene glycol vapor at 70 °C for 24 h. Measurements were made using an EMPYREAN XRD diffractometer operating with an accelerating voltage of 45 kV and a filament current of 40 mA, using CuK $\alpha$  step size of 0.04° (2 $\theta$ ) and 40 s of scan step time. Clay samples were examined by XRD in the air-dried form, saturated with ethylene glycol (EG) and after heating (550 °C). The preparations were measured over a 2 $\theta$  angle range of 2–70° (air-dried) and 2–30° (glycolated and heated).

Pedogenic Fe-oxides (Fed) were extracted by dithionite-citrate-bicarbonate (DCB) solution (Mehra and Jackson, 1960). The nanocrystalline Fe (Fe<sub>o</sub>), Al (Al<sub>o</sub>) and Si (Si<sub>o</sub>) compounds were extracted by shaking 2.5 g of soil 100 mL 0.2 M acid ammonium oxalate (pH 3) for 4 h in the dark (Schwertmann, 1964). The proportion of crystalline pedogenic iron against the total amount of iron was determined using the following Eq. (2) (after Arduino et al., 1984).

$$\text{Crystalline iron: } (\text{Fe}_d - \text{Fe}_o) / \text{Fe}_t \quad (2)$$

where Fe<sub>t</sub> is the total Fe<sub>2</sub>O<sub>3</sub>, measured by X-ray fluorescence (XRF).

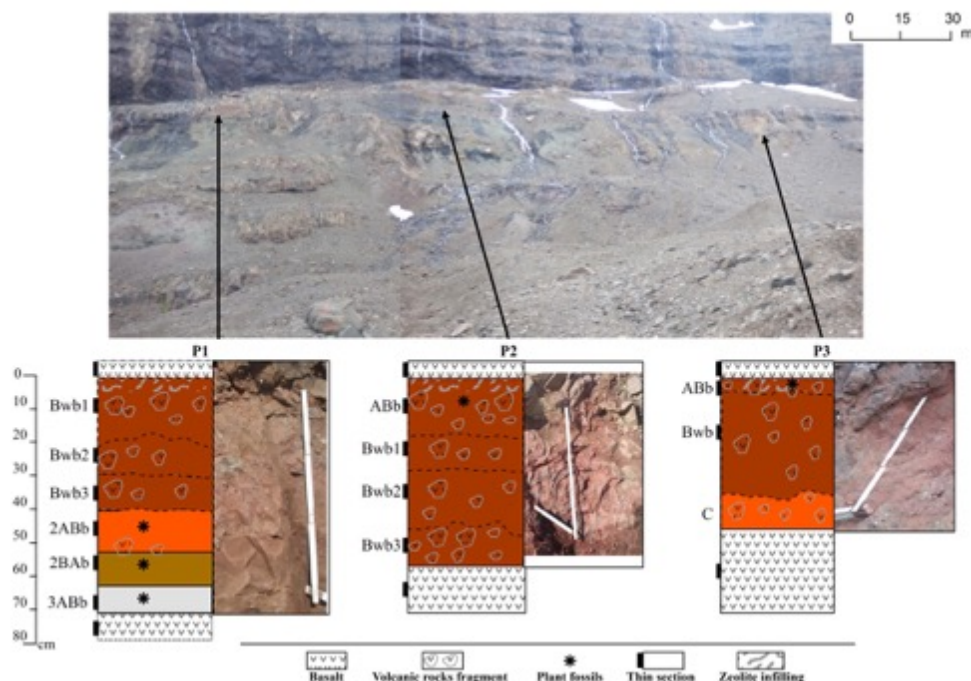


**Figure 2.** Distribution of the paleosols on the landscape at the Cytadela outcrop and their schematic representation.

### 3. Results

#### 3.1. Physical properties

The investigated profiles are located between basalt flows. Whereas the contact to the covering basalt flow was clear, the contact with the saprolite and the underlying basalt was not accessible. Therefore, all profiles should be thicker than originally described. The covering basalt flow is thin, no more than 1 m thick. Although it is probable that the original lava has been eroded.

The profiles are reddish-brown with gradual colour changes with depth. They have predominantly strong blocky (more angular) and platy structure with variable size with depth. With the exception of P1, rock fragments became more abundant and larger with depth (Table 1). Most of the horizons have sandy loam as texture. The horizons 2ABb-2BAb and 3ABb of the P1 are slightly finer with a sandy clay loam texture. Because of the difficulty to disperse the material, some amount of clay should have been accounted for silt or sand. Thus, the texture of the samples should be finer.

P1 is the most heterogeneous profile based on colour, which varies from red to gray, structure type and size, and the distribution of the rock fragments through the horizons. It is the thickest (> 73 cm) profile and has two lithic discontinuities (LD). The first LD was identified between the Bwb3 and 2ABb horizons, because of an abrupt lack of rock fragments in the 2ABb horizon. The second LD was identified between the 2BAb and 3ABb horizons because of the first appearance of dark fossil plant leaves and a grayish colour (hue = 5Y) being a marker of a buried A horizon.

The horizon boundaries in P2 are gradual and diffuse based on differences in structure type, varying between subangular/angular blocky and platy. The profile is reddish-brown (hue-2.5YR), with slight colour variations.

P3 has only minor differences of properties and gradual transitions between horizons. Based on colour and structure, three horizons could be distinguished. The colour grades from reddish-brown (hue = 2.5YR) to dull (hue = 7.5YR) and the peds becomes larger downwards.

Following the scale for the strength of paleosols (Ollier, 1965; Retallack, 2001), the horizons are moderately to strongly indurated, but no cements were detected. Small veins of zeolites crystals (up to 1 cm) were identified only at the basal contact of the overlying basalt with the uppermost red layer in all profiles.

**Table 1.** Selected main macromorphological properties (after FAO, 2006).

| Profile   | Horizon | Depth<br>[cm] | Horizon boundaries<br>(distinctness -<br>topography) | Structure <sup>1</sup> |           | Colour (Munsell) |                    | Rock fragments     | Plant fossil | Particle size % |                 |                    | Textural class  |
|-----------|---------|---------------|--|------------------------|-----------|------------------|--------------------|--------------------|--------------|-----------------|-----------------|--------------------|-----------------|
|           |         |               |  | Type                   | Size      | Dry              | Name               |                    |              | Clay (<2μ)      | Silt (2 μ-63 μ) | Sand (63μ - 2000μ) |                 |
| <b>P1</b> | Bwb1    | 0 - 23        | clear - wavy   | sb +pl                 | very fine | 5YR 5/4          | Dull reddish brown | many               |              | 15              | 18              | 67                 | Sandy loam      |
|           | Bwb2    | 23 - 34       | gradual – smooth                                     | sb+pl                  | fine/thin | 2.5YR 5/4        | Dull reddish brown | common             |              | 15              | 19              | 66                 | Sandy loam      |
|           | Bwb3    | 34 - 45       | abrupt- smooth                                       | ab                     | fine      | 2.5YR 5/4        | Dull reddish brown | common             |              | 14              | 19              | 67                 | Sandy loam      |
|           | 2ABb    | 45 - 60       | clear - smooth                                       | ab                     | fine      | 7.5YR 7/4        | Dull orange        | none               |              | 17              | 21              | 62                 | Sandy loam      |
|           | 2BAb    | 60 - 73       | abrupt - smooth                                      | ab+pl                  | coarse    | 10YR 6/4         | Dull yellow orange | none               |              | 20              | 22              | 58                 | Sandy clay loam |
|           | 3ABb    | 73+           |  |                        | pl+ab     | medium           | 5Y 4/1             | Gray               | none         | x               | 20              | 15                 | 65              |
| <b>P2</b> | ABb     | 0 - 20        | abrupt - smooth                                      | sb                     | medium    | 2.5YR 5/4        | Dull reddish brown | few                |              | 19              | 17              | 64                 | Sandy clay loam |
|           | Bwb1    | 20 - 30       | gradual - smooth                                     | ab+pl                  | coarse    | 2.5YR 2/4        | Reddish            | few                |              | 15              | 19              | 66                 | Sandy loam      |
|           | Bwb2    | 30 - 53       | diffuse - irregular                                  | ab+pl                  | medium    | 2.5YR 5/4        | Dull reddish brown | common             |              | 15              | 18              | 67                 | Sandy loam      |
|           | Bwb3    | 53+           |  |                        | ab+sb     | medium           | 2.5YR 5/4          | Dull reddish brown | many         |                 | 15              | 13                 | 72              |
| <b>P3</b> | ABb     | 0 - 10        | diffuse  | sb+pl                  | fine/thin | 2.5YR 5/4        | Dull reddish brown | common             |              | 12              | 15              | 73                 | Sandy loam      |
|           | Bwb     | 10 - 57       | gradual  | sb+pl                  | medium    | 2.5YR 5/4        | Dull reddish brown | common             |              | 14              | 20              | 66                 | Sandy loam      |
|           | C       | 57+           |  | sb+pl                  | coarse    | 7.5YR 5/3        | Dull               | many               |              | 11              | 10              | 79                 | Sandy loam      |

<sup>1</sup>**Structure type:** ab= angular blocky., sb= subangular blocky., pl= platy. **Size:** vf= very fine/thin., fi= fine/thin., me=medium., co= coarse/thick

### 3.2. Micromorphology

A petrographic analysis reveals that the red layers were formed on a tephra deposit rather than directly on the underlying basalt flow. The parent material is a basaltic lapilli tuff, with hypocrystalline crystallinity and with porphyritic texture, composed of predominantly large ( $> 0.5$  mm) plagioclases, olivines, pyroxenes and smaller ( $< 0.5$  mm) opaque phenocrysts embedded in a dark or orange groundmass. Another common mineral in all samples is a yellowish anisotropic sand-sized clay-body with mosaic-speckled b-fabric, showing second order yellow and red interference colours (Fig. 4).

The pyroclasts fragments of the profiles are very similar, suggesting the same parent material, with the exception of the horizons 2ABb, 2BAb and 3ABb in P1. They have pyroclasts with similar mineralogical composition, but smaller in size than in the overlying horizons and silt-sized quartz becomes more abundant (especially in the 3ABb) confirming the field observations of a lithic discontinuity.

In general, the pyroclastic fragments are moderately to strongly weathered in all profiles, with an upward increasing intensity. Under PPL, they have a blackish or orange groundmass, which becomes dark/ light reddish under OIL due to oxidation of released iron (Fig. 3).

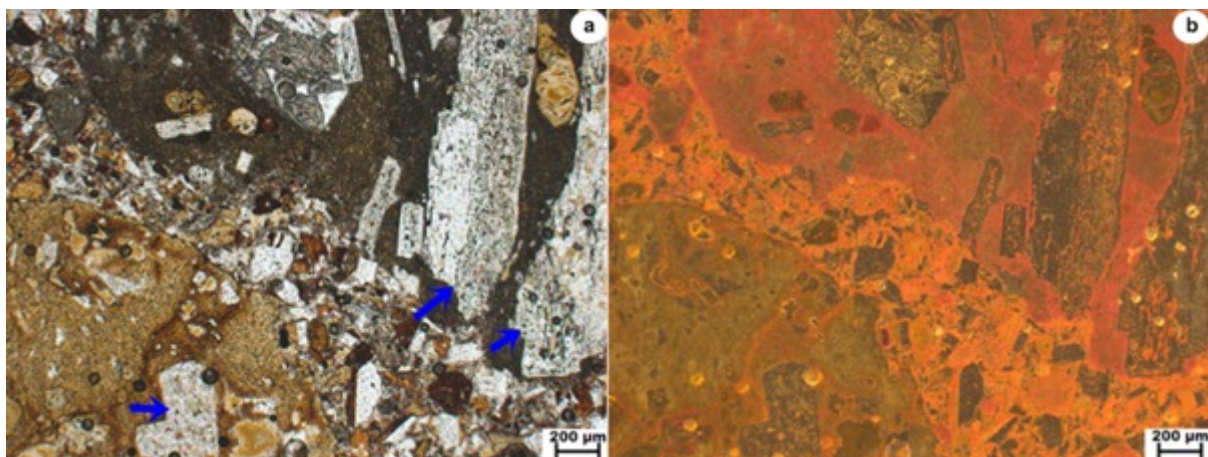


**Figure 3.** Weathered pyroclasts fragments. P1-Bwb3, 45cm. a) under PPL; b) same figure under OIL. Note the strong iron oxide pigmentation and the plagioclase weathering (blue arrows).

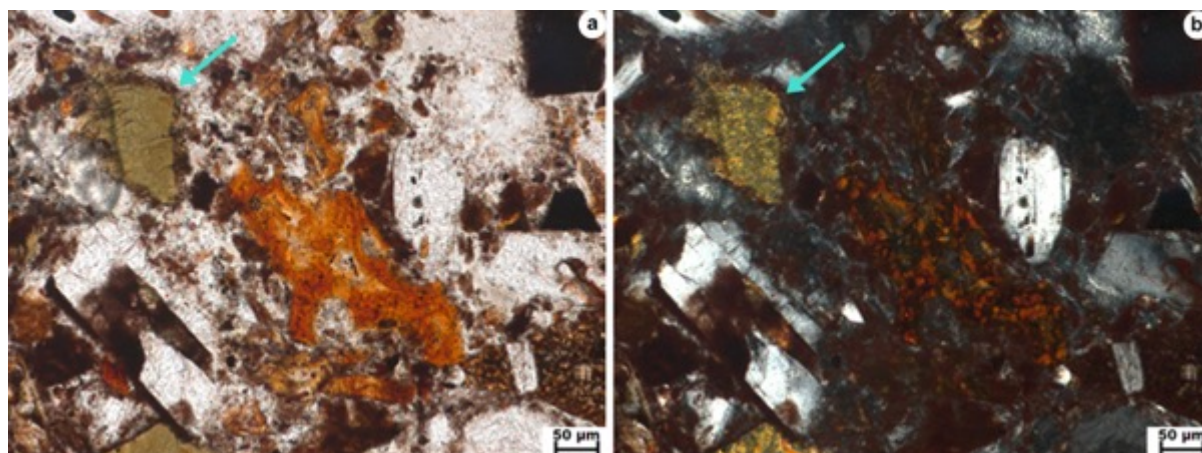


**Figure 4.** Mineral weathering. P2-Bwb1, 30cm. a) a yellowish sand-sized clay-body with mosaic-speckled b-fabric (blue arrow), orange glass fragment at the center of the figure (PPL); b) minerals showing speckled b-fabric due to clay neof ormation, note the preservation of the shape of both alteromorphs (XPL).

The phenocrysts show various degrees of weathering with a stronger alteration upwards in the profiles, with the exception of P1 because of the lithic discontinuity. A pellicular and/or irregular linear alteration of olivine to reddish-brownish alteromorphs. Alteromorphs are the secondary weathering products with shape preservation of the primary mineral, iddingsite (a mixture of iron oxide with phyllosilicates) is one of the most common alteromorph after olivine (Delvigne et al., 1979). Glass shards are abundant in all horizons but less in the 2ABb, 2BAb and 3ABb horizons of the P1. They show a range of colours, such as red, yellow, orange, brown and black. The main observed glass morphology were cusped to platy. Despite their abundance, most of the glass shards are no longer fresh, and therefore considered as alteromorphs. The orange and yellow glasses are often anisotropic (fibro palagonite-like, after Stroncik and Schmincke, 2002) (Fig. 4). Most of the plagioclases are fresh but some reveal a dotted and complex weathering pattern with isotropic brown, black and red clay fillings (Fig. 3). Pyroxenes show generally a dotted weathering pattern with a congruent dissolution. The planar voids, channels (Fig. 5a, b) and vugs are the predominant void types (Table 2). Accommodated to partially accommodated planar voids are most common but unaccommodated planar voids were also observed (Fig. 6). Passage features are present in all horizons, except in P2 (the ABb horizon) and P3 (the Bwb horizon). The occurrences of channels combined with passage features and unaccommodated planar voids is noteworthy, because it points to bioturbation.

**Table 2.** Selected main micromorphological characteristics.

| Profile   | Horizon | Depth<br>[cm] | Pedality |    |    | Voids |     |     |    |    |    | Accomodation |   |    | Microstructure | Micromass      |        |     |          |     | Plant residue | Pedofeatures |    |           | Zeolite |     |   |
|-----------|---------|---------------|----------|----|----|-------|-----|-----|----|----|----|--------------|---|----|----------------|----------------|--------|-----|----------|-----|---------------|--------------|----|-----------|---------|-----|---|
|           |         |               | sp       | mp | wp | spv   | cmv | cxp | ch | cm | ve | vu           | a | pa |                | un             | Colour |     | b-fabric |     |               | cc           | pf | Fe/Mn nod |         |     |   |
|           |         |               |          |    |    |       |     |     |    |    |    |              |   |    |                |                | ppl    | oil | u        | ssp |               | gs           |    |           |         |     |   |
| <b>P1</b> | Bwb1    | 0 - 23        | x        |    |    | x     |     |     | x  | x  |    | x            | x | x  | sb, (gr-cr)    | br, rd, lb, bl | rd     | x   |          |     |               |              |    | x         | x       |     | x |
|           | Bwb2    | 23 - 34       |          |    | x  |       |     |     |    | x  |    |              | x |    | (sb)           | br, rd, lb, bl | rd     | x   |          |     |               |              |    |           | x       |     |   |
|           | Bwb3    | 34 - 45       |          | x  |    |       |     |     | x  |    |    |              | x | x  | sb, (gr)       | br, rd, lb, bl | rd     | x   |          |     |               |              |    |           | x       |     |   |
|           | 2ABb    | 45 - 60       |          |    | x  |       |     |     | x  |    |    |              | x |    | (sb)           | lb, br, rd     | lb, br | x   | (x)      | (x) |               |              | x  |           | x       | x   |   |
|           | 2BAb    | 60 - 73       |          | x  |    |       |     |     |    |    | x  |              | x |    | (gr)           | lb, br, rd     | lb, br | x   | (x)      | (x) |               |              | x  |           | x       | x   |   |
| 3ABb      | 73+     |               |          |    |    |       |     |     |    |    |    |              |   |    | gr, lb, br     | ol, lb         | x      | (x) | (x)      |     |               |              |    | x         | x       |     |   |
| <b>P2</b> | ABb     | 0 - 20        |          | x  |    | x     | x   | x   | x  |    | x  | x            | x | x  | sb, gr         | br, lb, rd, bl | rd     | x   |          |     |               |              | x  |           |         | x   | x |
|           | Bwb1    | 20 - 30       |          | x  |    |       |     |     | x  |    |    | x            | x | x  | sb, (gr-cr)    | br, lb, rd, bl | rd     | x   |          |     |               |              |    |           | x       | x   |   |
|           | Bwb2    | 30 - 53       |          |    | x  |       |     |     | x  |    | x  | x            |   |    | (sb)           | br, lb, rd, bl | rd     | x   |          |     |               |              |    |           | x       | x   |   |
|           | Bwb3    | 53+           |          |    | x  |       |     |     | x  |    |    | x            | x |    | (sb)           | br, lb, rd, bl | rd     | x   |          |     |               |              |    |           | x       | x   |   |
| <b>P3</b> | ABb     | 0 - 10        |          | x  |    |       |     |     | x  |    |    | x            | x | x  | sb             | br, lb, rd, bl | rd     | x   |          | (x) |               |              | x  |           | x       | (x) | x |
|           | Bwb     | 10 - 57       |          |    | x  |       |     |     | x  |    |    | x            | x | x  | sb, (gr-cr)    | br, lb, rd, bl | rd     | x   |          |     |               |              |    |           |         |     |   |

The micromorphological property is shown by the presence (cross) or absence (no cross).

The brackets are used when the property is weakly expressed

**Pedality:** sp=strongly developed pedality., mp=moderately developed., wp=weakly developed

**Voids:** spv= simple packing voids., cmv= compound packing voids., cxp= complex packing voids., ch= channels., cm= chamber., ve= vesicles., vu= vughs

**Accomodation of planar voids:** a= accommodated., pa= partially accommodated., un= unaccommodated

**Microstructure:** sb= subangular., gr= granular., cr= crumb

**Colour:** PPL (Plane Polarized Light); OIL (Oblique Incident Light): rd= red., br= brown., bl= black., lb= light brown., ol= olive, gr= grey

**b-fabric:** u= undifferentiated., ssp= stipple speckled., gs= granostriated

**Pedofeatures:** cc = clay coatings, pf= passage features, Fe/Mn nod = iron/manganese nodules

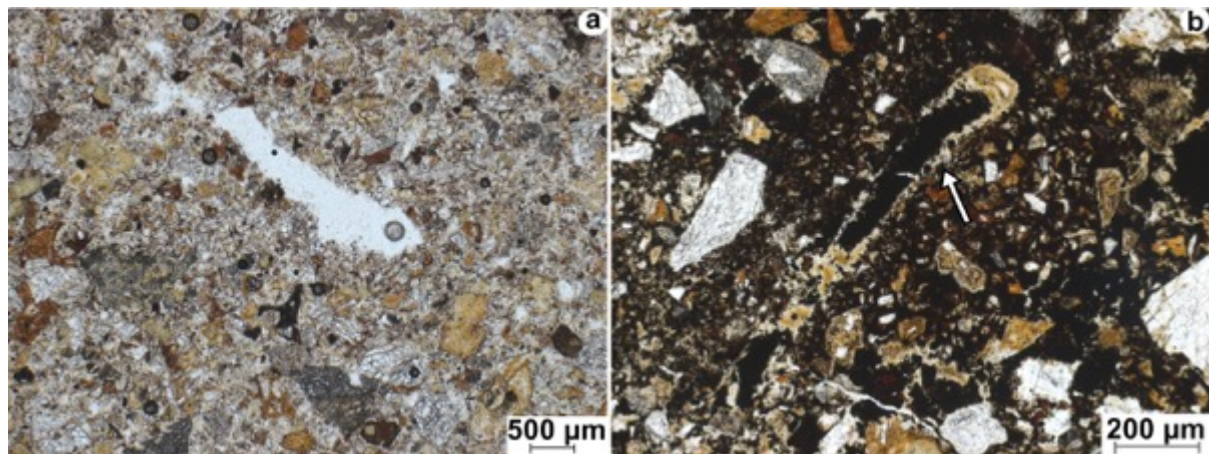


**Figure 5.** Bioturbation voids: a) P1-ABb, 60cm: a channel; b) P1-2BAb, 73cm: a channel (white arrow) filled by Fe/Mn oxide.

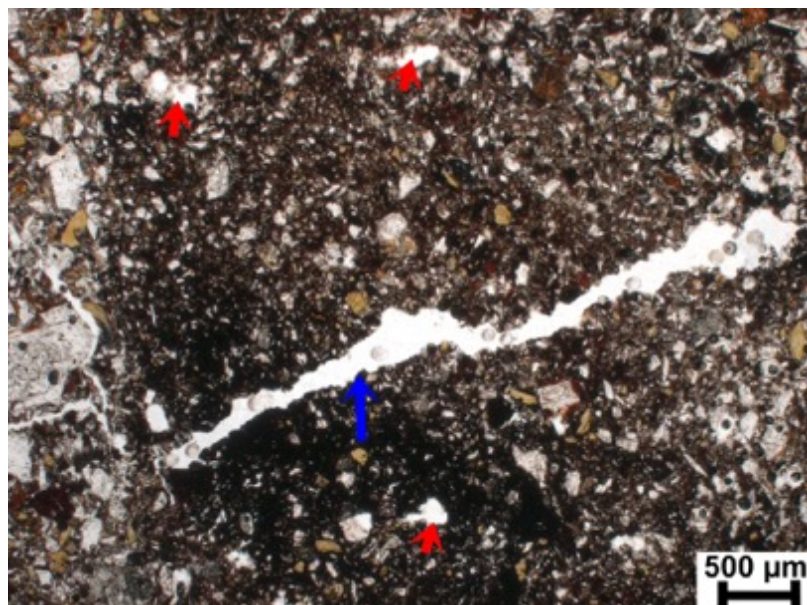


**Figure 6.** Bioturbation voids. P2-Bwb1, 30cm: unaccommodated void (blue arrow) and several channels around (red arrows). Note the void is crossing a moderately impregnated area by Fe/Mn oxides.

Angular, subangular blocky, platy and, less common granular and crumb microstructures are most prominent in all profiles. However, they are not well developed because pedality or planes of weakness are poorly or moderately expressed.

Undifferentiated b-fabric predominantly occurs in all horizons and weakly expressed granostriated and stipple-speckled b-fabrics were detected in the 2ABb, 2BAb and 3ABb horizons of P1 and in the ABb horizon of P3 (Fig. 7a, b).

The colours are heterogeneous in all samples, having a speckled and dotted limpidity under PPL. Under OIL, the reddish colour is predominant in all horizons. Only the

2ABb and 2BAb horizons in P1 have a brown to light brown colour, turning into olive in the 3ABb horizon.

Typical Fe/Mn nodules were noticed in all horizons except in the Bwb1, Bwb2 and Bwb3 horizons of P1. The nodules are orthic or disorthic having disjointed/digitate shapes. In the 2ABb, 2BAb and 3ABb horizons of P1 they are more abundant, more rounded and with sharper boundaries in comparison with those in other horizons (Fig. 7c). Further, they often reveal a granostriated b-fabric with XPL. Dendritic Mn nodules were also detected in the 3ABb horizon of P1. Because of the more gradual boundaries and irregular shape of the nodules in P2 and P3, the difference between nodules to a strongly impregnated feature is not clear (Fig. 7d).

A rare occurrence of yellowish, anisotropic, limpid, and coarse laminated clay coatings was only found in the Bwb1 horizon of P1. On the other hand, clay alteromorphs after glass were common in all samples. Clay infillings with speckled birefringence (not well-oriented clay) in the centre and boundaries with clear extinction bands (well-oriented clay) were detected in all samples, being very abundant in topmost horizon in P1 down to the Bw3b horizon. These infillings are yellowish- brown under PPL (Fig. 7e) in P1 showing yellow interference colours of the second order and speckled b-fabrics under XPL. In the P2 and P3 profiles the infillings have the same properties, but are almost transparent under PPL (Fig. 7f) having first order white with XPL and a speckled b-fabric.

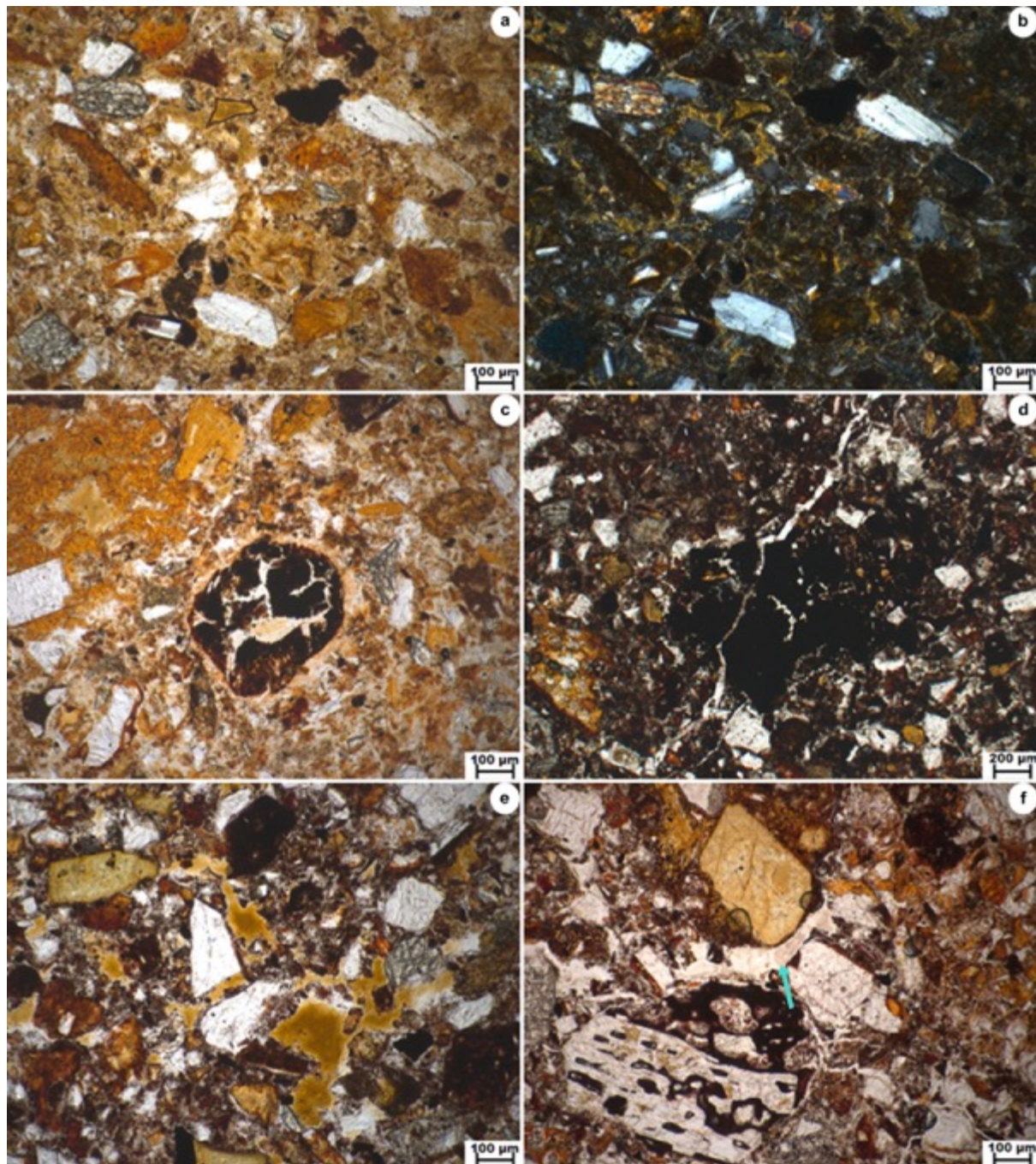


**Figure 7.** Groundmass and pedogenic features: a) P1-2BAb, 70cm: brownish fine mass (PPL); b) granostriated and stipple-speckled b-fabric (XPL); c) P1-2BAb, 70cm: typical disorthic disjointed Mn nodule (PPL); d) P2-Bwb2, 53cm: typical orthic digitate Mn nodule (PPL); e) P1-Bwb3, 45cm: yellowish-orange clay infilling (PPL); f) P2-Bwb2, 53cm: white/grey clay infilling (blue arrow) (PPL).

Plant residues were found in all profiles and particularly in the 2ABb, 2BAb and 3ABb horizons of P1. Organ (mainly roots) and tissue residues with reddish and orange/yellowish colours, probably impregnated by iron oxide (Fig. 8a), were found in the 2ABb and 2BAb horizons. Charcoal was found in the 3ABb horizon (Fig. 8b). Plant residues are scarce in P2 and P3 and were found only in A horizons.



**Figure 8.** Plant residues, under PPL. a) P1-ABb, 60cm: root fragment; b) P1-3ABb, 73+cm: charcoal fragment.

Voids filled with zeolite crystals were detected only in the uppermost horizons of all profiles. This finding corresponds with the field observations; thus, an effect of the covering lava flows has to be considered. Euhedral zeolite crystals occur in the fillings of the uppermost horizons of P1 and P2, whereas anhedral crystals are characteristic for the fillings in the uppermost horizon of P3 (Fig. 9). The induration of the samples can be considered a post-burial feature since it is a homogeneous feature across all horizons.



**Figure 9.** Types of zeolite crystallization in the horizons in contact with the lava flow, under XPL. a) P1- Bwb1, 23cm: euhedral zeolite crystals filling a large void; b) P2-ABb, 20cm: euhedral zeolite crystals filling a large void; c) P3-ABb, 10cm: anhedral zeolite crystals filling a large void.

### 3.3. Chemical and mineralogical properties

TOC and carbonates are present in negligible concentration in all samples (Table 3). The values are slightly higher in the 2ABb horizon of P1 with 0.3% of TOC and 2.6% of  $\text{CaCO}_3$ . This means that the TOC content does not reflect the occurrence of (once) organic material, detected by micromorphology. The source of the  $\text{CaCO}_3$  in the 2ABb horizon was not detected in the thin sections. Therefore, their origin could not be traced.

**Table 3.** Selected chemical characteristics: chemical index of alteration minus K (CIA-K)<sup>1</sup>; ratio of crystalline pedogenic iron oxides; amounts of carbonate ( $\text{CaCO}_3$ ) and total organic carbon (TOC).

| Profile | Horizon | Depth<br>[cm] | CIA-K <sup>1</sup> | $(\text{Fe}_d - \text{Fe}_o) / (\text{Fe}_t) * 100^2$ | CaCO <sub>3</sub> | TOC |
|---------|---------|---------------|--------------------|---|-------------------|-----|
|         |         |               |                    |   | %                 |     |
| P1      | Bwb1    | 0 - 23        | 50                 | 11  | 0,2               | 0,0 |
|         | Bwb2    | 23 - 34       | 53                 | 12  | 0,5               | 0,0 |
|         | Bwb3    | 34 - 45       | 54                 | 15  | 0,6               | 0,0 |
|         | 2ABb    | 45 - 60       | 54                 | 10  | 2,6               | 0,3 |
|         | 2BAb    | 60 - 73       | 56                 | 10  | 0,6               | 0,0 |
|         | 3ABb    | 73+           | 56                 | 5   | 0,6               | 0,1 |
| P2      | ABb     | 0 - 20        | 52                 | 14  | 0,0               | 0,0 |
|         | Bwb1    | 20 - 30       | 52                 | 18  | 0,1               | 0,0 |
|         | Bwb2    | 30 - 53       | 52                 | 14  | 0,1               | 0,0 |
|         | Bwb3    | 53+           | 52                 | 14  | 0,2               | 0,0 |
| P3      | ABb     | 0 - 10        | 52                 | 12  | 0,1               | 0,0 |
|         | Bwb     | 10 - 57       | 53                 | 11  | 0,3               | 0,0 |
|         | C       | 57+           | 50                 | 8   | 0,1               | 0,0 |

<sup>1</sup>after Maynard (1992)

<sup>2</sup>after Arduino et al., (1984)

The CIA-K (wt%) of the major elements is given in supplementary Table 1. Values show weak variations with depth in each profile and between the profiles, with an average value of 51 (Table 3, Fig. 10). P1 is an inverted profile. The lowermost horizon (3ABb) is the most weathered (CIA-K = 56) followed by two overlying horizons 2ABb (CIA-K = 56) and 2BAb (CIA-K = 54), whereas the Bwb1 horizon has a CIA-K of 50. P2 is very homogeneous, showing no variation throughout the profile, with a CIA-K of 52. P3 shows a similar degree of weathering in the ABb (CIA-K = 51) and Bwb (CIA-K = 51) horizons, which are slightly more weathered than the C horizon (CIA-K = 48). The  $Fe_d - Fe_o / Fe_t$  ratio depicts the proportion of crystalline pedogenic iron oxyhydroxides (e.g. hematite or goethite) in relation to total iron ( $Fe_t$ ) (Table 3). There were no measurable nanocrystalline compounds of Fe (e.g. ferrihydrite), which may indicate that all Fe released by weathering from Fe-bearing minerals was converted into crystalline forms. The lack of nanocrystalline Fe oxyhydroxides also indicates that no modern pedogenetic influence took place.

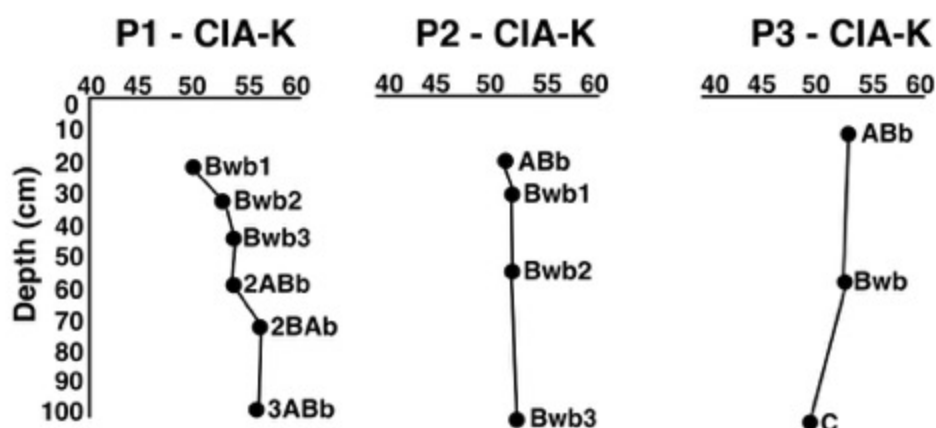


**Figure 10.** Depth function of the CIA-K values.

The content of pedogenic iron shows difference with depth, with values ranging from 5 to 18. In P1, the values increase with depth in the upper three horizons from 11 to 15. The upper LD is marked by a lower ratio of 10 and the second LD by a value 5. The values of 14 in P2 are the highest among the profiles, with a higher concentration in the Bwb1 horizon ( $Fe_d - Fe_o / Fe_t = 18$ ). The ratio in P3 decreases with depth, which may be attributed to undisturbed pedogenesis.

The presence of smectite in the samples was confirmed by a very strong (001) reflection at about  $6^\circ 2\theta$  in the air-dried condition that shifted to about  $5.2^\circ 2\theta$  in the ethylene glycol treated sample and collapsed to  $10 \text{ \AA}$  by heating (Fig. 11). The clay mineralogical composition is rather homogeneous throughout the samples and no primary minerals were identified. No nanocrystalline Al and Si compounds could be extracted by ammonium oxalate method (Supplementary Table 2), indicating these minerals are no longer stable after a long-term burial, probably being converted to crystalline forms.

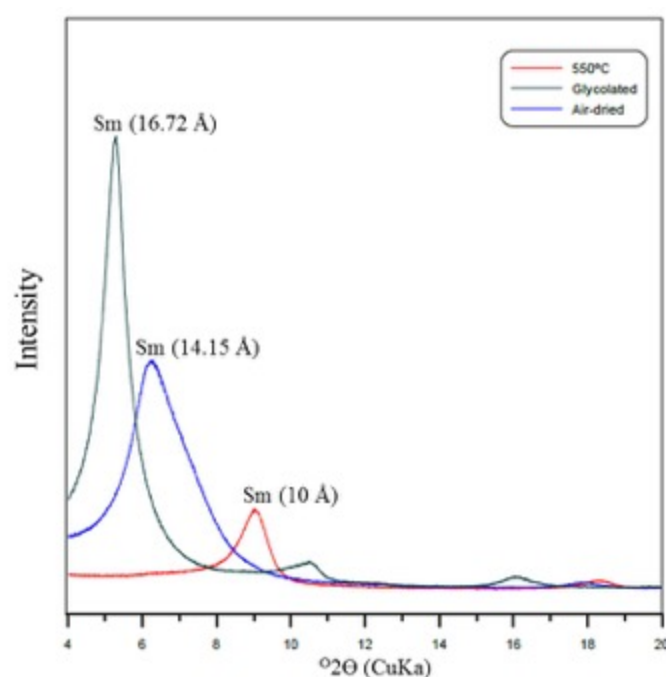


**Figure 11.** X-ray diffraction graph of a representative sample pointing to the presence of smectite (Sm). P1-Bwb2, 34cm. The clay fraction was air-dried oriented, glycolated and heated up to  $550^\circ$ . The other samples show very similar peaks.

## 4. Discussion

### 4.1. Macromorphological and mineralogical properties

The combination of diffuse transitions of colour and changes in structure can be taken as main physical properties indicating pedogenesis (Retallack, 1988). The differences noticed in structure, either shape or size of peds across the horizons of the investigated profiles, can be considered as ample features of pedogenesis (Fenwick, I., 1985).

The predominant blocky and platy structure may point at a finer texture like sandy clay loam. On the other hand (Shoji et al., 1993) published several soil morphological descriptions and textural analyses of volcanic soils, where most of them have at least

one horizon with blocky structure and a lower clay content compared with our results. Thus, we understand that our textural analysis and the structure described in field are not in disagreement, being aware of a possible underestimation of the content clay. The profiles reveal gradual changes of predominantly reddish-brown colours and structure with depth. Although red soils are predominantly found in tropical regions and on land surfaces hundreds of thousands to millions of years old (Blodgett et al., 1993), they can also be formed under well drained conditions even in temperate areas (Schwertmann et al., 1982).

In paleopedology, the interpretation of red colours must be done carefully (Wright, 1992), because one of the most recognized diagenetic effects, especially in pre-Quaternary paleosols, is the burial dehydration of the previously formed iron oxides and hydroxides to hematite, the so-called burial reddening (Retallack, 2001, 1991). However, despite its importance, burial reddening is not ubiquitous. Studies in Paleogene paleosols have dismissed this effect because they detected a juxtaposition of goethite and hematite in the same horizons (Kraus, 1997; PiPujol and Buurman, 1994; Srivastava and Sauer, 2014). Late diagenesis should have transformed goethite into hematite by dehydration.

Another possible post-burial effect known to occur in paleosols covered by basalt flows is the hematization through “fritting” (also called “baking”) of the uppermost horizons (Graef et al., 1997; Singer, 1970; Singer and Ben-Dor, 1987; Solleiro-Rebolledo et al., 2016). However, we ruled out this effect because the horizons directly buried by the lava flow are not redder compared to the horizons below.

Pedogenic processes preceding the volcanic activity (covering by the basalt flow) combined with limited post-burial reddening are to be considered responsible for the colours in the investigated horizons. One evidence for post-burial reddening is the intense red colour despite a moderate and little weathering, as verified by micromorphology and CIA-K, respectively. The role of pedogenic processes is demonstrated by the diffuse transition of the colours between the horizons, a common behavior in soils (Fenwick.I, 1985; Retallack, 1988).

The  $Fe_d - Fe_o / Fe_t$  ratio also supports the combination of pedogenesis with post-burial reddening. The reddish horizons, which have similar colours, display varied  $Fe_d - Fe_o / Fe_t$  ratios. The Bwb1 horizon in P2 for example, with the highest ratio of 18, has a

similar colour compared with the other horizons (hue 2.5YR). This indicates that the iron released during pedogenesis was different among the horizons but they caused almost the same colours. On the other hand, the yellowish horizons 2ABb and 2BAb in P1 have values of 10, which is not much different compared to the reddish horizons. This suggests that the burial reddening did not, or only partly, affect these horizons. Following this rationale, P1-3ABb is gray (5Y 4/1) and have measurable crystalline iron (=5). It means that this horizon was not affected by post-burial reddening. Hence, the paleo pedogenesis also played an important role forming a yellowish/gray colour in these horizons.

#### **4.2. Micromorphological and mineralogical properties**

The occurrence of channels, passage features and unaccommodated voids indicates biological activity in all profiles (Stoops, 2003). Although bioturbation can also occur in e.g. marine/lake sediments (Buurman, 1975), the presence of channels is a useful feature to differentiate paleosols from other materials (Singer, 1970). Moreover, neither sedimentary structures nor features were found, ruling out such a marine or lacustrine paleoenvironment.

We detected a weak granostriated and stipple-speckled b-fabric in the ABb horizon of P3 and in three horizons of P1 (2ABb, 2BAb and 3ABb). These b-fabrics are a signal of wet/dry cycles leading to swelling and shrinking processes, which are related to the presence of 2:1 phyllosilicates (Kovda and Mermut, 2010). However, these b-fabrics are weakly expressed, which may indicate short periods of wet/dry cycles. The simultaneous presence of Fe/Mn nodules without depletion features in the groundmass supports this assumption (Veneman et al., 1976). The occurrence of more concentric nodules in a higher abundance in the 2ABb, 2BAb and 3ABb horizons of P1 suggests multiple wet/dry cycles (Bouma et al., 1990; D'Amore et al., 2004). Further evidence supporting short periods of waterlogging are the better preservation of plant residues and paler colours of these horizons. Altogether, these features point to poorer drainage conditions for the 2ABb, 2BAb and 3ABb horizons in P1 compared to better drainage conditions in the reddish horizons.

The XRD data confirmed the presence of smectite, which could be responsible for the granostriated b-fabrics in some horizons because of its shrinking swelling properties. Smectite and kaolinite were found in other paleosols in that area as well (Birkenmajer and Łydka, 1990). Nonetheless, the origin of 2:1 minerals in volcanic soils is much

debated. They could be of hydrothermal (Dudas and Harward, 1975; Fiore, 1993; A. G. Jongmans et al., 1994; Pevear et al., 1982; Ugolini and Dahlgren, 2002), aeolian (Colman, 1982; Mizota and Takahashi, 1982; Mokma et al., 1972) or pedogenic origin (Berkhaut et al., 1994; McDaniel et al., 1995; Prudencio et al., 2002; Righi et al., 1998; Van der Gaast et al., 1986; Yousefifard et al., 2015). In the volcanic paleosol sequences of central Mexico (e.g. Nevado de Toluca or Teotihuacan) besides the higher amount of kaolinite, smectite has been also detected, related to the pedogenetic processes (Sánchez, 2015; Sedov et al., 2003). Therefore, further studies are necessary to understand the genesis of smectite on these samples.

In this study, different sources of clay minerals were detected by micromorphology. A limpid, laminated, clay coating occurred in the Bwb1 horizon of P1. This kind of morphology is generally associated with translocation processes (Kühn et al., 2010). However, this type of clay coating was infrequently found across the thin section and occurred particularly in former voids filled by zeolites. Since we detected these clay coatings only in a horizon in contact with the overlying basalt flow, a post-burial effect seems to be plausible. Similar clay coatings were described by (Graef et al., 1997) in paleosol horizons directly affected by lava and interpreted as a post-burial feature. The yellow interference colour of these coatings after inserting a retardation plate indicates that the clay particles are oriented perpendicular to the void walls, supporting the evidence for neoformation rather than translocation (Kühn and Pietsch, 2013; Stoops, 2003).

The yellowish clay infilling, which was a very frequent feature in all horizons, is also unlikely to have been effect of illuviation, because it also shows yellow interference colour after inserting a retardation plate (neoformation). However, with our data, is not possible to determine whether this infilling is inherited from the parent material or pedogenic. On the other hand, anisotropic alteromorphs after glass are abundant in all horizons, indicating pedogenic neoformation of phyllosilicates (Gérard et al., 2007). Beyond the other clay types mentioned, the abundant presence of sand-sized clay bodies could be one of the main sources of the 2:1 phyllosilicates. It is most probably an alteromorph after olivine and occurs both in soil and within the pyroclasts fragments. Similar phenomena were described by Jongmans et al. (1994) for an Andosol developed under equatorial climatic conditions and by (Bakker et al., 1996) in a tephra age sequence under a cool temperate climate. Both studies described this

type of clay-body as hydrothermal alteration of the rock fragments (hypogene alteration after Delvigne, 1990).

Another important indicator of a former land surface is the occurrence of plant residues (Sheldon, 2003; Singer, 1970). A few plant residues were detected in the reddish A horizons of P2 and P3, whereas in P1 they frequently occurred in the yellowish 2ABb, 2BAb and in the gray 3ABb horizons. Possible explanations for better preservation and higher abundance of plant residues in these horizons are: (i) these horizons were subject to weaker oxidation processes (i.e. paler colours, Fe/ Mn nodules) than other horizons, implying better plant preservation in the paleosol (McPherson, 1980), (ii) these horizons were buried by new tephra deposits, which is a common feature in volcanic paleosols (Sedov et al., 2010). Since this kind of burial is a rapid process, it leads to good conditions for preservation of plant residues.

### **4.3. Soil forming processes**

Soil forming processes have occurred in all profiles. Evidence for soil horizons formation was seen by differences in colour and structure. The soil colours were formed by brunification, weak redoximorphism and rubification combined with subsequent effect of diagenesis. The formation of soil structure was driven by pedoturbation/bioturbation (Materchera et al., 1992), being an important process visible both on the macroscopic and microscopic scale.

The results of soil forming processes detected by micromorphology were chemical and physical weathering of pyroclasts fragments. This is particularly illustrated by the formation of fine soil material and reddening of the groundmass of pyroclasts. The occurrence of passage features, channels and unaccommodated voids indicates bioturbation. Weak redoximorphic conditions, caused by a perched water table rather than influence of groundwater, gave rise to the Fe/Mn nodules (Veneman et al., 1976). The formation of weak anisotropic b-fabrics (i.e. granostriated and speckled) is an evidence for argilliturbation (Dalrymple and Jim, 1984). Although these two last features indicate repeated wet/dry cycles, none of the samples meet the requirements for Vertisols (IUSS Working Group WRB, 2014).

The presence of weathered volcanic glass suggests that andosolization processes took place (Retallack, 2001; Shoji et al., 1993). This process is characterized by formation of nanocrystalline materials and accumulation of organic matter (Shoji et al.,

1993). However, none of these two processes would still be detectable because of decomposition of organic matter after burial (Retallack, 2001) and the unlikely presence of nanocrystalline minerals (i.e. allophane, imogolite and ferrihydrite) after a long-term burial.

#### **4.4. Diagenetic processes**

The identified diagenetic features were the reddening of oxyhydroxides by dehydration, burial compaction, loss of organic matter and induration. The loss of organic matter is one of the most well-known post-burial effects in paleosols (Retallack, 2001), even for younger paleosols of Pleistocene-Holocene age, the depletion of organic carbon occurs soon after the burial (Dahms, 1994; Holliday, 1988). Zeolite crystals were also considered as a diagenetic feature provoked by the lava deposition. Even though zeolites can be present in natural soils, their occurrence is very rare (Ming and Boettinger, 2001). Zeolite filling voids of the former surficial horizons are an evidence of circulation of hydrothermal fluids with a temperature range of 40° to 250°C (Kristmannsdottir and Tomasson, 1978). García-Romero et al. (2005) described the presence of zeolite fillings in a paleosol buried by a lava flow. Gérard et al. (2007) and Parra et al. (1987) also found infillings of zeolites in red layers between basalt flows. However, in the case of the two last authors cases the zeolites were found throughout the profile, not only in the uppermost horizons as in the present study. Consequently, they attributed a hydrothermal origin to these red layers.

The cause of the induration of the paleosol is not clear so far. Solleiro-Rebolledo et al. (2016) and Singer and Ben-Dor (1987) reported induration of lava-covered paleosols caused by the heating of the lava flow. However, our profiles are homogeneously indurated with depth, thus excluding the heating effect. Another two possible causes for induration in paleosols are cementation of primary porosity and compaction by overburden (Buurman, 1975; Retallack, 2001). Since no cements were detected, compaction by overburden seems more plausible. The lack of a well-structured and open void network seen in the thin section supports this explanation. On the other hand, the compaction effects seem to have been limited, because fragile structures (e.g. plant residues) have their shapes still preserved.

Despite the occurrence of diagenetic processes, they were not intense enough provoke major changes in the paleosols with an exception of the geochemistry, which seems to have been affected, at some extent, by a circulation of hydrothermal fluids

after the lava deposition on the paleosol surface. These fluids can promote a geochemical rejuvenation effect by adding basic cations. The degree of weathering of the samples was below the expected because the average CIA-K values (=51) were lower than for volcanic soils under current periglacial climate in King George Island (average CIA-K = 61 in Lee et al., 2004). In addition, the uppermost horizons of the profiles are less weathered than the others below, which is not a normal pedogenic behaviour (except for arid areas). P1 is an inverted profile, where the lowermost horizon is the most weathered. In this case, the presence of two LD is the explanation. Although zeolite infillings were only found in the horizons in contact with the uppermost lava flow, it seems likely that a rejuvenation and a geochemical homogenization effect by percolation of hydrothermal fluids after the burial has occurred. Another potential geochemical rejuvenation in volcanic soils, which can disturb the weathering indices, is the upbuilding pedogenesis by an eventual addition of fresh volcanic ash (Lowe, 2000; Lowe and Tonkin, 2010; Sedov et al., 2010). Hence, the CIA-K should be used with caution in such circumstances.

## 5. Conclusions

Our results support both our hypotheses, i.e. that: (i) the red layers at the Cytadela area on King George Island are paleosols and (ii) they are suitable proxies for paleoenvironmental reconstruction.

Several features related to soil formation were identified: soil horizons (defined by colour and peds), bioturbation, Fe/Mn nodules, clay neoformation, clay infilling, striated b-fabrics and plant residues. The main andic properties are unlikely to be preserved in these paleosols. Nonetheless, the abundant presence of pyroclastic material, plant residues, Fe/Mn nodules, moderate weathering, lack of carbonates and presence of some yellowish/gray horizons are indicative of a humid temperate environment. Although diagenetic processes were also present (i.e. burial reddening, compaction, loss of organic matter, induration and zeolite infilling) the paleoenvironmental record was still detectable. Another possible diagenetic effect was geochemical rejuvenation and homogenization of the profiles, which compromised the use of CIA-K.

Overall, our findings are in agreement with previous studies (Mozer, 2012; Poole et al., 2003) indicating a humid temperate paleoclimate for King George Island during the Early Eocene. These results are a first step to a detailed understanding of the soil

forming processes of Early Eocene paleosols on Maritime Antarctica.

### **Acknowledgments**

The present work was possible with financial support of the National Counsel of Technological and Scientific Development (CNPq), Brazil. We thank the Brazilian Navy and the colleagues (38. Polska Wyprawa Antarktyczna) from the Henry Arctowski Station for all logistics and much additional support to realize the successful field work during the Antarctic expedition in the summer of 2013/2014. DNS is greatly indebted to Panagiotis Kritikakis (Tübingen University), who helped a lot with the production of the thin sections. We thank Dr. Ann-Kathrin Schatz (University of Tübingen) for comments and proofreading of the manuscript. We also are thankful to the three unknown reviewers for their helpful comments on an earlier version of the manuscript.

## Supplementary data

Supplementary Table 1. Major element data for the paleosols.

| Profile | Horizon | Depth<br>[cm] | [%]              |                  |                                |                                |     |     |     |                   |                  |                               |     |       |
|---------|---------|---------------|------------------|------------------|--------------------------------|--------------------------------|-----|-----|-----|-------------------|------------------|-------------------------------|-----|-------|
|         |         |               | SiO <sub>2</sub> | TiO <sub>2</sub> | Al <sub>2</sub> O <sub>3</sub> | Fe <sub>2</sub> O <sub>3</sub> | MnO | MgO | CaO | Na <sub>2</sub> O | K <sub>2</sub> O | P <sub>2</sub> O <sub>5</sub> | LOI | SUM   |
| P1      | Bwb1    | 0 - 23        | 54,9             | 0,8              | 19,2                           | 8,0                            | 0,2 | 4,4 | 7,4 | 3,4               | 1,0              | 0,3                           | 3,4 | 100,6 |
|         | Bwb2    | 23 - 34       | 55,6             | 0,8              | 19,6                           | 7,9                            | 0,1 | 4,4 | 6,8 | 3,1               | 1,0              | 0,2                           | 3,6 | 100,4 |
|         | Bwb3    | 34 - 45       | 54,7             | 0,8              | 19,6                           | 8,9                            | 0,1 | 4,6 | 6,7 | 3,0               | 1,1              | 0,2                           | 3,9 | 100,4 |
|         | 2ABb    | 45 - 60       | 54,9             | 0,8              | 19,2                           | 8,0                            | 0,2 | 4,6 | 7,3 | 3,3               | 1,2              | 0,2                           | 5,1 | 100,8 |
|         | 2BAb    | 60 - 73       | 55,5             | 0,8              | 20,0                           | 8,4                            | 0,1 | 4,6 | 6,1 | 2,8               | 1,1              | 0,2                           | 4,3 | 100,8 |
|         | 3ABb    | 73+           | 54,3             | 0,8              | 20,1                           | 9,0                            | 0,2 | 4,9 | 6,3 | 2,7               | 1,0              | 0,2                           | 5,0 | 99,9  |
| P2      | ABb     | 0 - 20        | 52,5             | 0,8              | 19,6                           | 10,7                           | 0,1 | 4,6 | 7,2 | 3,4               | 0,5              | 0,2                           | 4,3 | 99,9  |
|         | Bwb1    | 20 - 30       | 54,0             | 0,8              | 20,0                           | 8,8                            | 0,1 | 4,6 | 7,4 | 3,2               | 0,4              | 0,2                           | 4,6 | 100,6 |
|         | Bwb2    | 30 - 53       | 54,0             | 0,8              | 20,2                           | 8,9                            | 0,1 | 4,4 | 7,5 | 3,1               | 0,4              | 0,2                           | 4,3 | 100,6 |
|         | Bwb3    | 53+           | 54,8             | 0,8              | 20,1                           | 8,4                            | 0,1 | 4,3 | 7,3 | 3,2               | 0,4              | 0,2                           | 4,6 | 100,7 |
|         | Basalt  |               | 53,6             | 0,7              | 18,7                           | 7,9                            | 0,2 | 4,8 | 7,6 | 4,1               | 1,8              | 0,2                           | 1,6 | 100,7 |
| P3      | ABb     | 0 - 10        | 55,5             | 0,8              | 19,3                           | 8,5                            | 0,1 | 4,1 | 7,1 | 3,0               | 0,9              | 0,2                           | 4,1 | 99,7  |
|         | Bwb     | 10 - 57       | 55,8             | 0,8              | 19,4                           | 8,1                            | 0,1 | 4,1 | 7,2 | 2,9               | 0,9              | 0,2                           | 3,9 | 99,8  |
|         | C       | 57+           | 53,7             | 0,8              | 19,8                           | 8,1                            | 0,2 | 4,5 | 8,3 | 3,3               | 0,7              | 0,2                           | 2,9 | 99,5  |

**Supplementary Table 2.** Al, Si and Fe extracted by ammonium oxalate.

| <b>Profile</b> | <b>Horizon</b> | <b>Depth<br/>[cm]</b> | <b>Al<sub>o</sub></b> | <b>Si<sub>o</sub><br/>[%]</b> | <b>Fe<sub>o</sub></b> |
|----------------|----------------|-----------------------|-----------------------|-------------------------------|-----------------------|
| <b>P1</b>      | Bwb1           | 0 - 23                | 0,0                   | 0,0                           | 0,0                   |
|                | Bwb2           | 23 - 34               | 0,0                   | 0,0                           | 0,0                   |
|                | Bwb3           | 34 - 45               | 0,0                   | 0,0                           | 0,0                   |
|                | 2ABb           | 45 - 60               | 0,0                   | 0,0                           | 0,0                   |
|                | 2BAb           | 60 - 73               | 0,0                   | 0,0                           | 0,0                   |
|                | 3ABb           | 73+                   | 0,0                   | 0,0                           | 0,0                   |
| <b>P2</b>      | ABb            | 0 - 20                | 0,0                   | 0,0                           | 0,0                   |
|                | Bwb1           | 20 - 30               | 0,0                   | 0,0                           | 0,0                   |
|                | Bwb2           | 30 - 53               | 0,0                   | 0,0                           | 0,0                   |
|                | Bwb3           | 53+                   | 0,0                   | 0,0                           | 0,0                   |
| <b>P3</b>      | ABb            | 0 - 10                | 0,0                   | 0,0                           | 0,0                   |
|                | Bwb            | 10 - 57               | 0,0                   | 0,0                           | 0,0                   |
|                | C              | 57+                   | 0,0                   | 0,0                           | 0,0                   |

**Supplementary Table 3:** Number of standards, standard errors and detection limit for XRF calibration.

| <b>Element</b>                     | <b>Standards<sup>(1)</sup><br/>(n)</b> | <b>Calibration<br/>Standard error</b> | <b>Detection limit<sup>(2)</sup></b> | <b>Covered range of<br/>Standard-<br/>concentrations<sup>(3)</sup></b> |
|------------------------------------|--|---------------------------------------|--------------------------------------|--|
|                                    | 30                                     | ± 0,137%                              | 240 ppm                              | 34,46 – 88,20%   |
| <b>SiO<sub>2</sub></b>             |  |                                       |                                      |  |
| <b>TiO<sub>2</sub></b>             | 31                                     | ± 0,0195%                             | 12 ppm                               | 0,01 – 3,78%   |
| <b>Al<sub>2</sub>O<sub>3</sub></b> | 31                                     | ± 0,230%                              | 244 ppm                              | 0,03 – 59,27%  |
| <b>Fe<sub>2</sub>O<sub>3</sub></b> | 31                                     | ± 0,0569%                             | 180 ppm                              | 0,08 – 25,70%  |
| <b>MnO</b>                         | 22                                     | ± 22 ppm                              | 5,0 ppm                              | 0 – 0,35%  |
| <b>MgO</b>                         | 30                                     | ± 0,141%                              | 88 ppm                               | 0 – 43,51%   |
| <b>CaO</b>                         | 32                                     | ± 0,098%                              | 48 ppm                               | 0,04 – 21,36%  |
| <b>Na<sub>2</sub>O</b>             | 28                                     | ± 0,066%                              | 75 ppm                               | 0,04 – 10,59%  |
| <b>K<sub>2</sub>O</b>              | 31                                     | ± 0,040%                              | 24 ppm                               | 0,01 – 15,35%  |
| <b>P<sub>2</sub>O<sub>5</sub></b>  | 28                                     | ± 0,0087%                             | 14 ppm                               | 0,01 – 1,39%   |

<sup>(1)</sup> number of standards used for calibration.

<sup>(2)</sup> matrix-dependent; may change from sample to sample

<sup>(3)</sup> samples not within this range will be measured again with an internal calibration (independent of concentration). Error and detection limit may be different with each sample.

## References

- Arduino, E., Barberis, E., Carraro, F., Forno, M.G., 1984. Estimating relative ages from Iron-oxide/Total-Iron ratio of soils in the Western Po Valley, Italy. *Geoderma* 33, 39–52.
- Askin, R.A., 1991. Late Cretaceous-Early Tertiary Antarctic outcrop evidence for past vegetation and climates, in: Kennett, J.P., Warnke, D.. (Eds.), *The Antarctic Paleoenvironment: A Perspective on Global Change*. Antarctic Research Series. American Geophysical Union, Washington D.C, pp. 61–73.
- Bakker, L., Lowe, D.J., Jongmans, A.G., 1996. A micromorphological study of pedogenic processes in an evolutionary soil sequence formed on Late Quaternary rhyolitic tephra deposits, North Island, New Zealand. *Quat. Int.* 34–36, 249–261. doi:10.1016/1040-6182(95)00090-9
- Barrett, P., 2008. A History of Antarctic Cenozoic Glaciation - View from the Margin. *Dev. Earth Environ. Sci.* 8, 33–83. doi:10.1016/S1571-9197(08)00003-7
- Barrón, V., Montealegre, L., 1986. Iron Oxides and Colour of Triassic Sediments: Application of the Kubelka-Munk Theory. *Am. J. Sci.* doi:10.2475/ajs.286.10.792
- Berggaut, V., Singer, A., Stahr, K., 1994. Palagonite reconsidered: Paracrystalline illite-smectites from regoliths on basic pyroclastics. *Clays Clay Miner.* 42, 582–592. doi:10.1346/CCMN.1994.0420511
- Bijl, P.K., Schouten, S., Sluijs, A., Reichert, G.-J., Zachos, J.C., Brinkhuis, H., 2009. Early Palaeogene temperature evolution of the southwest Pacific Ocean. *Nature* 461, 776–779. doi:10.1038/nature08399
- Birkenmajer, K., 1988. Tertiary glacial and interglacial deposits, South Shetland Islands, Antarctica: geochronology versus biostratigraphy. *Bull. Polish Acad. Sci. Earth Sci.* 36, 133–145.
- Birkenmajer, K., 1980a. Tertiary volcanic-sedimentary succession at Admiralty Bay, King George Island (South Shetland Islands, Antarctica). *Stud. Geol. Pol.* 64, 7–65.
- Birkenmajer, K., 1980b. Geology of Admiralty Bay, King George Island (South Shetland Islands) — An outline. *Polish Polar Res.* 1, 29–54.
- Birkenmajer, K., Gaździcki, A., Krajewski, K.P., Przybycin, A., Solecki, A., Tatur, A., Yoon, H.I., 2005. First Cenozoic glaciers in West Antarctica. *Polish Polar Res.* 26, 3–12.
- Birkenmajer, K., Łydka, K., 1990. Mineralogical evidence for warm Palaeogene

- climate from the Ezcurra Inlet Group, King George Island, West Antarctica. *Bull. Polish Acad. Sci. Earth Sci.* 38, 25–38.
- Birkenmajer, K., Zastawniak, E., 1989. Late Cretaceous-early Tertiary floras of King George Island, West Antarctica: their stratigraphic distribution and palaeoclimatic significance. *Geol. Soc. London, Spec. Publ.* 47, 227–240. doi:10.1144/GSL.SP.1989.047.01.17
- Blesa, M., Matijević, E., 1989. Phase transformations of iron oxides, oxohydroxides, and hydrous oxides in aqueous media. *Adv. Colloid Interface Sci.* 29, 173–221. doi:10.1016/0001-8686(89)80009-0
- Blodgett, R., Crabaugh, J., McBride, E.F., 1993. The colour of red beds: a geologic perspective, in: Bigham, J.H., Ciolkosz, E. (Eds.), *Soil Colour*. Soil Science Society of America Special Publication, pp. 127–159.
- Borchardt, G., 1989. Smectites, in: Dixon, J., Weed, S. (Eds.), *Minerals in Soil Environments*. Soil Science Society of America, Madison, Wisconsin, pp. 675–727.
- Bouma, J., Fox, C., Miedma, R., 1990. Micromorphology of hydromorphic soils: applications for soil genesis and land evaluation, in: Douglas, L. (Ed.), *Soil Micromorphology: A Basic and Applied Science*. Elsevier, Amsterdam, pp. 257–278.
- Bronger, A., Heinkele, T., 1990. Mineralogical and clay mineralogical aspects of loess research. *Quat. Int.* 7/8, 37–51.
- Buurman, P., 1975. Possibilities of paleopedology. *Sedimentology* 22, 289–298.
- Canile, F.M., 2010. Evidências geológicas de mudanças climáticas (greenhouse-icehouse) na Antártica Ocidental durante a passagem Eoceno-Oligoceno. Universidade Federal de São Paulo.
- Churchman, G.J., Lowe, D., 2012. Alteration, formation, and occurrence of minerals in soils. *Handb. Soil Sci. Prop. Process.* 1, 20–72. doi:doi:10.1201/b11267-24
- Colman, S.M., 1982. Clay mineralogy of weathering rinds and possible implications concerning the sources of clay minerals in soils. *Geology* 10, 370–375.
- Commission Internationale de L'Eclairage, 1978. Recommendations on uniform colour spaces colour difference equations psychometric colour terms, Supplement 2. CIE Publ. 15 (E-1.3.1) 1971/(TC-1.3). Bur. Centrale de la CIE. Paris. Paris.
- Cornell, R.M., Schwertmann, U., 2003. *The Iron Oxides - Structure, properties,*

- reactions, occurrences and uses, 2nd ed. Wiley-VCH Verlag, Weinheim.
- Coxall, H.K., Wilson, P.A., Pälike, H., Lear, C.H., Backman, J., 2005. Rapid stepwise onset of Antarctic glaciation and deeper calcite compensation in the Pacific Ocean. *Nature* 433, 53–57. doi:10.1038/nature03135
- Craig, P., Chevrier, V., Sayyed, M.R.G., Islam, R., 2017. Spectral analysis of Deccan intrabasaltic bole beds: Implications for the formation and alteration of phyllosilicates on Mars. *Planet. Space Sci.* 135, 55–63. doi:10.1016/j.pss.2016.11.008
- D'Amore, D. V., Stewart, S.R., Huddleston, J.H., 2004. Saturation, Reduction, and the Formation of Iron–Manganese Concretions in the Jackson-Frazier Wetland, Oregon. *Soil Sci. Soc. Am. J.* 68, 1012. doi:10.2136/sssaj2004.1012
- Dahms, D., 1994. Mid-holocene erosion of soil catenas on moraines near the type pinedale till, wind river range, Wyoming. *Quat. Res.* 42, 41–48.
- Dalrymple, J.B., Jim, C.Y., 1984. Experimental study of soil microfabrics induced by isotropic stresses of wetting and drying. *Geoderma* 34, 43–68. doi:10.1016/0016-7061(84)90005-3
- Dawit, E.L., 2016. Paleoclimatic records of Late Triassic paleosols from Central Ethiopia. *Palaeogeogr. Palaeoclimatol. Palaeoecol.* 449, 127–140. doi:10.1016/j.palaeo.2016.02.011
- Dearing, J.A., 1999. Environmental Magnetic Susceptibility Using the Bartington MS2 System. *Interpret. A J. Bible Theol.* 52.
- Dearing, J.A., Hay, K.L., Baban, S.M.J., Huddleston, A.S., Wellington, E.M.H., Loveland, P.J., 1996. Magnetic susceptibility of soil: An evaluation of conflicting theories using a national data set. *Geophys. J. Int.* 127, 728–734. doi:10.1111/j.1365-246X.1996.tb04051.x
- DeConto, R.M., Pollard, D., 2003. Rapid Cenozoic glaciation of Antarctica induced by declining atmospheric CO<sub>2</sub>. *Nature* 421, 245–249. doi:10.1038/nature01290
- Delvigne, J., 1998. Atlas of Micromorphology of Mineral Alteration and Weathering, ORSTOM. ed. Mineralogical Association of Canada, Ottawa.
- Delvigne, J., 1990. Hypogene and supergene alteration of orthopyroxene in the Koua Bocca ultra mafic intrusion, Ivory Coast. *Chem. Geol.* 84, 49–53.
- Delvigne, J., Bisdorf, E.B., Sleeman, J., Stoops, G., 1979. Olivines, their pseudomorphs and secondary products. *Pedologie* 3, 247–309.
- DIN ISO 10693, 1995. Bodenbeschaffenheit Bestimmung des Carbonatgehaltes e

- Volumetrisches Verfahren. Beuth, Berlin.
- DIN ISO 10694, 1995. Bodenbeschaffenheit Bestimmung von organischem Kohlenstoff und Gesamtkohlenstoff nach trockener Verbrennung (Elementaranalyse). Beuth, Berlin.
- Dingle, R.V., Lavelle, M., 2000. Antarctic Peninsula Late Cretaceous-Early Cenozoic paleoenvironments and Gondwana paleogeographies. *J. African Earth Sci.* 31, 91–105. doi:10.1016/S0899-5362(00)00075-0
- Dingle, R. V., Lavelle, M., 1998a. Antarctic Peninsular cryosphere: Early Oligocene (c. 30 Ma) initiation and a revised glacial chronology. *J. Geol. Soc. London.* 155, 433–437. doi:10.1144/gsjgs.155.3.0433
- Dingle, R. V., Lavelle, M., 1998b. Late Cretaceous-Cenozoic climatic variations of the northern Antarctic Peninsula: New geochemical evidence and review. *Palaeogeogr. Palaeoclimatol. Palaeoecol.* 141, 215–232. doi:10.1016/S0031-0182(98)00056-X
- Dudas, M.J., Harward, M.E., 1975. Inherited and detrital 2:1 type phyllosilicates in soils developed from Mazama ash. *Soil Sci. Soc. Am. J.* 39, 571–577. doi:10.2136/sssaj1975.03615995003900030050x
- Eberl, D.D., 1984. Clay mineral formation and transformation in rocks and soils. *Philos. Trans. R. Soc. London* 311, 241–257.
- Ehrmann, W.U., Melles, M., Kuhn, G., Grobe, H., 1992. Significance of clay mineral assemblages in the Antarctic Ocean. *Mar. Geol.* 107, 249–273. doi:10.1016/0025-3227(92)90075-S
- Elliot, D.H., Askin, R.A., Kyte, F.T., Zinsmeister, W.J., 1994. Iridium and dinocysts at the Cretaceous-Tertiary boundary on Seymour Island, Antarctica: implications for the K-T event. *Geology* 22, 675–678. doi:10.1130/0091-7613
- Emeleus, C.H., Allwright, E.A., Kerr, A.C., Williamson, I.T., 1996. Red tuffs in the Palaeocene lava successions of the Inner Hebrides. *Scottish J. Geol.* 32, 83–90. doi:10.1144/sjg32010083
- FAO, 2006. Guidelines for soil description, 4th ed. Rome.
- Fedoroff, N., Courty, M.-A., Guo, Z., 2010. Paleosoils and Relict Soils, in: Stoops, G. Marcelino, V. Mees, F. (Ed.), *Interpretation of Micromorphological Features of Soils and Regoliths*. Elsevier, Amsterdam, pp. 623–662. doi:10.1016/B978-0-444-53156-8.00027-1
- Feldmann, R., Woodburne, M., 1988. Geology and paleontology of Seymour Island,

- Antarctic Peninsula. Geological Society of America, Memoir 169.
- Fenwick, I., M., 1985. Paleosols: problems of recognition and interpretation, in: Boardman, J. (Ed.), *Soils and Quaternary Landscape Evolution*. John Wiley and Sons, Norwich, p. 391.
- Fiore, S., 1993. The occurrences of smectite and illite in a pyroclastic deposit prior to weathering: implications on the genesis of 2:1 clay minerals in volcanic soils. *Appl. Clay Sci.* 8, 249–259. doi:10.1016/0169-1317(93)90007-N
- Fiore, S., Huertas, F., Linares, J., 1992. Mineralogy and geochemistry of some “so-called” paleosols from Mt. Vulture volcano (southern Italy). *Chem. Geol.* 99, 237–252. doi:10.1016/0009-2541(92)90179-9
- Fleck, R., Sutter, J., Elliot, D., 1977. Interpretation of discordant  $^{40}\text{Ar}/^{39}\text{Ar}$  age-spectra of Mesozoic tholeiites from Antarctica. *Geochim. Cosmochim. Acta* 41, 15–32.
- Francis, J., Poole, I., 2002. Cretaceous and early Tertiary climates of Antarctica: evidence from fossil wood. *Palaeogeogr. Palaeoclimatol. Palaeoecol.* 182, 47–64.
- Francis, J.E., Ashworth, A., Cantrill, D.J., Crame, J.A., Howe, J., Stephens, R., Tosolini, A.-M., Thorn, V., 2007. 100 Million Years of Antarctic Climate Evolution: Evidence from Fossil Plants. *Proc. 10th Int. Symp. Antarct. Earth Sci.* 19–27. doi:10.3133/of2007-1047.kp03
- Francis, J.E., Marensi, S., Levy, R., Hambrey, M., Thorn, V.C., Mohr, B., Brinkhuis, H., Warnaar, J., Zachos, J., Bohaty, S., DeConto, R., 2009. From Greenhouse to Icehouse - The Eocene/Oligocene in Antarctica. *Dev. Earth Environ. Sci.* 8, 309–368. doi:10.1016/S1571-9197(08)00008-6
- Galán, E., 2006. Genesis of Clay Minerals, in: *Developments in Clay Science*. pp. 1129–1162. doi:10.1016/S1572-4352(05)01042-1
- García-Romero, E., Vegas, J., Baldonado, J.L., Marfil, R., 2005. Clay minerals as alteration products in basaltic volcanoclastic deposits of La Palma (Canary Islands, Spain). *Sediment. Geol.* 174, 237–253. doi:10.1016/j.sedgeo.2004.12.007
- Gérard, M., Caquineau, S., Chenet, A., Fluteau, F., Courtillot, V., Subbarao, K. V., 2006. Red boles in the Deccan traps: time constraints from alteration processes, in: *Geophysical Research Abstracts*. p. 7092.
- Gérard, M., Caquineau, S., Pinheiro, J., Stoops, G., 2007. Weathering and allophane

- neof ormation in soils developed on volcanic ash in the Azores. *Eur. J. Soil Sci.* 58, 496–515. doi:10.1111/j.1365-2389.2007.00910.x
- Ghosh, P., Sayeed, M.R.G., Islam, R., Hundekari, S.M., 2006. Inter-basaltic clay (bole bed) horizons from Deccan traps of India: Implications for palaeo-weathering and palaeo-climate during Deccan volcanism. *Palaeogeogr. Palaeoclimatol. Palaeoecol.* 242, 90–109. doi:10.1016/j.palaeo.2006.05.018
- Gialanella, S., Girardi, F., Ischia, G., Lonardelli, I., Mattarelli, M., Montagna, M., 2010. On the goethite to hematite phase transformation. *J. Therm. Anal. Calorim.* 102, 867–873. doi:10.1007/s10973-010-0756-2
- Graef, F., Singer, A., Stahr, K., Jahn, R., 1997. Genesis and diagenesis of paleosols from Pliocene volcanics on the Golan Heights. *Catena* 30, 149–167. doi:10.1016/S0341-8162(97)00026-X
- Greenwood, D.R., Wing, S.L., 1995. Eocene continental climates and latitudinal temperature gradients. *Geology* 23, 1044–1048.
- Griener, K.W., Nelson, D.M., Warny, S., 2013. Declining moisture availability on the Antarctic Peninsula during the Late Eocene. *Palaeogeogr. Palaeoclimatol. Palaeoecol.* 383–384, 72–78. doi:10.1016/j.palaeo.2013.05.004
- Gualtieri, A.F., Venturelli, P., 1999. In situ study of the goethite-hematite phase transformation by real time synchrotron powder diffraction. *Am. Mineral.* 84, 895–904. doi:10.2138/am-1999-5-624
- Halama, R., Konrad-Schmolke, M., Sudo, M., Marschall, H., Wiedenbeck, M., 2014. Effects of fluid-rock interaction on  $^{40}\text{Ar}/^{39}\text{Ar}$  geochronology in high-pressure rocks (Sesia-Lanzo Zone, Western Alps). *Geochim. Cosmochim. Acta* 126, 475–494.
- Heidari, A., Mahmoodi, S., Stoops, G., Mees, F., 2004. Micromorphological Characteristics of Vertisols of Iran, Including Nonsmectitic Soils. *Arid L. Res. Manag.* 19, 29–46. doi:10.1080/15324980590887164
- Hekinian, R., 1982. *Petrology of the Ocean Floor*, Elsevier O. ed. Elsevier, Amsterdam-Oxford-New York. doi:10.1016/S0422-9894(08)70937-1
- Holliday, V., 1988. Genesis of a late-holocene soil chronosequence at the Lubbock lake archeological site, Texas. *Ann. Assoc. Am. Geogr.* 78, 594–610.
- Huber, M., Brinkhuis, H., Stickley, C.E., Döös, K., Sluijs, A., Warnaar, J., Schellenberg, S.A., Williams, G.L., 2004. Eocene circulation of the Southern Ocean: Was Antarctica kept warm by subtropical waters? *Paleoceanography*

- 19, 1–12. doi:10.1029/2004PA001014
- Hund, F., 1981. Inorganic Pigments: Bases for Coloured, Uncoloured, and Transparent Products. *Angew. Chemie Int. Ed. English* 20, 723–730. doi:10.1002/anie.198107231
- Hunt, R.J., Poole, I., 2003. Paleogene West Antarctic climate and vegetation history in light of new data from King George Island. *Geol. Soc. Am. Spec. Pap.* 369, 395–412. doi:10.1130/0-8137-2369-8.395
- IREN, 1978. Estudio de suelos de la provincia de Valdivia.
- Ishizuka, O., 1998. Vertical and horizontal variation of the fast neutron flux in a single irradiation capsule and their significance in the laser-heating  $^{40}\text{Ar}/^{39}\text{Ar}$  analysis: Case study for the hydraulic rabbit facility of the JMTR reactor, Japan. *Geochem. J* 32, 243–252.
- IUSS Working Group WRB, 2014. World reference base for soil resources 2014. International soil classification system for naming soils and creating legends for soil maps, World Soil Resources Reports No. 106. doi:10.1017/S0014479706394902
- Jeong, G.Y., Yoon, H. II, Lee, S.Y., 2004. Chemistry and microstructures of clay particles in smectite-rich shelf sediments, South Shetland Islands, Antarctica. *Mar. Geol.* 209, 19–30. doi:10.1016/j.margeo.2004.05.027
- Jiang, L., Chen, G., Grapes, R., Peng, Z., 2015. Journal of Asian Earth Sciences Thermal origin of continental red beds in SE China : An experiment study. *J. Asian Earth Sci.* 101, 14–19. doi:10.1016/j.jseaes.2015.01.019
- Jongmans, A.G., Nieuwenhuysse, A., Buurman, P., van Doesburg, J.D.J., van Oort, F., Jaunet, A.M., 1994. Inheritance of 2:1 phyllosilicates in Costa Rican Andisols. *Soil Sci. Soc. Am. J.* 58, 494–501. doi:10.2136/sssaj1994.03615995005800020035x
- Jongmans, a. G., Nieuwenhuysse, a., Buurman, P., van Doesburg, J.D.J., van Oort, F., Jaunet, a. M., 1994. Inheritance of 2:1 Phyllosilicates in Costa Rican Andisols. *Soil Sci. Soc. Am. J.* 58, 494. doi:10.2136/sssaj1994.03615995005800020035x
- Kovda, I., Mermut, A.R., 2010. Vertic Features, in: Stoops, G., Marcelino, V., Mees, F. (Eds.), *Interpretation of Micromorphological Features of Soils and Regoliths*. Elsevier, Amsterdam, pp. 109–122. doi:10.1016/B978-0-444-53156-8.00013-1
- Kraus, M.J., 1997. Lower Eocene alluvial paleosols: Pedogenic development,

- stratigraphic relationships, and paleosol/landscape associations. *Palaeogeogr. Palaeoclimatol. Palaeoecol.* 129, 387–406. doi:10.1016/S0031-0182(96)00056-9
- Kraus, M.J., Hasiotis, S.T., 2006. Significance of different modes of rhizolith preservation to interpreting paleoenvironmental and paleohydrologic settings: Examples from Paleogene paleosols, Birghorn Basin, Wyoming, U.S.A. *J. Sediment. Res.* 76, 633–646. doi:10.2110/jsr.2006.052
- Kristmannsdottir, H., Tomasson, J., 1978. Zeolite zones in geothermal areas of Iceland, in: Sand, L.B., Mumpton, F.M. (Eds.), *Natural Zeolite Occurrence, Properties and Use*. Pergamon Press, Oxford, pp. 277–284.
- Kühn, P., Aguilar, J., Miedma, R., 2010. Textural features and their related horizons, in: Stoops, G., Marcelino, V., Mees, F. (Ed.), *Micromorphological Features of Soils and Regoliths. Their Relevance for Pedogenic Studies and Classifications*. Elsevier B.V., pp. 217–250. doi:10.1016/B978-0-444-53156-8.00011-8
- Kühn, P., Pietsch, D., 2013. Soil micromorphogenesis and Early Holocene paleoclimate at the desert margin of Southern Arabia 3, 59–77. doi:10.3232/SJSS.2013.V3.N2.04
- Kühn, P., Techmer, A., Weidenfeller, M., 2013. Lower to middle Weichselian pedogenesis and palaeoclimate in Central Europe using combined micromorphology and geochemistry: The loess-paleosol sequence of Alsheim (Mainz Basin, Germany). *Quat. Sci. Rev.* 75, 43–58. doi:10.1016/j.quascirev.2013.05.019
- Lange, F.M., Frick, C., Stahr, K., Graef, F., Singer, A., 2002a. Fritted Paleosols as Indicators for the Local Paleoclimate - Examples from the Golan Heights. *Die Erde* 133, 259–274.
- Lange, F.M., Frick, C., Stahr, K., Graef, F., Singer, A., 2002b. Fritted paleosols as indicators for the local paleoclimate - examples from the Golan Heights. *Die Erde* 133, 259–274.
- Lanson, B., 1997. Decomposition of experimental x-ray diffraction patterns (profile fitting): A convenient way to study clay minerals. *Clays Clay Miner.* 45, 132–146. doi:10.1346/CCMN.1997.0450202
- Lee, Y. II, Lim, H.S., Yoon, H. II, 2004. Geochemistry of soils of King George Island, South Shetland Islands, West Antarctica: Implications for pedogenesis in cold polar regions. *Geochim. Cosmochim. Acta* 68, 4319–4333.

doi:10.1016/j.gca.2004.01.020

Lessovaia, S.N., Plötze, M., Inozemzev, S., Goryachkin, S., 2016. Traprock transformation into clayey materials in soil environments of the central Siberian plateau, Russia. *Clays Clay Miner.* 64, 668–676.

doi:10.1346/CCMN.2016.064042

Lowe, D.J., 2000. Upbuilding pedogenesis in multisequal tephra- derived soils in the Waikato region, in: Adams, J., Metherell, A. (Eds.), *Soil 200: New Horizons for a New Century. Australian and New Zealand Second Joint Soils Conference Volume 2: Lincoln University. New Zealand Society of Soil Science*, pp. 183–184.

Lowe, D.J., Tonkin, P.J., 2010. Unravelling upbuilding pedogenesis in tephra and loess sequences in New Zealand using tephrochronology, in: Gilkes, R.J., Prakongkep, N. (Eds.), *Proceedings of the 19th World Congress of Soil Science “Soil Solutions for a Changing World” (1-6 Aug., 2010, Brisbane), Symposium 1.3.2 Geochronological Techniques and Soil Formation. Brisbane*, pp. 34–37.

Lu, S.G., Xue, Q.F., Zhu, L., Yu, J.Y., 2008. Mineral magnetic properties of a weathering sequence of soils derived from basalt in Eastern China. *Catena* 73, 23–33. doi:10.1016/j.catena.2007.08.004

Luque, E., 2008. *Propiedades magnéticas de los óxidos de hierro en suelos mediterráneos. Universidad de Córdoba.*

Mackensen, A., Ehrmann, W.U., 1992. Middle Eocene through Early Oligocene climate history and paleoceanography in the Southern Ocean: Stable oxygen and carbon isotopes from ODP Sites on Maud Rise and Kerguelen Plateau. *Mar. Geol.* 108, 1–27. doi:10.1016/0025-3227(92)90210-9

Maher, B., 1986. Characterisation of soils by mineralmagnetic measurements. *Phys. Earth Planet. Inter.* 42, 76–92. doi:10.1016/S0031-9201(86)80010-3

Mansilla, H.G., De Valais, S., Stinnesbeck, W., Varela, N.A., Leppe, M.A., 2012. New Avian tracks from the lower to middle Eocene at Fossil Hill, King George Island, Antarctica. *Antarct. Sci.* 24, 500–506. doi:10.1017/S0954102012000260

Mansilla, H.G., Stinnesbeck, W., Varela, N., Leppe, M., 2013. Eocene fossil feather from King George Island, South Shetland Islands, Antarctica. *Antarct. Sci.* 26, 384–388. doi:10.1017/S0954102013000771

Marques, R., Prudêncio, M.I., Waerenborgh, J.C., Rocha, F., Dias, M.I., Ruiz, F., Ferreira, E.S., Abad, M., Muñoz, A.M., 2014. Origin of reddening in a paleosol

- buried by lava flows in Fogo island (Cape Verde). *J. African Earth Sci.* 96, 60–70. doi:10.1016/j.jafrearsci.2014.03.019
- Materechera, S.A., Dexter, A.R., Alston, A.M., 1992. Formation of aggregates by plant roots in homogenised soils. *Plant Soil* 142, 69–79. doi:10.1007/BF00010176
- Maynard, J.B., 1992. Chemistry of modern soils as a guide to interpreting Precambrian paleosols. *J. Geol.* 100, 279–289.
- McDaniel, P.A., Falen, A.L., Tice, K.R., Graham, R.C., Fendorf, S.E., 1995. Beidellite in e horizons of Northern Idaho spodosols formed in Volcanic ash. *Clays Clay Miner.* 43, 525–532. doi:10.1346/CCMN.1995.0430502
- McPherson, J., 1980. Genesis of variegated redbeds in the fluvial Aztec siltstone (Late Devonian), Southern Victoria Land, Antarctica. *Sediment. Geol.* 27.
- Mehra, O.P., Jackson, M.L., 1960. Iron Oxide Removal from Soils and Clays by a Dithionite-Citrate System Buffered with Sodium Bicarbonate. *Clays Clay Miner.* 7, 317–327. doi:10.1346/CCMN.1958.0070122
- Ming, D.W., Boettinger, J.L., 2001. Zeolites in Soil Environments. *Rev. Mineral. Geochemistry* 45, 323–345. doi:10.2138/rmg.2001.45.11
- Mirabella, A., Egli, M., Raimondi, S., Giaccari, D., 2005. Origin of clay minerals in soils on pyroclastic deposits in the Island of Lipari (Italy). *Clays Clay Miner.* 53, 409–421. doi:10.1346/CCMN.2005.0530409
- Mizota, C., Takahashi, Y., 1982. Eolian origin of quartz and mica in soils developed on basalts in northwestern Kyushu and San-in, Japan. *Soil Sci. Plant Nutr.* 28, 369–378. doi:10.1080/00380768.1982.10433652
- Mokma, D., Syers, J., Jackson, M., Clayton, R., Rex, R., 1972. Eolian additions to soils and sediments in the South Pacific area. *J. Soil Sci.* 23, 147–162.
- Moore, D., Reynolds Jr, R., 1997. *X-ray Diffraction and the Identification of Clay Minerals*, 2nd ed. Oxford University.
- Mozer, A., 2012. Pre-glacial sedimentary facies of the Point Thomas Formation (Eocene) at Cytadela, Admiralty Bay, King George Island, West Antarctica. *Polish Polar Res.* 33, 41–62. doi:10.2478/v10183-012-0002-7
- Müller, H., Schwaighofer, B., 1979. Frittung oder tertiäre Verwitterung — Zur Frage der Rotfärbung in den tertiären Liegendsedimenten des Basalts von Stoob (Burgenland, Österreich). *Verh.Geol.B.-A* 2, 133–160.
- Nahon, D., Colin, F., Tardy, Y., 1982. Formation and distribution of Mg,Fe,Mn-

- smectites in the first stages of the lateritic weathering of forsterite and tephroite. *Clay Miner.* 17, 339–348. doi:10.1180/claymin.1982.017.3.06
- Nawrocki, J., Pańczyk, M., Williams, I.S., 2011. Isotopic ages of selected magmatic rocks from King George Island (West Antarctica) controlled by magnetostratigraphy. *Geol. Q.* 55, 301–322.
- NRCS, 1996. Soil Survey Laboratory Methods Manual 716. doi:10.1021/ol049448l
- Ollier, C., 1965. Some features of granite weathering in Australia. *Zeitschrift für Geomorphol.* 9, 285–304.
- Pagani, M., Zachos, J.C., Freeman, K.H., Tripple, B., Bohaty, S., 2005. Marked decline in Atmospheric Carbon Dioxide Concentrations during the Paleocene. *Science* (80-. ). 309, 600–603. doi:10.1126/science.1110063
- Parra, M., Delmont, P., Dumon, J.C., Ferragne, A., Pons, J.C., 1987. Mineralogy and origin of Tertiary interbasaltic clays from the Faeroe island, Northeastern Atlantic. *Clay Miner.* 22, 63–82.
- Pearson, P.N., Foster, G.L., Wade, B.S., 2009. Atmospheric carbon dioxide through the Eocene–Oligocene climate transition. *Nature* 461, 1110–1113. doi:10.1038/nature08447
- Pearson, P.N., Palmer, M.R., 2000. Atmospheric carbon dioxide concentrations over the past 60 million years. *Nature* 406, 695–699. doi:10.1038/35021000
- Pevear, D., Dethier, D., Frank, D., 1982. Clay minerals in the 1980 deposits from Mount St. Helens. *Clays Clay Miner.* 30, 241–252. doi:10.1346/CCMN.1982.0300401
- Pietsch, D., Kühn, P., 2012. Early Holocene paleosols at the southwestern Ramlat As-Sab'atayn desert margin: New climate proxies for southern Arabia. *Palaeogeogr. Palaeoclimatol. Palaeoecol.* 365–366, 154–165. doi:10.1016/j.palaeo.2012.09.023
- PiPujol, M.D., Buurman, P., 1994. The distinction between ground-water gley and surface-water gley phenomena in Tertiary paleosols of the Ebro basin, NE Spain. *Palaeogeogr. Palaeoclimatol. Palaeoecol.* 110, 103–113. doi:10.1016/0031-0182(94)90112-0
- Poole, I., Cantrill, D., Utescher, T., 2005. A multi-proxy approach to determine Antarctic terrestrial palaeoclimate during the Late Cretaceous and Early Tertiary. *Palaeogeogr. Palaeoclimatol. Palaeoecol.* 222, 95–121. doi:10.1016/j.palaeo.2005.03.011

- Poole, I., Hunt, R.J., Cantrill, D.J., 2001. A fossil wood flora from King George Island: ecological implications for an Antarctic Eocene vegetation. *Ann. Bot.* 88, 33–54. doi:10.1006/anbo.2001.1425
- Poole, I., Mennega, A.M.W., Cantrill, D.J., 2003. Valdivian ecosystems in the Late Cretaceous and Early Tertiary of Antarctica: Further evidence from myrtaceous and eucryphiaceous fossil wood. *Rev. Palaeobot. Palynol.* 124, 9–27. doi:10.1016/S0034-6667(02)00244-0
- Porter, D.A., McCahont, T., Ransom, M.D., 1998. Differentiating pedogenic and diagenetic properties in a Cretaceous paleosol in Kansas. *Quat. Int.* 51/52, 35–54.
- Preetz, H., Igel, J., Hannam, J.A., Stadler, S., 2017. Relationship between magnetic properties and reddening of tropical soils as indicators of weathering. *Geoderma* 303, 143–149. doi:10.1016/j.geoderma.2017.05.007
- Pross, J., Contreras, L., Bijl, P.K., Greenwood, D.R., Bohaty, S.M., Schouten, S., Bendle, J. a, Röhl, U., Tauxe, L., Raine, J.I., Huck, C.E., van de Flierdt, T., Jamieson, S.S.R., Stickley, C.E., van de Schootbrugge, B., Escutia, C., Brinkhuis, H., 2012. Persistent near-tropical warmth on the Antarctic continent during the early Eocene epoch. *Nature* 488, 73–7. doi:10.1038/nature11300
- Prudencio, M.I., Sequeira Braga, M.A., Paquet, H., Waerenborgh, J.C., Pereira, L.C.J., Gouveia, M.A., 2002. Clay mineral assemblages in weathered basalt profiles from central and southern Portugal: Climatic significance. *Catena* 49, 77–89. doi:10.1016/S0341-8162(02)00018-8
- Rasmussen, C., Dahlgren, R. a., Southard, R.J., 2010. Basalt weathering and pedogenesis across an environmental gradient in the southern Cascade Range, California, USA. *Geoderma* 154, 473–485. doi:10.1016/j.geoderma.2009.05.019
- Rasmussen, C., Matsuyama, N., Dahlgren, R.A., Southard, R.J., Brauer, N., 2007. Soil genesis and mineral transformation across an environmental gradient on andesitic lahar. *Soil Sci. Soc. Am.* 71, 225–237.
- Reguero, M.A., Marensi, S.A., Santillana, S.N., 2002. Antarctic Peninsula and South America (Patagonia)\nPaleogene terrestrial faunas and environments: biogeographic\nrelationships. *Palaeogeogr. Palaeoclimatol. Palaeoecol.* 2776, 1–22.
- Retallack, G.J., 2001. *Soils of the Past: An Introduction to Paleopedology*, second. ed. Blackwell Science, United Kingdom. doi:10.1002/9780470698716

- Retallack, G.J., 1991. Untangling the effects of burial alteration and ancient soil formation. *Annu. Rev. Earth Planet. Sci.* 19, 183–206.  
doi:10.1146/annurev.earth.19.1.183
- Retallack, G.J., 1988. Field recognition of paleosols. *Geol. Soc. Am. Spec. Pap.* 1–20. doi:10.1130/SPE216-p1
- Righi, D., Terribile, F., Petit, S., 1998. Pedogenic formation of high-charge beidellite in a Vertisol of Sardinia (Italy). *Clays Clay Miner.* 46, 167–177.  
doi:10.1346/CCMN.1998.0460207
- Rivas, J., Ortega, B., Sedov, S., Solleiro, E., Sychera, S., 2006. Rock magnetism and pedogenetic processes in Luvisol profiles: Examples from Central Russia and Central Mexico. *Quat. Int.* 156–157, 212–223.  
doi:10.1016/j.quaint.2006.05.007
- Robert, C., Kennett, J.P., 1997. Antarctic continental weathering changes during Eocene-Oligocene cryosphere expansion: Clay mineral and oxygen isotope evidence. *Geology* 25, 587–590. doi:10.1130/0091-7613
- Sánchez, S., 2015. Los paleosuelos “negros” como indicadores de cambios ambientales naturales e inducidos por el hombre en el periodo de ocupacion teotihuacano. UNAM.
- Sayyed, M.R.G., Pardeshi, R.G., Islam, R., 2014. Palaeoweathering characteristics of an intrabasaltic red bole of the Deccan Flood Basalts near Shrivardhan of western coast of India. *J. Earth Syst. Sci.* 1717–1728. doi:10.1007/s12040-014-0481-5
- Schatz, A.-K., Scholten, T., Kühn, P., 2015. Paleoclimate and weathering of the Tokaj (Hungary) loess–paleosol sequence. *Palaeogeogr. Palaeoclimatol. Palaeoecol.* 426, 170–182. doi:10.1016/j.palaeo.2015.03.016
- Scheinost, A., Chavernas, A., Barrón, V., Torrent, J., 1998. Use and limitations of second-derivative diffuse reflectance spectroscopy in the visible to near-infrared range to identify and quantify Fe oxide minerals in soils. *Clays Clay Miner.* 46, 528–536.
- Schulze, D., 1981. Identification of soil iron oxide minerals by Differential X-ray Diffraction. *Soil Sci. Soc. Am. J.* 45, 437–440.
- Schwertmann, U., 1964. Differenzierung der Eisenoxide des Bodens durch Extraktion mit Ammoniumoxalat-Lösung. *J. Plant Nutr. Soil Sci.* 105, 194–202.
- Schwertmann, U., Fechter, H., 1984. The Influence of aluminum on iron oxides: XI.

- Aluminum-substituted maghemite in soils and its formation. *Soil Sci. Soc. Am.* 48, 1462–1463. doi:10.2136/sssaj1984.03615995004800060054x
- Schwertmann, U., Friedl, J., Stanjek, H., 1999. From Fe(III) ions to Ferrihydrite and then to Hematite. *J. Colloid Interface Sci.* 209, 215–223.  
doi:10.1006/jcis.1998.5899
- Schwertmann, U., Murad, E., Schulze, D.G., 1982. Is there Holocene reddening (hematite formation) in soils of axeric temperate areas? *Geoderma* 27, 209–223.
- Schwertmann, U., Taylor, R., 1989. Iron Oxides, in: Dixon, J., Weed, S. (Eds.), *Minerals in Soil Environments*. Soil Science Society of America, Madison, Wisconsin, pp. 379–438.
- Sedov, S., Solleiro-Rebolledo, E., Morales-Puente, P., Arias-Herreia, A., Vallejo-Gomez, E., Jasso-Castaneda, C., 2003. Mineral and organic components of the buried paleosols of the Nevado de Toluca, Central Mexico as indicators of paleoenvironments and soil evolution. *Quat. Int.* 106–107, 169–184.  
doi:10.1016/S1040-6182(02)00171-4
- Sedov, S., Stoops, G., Shoba, S., 2010. Regoliths and Soils on Volcanic Ash, in: Stoops, G., Marcelino, V., Mees, F. (Ed.), *Interpretation of Micromorphological Features of Soils and Regoliths*. Elsevier, Amsterdam, pp. 275–303.  
doi:10.1016/B978-0-444-53156-8.00013-1
- Sheldon, N.D., 2005. Do red beds indicate paleoclimatic conditions? A Permian case study. *Palaeogeogr. Palaeoclimatol. Palaeoecol.* 228, 305–319.  
doi:10.1016/j.palaeo.2005.06.009
- Sheldon, N.D., 2003. Pedogenesis and geochemical alteration of the Pacific Gorge subgroup Columbia River basalt, Oregon. *Bull. Geol. Soc. Am.* 115, 1377–1387.  
doi:10.1130/B25223.1
- Sheldon, N.D., Retallack, G.J., 2004. Regional paleoprecipitation records from the Late Eocene and Oligocene of North America. *J. Geol.* 112, 487–494.  
doi:10.1086/421076
- Sheldon, N.D., Tabor, N.J., 2009. Quantitative paleoenvironmental and paleoclimatic reconstruction using paleosols. *Earth-Science Rev.* 95, 1–52.  
doi:10.1016/j.earscirev.2009.03.004
- Shoji, S., Nanzyo, M., Dahlgren, R.A., 1993. *Volcanic ash soils - Genesis, properties and utilization*, Statewide Agricultural Land Use Baseline 2015. Elsevier Science, Amsterdam.

- Shukla, A.D., Ray, D., Pande, K., Shukla, P.N., 2014. Formation of paleosol (fossil soil) in Deccan continental flood basalt: alteration style and implications towards aqueous environments of early mars, in: Eighth International Conference on Mars. Pasadena, California, p. 1194.
- Singer, A., 1980. The palaeoclimate interpretation of clay minerals in soil and weathering profiles. *Earth-Science Rev.* 15, 303–326.
- Singer, A., 1970. Edaphoids and paleosols of basaltic origin in The Galilee, Israel. *J. Soil Sci.* 21.
- Singer, A., Ben-Dor, E., 1987. Origin of red clay layers interbedded with basalts of the Golan Heights. *Geoderma* 39, 293–306. doi:10.1016/0016-7061(87)90049-8
- Singer, A., Navrot, J., 1977. Clay formation from basic volcanic rocks in a humid Mediterranean climate. *Soil Sci. Soc. Am. J.* 41, 645–650.
- Solleiro-Rebolledo, E., Straubinger, M., Terhorst, B., Sedov, S., Ibarra, G., Sánchez-Alaniz, J.I., Solanes, M.C., Marmolejo, E., 2016. Paleosols beneath a lava flow in the southern basin of Mexico: The effect of heat on the paleopedological record. *Catena* 137, 622–634. doi:10.1016/j.catena.2014.12.002
- Spinola, D.N., Pi-Puig, T., Solleiro-Rebolledo, E., Egli, M., Sudo, M., Sedov, S., Kühn, P., 2017a. Origin of clay minerals in Early Eocene volcanic paleosols on King George Island, Maritime Antarctica. *Sci. Rep.* doi:10.1038/s41598-017-06617-x
- Spinola, D.N., Portes, R. de C., Schaefer, C.E.G.R., Solleiro-Rebolledo, E., Pi-Puig, T., Kühn, P., 2017b. Eocene paleosols on King George Island, Maritime Antarctica: Macromorphology, micromorphology and mineralogy. *Catena*. doi:10.1016/j.catena.2017.01.004
- Srivastava, P., Sangode, S.J., Meshram, D.C., Gudadhe, S.S., Nagaraju, E., Kumar, A., Venkateshwarlu, M., 2012. Paleoweathering and depositional conditions in the inter-flow sediment units (bole beds) of Deccan Volcanic Province, India: A mineral magnetic approach. *Geoderma* 177–178, 90–109. doi:10.1016/j.geoderma.2012.01.034
- Srivastava, P., Sangode, S.J., Torrent, J., 2015. Mineral magnetic and diffuse reflectance spectroscopy characteristics of the Deccan volcanic bole beds : Implications to genesis and transformations of iron oxides. *Geoderma* 239–240, 317–330. doi:10.1016/j.geoderma.2014.11.010
- Srivastava, P., Sauer, D., 2014. Thin-section analysis of lithified paleosols from

- Dagshai Formation of the Himalayan Foreland: Identification of paleopedogenic features and diagenetic overprinting and implications for paleoenvironmental reconstruction. *Catena* 112, 86–98. doi:10.1016/j.catena.2013.08.008
- Steiger, R., Jäger, E., 1977. Subcommittee on geochronology: convention on the use of decay constants in geo- and cosmochronology. *Earth Planet. Sci. Lett.* 36, 359–362.
- Stickley, C.E., Brinkhuis, H., Schellenberg, S.A., Sluijs, A., Röhl, U., Fuller, M., Grauert, M., Huber, M., Warnaar, J., Williams, G.L., 2004. Timing and nature of the deepening of the Tasmanian Gateway. *Paleoceanography* 19, 1–18. doi:10.1029/2004PA001022
- Stoops, G., 2003. *Guidelines for Analysis and Description of Soil and Regolith Thin Sections*. Soil Science Society of America, Madison, Wisconsin.
- Stronck, N.A., Schmincke, H.U., 2002. Palagonite - A review. *Int. J. Earth Sci.* 91, 680–697. doi:10.1007/s00531-001-0238-7
- Torrent, J., Barrón, V., 2002. Diffuse reflectance spectroscopy of iron oxides. *Encycl. Surf. Colloid Sci.* 1438–1446.
- Torrent, J., Barrón, V., Liu, Q., 2006. Magnetic enhancement is linked to and precedes hematite formation in aerobic soil. *Geophys. Res. Lett.* 33, 4–7. doi:10.1029/2005GL024818
- Torrent, J., Liu, Q., Bloemendal, J., Barrón, V., 2007. Magnetic enhancement and iron oxides in the Upper Luochuan Loess-Paleosol sequence, Chinese Loess Plateau. *Soil Sci. Soc. Am. J.* 71, 1570–1578. doi:10.2136/sssaj2006.0328
- Torrent, J., Schwertmann, U., 1987. Influence of hematite on the colour of Red Beds. *J. Sediment. Petrol.* 57, 682–686.
- Ugolini, F.C., Dahlgren, R.A., 2002. Soil development in volcanic ash. *Glob. Environ. Res.* 6, 69–81.
- Uto, K., Ishizuka, O., Matsumoto, A., Kamioka, H., Togashi, S., 1997. Laser-heating  $^{40}\text{Ar}/^{39}\text{Ar}$  dating system of the Geological Survey of Japan: System outline and preliminary results. *Bull. Geol. Surv. Japan* 48, 23–46.
- Vacca, A., Ferrara, C., Matteucci, R., Murru, M., 2012. Ferruginous paleosols around the Cretaceous-Paleocene boundary in central-southern Sardinia (Italy) and their potential as pedostratigraphic markers. *Quat. Int.* 265, 179–190. doi:10.1016/j.quaint.2011.07.036
- Van der Gaast, S.J., Mizota, C., Jansen, J.H.F., 1986. Curved smectite in soils from

- volcanic ash in Kenya and Tanzania: a low-angle X-ray powder diffraction study. *Clays Clay Miner.* 34, 665.
- Van Houten, F., 1973. Origin of red beds - A review - 1961 - 1972. *Annu. Rev. Earth Planet. Sci.* 1, 39–61.
- Veblen, T., Alaback, P., 1996. High-Latitude Rainforests and Associated Ecosystems of the West Coast of the Americas, in: Lawford, R., Fuentes, E., Alaback, P. (Eds.), *High-Latitude Rainforest and Associated Ecosystems of the West Coast of the Americas*. Springer Verlag, New York, pp. 173–213.  
doi:10.1007/978-1-4612-3970-3
- Velde, B., Meunier, A., 2008. *The Origin of Clay Minerals in Soil and Weathered Rocks*. Springer-Verlag, Berlin Heidelberg.
- Veneman, P.L., Vepraskas, M., Bouma, J., 1976. The physical significance of soil mottling in a Wisconsin toposequence. *Geoderma* 15, 103–118.
- Weibel, R., 1999. Effects of burial on the clay assemblages in the Triassic Skagerrak Formation, Denmark. *Clay Miner.* 34, 619–635.  
doi:10.1180/claymin.1999.034.4.08
- Widdowson, M., Walsh, J.N., Subbarao, K. V., 1997. The geochemistry of Indian bole horizons: palaeoenvironmental implications of Deccan intravolcanic palaeosurfaces, in: Widdowson, M. (Ed.), *Paleosurfaces: Recognition, Reconstruction and Palaeoenvironmental Interpretation*. Geological Society Special Publication, pp. 269–281. doi:10.1144/GSL.SP.1997.120.01.17
- Wilke, F.D., O'Brien, P., Gerdes, A., Timmerman, M., Sudo, M., Khan, M.A., 2010. The multistage exhumation history of the Kaghan Valley UHP series, NW Himalaya, Pakistan from U-Pb and  $40\text{Ar}/39\text{Ar}$  ages. *Eur. J. Mineral.* 22, 703–719.
- Wilson, M.J., 1999. The origin and formation of clay minerals in soils: past, present and future perspectives. *Clay Miner.* 34, 7–25. doi:10.1180/000985599545957
- Wojdyr, M., 2010. Fityk: a general-purpose peak fitting program. *J. Appl. Crystallogr.* 43, 1126–1128. doi:10.1107/S0021889810030499
- Wright, V.P., 1992. *Paleosol recognition: A guide to early diagenesis in terrestrial settings*, *Developments in Sedimentology, Diagenesis III*. Elsevier.  
doi:10.1016/S0070-4571(08)70574-0
- Wyszecki, G., Stiles, W., 1982. *Colour science: Concepts and methods, quantitative data and formulae*. Wiley, New York.

- York, D., 1969. Least squares fitting of a straight line with correlated errors. *Earth Planet. Sci. Lett.* 5, 320–324.
- Yousefifard, M., Ayoubi, S., Poch, R.M., Jalalian, A., Khademi, H., Khormali, F., 2015. Clay transformation and pedogenic calcite formation on a lithosequence of igneous rocks in northwestern Iran. *Catena* 133, 186–197.  
doi:10.1016/j.catena.2015.05.014
- Zachos, J., Pagani, M., Sloan, L., Thomas, E., Billups, K., 2001. Trends, Rhythms, and Aberrations in Global Climate 65 Ma to Present. *Science* 292, 686–693. doi:10.1126/science.1059412
- Zachos, J.C., Quinn, T.M., Salamy, K.A., 1996. High-resolution deep-sea foraminiferal stable isotope records of the Eocene-Oligocene transition. *Paleoceanography*.

**Manuscript 2**

Scientific Reports: Volume 152, May 2017, Pages 69-81

10.1038/s41598-017-06617-x

<https://doi.org/10.1038/s41598-017-06617-x>

**Origin of clay minerals in Early Eocene volcanic paleosols on King George Island, Maritime Antarctica**

Diogo Noses Spinola<sup>a\*</sup>, Teresa Pi-Puig<sup>b</sup>, Elizabeth Solleiro-Rebolledo<sup>b</sup>, Markus Egli<sup>c</sup>, Masafumi Sudo<sup>d</sup>, Sergey Sedov<sup>b</sup>, Peter Kühn<sup>a</sup>

<sup>a</sup> Institute of Geography, University of Tübingen, Germany.

<sup>b</sup> Institute of Geology, Nacional Autonomous University of Mexico, Mexico.

<sup>c</sup> Department of Geography, University of Zurich, Switzerland.

<sup>d</sup> Institute of Earth and Environmental Science, University of Potsdam, Germany.

### **Abstract**

The paleoclimate during the Early Eocene in Maritime Antarctica is characterized by cool conditions without a pronounced dry season. Soils formed on volcanic material under such climate conditions in modern analogue environments are usually Andosols rich in nanocrystalline minerals without pedogenic smectite. The paleosols formed on volcanic material on King Georges Island are covered by basalts, dated by 6 new  $^{40}\text{Ar}/^{39}\text{Ar}$  datings to 51 – 48 Ma, and are rich in smectite. A pedogenic origin of the smectites would suggest a semi-arid rather than a wet non-seasonal humid paleoclimate. To investigate the origin of the smectites in these paleosols we used X-ray diffraction and microscopic techniques. Minor mineralogical changes between the volcanic parent material and the paleosols and a homogenous distribution of smectites throughout the paleosol horizons indicate that these smectites were mainly inherited from the pyroclastic parent material, which was altered prior to surficial weathering. Nevertheless, the mineralogical properties, such as degree of crystallinity and octahedral site occupancy, of these smectites were modified during the ancient soil formation. Our findings highlight that trioctahedral smectites were a product of deuteric alteration of pyroclastic rocks and were progressively transformed to dioctahedral smectites during weathering in a soil environment on King George Island.

## Introduction

The paleoclimate during the Early Eocene in Maritime Antarctica is characterized by cool conditions without a pronounced dry season. Studies based on plant fossil assemblages suggest a paleoenvironment similar to the Valdivian rainforest in southern Chile (Francis et al., 2009; Poole et al., 2003, 2001). The Valdivian rainforest is considered as a suitable modern analogue because of similar plant assemblages and because of volcanic substrates (Poole et al., 2001).

Andosols are the predominant type of volcanic soils formed under a cool temperate environment, like the Valdivian rainforest. Nanocrystalline minerals (i.e. allophane and ferrihydrite) and imogolite are the predominant secondary minerals in these soils (Churchman and Lowe, 2012; IUSS Working Group WRB, 2014; Shoji et al., 1993; Ugolini and Dahlgren, 2002). In environments having a pronounced dry-season, the occurrence of halloysite and smectite becomes more common (Galán, 2006; Velde and Meunier, 2008). So far the origin of smectites within this material is not clarified and mainly three different origins are proposed: (i) many authors suggest an inheritance origin, when the volcanic substrate was subject to a hydrothermal or deuteric alteration (a low-temperature magmatic alteration related to the solidification of a melt) leading to a formation of smectites prior to a subsequent surficial weathering (Dudas and Harward, 1975; Fiore, 1993; A. G. Jongmans et al., 1994; Mirabella et al., 2005; Pevear et al., 1982; Rasmussen et al., 2007). (ii) Smectites are of pedogenic origin as a product of *in-situ* weathering of primary minerals (McDaniel et al., 1995; Prudencio et al., 2002; Rasmussen et al., 2010; Van der Gaast et al., 1986; Yousefifard et al., 2015). (iii) Aeolian input of smectites may have played a major role (Colman, 1982; Mizota and Takahashi, 1982).

The importance of clay mineralogy for paleoenvironmental interpretation is well recognized (Bronger and Heinkele, 1990; Sheldon and Retallack, 2004). Nonetheless, clay minerals are only suitable for a paleoenvironmental interpretation when their origin in paleosols is confirmed as being pedogenic (Singer, 1980). For this reason, before interpreting clay minerals as weathering products of the tephra, a potential hydrothermal or deuteric and/or aeolian origin must be excluded.

King George Island (KGI), Maritime Antarctica, is one of the few sites in Antarctica where Eocene paleosols were recognized. In a first attempt for a paleoenvironmental

reconstruction based on its clay mineralogy, Birkenmajer and Łydka (1990) attributed the presence of smectite and kaolinite in paleosols as a record of a warm-wet paleoclimate. However, no further studies were made to understand the origin of these clays. In a recent publication, smectite was identified in Eocene paleosols on KGI (Spinola et al., 2017b). A predominance of smectite, however, should not exist, because these paleosols correlate with fossil plants layers that indicate a cool paleoenvironment. Thus, to avoid misinterpretations of the Eocene paleoclimate using the clay mineralogy of these paleosols, the origin of these clay minerals must be understood.

The objective of this study was, therefore, to investigate – by using X-ray diffraction, microscopic and sub-microscopic techniques (SEM-EDS) - the origin of smectites in Eocene paleosols on KGI. The occurrence of smectite in these paleosols have a potential to give additional paleoenvironmental information, e.g. pedogenic smectites would suggest a dryer climate for the Early Eocene which would be in contrast to the wet non-seasonal paleoclimate model (Francis et al., 2009; Mozer, 2012; Poole et al., 2003, 2001).

## **Results**

### **Field – General characteristics**

The two investigated profiles are morphologically similar (Supplementary Table 1). Both are relatively thick paleosols profiles (P1: >73cm, P2: >56cm) occurring between basalt flows (Fig. 1). Whereas the contact with the covering basalt flow is clear, the contact with the saprolite and the underlying basalt was not accessible. Both profiles are reddish-brown with gradual colour changes with depth. They are characterized by a predominantly strong blocky (more angular) and platy structure and a variable size of aggregates with depth. Most of the horizons have a sandy loam texture (Table 1). The 2BAb and 3ABb horizons of P1 and ABb of P2 have a slightly finer texture with a sandy clay loam.

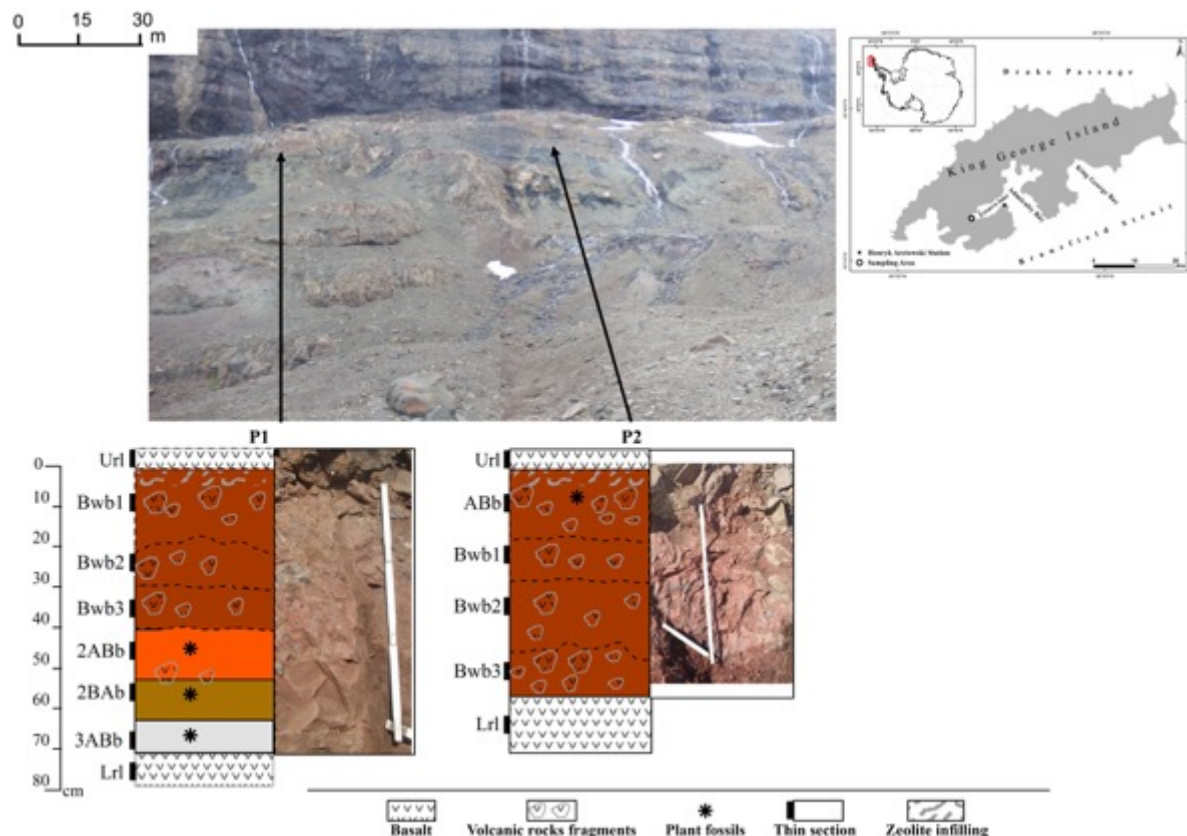


**Figure 1.** Overview of the sampling site at King George Island, location of the paleosols at the Cytadela outcrop and their schematic profile description.

Based on the colour, P1 is the more heterogeneous profile. The colours vary from red to grey, between structure type and size, and the rock fragments in the horizons. It is also thicker than P2 and has two lithic discontinuities (LD). The first LD is between the Bwb3 and 2ABb horizons due to an abrupt lack in rock fragments in the 2ABb horizon. The second LD is between the 2BAb and 3ABb horizons, indicated by the appearance of dark fossil plant leaves and a greyish colour (hue = 5Y) being a marker of a buried A horizon. The horizon boundaries in P2 are gradual and diffuse. The horizons can be distinguished mostly by differences in the structure type that varies between subangular/angular blocky and platy. P2 has a predominantly reddish-brown (hue-2.5YR) colour.

**Table 1.** Selected textural and mineralogical properties.

| Profile   | Horizon         | Depth<br>[cm]     | Particle size<br>%  |                              |                                 | Textural class  | Octahedral occupancy of smectites<br>% |                | Smectite in the parent material<br>% |      |
|-----------|-----------------|-------------------|---------------------|------------------------------|---------------------------------|-----------------|--|----------------|--------------------------------------|------|
|           |                 |                   | Clay<br>( $<2\mu$ ) | Silt<br>( $2\mu$ - $63\mu$ ) | Sand<br>( $63\mu$ - $2000\mu$ ) |                 | Di octahedral                          | Tri octahedral |                                      |      |
| <b>P1</b> | Bwb1            | 0 - 23            | 15                  | 18                           | 67                              | Sandy loam      | 92                                     | 8              |                                      |      |
|           | Bwb2            | 23 - 34           | 15                  | 19                           | 66                              | Sandy loam      | 97                                     | 3              |                                      |      |
|           | Bwb3            | 34 - 45           | 14                  | 19                           | 67                              | Sandy loam      | 92                                     | 8              |                                      |      |
|           | Parent material | from Bwb3 horizon |                     |                              |                                 |                 |  | 55             | 45                                   | 28.4 |
|           | 2ABb            | 45 - 60           | 17                  | 21                           | 62                              | Sandy loam      | 81                                     | 19             |                                      |      |
|           | 2BAb            | 60 - 73           | 20                  | 22                           | 58                              | Sandy clay loam | 91                                     | 9              |                                      |      |
|           | Parent material | from 2ABb horizon |                     |                              |                                 |                 |  | 68             | 32                                   | 33.6 |
|           | 3ABb            | 73+               | 20                  | 15                           | 65                              | Sandy clay loam | 99                                     | 1              |                                      |      |
|           | Parent material | from 3ABb horizon |                     |                              |                                 |                 |  | 72             | 28                                   | 41.8 |
| <b>P2</b> | ABb             | 0 - 20            | 19                  | 17                           | 64                              | Sandy clay loam | 98                                     | 2              |                                      |      |
|           | Bwb1            | 20 - 30           | 15                  | 19                           | 66                              | Sandy loam      | 98                                     | 2              |                                      |      |
|           | Bwb2            | 30 - 53           | 15                  | 18                           | 67                              | Sandy loam      | 99                                     | 1              |                                      |      |
|           | Bwb3            | 53+               | 15                  | 13                           | 72                              | Sandy loam      | 97                                     | 3              |                                      |      |
|           | Parent material | from Bwb3 horizon |                     |                              |                                 |                 |  | 75             | 25                                   | 29.7 |

### **$^{40}\text{Ar}/^{39}\text{Ar}$ dating**

The  $^{40}\text{Ar}/^{39}\text{Ar}$  age of the lava flows confirms a late Early Eocene age (Fig. 2, Table 2, Supplementary Fig. 1 and Supplementary Table 2). The ages of the basalts covering the profiles should be identical because they belong to the same lava flow (Fig. 1), within 60 m horizontally from P1 to P2 and also 90 m from P2 to P3 (not studied in the present manuscript). The ages from upper (Url) and lower (Lrl) basaltic lava flows at P1 (P1-Url and P1-Lrl) are  $50.47 \pm 0.08$  (error: 1 sigma, Lab ID: C16047) and  $48.57 \pm 0.29$  Ma (C17003). The ages are similar, although the upper flow is slightly older than the lower one beyond 2 sigma error. The ages from the upper and lower basaltic lava flows at P2 (P2-Url and P2-Lrl) are  $42.66 \pm 0.20$  (C16048) and  $50.21 \pm 0.15$  Ma (C17004). Thus, the age only from P2-Url is much younger than the other three ages from 50.5 to 48.5 Ma. Especially the result of sample P2-Lrl is excellent result because the plateau age and isochron ages from the plateau steps correspond very well (Fig.

2 and Table 2). Therefore, the age 50.21 Ma of P2-Lrl will be used as the best inferior age for the basaltic units. The younger age of 42.66 Ma from P2-Url could be explained by the larger loss of radiogenic  $^{40}\text{Ar}$  from the sample due to alteration, which is consistent with the petrographic observation, and the Ar loss curve in the lower temperature steps in the age spectrum (Supplementary Fig. 1). For the ages of P1-Url and P3-Url is the most probable age for the upper basaltic unit 50.5 to 48 Ma. Therefore, the new  $^{40}\text{Ar}/^{39}\text{Ar}$  datings propose an age for the basalt flows ranging between 51 Ma and 48 Ma, thus, dating to the late Early Eocene.

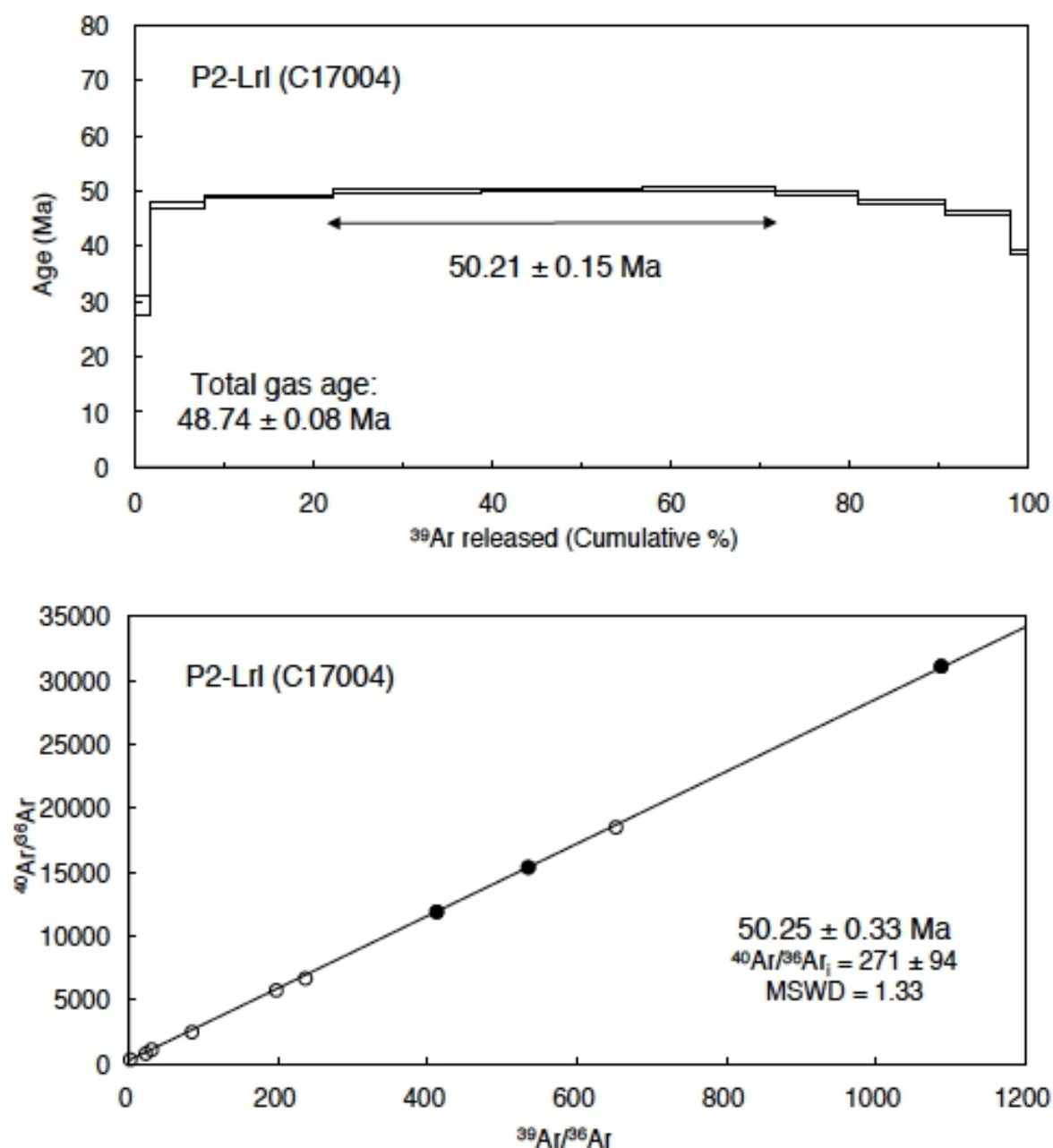


**Figure 2.**  $^{40}\text{Ar}/^{39}\text{Ar}$  age spectrum and normal isochron plot obtained by the stepwise heating analysis of



complete transformation to secondary products (i.e. alteration of olivine to smectite and less frequently to serpentine). The other three clay types were neoformed and are characterized by a brown, grey and green infillings. Infillings and alteromorphs of olivine were the most frequent alterations types followed by alterations of glass and plagioclase.

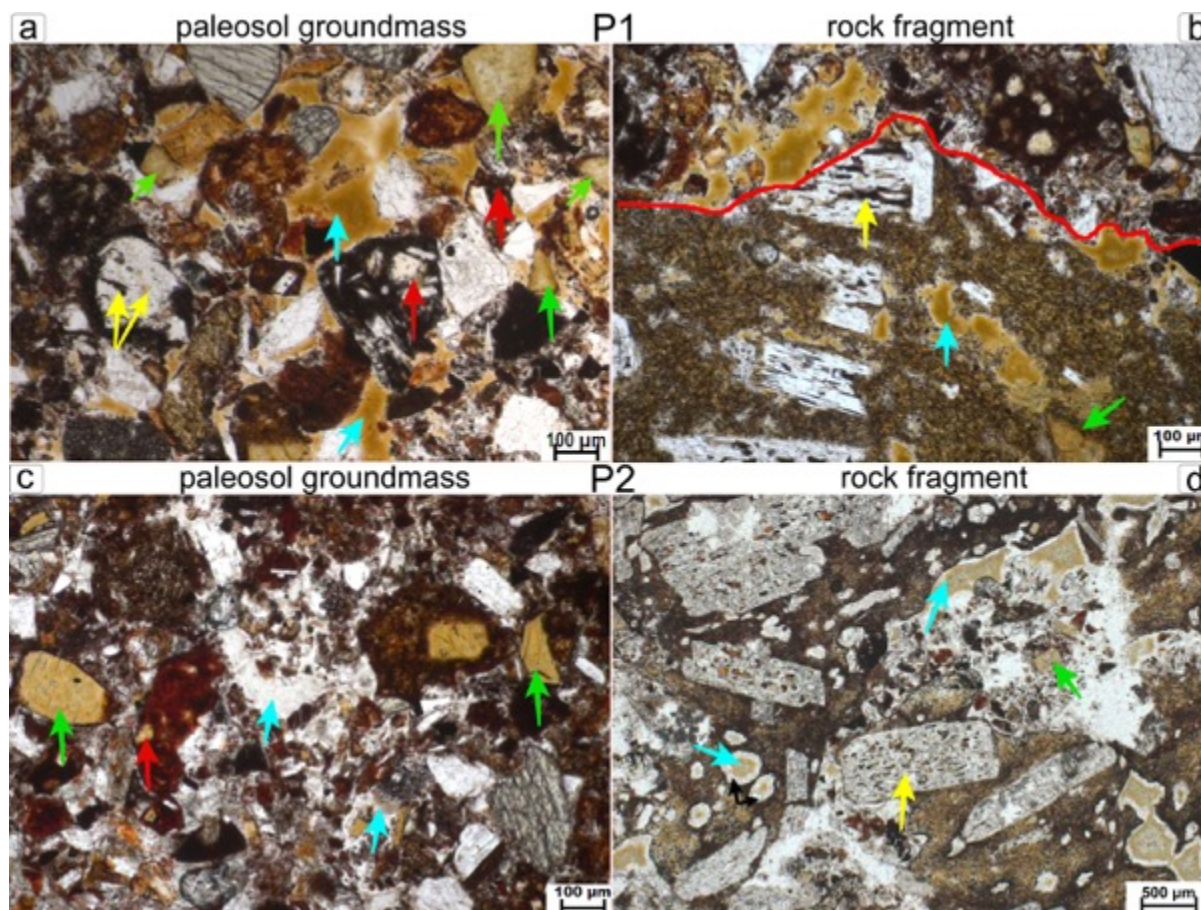


**Figure 3.** Alterations types occurring in the groundmass of paleosols and in rock fragments under Plane Polarized Light (PPL). a-) P1-Bwb2, 23-34cm: brown infillings (blue arrows); clay filling vesicles in glass shards (red arrows); brownish clays of former olivines (green arrows); yellow arrows: alterations of plagioclase b-) P1-Bwb2, 23-34cm: similar alterations occurring inside a rock fragment, the red line defines the limit between rock (below the line) and paleosol (above the line). c-) P2-Bwb1, 20-30cm: grey infillings are almost transparent under PPL (blue arrows); clay (red arrow) filling vesicles in glass shards; brownish clays in former olivine (green arrows). d-) P2-Bwb1, 20-30cm: same alterations occurring in a rock fragment, note the brown infilling (blue arrow) surrounded by a white rim due to Fe depletion (black arrows); alteration of plagioclase (yellow arrow).

Alteromorphs of primary minerals occur with similar features in both profiles. Brown clay with a mosaic-speckled b-fabric replaced olivine crystals, showing second order yellow and red interference colours under crossed polarizers (XPL). Plagioclases revealed a dotted and complex alteration pattern composed of brown, black and red clay infillings. Glass shards have mainly a cusped to platy shape, with red, yellow, orange, brown and black colours; their voids and vesicles are often filled with brown

clay. In addition, the orange and yellow shards are usually anisotropic under XPL.

Neoformation of clays occurs generally as infillings. These are a common feature in both profiles. The centre of the infilling has a speckled b-fabric (not well-oriented clay) and the boundaries of the infilling has extinction bands (well-oriented clay). These infillings are predominantly brown in P1, whereas they are mostly light-grey and nearly transparent in P2 (Fig. 3) together with brown and green colours. Another common characteristic of the infillings is the abrupt transition to the surrounding soil or rock.

Despite of the lithic discontinuities in P1, the alteration products are very similar in all horizons. The infillings are less abundant and more incorporated into the soil groundmass in the horizons 2ABb, 2BAb and 3ABb than in the upper horizons. A finer soil texture (sandy clay loam) in comparison to the horizons Bwb1, Bwb2 and Bwb3 (sandy loam), and the presence of speckled/granostriated b-fabrics in the micromass of these horizons can be taken as an evidence for a better incorporation of clays into the soil groundmass (Supplementary Table 3). Infillings are not incorporated into the soil and have well-defined borders in the horizons Bwb1, Bwb2 and Bwb3.

There are no major changes in the alterations types across all horizons of P2. The most relevant difference is the green colour of the clay infillings in the lowermost horizon (Bwb3), which have brown and grey colours in the other horizons. Grey infillings are predominant in the soil groundmass of the horizons Bwb1 and Bwb2, whereas infillings in the rock fragments are mostly brown, but progressively becoming grey (Fig. 3 and Fig. 4). In the uppermost horizon (ABb) brown infillings turning into grey was also detected in the soil groundmass.

### **SEM-EDS**

The alteromorphs of olivine and the infillings (of all colours) have radial textures in wider cracks in olivines. These infillings that occur in the soil groundmass tend to be exhibit thinner cracks than those in rock fragments. Nevertheless, the overall texture of infillings in soil and rock fragments is the same. They have a centre with cracks and smoother borders and are surrounded by a large crack near the contact with the soil or rock (Fig. 4b). Such differences in texture may explain the speckled b-fabric (cracked centre), the extinction bands (smooth borders) and the abrupt interface to soil or rock (large cracks) seen under the petrographic microscope. The alterations after plagioclase and glass shards are more irregular. Primary mineral textures of

plagioclase are still detectable. The transformation of glass shards into clays is better expressed around their vesicles and voids.

The EDS results show that alteromorphs of olivine having brown and green infillings are chemically similar. These types of alterations are richer in Fe and Mg, regardless if they occur in the soil groundmass or in the rock fragments (Supplementary Fig. 2 online). In contrast, the transitions of brown to grey infillings in P2 have a gradual loss of Fe at the boundaries of the infilling (Fig. 4f). The alteration of plagioclase reflects the composition of the primary mineral, with higher amounts of Al-Si-Ca than other alterations. The chemical composition of the major cations of volcanic shards is varying without a clear pattern.

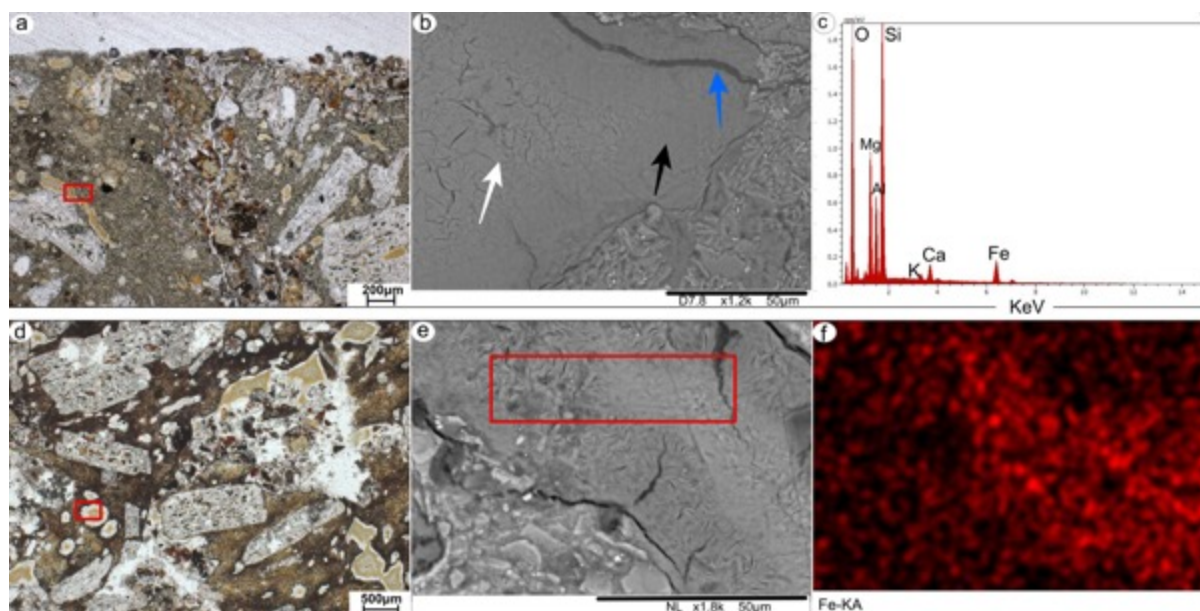


**Figure 4.** Petrographic and SEM images of selected alterations. a-) P1-Bwb3, 34-45cm: brown infilling in a rock fragment (red rectangle). b-) the same infilling analysed with SEM. Note the abundant cracks in the centre of the infilling (white arrow) with smoother boundaries (black arrow) and a large crack next to the contact with the rock (blue arrow). c-) EDS spectrum of the infilling. d-) P2-Bwb1, 20-30cm: brown infilling with a white rim in a rock fragment. e-) the same infilling analysed with SEM. Red rectangle indicate the selected area for elemental mapping f-) distribution of Fe in the infilling. Darker areas (borders) indicate a lower content, whereas brighter red colours (towards the centre of the image) indicate a higher Fe content.

### X-ray diffraction (XRD)

The clay mineralogy of the profiles is generally homogeneous. The clays are composed of smectite having some randomly interstratified components. Smectite was confirmed by a strong  $d_{001}$  reflection at about 1.4 nm under air-dried conditions that shifted to about 1.7 nm after ethylene glycol treatment and collapsed to 1.0 nm after heating at 550°C (Fig. 5). The presence of a shoulder in the  $d_{001}$  peak in some

samples indicated a presence of randomly interstratified illite-smectite (I/S), which was better detectable after decomposing the spectra using profile fitting techniques (Wojdyr, 2010) (Fig. 6).

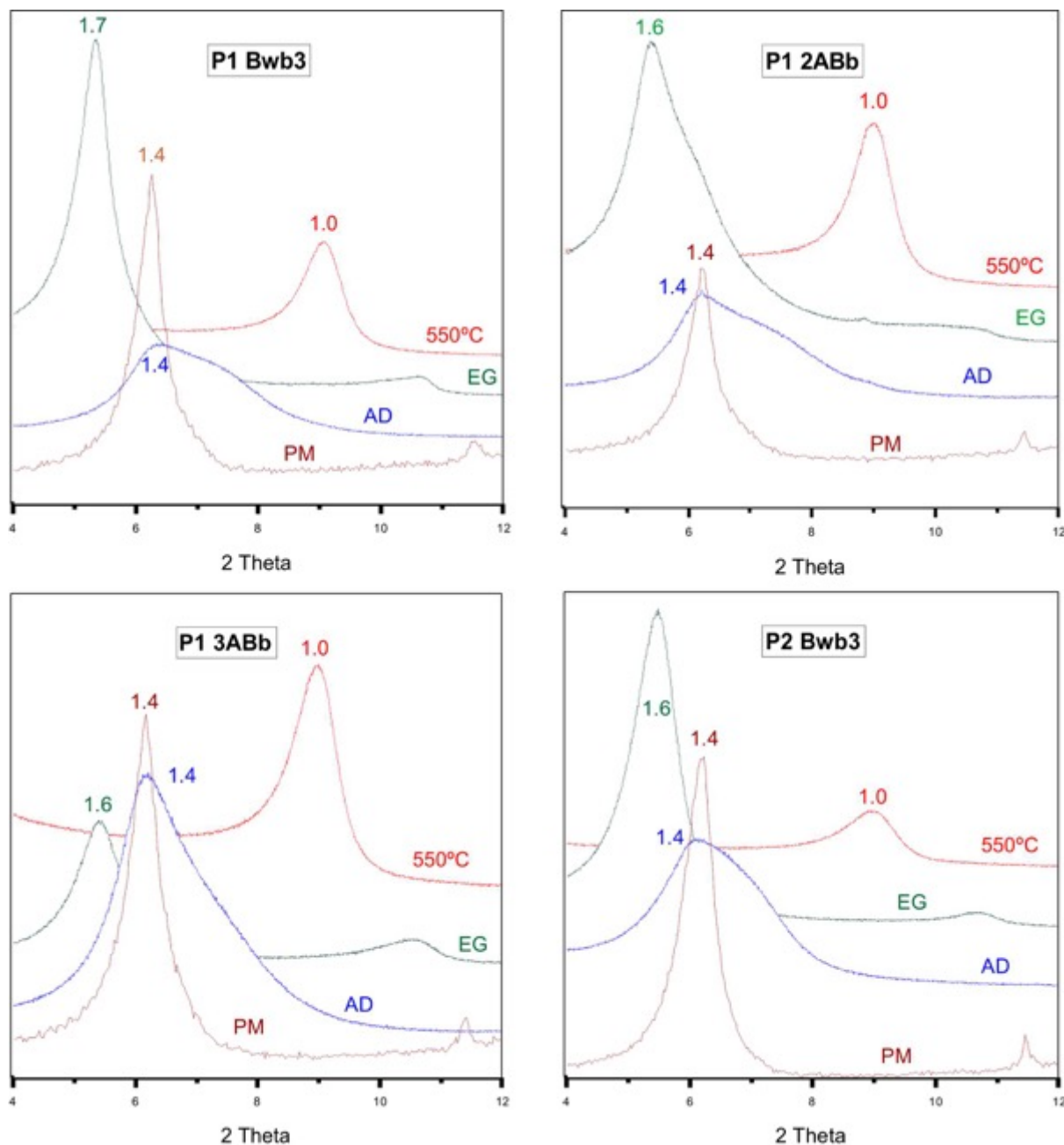


**Figure 5.** XRD patterns of clay samples from selected horizons. The d-spacing are given in nm. AD = Air dried, EG = Ethylene glycol solvation, 550°C = sample heated at 550°C, PM = parent material.

The main minerals in the parent material (rock fragments extracted from paleosol horizons) are plagioclase, pyroxene, quartz, and a considerable amount of smectite, reaching almost 42% in the horizon 3ABb in P1 (Table 1).

The clay association in P1 shows slight variations, having predominantly smectitic components with a minor portion of I/S. The presence of a broader shoulder of the (001) peak indicated a more developed I/S in the horizons Bwb3, 2ABb, 2BAb and 3ABb. The P2 is more homogenous and the interstratified component is only identifiable after decomposing the XRD pattern (no shoulders were visible). In both profiles, the smectitic component is better crystallized, having sharper peaks and a lower *Full Width at Half Maximum* (FWHM) value than the interstratified component. In the rock samples, the smectites have a higher degree of crystallinity, with sharper peaks (Fig. 5) and lower FWHM values than the smectitic component in the paleosols (Fig. 6).

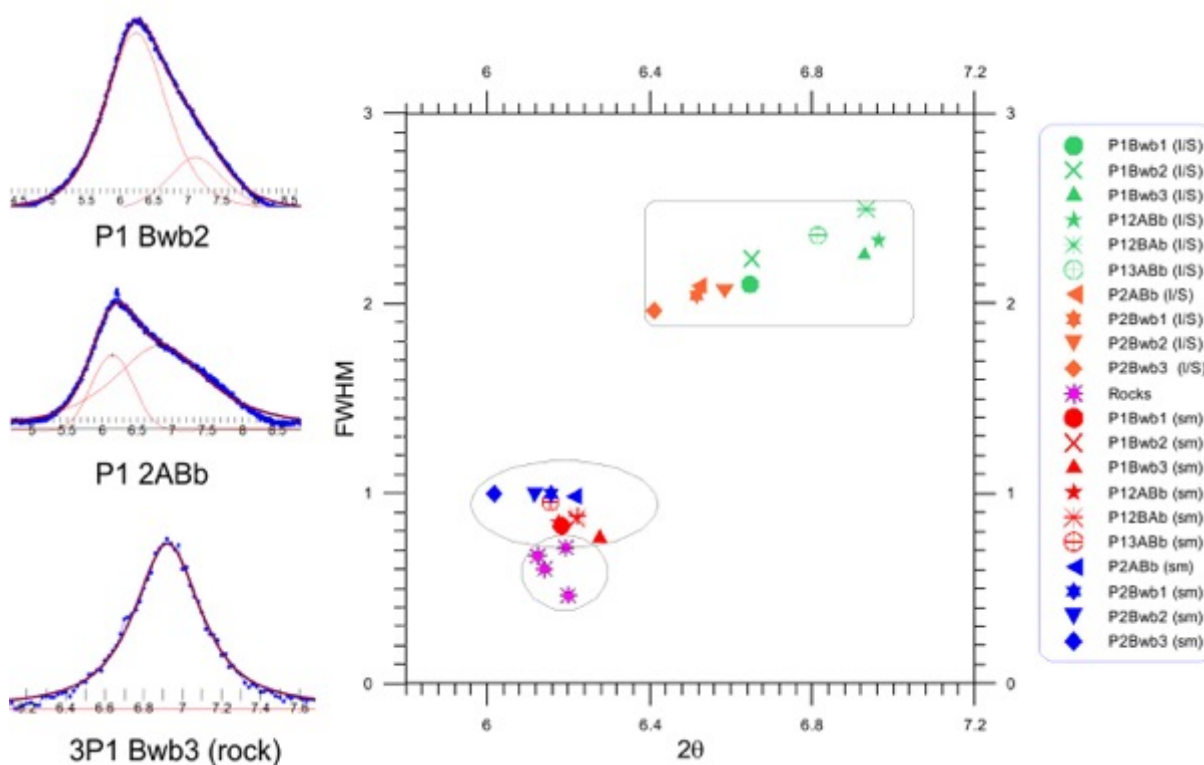


**Figure 6.** Degree of crystallinity of smectitic and interstratified components of the paleosol samples and the parent material. a-) Examples of profile fitting analysis obtained for clay samples of selected horizons; b-) Full width at half maximum (FWHM) of paleosols and rock samples. The lower the FWHM, the better the crystallinity and vice-versa. Smectitic component of P1 and P2 in red and blue, respectively. Interstratified component of P1 and P2 in green and orange, respectively. Smectite of rocks samples in pink. Each symbol represents one horizon. Note the smectitic component is more crystalline than the I/S component. Smectite from the rocks has a higher crystallinity with lower FWHM values.

There is a dominance of dioctahedral smectite over trioctahedral smectite with more than 80% of dioctahedral smectite in all horizons (Table 1). This is detected by the (060) reflectance on randomly oriented samples. The portions of the dioctahedral and trioctahedral smectites in the rocks samples are similar, but the dioctahedral

component still predominates. An increase of the clay amount and of the proportion of dioctahedral smectite in the rock fragments can be detected in the horizons 2ABb and 3ABb of P1, which have a finer texture and less rock fragments.

Generally, there were no major differences of the clay assemblages throughout the paleosols horizons. The differences between paleosol and parent material were more perceptible. The clearest difference was a predominance of dioctahedral smectite, the presence of an interstratified component, and less crystallinity of the smectite in the paleosols.

### **Discussion**

While the microscopic and submicroscopic analyses showed the sources, shape and semi-quantitative chemistry of the clays, the XRD results provided the identification, degree of crystallinity and the octahedral site occupation (di- and trioctahedral) of the smectites.

Alteromorphism of primary minerals, such as the plagioclases or olivine, is often used as a proof of deuteritic alterations (Hekinian, 1982). Delvigne et al. (1979), however, demonstrated that either deuteritic alteration or weathering of olivine can produce similar products. Nonetheless, it seems that rock weathering has left the infillings and olivines alteromorphs in the soil groundmass as a residuum (Jongmans et al., 1994). The alteration of plagioclase in the present study was caused by deuteritic alteration. One proof is that the plagioclase phenocrysts within rock fragments are more weathered than the glassy groundmass. As a result of weathering and pedogenic processes the glassy groundmass should have been much more weathered than plagioclases in rock fragments.

The differences between the profiles are most probably related to paleodrainage conditions. The colour of the infillings in P1 is brown while in P2 is predominantly grey, with minor brown and green. In P2, the green infilling was only detected in the lowermost horizon (Bwb3), while a brown colour was present in rock fragments upwards in the profile. This suggests that the brown colour was the original colour that turned into green in Bwb3 horizon under more reducing conditions. In addition, the predominant grey colour in the soil groundmass of all horizons indicates Fe depletion, suggesting slightly reductive conditions with decreasing intensity in the uppermost horizon (ABb). In this horizon, the infillings in the soil groundmass are still brown.

Even though the horizons P1-ABb; P1-BAb and P1-3ABb have Fe nodules and have a more yellowish/greyish than reddish field colour, they generally have brown infillings. Due to weathering and biological activity these infillings are more incorporated into the soil groundmass because their boundaries are barely seen (Jongmans et al., 1994). In addition, they have granostriated b-fabric (Spinola et al., 2017b), which are signs of pedoturbation (Heidari et al., 2004).

The smectites in the paleosols are predominantly dioctahedral whereas the distribution with trioctahedral smectites is more balanced in the rock samples. Nevertheless, the percentage of trioctahedral smectites in the rocks is likely lower than the presented results because of the interference on the (060) peak with the quartz peak (0,15 nm) and with the basal peak of serpentine (Moore and Reynolds Jr, 1997). Despite this, our results are in accordance with the common knowledge that dioctahedral smectites are more common in soils because of its higher stability than the trioctahedral types (Borchardt, 1989; Velde and Meunier, 2008; Wilson, 1999). Even in soils formed in Siberia, with limited chemical weathering, Lessovaia et al. (2016) reported an increase in the proportion of dioctahedral smectites in relation to trioctahedral ones from bottom to top soil horizons. Nahon et al. (1982) demonstrated in a study about weathering of olivine-bearing rocks that the formation of smectites started with trioctahedral species being progressively replaced by dioctahedral smectites. Some paleosols between basalts in India also had smectites formed by deuteric alteration followed by weathering (Craig et al., 2017). Thus, it can be inferred that trioctahedral smectites in the present study were a product of deuteric alteration of the pyroclastic rocks and were progressively transformed to dioctahedral smectites during weathering in a soil environment.

The degree of crystallinity of the smectitic component is also an important difference between the paleosols and rocks samples. Pedogenic smectites tend to be less crystalline (Velde and Meunier, 2008), producing broader peaks or higher FWHM values, which corresponds to our findings. The smectites of the paleosols were less crystalline (higher FWHM) than those in rocks.

The presence of interstratified I/S is commonly attributed to an early stage of burial diagenesis, progressively turning smectite into illite (Eberl, 1984; Velde and Meunier, 2008). There is, however, no enrichment of K detectable in all soil horizons (Spinola et al., 2017b). There are further explanations for the presence of I/S in volcanic

soils/paleosols, such as inheritance from the deuteric altered parent material (Fiore, 1993; Jeong et al., 2004), aeolian deposition (Singer and Navrot, 1977) and also pedogenic, via weathering of tephra under semi-arid conditions (Berkhaut et al., 1994). Although all hypotheses are sound, we have no strong evidences supporting any of them.

No evidences for other typical secondary minerals of volcanic soils were found in the XRD pattern, such as nanocrystalline minerals (allophane and ferrihydrite) imogolite and halloysite. Whereas allophane is indicative of more humid climates, halloysite is often found on environments with high [Si] (silica activity), usually associated with semi-arid environments (Churchman and Lowe, 2012; Sedov et al., 2010, 2003).

The morphological similarity between smectites of the paleosols and its parent material suggests inheritance from a deuteric altered parent material as the origin. Further weathering in a soil paleoenvironment produced the differences discussed above, such as differences in crystallinity, octahedral occupancy, and interstratification. Similar clay composition between parent material and soil was previously described in other volcanic areas such as in Italy (Fiore, 1993; Fiore et al., 1992; Mirabella et al., 2005), Costa Rica (Jongmans et al., 1994) and US (Dudas and Harward, 1975; Pevear et al., 1982). In all these cases, the smectites were proven to be inherited from deuteric or hydrothermally altered parent material.

Homogeneity in clay assemblage and crystallinity in depth within each profile and between the profiles also support the inheritance origin (Mirabella et al., 2005). A clay assemblage formed by pedogenesis should be more heterogeneous, since each soil horizon gather specific chemical-physical and biological conditions (Churchman and Lowe, 2012; Singer, 1980). Only the smectite after glass shards seems to be purely pedogenic because of heterogeneous chemistry and morphology even within the same horizon. The formation of clay inside glass vesicles also indicate authigenesis (Fiore, 1993). Aeolian deposition seems also unlikely or played a minor role, otherwise, a distinct signature (textural, microscopic or XRD) should be expected in the paleo A horizons.

## Conclusions

$^{40}\text{Ar}/^{39}\text{Ar}$  dating was performed for the first time on these paleosols. Over- and underlying basaltic lava flows gave consistent ages ranging between 51 and 48 Ma

dating the paleosols to the late Early Eocene. The mineralogical data indicate that smectites in Eocene paleosols on KGI are generally inherited from the parent material that was subjected to deuteritic alterations prior to pedogenesis. The most important evidences are the homogeneity of clay assemblage between paleosols and parent material. The visual and chemical homogeneity of the clay concentrations detected under petrographic microscope and SEM/EDS and a homogeneous distribution of clays with depth in each profile supports our conclusion. Nevertheless, pedogenesis was responsible for the almost complete transformation of the inherited trioctahedral smectites (which are still present in the rocks) to dioctahedral smectites in the paleosols. Furthermore, the smectite in the paleosols are less crystalline and have an interstratified component.

The octahedral layer of the inherited smectites in the paleosols was altered by pedogenic processes, but the smectite was not further weathered to kaolinite. The imperfect drainage combined with a base-rich parent material (basaltic tephra), and likely a high pH, may have been important paleoenvironmental factors for the relative stability of the smectites. Nevertheless, since the smectite was subjected to alterations, more detailed paleoenvironmental information can potentially be taken from its isotope composition.

The question if clay minerals (e.g. smectite) are pedogenic or inherited from the parent material should be more frequently investigated in paleoenvironmental studies using clay mineralogy as a proxy since only clay minerals in soils/paleosols that are of pedogenic origin bear information of the paleoclimate.

## **Methods**

### **Site description and geological background**

The samples were collected on King George Island, South Shetland Islands, Maritime Antarctica. The specific outcrop is located at the Cytadela area of the Ezcurra Inlet in the Admiralty Bay (62° 11.057'S - 58° 35.209'W) (Fig. 1).

The outcrop stratigraphically belongs to the Point Thomas Formation, Ezcurra Inlet Group, which comprises a 500 m thick Paleogene (Eocene-Oligocene) volcanic succession (Birkenmajer, 1980b; Birkenmajer and Zastawniak, 1989). This formation was deposited during the Arctowski interglacial period (ca 50 to ca 32 Ma), a climostratigraphic unit introduced by Birkenmajer (1988).

Two informal units of the Point Thomas Formation are recognized at the Cytadela outcrop, the Lower Member (LM) and Upper Member (UM) (Birkenmajer, 1980b). The LM is a 20–40 m thick regular high-Al flow basalt with a thickness of 1–6 m alternating with pyroclastic deposits. The UM comprises 150–450 m of irregular, lenticular basalt lavas alternating with feldspathic tuff, interbedded with coarse vent breccia and plant-bearing tuff.

We sampled two profiles (P1 and P2), which are located in a distance of 60 m (Fig. 2). Samples were taken from paleosols below the 6<sup>th</sup> basalt flow (from bottom to top) in the LM of schematic field section by Mozer (2012).

### **<sup>40</sup>Ar/<sup>39</sup>Ar dating**

The groundmass samples with 250–500 µm size were prepared by crushing the fresh part of the rock, sieving, washing and the removal of phenocrysts with a magnetic separator and by handpicking. Finally, the samples are soaked in 1N HCl for a few minutes to remove secondary minerals on their surface.

Neutron activation of the groundmass was performed at the Oregon State TRIGA Reactor (OSTR) in the University of Oregon, USA. The samples were irradiated by the fast neutrons in the CLICIT facility, in which a Cd tube with 0.51 mm thickness is equipped. Samples were wrapped by commercial Al foils, then were loaded into the 99.999% pure Al sample container together with the neutron-flux monitoring mineral, Fish Canyon Tuff sanidine (FC3), prepared by Geological Survey of Japan (27.5 Ma; Ishizuka, 1998; Uto et al., 1997) crystals of K<sub>2</sub>SO<sub>4</sub> and CaF<sub>2</sub> for correction of interference by the Ar isotopes produced from K and Ca in the samples. They all had been irradiated for 4 hours with the fast neutron flux of  $2.5 \times 10^{13}$  n/cm<sup>2</sup>/s. After cooling of samples, they were sent back to Potsdam then their Ar isotopes were analysed at the <sup>40</sup>Ar/<sup>39</sup>Ar geochronology laboratory in the University of Potsdam (Halama et al., 2014; Wilke et al., 2010)

The Ar isotopic analytical system consists of, (1) a New Wave Gantry Dual Wave laser ablation system with a 50W CO<sub>2</sub> laser (wavelength 10.6 micrometre) for heating samples and extracting gases, (2) an ultra-high vacuum purification line equipped with SAES getters and the cold trap held at the frozen temperature of ethanol, and (3) a high-sensitivity Micromass 5400 noble gas mass spectrometer equipped with an electron multiplier conducting the pulse-counting analysis. All groundmass samples of

about 13 mg each were firstly loaded into the sample chamber. Then the sample chamber and the purification line were baked for 24 hours at 100 and 200°C. The groundmass samples were firstly preheated and pumped with 1.2% output (0.6W), then were analysed by stepwise heating for two minutes with 10-15 steps with a continuous CO<sub>2</sub> laser beam with 1.5 mm diameter. The obtained Ar isotope ratios by the analysis are corrected for blank, mass discrimination, interferences and decay corrections following Uto et al. (1997), and then the plateau age, total gas age, normal and inverse isochron ages are calculated for each sample. Decay constants and atmospheric Ar isotope ratios follow Steiger and Jäger (1977) and the calculation of isochron ages follows York (1969). Plateau ages were determined by the criteria of Fleck et al. (1977). Finally concluded ages for each sample were obtained by the comparison among plateau age, normal and inverse isochron ages from plateau steps or all steps and total gas age with considering if the initial <sup>40</sup>Ar/<sup>36</sup>Ar ratios obtained by isochrons were valid. All results not shown in the text (i.e. Fig. 2 and Table 2) are in Supplementary Fig. 1 and Supplementary Table 2.

### **Micromorphological and SEM-EDS analyses**

We described 10 undisturbed and oriented samples. Detailed micromorphological description can be found in the Supplementary Table 3. The analysis were made in 9 x 6 cm thin sections and photographed using a polarizing microscope (Zeiss Axio Imager.A2m, Software AxioVision 4.7.2) with plane polarized light (PPL) and crossed polarized light (XPL). The most important alteration types were grouped into six categories (Table 2). The textures and microchemistry of the alterations were determined using a Hitachi TM3030 Plus Scanning electron microscope (SEM) coupled with a Bruker Quantax 70 X-ray microanalysis detector (EDS) on polished uncoated thin sections at the Institute of Mineralogy and Geodynamics, University of Tübingen.

### **X-ray diffraction (XRD)**

We analyzed the clay fraction (<2µm) of all horizons and the coarse fraction (>2mm) of selected horizons in a total of 10 and 4 samples, respectively. The coarse fraction is the rocks fragments (pyroclastic material) forming the paleosol parent material.

The clay fraction was separated in distilled water according to Stoke's law and was prepared using two different methods:

air-dried oriented preparations were obtained by pipetting some drops of the

suspensions onto a glass slide, which was then dried at 30°C for a few hours (Moore and Reynolds Jr, 1997). Ethylene glycol solvation of the slides was achieved by exposing them to ethylene glycol vapor at 70°C for a minimum of 12 hours.

randomly oriented samples, to measure the 060 reflections that allowed the distinction between dioctahedral and trioctahedral clay minerals, were prepared using a back-loading procedure (Moore and Reynolds Jr, 1997).

Measurements were made using an Empyrean diffractometer operating with an accelerating voltage of 45V and a filament current of 30mA, using  $\text{CuK}\alpha$  radiation, nickel filter and PixCELL 3D detector. Oriented samples were examined by XRD in the air-dried form, saturated with ethylene glycol (EG) and after heating (550°C). The preparations were measured over a  $2\theta$  angle range of 2-70° (air-dried) and 2-30° (glycolated and heated) with a step size of 0.04° ( $2\theta$ ) and 40s of scan step time. For randomly samples the peaks were resolved from the background by small step scan (0.002°  $2\theta$ ) and long count time (100s) measurements.

Profile fitting was calculated from oriented samples using simple peak weighting factors. For area estimation, we used Fityk (Wojdyr, 2010), a software for data processing and nonlinear **curve fitting**, simple background subtraction and easy placement of peaks and changing of peak parameters. The smectite peak was evaluated by peak fitting that is based on a pseudo-Voigt function. The decomposition of peaks using profile fitting (Lanson, 1997; Wojdyr, 2010) allows the identification of clay assemblage and provides information of peak position and full width at half maximum intensity (FWHM). For the FWHM measurement, instrumental broadening effects were calibrated via a LaB6 standard (NIST 660a).

### **Acknowledgments**

The present work was possible with financial support of the National Counsel of Technological and Scientific Development (CNPq), Brazil. We acknowledge support by Deutsche Forschungsgemeinschaft and Open Access Publishing Fund of University of Tübingen. We thank the Brazilian Navy and the colleagues (38. Polska Wyprawa Antarktyczna) from the Henry Arctowski Station for all logistics and much additional support to realize the successful field work during the Antarctic expedition in the summer of 2013/2014. We thank Dr. Michael Plötze (ETH Zürich) for providing X-ray diffraction data of rock samples. We also thank Stefan Kreißl (University of Tübingen) for helping with the SEM-EDS.

**Supplementary Table 1.** Selected main macromorphological properties (after FAO, 2006).

| Profile | Horizon | Depth<br>[cm] | Horizon<br>boundaries<br>(distinctness -<br>topography) | Structure <sup>1</sup> |           | Colour (Munsell) |                    | Rock<br>fragments  | Plant<br>fossil | Particle size<br>% |                    |                          | Textural<br>class  |
|---------|---------|---------------|---|------------------------|-----------|------------------|--------------------|--------------------|-----------------|--------------------|--------------------|--------------------------|--------------------|
|         |         |               |   | Type                   | Size      | Dry              | Name               |                    |                 | Clay<br>(<2μ)      | Silt<br>(2 μ-63 μ) | Sand<br>(63μ -<br>2000μ) |                    |
| P1      | Bwb1    | 0 - 23        | clear - wavy  | sb +pl                 | very fine | 5YR 5/4          | Dull reddish brown | many               |                 | 15                 | 18                 | 67                       | Sandy loam         |
|         | Bwb2    | 23 - 34       | gradual – smooth  | sb+pl                  | fine/thin | 2.5YR 5/4        | Dull reddish brown | common             |                 | 15                 | 19                 | 66                       | Sandy loam         |
|         | Bwb3    | 34 - 45       | abrupt- smooth  | ab                     | fine      | 2.5YR 5/4        | Dull reddish brown | common             |                 | 14                 | 19                 | 67                       | Sandy loam         |
|         | 2ABb    | 45 - 60       | clear - smooth  | ab                     | fine      | 7.5YR 7/4        | Dull orange        | none               |                 | 17                 | 21                 | 62                       | Sandy loam         |
|         | 2BAb    | 60 - 73       | abrupt - smooth   | ab+pl                  | coarse    | 10YR 6/4         | Dull yellow orange | none               |                 | 20                 | 22                 | 58                       | Sandy clay<br>loam |
|         | 3ABb    | 73+           |   |                        | pl+ab     | medium           | 5Y 4/1             | Gray               | none            | x                  | 20                 | 15                       | 65                 |
| P2      | ABb     | 0 - 20        | abrupt - smooth   | sb                     | medium    | 2.5YR 5/4        | Dull reddish brown | few                |                 | 19                 | 17                 | 64                       | Sandy clay<br>loam |
|         | Bwb1    | 20 - 30       | gradual - smooth  | ab+pl                  | coarse    | 2.5YR 2/4        | Reddish            | few                |                 | 15                 | 19                 | 66                       | Sandy loam         |
|         | Bwb2    | 30 - 53       | diffuse - irregular                                     | ab+pl                  | medium    | 2.5YR 5/4        | Dull reddish brown | common             |                 | 15                 | 18                 | 67                       | Sandy loam         |
|         | Bwb3    | 53+           |   |                        | ab+sb     | medium           | 2.5YR 5/4          | Dull reddish brown | many            |                    | 15                 | 13                       | 72                 |
| P3      | ABb     | 0 - 10        | diffuse   | sb+pl                  | fine/thin | 2.5YR 5/4        | Dull reddish brown | common             |                 | 12                 | 15                 | 73                       | Sandy loam         |
|         | Bwb     | 10 - 57       | gradual   | sb+pl                  | medium    | 2.5YR 5/4        | Dull reddish brown | common             |                 | 14                 | 20                 | 66                       | Sandy loam         |
|         | C       | 57+           |   |                        | coarse    | 7.5YR 5/3        | Dull               | many               |                 | 11                 | 10                 | 79                       | Sandy loam         |

<sup>1</sup>Structure type: ab= angular blocky., sb= subangular blocky., pl= platy. Size: vf= very fine/thin., fi= fine/thin., me=medium., co= coarse/thick

**Supplementary Table 2.**  $^{40}\text{Ar}/^{39}\text{Ar}$  analytical results of basaltic lava flows, P1-Url, P1-Lrl, P2-Url, P3-Url and P3-Lrl.

| Laser output  | $^{40}\text{Ar}/^{39}\text{Ar}$ Ar | $^{37}\text{Ar}/^{39}\text{Ar}$ Ar | $^{36}\text{Ar}/^{39}\text{Ar}$ Ar | K/Ca        | $^{40}\text{Ar}^*$ (%) | $^{39}\text{Ar}_K$ fraction (%) | $^{40}\text{Ar}^*/^{39}\text{Ar}_K$ Age ( $\pm 1 \sigma$ ) (Ma) |
|---|------------------------------------|------------------------------------|------------------------------------|-------------|------------------------|---------------------------------|---|
| <b>Sample ID: P1-Url</b> Laboratory ID: C16047 Neutron irradiation ID: PO-5 |                                    |                                    |                                    |             |                        |                                 |   |
| J= #####  |                                    |                                    | ( $\times 10^{-3}$ )               |             |                        |                                 |   |
| 1.6%  | 40.00                              | $\pm 0.19$                         | 0.361                              | $\pm 0.003$ | 39.24                  | $\pm 0.28$                      | 1.63 71.08 17.10 28.44 $\pm 0.16$ 49.44 $\pm 0.34$              |
| 2.0%  | 31.59                              | $\pm 0.04$                         | 0.521                              | $\pm 0.001$ | 4.12                   | $\pm 0.02$                      | 1.13 96.28 39.85 30.43 $\pm 0.04$ 52.85 $\pm 0.22$              |
| 2.2%  | 29.51                              | $\pm 0.09$                         | 0.942                              | $\pm 0.005$ | 2.88                   | $\pm 0.04$                      | 0.62 97.37 17.12 28.75 $\pm 0.09$ 49.98 $\pm 0.25$              |
| 2.4%  | 29.59                              | $\pm 0.14$                         | 1.265                              | $\pm 0.007$ | 3.37                   | $\pm 0.07$                      | 0.46 96.98 10.46 28.72 $\pm 0.14$ 49.93 $\pm 0.31$              |
| 2.8%  | 28.61                              | $\pm 0.16$                         | 1.640                              | $\pm 0.010$ | 4.15                   | $\pm 0.08$                      | 0.36 96.17 10.11 27.55 $\pm 0.16$ 47.91 $\pm 0.34$              |
| 3.4%  | 33.29                              | $\pm 0.23$                         | 2.451                              | $\pm 0.017$ | 27.90                  | $\pm 0.29$                      | 0.24 75.83 4.74 25.28 $\pm 0.20$ 44.02 $\pm 0.39$               |
| 4.0%  | 39.86                              | $\pm 0.29$                         | 5.778                              | $\pm 0.053$ | 59.70                  | $\pm 1.42$                      | 0.10 56.91 0.62 22.77 $\pm 0.47$ 39.69 $\pm 0.82$               |
| Plateau age (No Plateau)  |                                    |                                    |                                    |             |                        |                                 | $\pm$   |
| Total gas age   |                                    |                                    |                                    |             |                        |                                 | 50.47 $\pm 0.08$  |
| Normal isochron age (of all steps)  |                                    |                                    |                                    |             |                        |                                 | 51.93 $\pm 0.22$  |
| Inverse isochron age (of all steps)   |                                    |                                    |                                    |             |                        |                                 | 52.52 $\pm 0.22$  |
| <hr/>   |                                    |                                    |                                    |             |                        |                                 |   |
| Laser output  | $^{40}\text{Ar}/^{39}\text{Ar}$ Ar | $^{37}\text{Ar}/^{39}\text{Ar}$ Ar | $^{36}\text{Ar}/^{39}\text{Ar}$ Ar | K/Ca        | $^{40}\text{Ar}^*$ (%) | $^{39}\text{Ar}_K$ fraction (%) | $^{40}\text{Ar}^*/^{39}\text{Ar}_K$ Age ( $\pm 1 \sigma$ ) (Ma) |
| <b>Sample ID: P2-Url</b> Laboratory ID: C17003 Neutron irradiation ID: PO-5 |                                    |                                    |                                    |             |                        |                                 |   |
| J= #####  |                                    |                                    | ( $\times 10^{-3}$ )               |             |                        |                                 |   |
| 1.4%  | 345.24                             | $\pm 6.14$                         | 1.613                              | $\pm 0.049$ | #####                  | $\pm #####$                     | 0.36 10.03 1.93 34.66 $\pm 5.27$ 59.83 $\pm 8.96$               |
| 1.6%  | 100.1                              | $\pm 1.5$                          | 1.86                               | $\pm 0.03$  | 189                    | $\pm 2$                         | 0.32 44.33 6.55 44.4 $\pm 1.2$ 76 $\pm 2$                       |
| 1.8%  | 49.2                               | $\pm 0.8$                          | 2.42                               | $\pm 0.04$  | 43.6                   | $\pm 0.7$                       | 0.24 74.18 11.07 36.6 $\pm 0.7$ 63.1 $\pm 1.2$                  |
| 2.1%  | 35.9                               | $\pm 0.5$                          | 3.83                               | $\pm 0.05$  | 19.3                   | $\pm 0.3$                       | 0.15 85.00 19.39 30.6 $\pm 0.4$ 52.9 $\pm 0.8$                  |
| 2.4%  | 32.9                               | $\pm 0.5$                          | 5.33                               | $\pm 0.08$  | 14.1                   | $\pm 0.2$                       | 0.11 88.60 18.98 29.3 $\pm 0.4$ 50.6 $\pm 0.8$                  |
| 2.7%  | 34.91                              | $\pm 0.15$                         | 6.06                               | $\pm 0.04$  | 22.60                  | $\pm 0.18$                      | 0.10 82.27 15.13 28.83 $\pm 0.14$ 49.9 $\pm 0.3$                |
| 3.1%  | 31.6                               | $\pm 0.2$                          | 7.06                               | $\pm 0.05$  | 15.35                  | $\pm 0.18$                      | 0.08 87.44 12.76 27.73 $\pm 0.19$ 48.0 $\pm 0.4$                |
| 3.6%  | 35.7                               | $\pm 0.3$                          | 10.46                              | $\pm 0.10$  | 37.5                   | $\pm 0.5$                       | 0.06 71.29 8.45 25.6 $\pm 0.3$ 44.4 $\pm 0.5$                   |
| 4.2%  | 52.8                               | $\pm 0.5$                          | 13.80                              | $\pm 0.14$  | 95.7                   | $\pm 0.9$                       | 0.04 48.61 5.74 25.9 $\pm 0.4$ 44.9 $\pm 0.7$                   |
| Plateau age (Plateau: 3 steps from 2.1% to 2.7%)                            |                                    |                                    |                                    |             |                        |                                 | 50.38 $\pm 0.27$  |
| Total gas age   |                                    |                                    |                                    |             |                        |                                 | 53.04 $\pm 0.34$  |
| Normal isochron age (of all steps)  |                                    |                                    |                                    |             |                        |                                 | 48.72 $\pm 0.29$  |
| Inverse isochron age (of all steps)   |                                    |                                    |                                    |             |                        |                                 | 48.57 $\pm 0.29$  |
| <hr/>   |                                    |                                    |                                    |             |                        |                                 |   |
| Laser output  | $^{40}\text{Ar}/^{39}\text{Ar}$ Ar | $^{37}\text{Ar}/^{39}\text{Ar}$ Ar | $^{36}\text{Ar}/^{39}\text{Ar}$ Ar | K/Ca        | $^{40}\text{Ar}^*$ (%) | $^{39}\text{Ar}_K$ fraction (%) | $^{40}\text{Ar}^*/^{39}\text{Ar}_K$ Age ( $\pm 1 \sigma$ ) (Ma) |
| <b>Sample ID: P2-Lrl</b> Laboratory ID: C16048 Neutron irradiation ID: PO-5 |                                    |                                    |                                    |             |                        |                                 |   |
| J= #####  |                                    |                                    | ( $\times 10^{-3}$ )               |             |                        |                                 |   |
| 1.4%  | 230.86                             | $\pm 1.16$                         | 0.370                              | $\pm 0.006$ | 731.7                  | $\pm 3.8$                       | 1.59 6.35 2.51 14.67 $\pm 0.60$ 25.46 $\pm 1.04$                |
| 1.6%  | 43.30                              | $\pm 0.04$                         | 0.291                              | $\pm 0.001$ | 67.6                   | $\pm 0.1$                       | 2.02 53.93 49.97 23.36 $\pm 0.03$ 40.38 $\pm 0.17$              |
| 1.8%  | 39.15                              | $\pm 0.15$                         | 0.275                              | $\pm 0.002$ | 42.6                   | $\pm 0.2$                       | 2.14 67.87 17.17 26.57 $\pm 0.13$ 45.87 $\pm 0.28$              |
| 2.0%  | 45.94                              | $\pm 0.24$                         | 0.462                              | $\pm 0.003$ | 62.7                   | $\pm 0.3$                       | 1.27 59.78 8.46 27.47 $\pm 0.20$ 47.40 $\pm 0.39$               |
| 2.3%  | 57.61                              | $\pm 0.32$                         | 0.601                              | $\pm 0.004$ | 101.9                  | $\pm 0.6$                       | 0.98 47.80 5.61 27.55 $\pm 0.28$ 47.52 $\pm 0.52$               |
| 2.7%  | 56.19                              | $\pm 0.30$                         | 0.923                              | $\pm 0.008$ | 98.7                   | $\pm 0.5$                       | 0.64 48.25 6.14 27.13 $\pm 0.25$ 46.81 $\pm 0.46$               |
| 3.2%  | 55.19                              | $\pm 0.28$                         | 1.877                              | $\pm 0.012$ | 100.0                  | $\pm 0.6$                       | 0.31 46.73 7.67 25.82 $\pm 0.25$ 44.58 $\pm 0.47$               |
| 3.7%  | 95.53                              | $\pm 0.49$                         | 3.607                              | $\pm 0.022$ | 242.4                  | $\pm 1.3$                       | 0.16 25.32 2.30 24.24 $\pm 0.42$ 41.89 $\pm 0.73$               |
| 4.2%  | 343.02                             | $\pm 4.26$                         | 4.044                              | $\pm 0.067$ | 1150.1                 | $\pm 15.4$                      | 0.15 1.02 0.17 3.49 $\pm 2.95$ 6.10 $\pm 5.13$                  |
| Plateau age (No Plateau)  |                                    |                                    |                                    |             |                        |                                 | $\pm$   |
| Total gas age   |                                    |                                    |                                    |             |                        |                                 | 42.64 $\pm 0.08$  |
| Normal isochron age (of all steps)  |                                    |                                    |                                    |             |                        |                                 | 42.51 $\pm 0.20$  |
| Inverse isochron age (of all steps)   |                                    |                                    |                                    |             |                        |                                 | 42.66 $\pm 0.20$  |
| <hr/>   |                                    |                                    |                                    |             |                        |                                 |   |
| Laser output  | $^{40}\text{Ar}/^{39}\text{Ar}$ Ar | $^{37}\text{Ar}/^{39}\text{Ar}$ Ar | $^{36}\text{Ar}/^{39}\text{Ar}$ Ar | K/Ca        | $^{40}\text{Ar}^*$ (%) | $^{39}\text{Ar}_K$ fraction (%) | $^{40}\text{Ar}^*/^{39}\text{Ar}_K$ Age ( $\pm 1 \sigma$ ) (Ma) |
| <b>Sample ID: P3-Url</b> Laboratory ID: C17001 Neutron irradiation ID: PO-5 |                                    |                                    |                                    |             |                        |                                 |   |
| J= #####  |                                    |                                    | ( $\times 10^{-3}$ )               |             |                        |                                 |   |
| 1.4%  | 2006.4                             | $\pm 19.4$                         | 8.7                                | $\pm 0.2$   | 6539.6                 | $\pm 66.5$                      | 0.07 3.72 1.49 75.05 $\pm 12.38$ 130.55 $\pm 20.79$             |
| 1.6%  | 145.7                              | $\pm 2.8$                          | 5.6                                | $\pm 0.1$   | 362.1                  | $\pm 8.8$                       | 0.10 26.88 6.13 39.31 $\pm 2.91$ 69.57 $\pm 5.06$               |
| 1.8%  | 85.5                               | $\pm 2.1$                          | 8.3                                | $\pm 0.2$   | 179.2                  | $\pm 5.4$                       | 0.07 38.86 10.16 33.43 $\pm 1.99$ 59.32 $\pm 3.48$              |
| 2.0%  | 56.6                               | $\pm 1.0$                          | 11.0                               | $\pm 0.2$   | 87.6                   | $\pm 2.0$                       | 0.05 55.85 15.87 31.86 $\pm 0.90$ 56.59 $\pm 1.60$              |
| 2.2%  | 47.8                               | $\pm 0.5$                          | 13.9                               | $\pm 0.2$   | 69.8                   | $\pm 0.8$                       | 0.04 59.23 19.91 28.58 $\pm 0.43$ 50.84 $\pm 0.78$              |
| 2.4%  | 42.8                               | $\pm 0.5$                          | 16.2                               | $\pm 0.2$   | 59.4                   | $\pm 0.9$                       | 0.04 62.05 13.80 26.83 $\pm 0.45$ 47.77 $\pm 0.82$              |
| 2.7%  | 61.2                               | $\pm 0.8$                          | 16.4                               | $\pm 0.2$   | 117.5                  | $\pm 1.9$                       | 0.04 45.41 11.30 28.10 $\pm 0.73$ 50.00 $\pm 1.29$              |
| 3.2%  | 41.8                               | $\pm 0.6$                          | 21.1                               | $\pm 0.3$   | 61.4                   | $\pm 1.0$                       | 0.03 60.62 12.61 25.69 $\pm 0.54$ 45.76 $\pm 0.97$              |
| 3.8%  | 73.6                               | $\pm 1.0$                          | 31.8                               | $\pm 0.4$   | 177.9                  | $\pm 2.5$                       | 0.02 32.05 8.72 24.09 $\pm 0.82$ 42.94 $\pm 1.45$               |
| Plateau age (No Plateau)  |                                    |                                    |                                    |             |                        |                                 | $\pm$   |
| Total gas age   |                                    |                                    |                                    |             |                        |                                 | 53.14 $\pm 0.70$  |
| Normal isochron age (of all steps)  |                                    |                                    |                                    |             |                        |                                 | 47.89 $\pm 0.52$  |
| Inverse isochron age (of all steps)   |                                    |                                    |                                    |             |                        |                                 | 48.21 $\pm 0.52$  |
| <hr/>   |                                    |                                    |                                    |             |                        |                                 |   |
| Laser output  | $^{40}\text{Ar}/^{39}\text{Ar}$ Ar | $^{37}\text{Ar}/^{39}\text{Ar}$ Ar | $^{36}\text{Ar}/^{39}\text{Ar}$ Ar | K/Ca        | $^{40}\text{Ar}^*$ (%) | $^{39}\text{Ar}_K$ fraction (%) | $^{40}\text{Ar}^*/^{39}\text{Ar}_K$ Age ( $\pm 1 \sigma$ ) (Ma) |
| <b>Sample ID: P3-Lrl</b> Laboratory ID: C17005 Neutron irradiation ID: PO-5 |                                    |                                    |                                    |             |                        |                                 |   |
| J= #####  |                                    |                                    | ( $\times 10^{-3}$ )               |             |                        |                                 |   |
| 1.4%  | 267.44                             | $\pm 2.67$                         | 1.52                               | $\pm 0.04$  | 875.27                 | $\pm 7.86$                      | 0.39 3.34 2.06 8.93 $\pm 1.86$ 16.04 $\pm 3.32$                 |
| 1.6%  | 38.01                              | $\pm 0.47$                         | 0.87                               | $\pm 0.01$  | 32.63                  | $\pm 0.38$                      | 0.67 74.81 10.69 28.45 $\pm 0.42$ 50.62 $\pm 0.76$              |
| 1.8%  | 32.85                              | $\pm 0.15$                         | 1.04                               | $\pm 0.01$  | 5.91                   | $\pm 0.07$                      | 0.57 94.94 22.36 31.21 $\pm 0.15$ 55.44 $\pm 0.34$              |
| 2.0%  | 30.36                              | $\pm 0.25$                         | 2.26                               | $\pm 0.02$  | 6.46                   | $\pm 0.09$                      | 0.26 94.31 19.52 28.68 $\pm 0.24$ 51.01 $\pm 0.46$              |
| 2.2%  | 29.64                              | $\pm 0.19$                         | 3.32                               | $\pm 0.02$  | 7.04                   | $\pm 0.09$                      | 0.18 93.89 18.69 27.89 $\pm 0.18$ 49.63 $\pm 0.38$              |
| 2.4%  | 29.68                              | $\pm 0.16$                         | 4.20                               | $\pm 0.02$  | 8.02                   | $\pm 0.12$                      | 0.14 93.15 12.21 27.72 $\pm 0.15$ 49.33 $\pm 0.33$              |
| 2.7%  | 28.43                              | $\pm 0.15$                         | 5.10                               | $\pm 0.03$  | 8.25                   | $\pm 0.15$                      | 0.11 92.88 8.27 26.50 $\pm 0.15$ 47.18 $\pm 0.32$               |
| 3.1%  | 26.04                              | $\pm 0.28$                         | 8.37                               | $\pm 0.09$  | 18.14                  | $\pm 0.31$                      | 0.07 82.01 4.33 21.48 $\pm 0.27$ 38.34 $\pm 0.50$               |
| 3.7%  | 39.58                              | $\pm 0.48$                         | 17.45                              | $\pm 0.25$  | 79.59                  | $\pm 1.26$                      | 0.03 44.13 1.88 17.67 $\pm 0.48$ 31.60 $\pm 0.87$               |
| Plateau age (Plateau: 3 steps from 2.0% to 2.4%)                            |                                    |                                    |                                    |             |                        |                                 | 49.81 $\pm 0.22$  |
| Total gas age   |                                    |                                    |                                    |             |                        |                                 | 49.56 $\pm 0.16$  |
| Normal isochron age (of all steps)  |                                    |                                    |                                    |             |                        |                                 | 49.71 $\pm 0.23$  |
| Inverse isochron age (of all steps)   |                                    |                                    |                                    |             |                        |                                 | 50.83 $\pm 0.24$  |

#100% corresponds to 50W output of CO<sub>2</sub> laser. All the errors indicate 1 sigma error.  $^{40}\text{Ar}^*$ : radiogenic <sup>4</sup>

**Supplementary Table 3.** Selected main micromorphological characteristic

| Profile   | Horizon | Depth<br>[cm] | Pedality |    |    | Voids |     |    |    |    |    | Accomodation |   |             | Microstructure | Micromass |        |          | Plant residue | Pedofeatures |    |           | Zeolite |   |
|-----------|---------|---------------|----------|----|----|-------|-----|----|----|----|----|--------------|---|-------------|----------------|-----------|--------|----------|---------------|--------------|----|-----------|---------|---|
|           |         |               | sp       | mp | wp | spv   | cmv | cx | ch | cm | ve | vu           | a | pa          |                | un        | Colour | b-fabric |               | cc           | pf | Fe/Mn nod |         |   |
| <b>P1</b> | Bwb1    | 0 - 23        | x        |    |    | x     |     | x  | x  |    | x  | x            | x | sb, (gr-cr) | br, rd, lb, bl | rd        | x      |          |               | x            | x  |           | x       |   |
|           | Bwb2    | 23 - 34       |          |    | x  |       |     |    |    |    |    |              |   | (sb)        | br, rd, lb, bl | rd        | x      |          |               |              |    | x         |         |   |
|           | Bwb3    | 34 - 45       |          | x  |    |       |     | x  |    |    |    |              |   | sb, (gr)    | br, rd, lb, bl | rd        | x      |          |               |              |    | x         |         |   |
|           | 2ABb    | 45 - 60       |          |    | x  |       |     | x  |    |    |    |              |   | (sb)        | lb, br, rd     | lb, br    | x      | (x)      | (x)           | x            |    | x         | x       |   |
|           | 2BAb    | 60 - 73       |          | x  |    |       |     |    |    |    | x  | x            |   | (gr)        | lb, br, rd     | lb, br    | x      | (x)      | (x)           | x            |    | x         | x       |   |
|           | 3ABb    | 73+           |          |    |    |       |     |    |    |    |    |              |   |             | gr, lb, br     | ol, lb    | x      | (x)      | (x)           |              |    | x         | x       |   |
| <b>P2</b> | ABb     | 0 - 20        |          | x  |    | x     | x   | x  | x  |    | x  | x            | x | sb, gr      | br, lb, rd, bl | rd        | x      |          |               | x            |    |           | x       | x |
|           | Bwb1    | 20 - 30       |          | x  |    |       |     | x  |    |    | x  | x            | x | sb, (gr-cr) | br, lb, rd, bl | rd        | x      |          |               |              |    | x         | x       |   |
|           | Bwb2    | 30 - 53       |          |    | x  |       |     | x  |    | x  | x  |              |   | (sb)        | br, lb, rd, bl | rd        | x      |          |               |              |    | x         | x       |   |
|           | Bwb3    | 53+           |          |    | x  |       |     | x  |    |    | x  | x            |   | (sb)        | br, lb, rd, bl | rd        | x      |          |               |              |    | x         | x       |   |

The micromorphological property is shown by the presence (cross) or absence (no cross).

The brackets are used when the property is weakly expressed

Pedality: sp=strongly developed pedality., mp=moderately developed., wp=weakly developed

Voids: spv= simple packing voids., cmv= compound packing voids., cxp= complex packing voids., ch= channels., cm= chamber., ve= vesicles., vu= vughs

Accomodation of planar voids: a= accommodated., pa= partially accommodated., un= unaccommodated

Microstructure: sb= subangular., gr= granular., cr= crumb

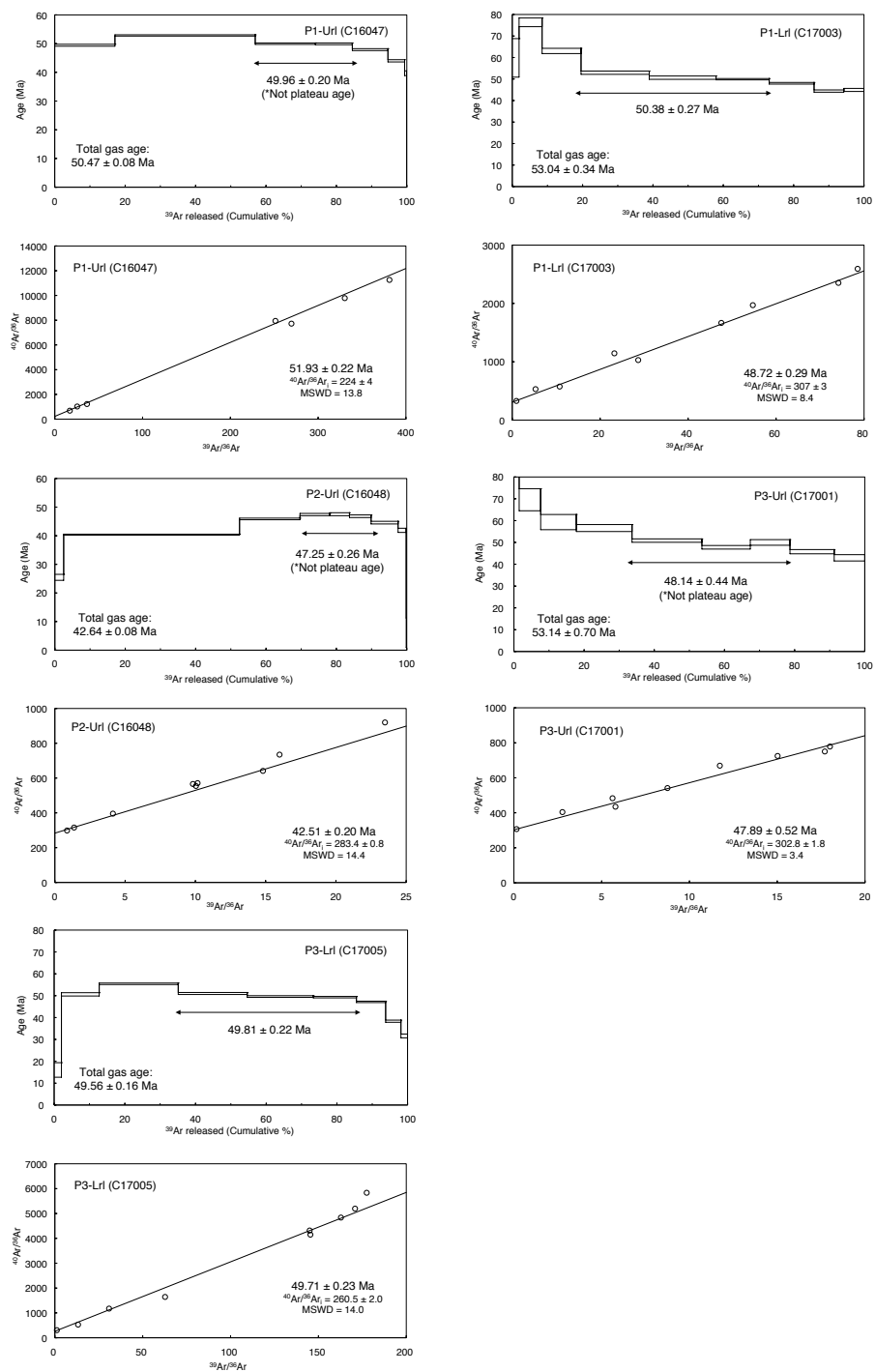
Colour: PPL (Plane Polarized Light); OIL (Oblique Incident Light): rd= red., br= brown., bl= black., lb= light brown., ol= olive, gr= grey

b-fabric: u= undifferentiated., ssp= stipple speckled., gs= granostriated

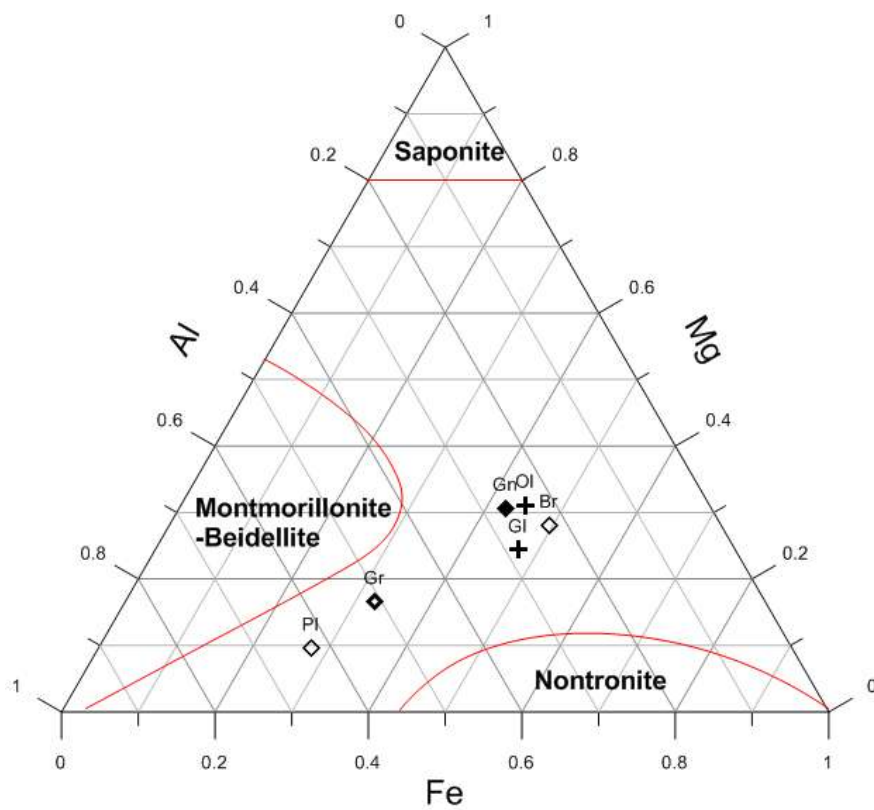
Pedofeatures: cc = clay coatings, pf= passage features, Fe/Mn nod = iron/manganese nodules

**Supplementary Table 4.** Alteration types distribution through the paleosols horizons.

| Profile   | Horizon | Depth<br>(cm) | Alteration type |             |       |                    |                   |                    |
|-----------|---------|---------------|-----------------|-------------|-------|--------------------|-------------------|--------------------|
|           |         |               | Transformation  |             |       | Neoformation       |                   |                    |
|           |         |               | Olivine         | Plagioclase | Glass | Brown<br>infilling | Grey<br>infilling | Green<br>infilling |
| <b>P1</b> | Bwb1    | 0-23          | x               | x           | x     | x                  |                   |                    |
|           | Bwb2    | 23-34         | x               | x           | x     | x                  |                   |                    |
|           | Bwb3    | 34-45         | x               | x           | x     | x                  |                   |                    |
|           | 2ABb    | 45-60         | x               | x           | x     | x                  |                   |                    |
|           | 2BAb    | 60-73         | x               | x           | x     | x                  |                   |                    |
|           | 3ABb    | 73+           | x               | x           | x     | x                  |                   |                    |
| <b>P2</b> | ABb     | 0-20          | x               | x           | x     | x                  | x                 |                    |
|           | Bwb1    | 20-30         | x               | x           | x     | (x)                | x                 |                    |
|           | Bwb2    | 30-53         | x               | x           | x     | (x)                | x                 |                    |
|           | Bwb3    | 53+           | x               | x           | x     | (x)                | x                 | x                  |



**Supplementary Figure 1.**  $^{40}\text{Ar}/^{39}\text{Ar}$  age spectra and normal isochron plots obtained by the stepwise heating analysis of the other five groundmass samples than the sample P2-LrI shown in Fig. 2 in the text. Sample-ID and Laboratory-ID are indicated in all figures. Closed circles in the isochron plot are derived from plateau steps instead open circles are not



**Supplementary Figure 2.**  $\text{Fe}_2\text{O}_3 - \text{Al}_2\text{O}_3 - \text{MgO}$  Ternary diagram with the average chemical composition (EDS values) of each alteration. Br = brown infilling; Gr = grey infilling; Gn = green infilling; OI = olivine alteration; PI = plagioclase alteration; GI = glass alteration.

## References

- Arduino, E., Barberis, E., Carraro, F., Forno, M.G., 1984. Estimating relative ages from Iron-oxide/Total-Iron ratio of soils in the Western Po Valley, Italy. *Geoderma* 33, 39–52.
- Askin, R.A., 1991. Late Cretaceous-Early Tertiary Antarctic outcrop evidence for past vegetation and climates, in: Kennett, J.P., Warnke, D.. (Eds.), *The Antarctic Paleoenvironment: A Perspective on Global Change*. Antarctic Research Series. American Geophysical Union, Washington D.C, pp. 61–73.
- Bakker, L., Lowe, D.J., Jongmans, A.G., 1996. A micromorphological study of pedogenic processes in an evolutionary soil sequence formed on Late Quaternary rhyolitic tephra deposits, North Island, New Zealand. *Quat. Int.* 34–36, 249–261. doi:10.1016/1040-6182(95)00090-9
- Barrett, P., 2008. A History of Antarctic Cenozoic Glaciation - View from the Margin. *Dev. Earth Environ. Sci.* 8, 33–83. doi:10.1016/S1571-9197(08)00003-7
- Barrón, V., Montealegre, L., 1986. Iron Oxides and Colour of Triassic Sediments: Application of the Kubelka-Munk Theory. *Am. J. Sci.* doi:10.2475/ajs.286.10.792
- Berggaut, V., Singer, A., Stahr, K., 1994. Palagonite reconsidered: Paracrystalline illite-smectites from regoliths on basic pyroclastics. *Clays Clay Miner.* 42, 582–592. doi:10.1346/CCMN.1994.0420511
- Bijl, P.K., Schouten, S., Sluijs, A., Reichert, G.-J., Zachos, J.C., Brinkhuis, H., 2009. Early Palaeogene temperature evolution of the southwest Pacific Ocean. *Nature* 461, 776–779. doi:10.1038/nature08399
- Birkenmajer, K., 1988. Tertiary glacial and interglacial deposits, South Shetland Islands, Antarctica: geochronology versus biostratigraphy. *Bull. Polish Acad. Sci. Earth Sci.* 36, 133–145.
- Birkenmajer, K., 1980a. Tertiary volcanic-sedimentary succession at Admiralty Bay, King George Island (South Shetland Islands, Antarctica). *Stud. Geol. Pol.* 64, 7–65.
- Birkenmajer, K., 1980b. Geology of Admiralty Bay , King George Island ( South Shetland Islands ) — An outline. *Polish Polar Res.* 1, 29–54.
- Birkenmajer, K., Gaździcki, A., Krajewski, K.P., Przybycin, A., Solecki, A., Tatur, A., Yoon, H.I., 2005. First Cenozoic glaciers in West Antarctica. *Polish Polar Res.* 26, 3–12.
- Birkenmajer, K., Łydka, K., 1990. Mineralogical evidence for warm Palaeogene

- climate from the Ezcurra Inlet Group, King George Island, West Antarctica. *Bull. Polish Acad. Sci. Earth Sci.* 38, 25–38.
- Birkenmajer, K., Zastawniak, E., 1989. Late Cretaceous-early Tertiary floras of King George Island, West Antarctica: their stratigraphic distribution and palaeoclimatic significance. *Geol. Soc. London, Spec. Publ.* 47, 227–240. doi:10.1144/GSL.SP.1989.047.01.17
- Blesa, M., Matijević, E., 1989. Phase transformations of iron oxides, oxohydroxides, and hydrous oxides in aqueous media. *Adv. Colloid Interface Sci.* 29, 173–221. doi:10.1016/0001-8686(89)80009-0
- Blodgett, R., Crabaugh, J., McBride, E.F., 1993. The colour of red beds: a geologic perspective, in: Bigham, J.H., Ciolkosz, E. (Eds.), *Soil Colour*. Soil Science Society of America Special Publication, pp. 127–159.
- Borchardt, G., 1989. Smectites, in: Dixon, J., Weed, S. (Eds.), *Minerals in Soil Environments*. Soil Science Society of America, Madison, Wisconsin, pp. 675–727.
- Bouma, J., Fox, C., Miedma, R., 1990. Micromorphology of hydromorphic soils: applications for soil genesis and land evaluation, in: Douglas, L. (Ed.), *Soil Micromorphology: A Basic and Applied Science*. Elsevier, Amsterdam, pp. 257–278.
- Bronger, A., Heinkele, T., 1990. Mineralogical and clay mineralogical aspects of loess research. *Quat. Int.* 7/8, 37–51.
- Buurman, P., 1975. Possibilities of paleopedology. *Sedimentology* 22, 289–298.
- Canile, F.M., 2010. Evidências geológicas de mudanças climáticas (greenhouse-icehouse) na Antártica Ocidental durante a passagem Eoceno-Oligoceno. Universidade Federal de São Paulo.
- Churchman, G.J., Lowe, D., 2012. Alteration, formation, and occurrence of minerals in soils. *Handb. Soil Sci. Prop. Process.* 1, 20–72. doi:doi:10.1201/b11267-24
- Colman, S.M., 1982. Clay mineralogy of weathering rinds and possible implications concerning the sources of clay minerals in soils. *Geology* 10, 370–375.
- Commission Internationale de L'Eclairage, 1978. Recommendations on uniform colour spaces colour difference equations psychometric colour terms, Supplement 2. CIE Publ. 15 (E-1.3.1) 1971/(TC-1.3). Bur. Centrale de la CIE. Paris. Paris.
- Cornell, R.M., Schwertmann, U., 2003. *The Iron Oxides - Structure, properties,*

- reactions, occurrences and uses, 2nd ed. Wiley-VCH Verlag, Weinheim.
- Coxall, H.K., Wilson, P.A., Pälike, H., Lear, C.H., Backman, J., 2005. Rapid stepwise onset of Antarctic glaciation and deeper calcite compensation in the Pacific Ocean. *Nature* 433, 53–57. doi:10.1038/nature03135
- Craig, P., Chevrier, V., Sayyed, M.R.G., Islam, R., 2017. Spectral analysis of Deccan intrabasaltic bole beds: Implications for the formation and alteration of phyllosilicates on Mars. *Planet. Space Sci.* 135, 55–63. doi:10.1016/j.pss.2016.11.008
- D'Amore, D. V., Stewart, S.R., Huddleston, J.H., 2004. Saturation, Reduction, and the Formation of Iron–Manganese Concretions in the Jackson-Frazier Wetland, Oregon. *Soil Sci. Soc. Am. J.* 68, 1012. doi:10.2136/sssaj2004.1012
- Dahms, D., 1994. Mid-holocene erosion of soil catenas on moraines near the type pinedale till, wind river range, Wyoming. *Quat. Res.* 42, 41–48.
- Dalrymple, J.B., Jim, C.Y., 1984. Experimental study of soil microfabrics induced by isotropic stresses of wetting and drying. *Geoderma* 34, 43–68. doi:10.1016/0016-7061(84)90005-3
- Dawit, E.L., 2016. Paleoclimatic records of Late Triassic paleosols from Central Ethiopia. *Palaeogeogr. Palaeoclimatol. Palaeoecol.* 449, 127–140. doi:10.1016/j.palaeo.2016.02.011
- Dearing, J.A., 1999. Environmental Magnetic Susceptibility Using the Bartington MS2 System. *Interpret. A J. Bible Theol.* 52.
- Dearing, J.A., Hay, K.L., Baban, S.M.J., Huddleston, A.S., Wellington, E.M.H., Loveland, P.J., 1996. Magnetic susceptibility of soil: An evaluation of conflicting theories using a national data set. *Geophys. J. Int.* 127, 728–734. doi:10.1111/j.1365-246X.1996.tb04051.x
- DeConto, R.M., Pollard, D., 2003. Rapid Cenozoic glaciation of Antarctica induced by declining atmospheric CO<sub>2</sub>. *Nature* 421, 245–249. doi:10.1038/nature01290
- Delvigne, J., 1998. Atlas of Micromorphology of Mineral Alteration and Weathering, ORSTOM. ed. Mineralogical Association of Canada, Ottawa.
- Delvigne, J., 1990. Hypogene and supergene alteration of orthopyroxene in the Koua Bocca ultra mafic intrusion, Ivory Coast. *Chem. Geol.* 84, 49–53.
- Delvigne, J., Bisdorf, E.B., Sleeman, J., Stoops, G., 1979. Olivines, their pseudomorphs and secondary products. *Pedologie* 3, 247–309.
- DIN ISO 10693, 1995. Bodenbeschaffenheit Bestimmung des Carbonatgehaltes e

Volumetrisches Verfahren. Beuth, Berlin.

- DIN ISO 10694, 1995. Bodenbeschaffenheit Bestimmung von organischem Kohlenstoff und Gesamtkohlenstoff nach trockener Verbrennung (Elementaranalyse). Beuth, Berlin.
- Dingle, R.V., Lavelle, M., 2000. Antarctic Peninsula Late Cretaceous-Early Cenozoic paleoenvironments and Gondwana paleogeographies. *J. African Earth Sci.* 31, 91–105. doi:10.1016/S0899-5362(00)00075-0
- Dingle, R. V., Lavelle, M., 1998a. Antarctic Peninsular cryosphere: Early Oligocene (c. 30 Ma) initiation and a revised glacial chronology. *J. Geol. Soc. London.* 155, 433–437. doi:10.1144/gsjgs.155.3.0433
- Dingle, R. V., Lavelle, M., 1998b. Late Cretaceous-Cenozoic climatic variations of the northern Antarctic Peninsula: New geochemical evidence and review. *Palaeogeogr. Palaeoclimatol. Palaeoecol.* 141, 215–232. doi:10.1016/S0031-0182(98)00056-X
- Dudas, M.J., Harward, M.E., 1975. Inherited and detrital 2:1 type phyllosilicates in soils developed from Mazama ash. *Soil Sci. Soc. Am. J.* 39, 571–577. doi:10.2136/sssaj1975.03615995003900030050x
- Eberl, D.D., 1984. Clay mineral formation and transformation in rocks and soils. *Philos. Trans. R. Soc. London* 311, 241–257.
- Ehrmann, W.U., Melles, M., Kuhn, G., Grobe, H., 1992. Significance of clay mineral assemblages in the Antarctic Ocean. *Mar. Geol.* 107, 249–273. doi:10.1016/0025-3227(92)90075-S
- Elliot, D.H., Askin, R.A., Kyte, F.T., Zinsmeister, W.J., 1994. Iridium and dinocysts at the Cretaceous-Tertiary boundary on Seymour Island, Antarctica: implications for the K-T event. *Geology* 22, 675–678. doi:10.1130/0091-7613
- Emeleus, C.H., Allwright, E.A., Kerr, A.C., Williamson, I.T., 1996. Red tuffs in the Palaeocene lava successions of the Inner Hebrides. *Scottish J. Geol.* 32, 83–90. doi:10.1144/sjg32010083
- FAO, 2006. Guidelines for soil description, 4th ed. Rome.
- Fedoroff, N., Courty, M.-A., Guo, Z., 2010. Paleosoils and Relict Soils, in: Stoops, G. Marcelino, V. Mees, F. (Ed.), *Interpretation of Micromorphological Features of Soils and Regoliths*. Elsevier, Amsterdam, pp. 623–662. doi:10.1016/B978-0-444-53156-8.00027-1
- Feldmann, R., Woodburne, M., 1988. Geology and paleontology of Seymour Island,

- Antarctic Peninsula. Geological Society of America, Memoir 169.
- Fenwick, I., M., 1985. Paleosols: problems of recognition and interpretation, in: Boardman, J. (Ed.), *Soils and Quaternary Landscape Evolution*. John Wiley and Sons, Norwich, p. 391.
- Fiore, S., 1993. The occurrences of smectite and illite in a pyroclastic deposit prior to weathering: implications on the genesis of 2:1 clay minerals in volcanic soils. *Appl. Clay Sci.* 8, 249–259. doi:10.1016/0169-1317(93)90007-N
- Fiore, S., Huertas, F., Linares, J., 1992. Mineralogy and geochemistry of some “so-called” paleosols from Mt. Vulture volcano (southern Italy). *Chem. Geol.* 99, 237–252. doi:10.1016/0009-2541(92)90179-9
- Fleck, R., Sutter, J., Elliot, D., 1977. Interpretation of discordant  $^{40}\text{Ar}/^{39}\text{Ar}$  age spectra of Mesozoic tholeiites from Antarctica. *Geochim. Cosmochim. Acta* 41, 15–32.
- Francis, J., Poole, I., 2002. Cretaceous and early Tertiary climates of Antarctica: evidence from fossil wood. *Palaeogeogr. Palaeoclimatol. Palaeoecol.* 182, 47–64.
- Francis, J.E., Ashworth, A., Cantrill, D.J., Crame, J.A., Howe, J., Stephens, R., Tosolini, A.-M., Thorn, V., 2007. 100 Million Years of Antarctic Climate Evolution: Evidence from Fossil Plants. *Proc. 10th Int. Symp. Antarct. Earth Sci.* 19–27. doi:10.3133/of2007-1047.kp03
- Francis, J.E., Marensi, S., Levy, R., Hambrey, M., Thorn, V.C., Mohr, B., Brinkhuis, H., Warnaar, J., Zachos, J., Bohaty, S., DeConto, R., 2009. From Greenhouse to Icehouse - The Eocene/Oligocene in Antarctica. *Dev. Earth Environ. Sci.* 8, 309–368. doi:10.1016/S1571-9197(08)00008-6
- Galán, E., 2006. Genesis of Clay Minerals, in: *Developments in Clay Science*. pp. 1129–1162. doi:10.1016/S1572-4352(05)01042-1
- García-Romero, E., Vegas, J., Baldonado, J.L., Marfil, R., 2005. Clay minerals as alteration products in basaltic volcanoclastic deposits of La Palma (Canary Islands, Spain). *Sediment. Geol.* 174, 237–253. doi:10.1016/j.sedgeo.2004.12.007
- Gérard, M., Caquineau, S., Chenet, A., Fluteau, F., Courtillot, V., Subbarao, K. V., 2006. Red boles in the Deccan traps: time constraints from alteration processes, in: *Geophysical Research Abstracts*. p. 7092.
- Gérard, M., Caquineau, S., Pinheiro, J., Stoops, G., 2007. Weathering and allophane

- neof ormation in soils developed on volcanic ash in the Azores. *Eur. J. Soil Sci.* 58, 496–515. doi:10.1111/j.1365-2389.2007.00910.x
- Ghosh, P., Sayeed, M.R.G., Islam, R., Hundekari, S.M., 2006. Inter-basaltic clay (bole bed) horizons from Deccan traps of India: Implications for palaeo-weathering and palaeo-climate during Deccan volcanism. *Palaeogeogr. Palaeoclimatol. Palaeoecol.* 242, 90–109. doi:10.1016/j.palaeo.2006.05.018
- Gialanella, S., Girardi, F., Ischia, G., Lonardelli, I., Mattarelli, M., Montagna, M., 2010. On the goethite to hematite phase transformation. *J. Therm. Anal. Calorim.* 102, 867–873. doi:10.1007/s10973-010-0756-2
- Graef, F., Singer, A., Stahr, K., Jahn, R., 1997. Genesis and diagenesis of paleosols from Pliocene volcanics on the Golan Heights. *Catena* 30, 149–167. doi:10.1016/S0341-8162(97)00026-X
- Greenwood, D.R., Wing, S.L., 1995. Eocene continental climates and latitudinal temperature gradients. *Geology* 23, 1044–1048.
- Griener, K.W., Nelson, D.M., Warny, S., 2013. Declining moisture availability on the Antarctic Peninsula during the Late Eocene. *Palaeogeogr. Palaeoclimatol. Palaeoecol.* 383–384, 72–78. doi:10.1016/j.palaeo.2013.05.004
- Gualtieri, A.F., Venturelli, P., 1999. In situ study of the goethite-hematite phase transformation by real time synchrotron powder diffraction. *Am. Mineral.* 84, 895–904. doi:10.2138/am-1999-5-624
- Halama, R., Konrad-Schmolke, M., Sudo, M., Marschall, H., Wiedenbeck, M., 2014. Effects of fluid-rock interaction on  $^{40}\text{Ar}/^{39}\text{Ar}$  geochronology in high-pressure rocks (Sesia-Lanzo Zone, Western Alps). *Geochim. Cosmochim. Acta* 126, 475–494.
- Heidari, A., Mahmoodi, S., Stoops, G., Mees, F., 2004. Micromorphological Characteristics of Vertisols of Iran, Including Nonsmectitic Soils. *Arid L. Res. Manag.* 19, 29–46. doi:10.1080/15324980590887164
- Hekinian, R., 1982. *Petrology of the Ocean Floor*, Elsevier O. ed. Elsevier, Amsterdam-Oxford-New York. doi:10.1016/S0422-9894(08)70937-1
- Holliday, V., 1988. Genesis of a late-holocene soil chronosequence at the Lubbock lake archeological site, Texas. *Ann. Assoc. Am. Geogr.* 78, 594–610.
- Huber, M., Brinkhuis, H., Stickley, C.E., Döös, K., Sluijs, A., Warnaar, J., Schellenberg, S.A., Williams, G.L., 2004. Eocene circulation of the Southern Ocean: Was Antarctica kept warm by subtropical waters? *Paleoceanography*

- 19, 1–12. doi:10.1029/2004PA001014
- Hund, F., 1981. Inorganic Pigments: Bases for Coloured, Uncoloured, and Transparent Products. *Angew. Chemie Int. Ed. English* 20, 723–730. doi:10.1002/anie.198107231
- Hunt, R.J., Poole, I., 2003. Paleogene West Antarctic climate and vegetation history in light of new data from King George Island. *Geol. Soc. Am. Spec. Pap.* 369, 395–412. doi:10.1130/0-8137-2369-8.395
- IREN, 1978. Estudio de suelos de la provincia de Valdivia.
- Ishizuka, O., 1998. Vertical and horizontal variation of the fast neutron flux in a single irradiation capsule and their significance in the laser-heating  $^{40}\text{Ar}/^{39}\text{Ar}$  analysis: Case study for the hydraulic rabbit facility of the JMTR reactor, Japan. *Geochem. J.* 32, 243–252.
- IUSS Working Group WRB, 2014. World reference base for soil resources 2014. International soil classification system for naming soils and creating legends for soil maps, World Soil Resources Reports No. 106. doi:10.1017/S0014479706394902
- Jeong, G.Y., Yoon, H. II, Lee, S.Y., 2004. Chemistry and microstructures of clay particles in smectite-rich shelf sediments, South Shetland Islands, Antarctica. *Mar. Geol.* 209, 19–30. doi:10.1016/j.margeo.2004.05.027
- Jiang, L., Chen, G., Grapes, R., Peng, Z., 2015. Journal of Asian Earth Sciences Thermal origin of continental red beds in SE China : An experiment study. *J. Asian Earth Sci.* 101, 14–19. doi:10.1016/j.jseaes.2015.01.019
- Jongmans, A.G., Nieuwenhuysse, A., Buurman, P., van Doesburg, J.D.J., van Oort, F., Jaunet, A.M., 1994. Inheritance of 2:1 phyllosilicates in Costa Rican Andisols. *Soil Sci. Soc. Am. J.* 58, 494–501. doi:10.2136/sssaj1994.03615995005800020035x
- Jongmans, a. G., Nieuwenhuysse, a., Buurman, P., van Doesburg, J.D.J., van Oort, F., Jaunet, a. M., 1994. Inheritance of 2:1 Phyllosilicates in Costa Rican Andisols. *Soil Sci. Soc. Am. J.* 58, 494. doi:10.2136/sssaj1994.03615995005800020035x
- Kovda, I., Mermut, A.R., 2010. Vertic Features, in: Stoops, G., Marcelino, V., Mees, F. (Eds.), *Interpretation of Micromorphological Features of Soils and Regoliths*. Elsevier, Amsterdam, pp. 109–122. doi:10.1016/B978-0-444-53156-8.00013-1
- Kraus, M.J., 1997. Lower Eocene alluvial paleosols: Pedogenic development,

- stratigraphic relationships, and paleosol/landscape associations. *Palaeogeogr. Palaeoclimatol. Palaeoecol.* 129, 387–406. doi:10.1016/S0031-0182(96)00056-9
- Kraus, M.J., Hasiotis, S.T., 2006. Significance of different modes of rhizolith preservation to interpreting paleoenvironmental and paleohydrologic settings: Examples from Paleogene paleosols, Birghorn Basin, Wyoming, U.S.A. *J. Sediment. Res.* 76, 633–646. doi:10.2110/jsr.2006.052
- Kristmannsdottir, H., Tomasson, J., 1978. Zeolite zones in geothermal areas of Iceland, in: Sand, L.B., Mumpton, F.M. (Eds.), *Natural Zeolite Occurrence, Properties and Use*. Pergamon Press, Oxford, pp. 277–284.
- Kühn, P., Aguilar, J., Miedma, R., 2010. Textural features and their related horizons, in: Stoops, G., Marcelino, V., Mees, F. (Ed.), *Micromorphological Features of Soils and Regoliths. Their Relevance for Pedogenic Studies and Classifications*. Elsevier B.V., pp. 217–250. doi:10.1016/B978-0-444-53156-8.00011-8
- Kühn, P., Pietsch, D., 2013. Soil micromorphogenesis and Early Holocene paleoclimate at the desert margin of Southern Arabia 3, 59–77. doi:10.3232/SJSS.2013.V3.N2.04
- Kühn, P., Techmer, A., Weidenfeller, M., 2013. Lower to middle Weichselian pedogenesis and palaeoclimate in Central Europe using combined micromorphology and geochemistry: The loess-paleosol sequence of Alsheim (Mainz Basin, Germany). *Quat. Sci. Rev.* 75, 43–58. doi:10.1016/j.quascirev.2013.05.019
- Lange, F.M., Frick, C., Stahr, K., Graef, F., Singer, A., 2002a. Fritted Paleosols as Indicators for the Local Paleoclimate - Examples from the Golan Heights. *Die Erde* 133, 259–274.
- Lange, F.M., Frick, C., Stahr, K., Graef, F., Singer, A., 2002b. Fritted paleosols as indicators for the local paleoclimate - examples from the Golan Heights. *Die Erde* 133, 259–274.
- Lanson, B., 1997. Decomposition of experimental x-ray diffraction patterns (profile fitting): A convenient way to study clay minerals. *Clays Clay Miner.* 45, 132–146. doi:10.1346/CCMN.1997.0450202
- Lee, Y. II, Lim, H.S., Yoon, H. II, 2004. Geochemistry of soils of King George Island, South Shetland Islands, West Antarctica: Implications for pedogenesis in cold polar regions. *Geochim. Cosmochim. Acta* 68, 4319–4333.

doi:10.1016/j.gca.2004.01.020

Lessovaia, S.N., Plötze, M., Inozemzev, S., Goryachkin, S., 2016. Traprock transformation into clayey materials in soil environments of the central Siberian plateau, Russia. *Clays Clay Miner.* 64, 668–676.

doi:10.1346/CCMN.2016.064042

Lowe, D.J., 2000. Upbuilding pedogenesis in multisequal tephra- derived soils in the Waikato region, in: Adams, J., Metherell, A. (Eds.), *Soil 200: New Horizons for a New Century. Australian and New Zealand Second Joint Soils Conference Volume 2: Lincoln University. New Zealand Society of Soil Science*, pp. 183–184.

Lowe, D.J., Tonkin, P.J., 2010. Unravelling upbuilding pedogenesis in tephra and loess sequences in New Zealand using tephrochronology, in: Gilkes, R.J., Prakongkep, N. (Eds.), *Proceedings of the 19th World Congress of Soil Science “Soil Solutions for a Changing World” (1-6 Aug., 2010, Brisbane), Symposium 1.3.2 Geochronological Techniques and Soil Formation. Brisbane*, pp. 34–37.

Lu, S.G., Xue, Q.F., Zhu, L., Yu, J.Y., 2008. Mineral magnetic properties of a weathering sequence of soils derived from basalt in Eastern China. *Catena* 73, 23–33. doi:10.1016/j.catena.2007.08.004

Luque, E., 2008. *Propiedades magnéticas de los óxidos de hierro en suelos mediterráneos. Universidad de Córdoba.*

Mackensen, A., Ehrmann, W.U., 1992. Middle Eocene through Early Oligocene climate history and paleoceanography in the Southern Ocean: Stable oxygen and carbon isotopes from ODP Sites on Maud Rise and Kerguelen Plateau. *Mar. Geol.* 108, 1–27. doi:10.1016/0025-3227(92)90210-9

Maher, B., 1986. Characterisation of soils by mineralmagnetic measurements. *Phys. Earth Planet. Inter.* 42, 76–92. doi:10.1016/S0031-9201(86)80010-3

Mansilla, H.G., De Valais, S., Stinnesbeck, W., Varela, N.A., Leppe, M.A., 2012. New Avian tracks from the lower to middle Eocene at Fossil Hill, King George Island, Antarctica. *Antarct. Sci.* 24, 500–506. doi:10.1017/S0954102012000260

Mansilla, H.G., Stinnesbeck, W., Varela, N., Leppe, M., 2013. Eocene fossil feather from King George Island, South Shetland Islands, Antarctica. *Antarct. Sci.* 26, 384–388. doi:10.1017/S0954102013000771

Marques, R., Prudêncio, M.I., Waerenborgh, J.C., Rocha, F., Dias, M.I., Ruiz, F., Ferreira, E.S., Abad, M., Muñoz, A.M., 2014. Origin of reddening in a paleosol

- buried by lava flows in Fogo island (Cape Verde). *J. African Earth Sci.* 96, 60–70. doi:10.1016/j.jafrearsci.2014.03.019
- Materechera, S.A., Dexter, A.R., Alston, A.M., 1992. Formation of aggregates by plant roots in homogenised soils. *Plant Soil* 142, 69–79. doi:10.1007/BF00010176
- Maynard, J.B., 1992. Chemistry of modern soils as a guide to interpreting Precambrian paleosols. *J. Geol.* 100, 279–289.
- McDaniel, P.A., Falen, A.L., Tice, K.R., Graham, R.C., Fendorf, S.E., 1995. Beidellite in e horizons of Northern Idaho spodosols formed in Volcanic ash. *Clays Clay Miner.* 43, 525–532. doi:10.1346/CCMN.1995.0430502
- McPherson, J., 1980. Genesis of variegated redbeds in the fluvial Aztec siltstone (Late Devonian), Southern Victoria Land, Antarctica. *Sediment. Geol.* 27.
- Mehra, O.P., Jackson, M.L., 1960. Iron Oxide Removal from Soils and Clays by a Dithionite-Citrate System Buffered with Sodium Bicarbonate. *Clays Clay Miner.* 7, 317–327. doi:10.1346/CCMN.1958.0070122
- Ming, D.W., Boettinger, J.L., 2001. Zeolites in Soil Environments. *Rev. Mineral. Geochemistry* 45, 323–345. doi:10.2138/rmg.2001.45.11
- Mirabella, A., Egli, M., Raimondi, S., Giaccari, D., 2005. Origin of clay minerals in soils on pyroclastic deposits in the Island of Lipari (Italy). *Clays Clay Miner.* 53, 409–421. doi:10.1346/CCMN.2005.0530409
- Mizota, C., Takahashi, Y., 1982. Eolian origin of quartz and mica in soils developed on basalts in northwestern Kyushu and San-in, Japan. *Soil Sci. Plant Nutr.* 28, 369–378. doi:10.1080/00380768.1982.10433652
- Mokma, D., Syers, J., Jackson, M., Clayton, R., Rex, R., 1972. Eolian additions to soils and sediments in the South Pacific area. *J. Soil Sci.* 23, 147–162.
- Moore, D., Reynolds Jr, R., 1997. *X-ray Diffraction and the Identification of Clay Minerals*, 2nd ed. Oxford University.
- Mozer, A., 2012. Pre-glacial sedimentary facies of the Point Thomas Formation (Eocene) at Cytadela, Admiralty Bay, King George Island, West Antarctica. *Polish Polar Res.* 33, 41–62. doi:10.2478/v10183-012-0002-7
- Müller, H., Schwaighofer, B., 1979. Frittung oder tertiäre Verwitterung — Zur Frage der Rotfärbung in den tertiären Liegendsedimenten des Basalts von Stoob (Burgenland, Österreich). *Verh.Geol.B.-A* 2, 133–160.
- Nahon, D., Colin, F., Tardy, Y., 1982. Formation and distribution of Mg,Fe,Mn-

- smectites in the first stages of the lateritic weathering of forsterite and tephroite. *Clay Miner.* 17, 339–348. doi:10.1180/claymin.1982.017.3.06
- Nawrocki, J., Pańczyk, M., Williams, I.S., 2011. Isotopic ages of selected magmatic rocks from King George Island (West Antarctica) controlled by magnetostratigraphy. *Geol. Q.* 55, 301–322.
- NRCS, 1996. Soil Survey Laboratory Methods Manual 716. doi:10.1021/ol049448l
- Ollier, C., 1965. Some features of granite weathering in Australia. *Zeitschrift für Geomorphol.* 9, 285–304.
- Pagani, M., Zachos, J.C., Freeman, K.H., Tripple, B., Bohaty, S., 2005. Marked decline in Atmospheric Carbon Dioxide Concentrations during the Paleocene. *Science* (80-. ). 309, 600–603. doi:10.1126/science.1110063
- Parra, M., Delmont, P., Dumon, J.C., Ferragne, A., Pons, J.C., 1987. Mineralogy and origin of Tertiary interbasaltic clays from the Faeroe island, Northeastern Atlantic. *Clay Miner.* 22, 63–82.
- Pearson, P.N., Foster, G.L., Wade, B.S., 2009. Atmospheric carbon dioxide through the Eocene–Oligocene climate transition. *Nature* 461, 1110–1113. doi:10.1038/nature08447
- Pearson, P.N., Palmer, M.R., 2000. Atmospheric carbon dioxide concentrations over the past 60 million years. *Nature* 406, 695–699. doi:10.1038/35021000
- Pevear, D., Dethier, D., Frank, D., 1982. Clay minerals in the 1980 deposits from Mount St. Helens. *Clays Clay Miner.* 30, 241–252. doi:10.1346/CCMN.1982.0300401
- Pietsch, D., Kühn, P., 2012. Early Holocene paleosols at the southwestern Ramlat As-Sab'atayn desert margin: New climate proxies for southern Arabia. *Palaeogeogr. Palaeoclimatol. Palaeoecol.* 365–366, 154–165. doi:10.1016/j.palaeo.2012.09.023
- PiPujol, M.D., Buurman, P., 1994. The distinction between ground-water gley and surface-water gley phenomena in Tertiary paleosols of the Ebro basin, NE Spain. *Palaeogeogr. Palaeoclimatol. Palaeoecol.* 110, 103–113. doi:10.1016/0031-0182(94)90112-0
- Poole, I., Cantrill, D., Utescher, T., 2005. A multi-proxy approach to determine Antarctic terrestrial palaeoclimate during the Late Cretaceous and Early Tertiary. *Palaeogeogr. Palaeoclimatol. Palaeoecol.* 222, 95–121. doi:10.1016/j.palaeo.2005.03.011

- Poole, I., Hunt, R.J., Cantrill, D.J., 2001. A fossil wood flora from King George Island: ecological implications for an Antarctic Eocene vegetation. *Ann. Bot.* 88, 33–54. doi:10.1006/anbo.2001.1425
- Poole, I., Mennega, A.M.W., Cantrill, D.J., 2003. Valdivian ecosystems in the Late Cretaceous and Early Tertiary of Antarctica: Further evidence from myrtaceous and eucryphiaceous fossil wood. *Rev. Palaeobot. Palynol.* 124, 9–27. doi:10.1016/S0034-6667(02)00244-0
- Porter, D.A., McCahont, T., Ransom, M.D., 1998. Differentiating pedogenic and diagenetic properties in a Cretaceous paleosol in Kansas. *Quat. Int.* 51/52, 35–54.
- Preetz, H., Igel, J., Hannam, J.A., Stadler, S., 2017. Relationship between magnetic properties and reddening of tropical soils as indicators of weathering. *Geoderma* 303, 143–149. doi:10.1016/j.geoderma.2017.05.007
- Pross, J., Contreras, L., Bijl, P.K., Greenwood, D.R., Bohaty, S.M., Schouten, S., Bendle, J. a, Röhl, U., Tauxe, L., Raine, J.I., Huck, C.E., van de Flierdt, T., Jamieson, S.S.R., Stickley, C.E., van de Schootbrugge, B., Escutia, C., Brinkhuis, H., 2012. Persistent near-tropical warmth on the Antarctic continent during the early Eocene epoch. *Nature* 488, 73–7. doi:10.1038/nature11300
- Prudencio, M.I., Sequeira Braga, M.A., Paquet, H., Waerenborgh, J.C., Pereira, L.C.J., Gouveia, M.A., 2002. Clay mineral assemblages in weathered basalt profiles from central and southern Portugal: Climatic significance. *Catena* 49, 77–89. doi:10.1016/S0341-8162(02)00018-8
- Rasmussen, C., Dahlgren, R. a., Southard, R.J., 2010. Basalt weathering and pedogenesis across an environmental gradient in the southern Cascade Range, California, USA. *Geoderma* 154, 473–485. doi:10.1016/j.geoderma.2009.05.019
- Rasmussen, C., Matsuyama, N., Dahlgren, R.A., Southard, R.J., Brauer, N., 2007. Soil genesis and mineral transformation across an environmental gradient on andesitic lahar. *Soil Sci. Soc. Am.* 71, 225–237.
- Reguero, M.A., Marensi, S.A., Santillana, S.N., 2002. Antarctic Peninsula and South America (Patagonia)\nPaleogene terrestrial faunas and environments: biogeographic\nrelationships. *Palaeogeogr. Palaeoclimatol. Palaeoecol.* 2776, 1–22.
- Retallack, G.J., 2001. *Soils of the Past: An Introduction to Paleopedology*, second. ed. Blackwell Science, United Kingdom. doi:10.1002/9780470698716

- Retallack, G.J., 1991. Untangling the effects of burial alteration and ancient soil formation. *Annu. Rev. Earth Planet. Sci.* 19, 183–206.  
doi:10.1146/annurev.earth.19.1.183
- Retallack, G.J., 1988. Field recognition of paleosols. *Geol. Soc. Am. Spec. Pap.* 1–20. doi:10.1130/SPE216-p1
- Righi, D., Terribile, F., Petit, S., 1998. Pedogenic formation of high-charge beidellite in a Vertisol of Sardinia (Italy). *Clays Clay Miner.* 46, 167–177.  
doi:10.1346/CCMN.1998.0460207
- Rivas, J., Ortega, B., Sedov, S., Solleiro, E., Sychera, S., 2006. Rock magnetism and pedogenetic processes in Luvisol profiles: Examples from Central Russia and Central Mexico. *Quat. Int.* 156–157, 212–223.  
doi:10.1016/j.quaint.2006.05.007
- Robert, C., Kennett, J.P., 1997. Antarctic continental weathering changes during Eocene-Oligocene cryosphere expansion: Clay mineral and oxygen isotope evidence. *Geology* 25, 587–590. doi:10.1130/0091-7613
- Sánchez, S., 2015. Los paleosuelos “negros” como indicadores de cambios ambientales naturales e inducidos por el hombre en el periodo de ocupacion teotihuacano. UNAM.
- Sayyed, M.R.G., Pardeshi, R.G., Islam, R., 2014. Palaeoweathering characteristics of an intrabasaltic red bole of the Deccan Flood Basalts near Shrivardhan of western coast of India. *J. Earth Syst. Sci.* 1717–1728. doi:10.1007/s12040-014-0481-5
- Schatz, A.-K., Scholten, T., Kühn, P., 2015. Paleoclimate and weathering of the Tokaj (Hungary) loess–paleosol sequence. *Palaeogeogr. Palaeoclimatol. Palaeoecol.* 426, 170–182. doi:10.1016/j.palaeo.2015.03.016
- Scheinost, A., Chavernas, A., Barrón, V., Torrent, J., 1998. Use and limitations of second-derivative diffuse reflectance spectroscopy in the visible to near-infrared range to identify and quantify Fe oxide minerals in soils. *Clays Clay Miner.* 46, 528–536.
- Schulze, D., 1981. Identification of soil iron oxide minerals by Differential X-ray Diffraction. *Soil Sci. Soc. Am. J.* 45, 437–440.
- Schwertmann, U., 1964. Differenzierung der Eisenoxide des Bodens durch Extraktion mit Ammoniumoxalat-Lösung. *J. Plant Nutr. Soil Sci.* 105, 194–202.
- Schwertmann, U., Fechter, H., 1984. The Influence of aluminum on iron oxides: XI.

- Aluminum-substituted maghemite in soils and its formation. *Soil Sci. Soc. Am.* 48, 1462–1463. doi:10.2136/sssaj1984.03615995004800060054x
- Schwertmann, U., Friedl, J., Stanjek, H., 1999. From Fe(III) ions to Ferrihydrite and then to Hematite. *J. Colloid Interface Sci.* 209, 215–223. doi:10.1006/jcis.1998.5899
- Schwertmann, U., Murad, E., Schulze, D.G., 1982. Is there Holocene reddening (hematite formation) in soils of axeric temperate areas? *Geoderma* 27, 209–223.
- Schwertmann, U., Taylor, R., 1989. Iron Oxides, in: Dixon, J., Weed, S. (Eds.), *Minerals in Soil Environments*. Soil Science Society of America, Madison, Wisconsin, pp. 379–438.
- Sedov, S., Solleiro-Rebolledo, E., Morales-Puente, P., Arias-Herreia, A., Vallejo-Gomez, E., Jasso-Castaneda, C., 2003. Mineral and organic components of the buried paleosols of the Nevado de Toluca, Central Mexico as indicators of paleoenvironments and soil evolution. *Quat. Int.* 106–107, 169–184. doi:10.1016/S1040-6182(02)00171-4
- Sedov, S., Stoops, G., Shoba, S., 2010. Regoliths and Soils on Volcanic Ash, in: Stoops, G., Marcelino, V., Mees, F. (Ed.), *Interpretation of Micromorphological Features of Soils and Regoliths*. Elsevier, Amsterdam, pp. 275–303. doi:10.1016/B978-0-444-53156-8.00013-1
- Sheldon, N.D., 2005. Do red beds indicate paleoclimatic conditions? A Permian case study. *Palaeogeogr. Palaeoclimatol. Palaeoecol.* 228, 305–319. doi:10.1016/j.palaeo.2005.06.009
- Sheldon, N.D., 2003. Pedogenesis and geochemical alteration of the Pacific Gorge subgroup Columbia River basalt, Oregon. *Bull. Geol. Soc. Am.* 115, 1377–1387. doi:10.1130/B25223.1
- Sheldon, N.D., Retallack, G.J., 2004. Regional paleoprecipitation records from the Late Eocene and Oligocene of North America. *J. Geol.* 112, 487–494. doi:10.1086/421076
- Sheldon, N.D., Tabor, N.J., 2009. Quantitative paleoenvironmental and paleoclimatic reconstruction using paleosols. *Earth-Science Rev.* 95, 1–52. doi:10.1016/j.earscirev.2009.03.004
- Shoji, S., Nanzyo, M., Dahlgren, R.A., 1993. *Volcanic ash soils - Genesis, properties and utilization*, Statewide Agricultural Land Use Baseline 2015. Elsevier Science, Amsterdam.

- Shukla, A.D., Ray, D., Pande, K., Shukla, P.N., 2014. Formation of paleosol (fossil soil) in Deccan continental flood basalt: alteration style and implications towards aqueous environments of early mars, in: Eighth International Conference on Mars. Pasadena, California, p. 1194.
- Singer, A., 1980. The palaeoclimate interpretation of clay minerals in soil and weathering profiles. *Earth-Science Rev.* 15, 303–326.
- Singer, A., 1970. Edaphoids and paleosols of basaltic origin in The Galilee, Israel. *J. Soil Sci.* 21.
- Singer, A., Ben-Dor, E., 1987. Origin of red clay layers interbedded with basalts of the Golan Heights. *Geoderma* 39, 293–306. doi:10.1016/0016-7061(87)90049-8
- Singer, A., Navrot, J., 1977. Clay formation from basic volcanic rocks in a humid Mediterranean climate. *Soil Sci. Soc. Am. J.* 41, 645–650.
- Solleiro-Rebolledo, E., Straubinger, M., Terhorst, B., Sedov, S., Ibarra, G., Sánchez-Alaniz, J.I., Solanes, M.C., Marmolejo, E., 2016. Paleosols beneath a lava flow in the southern basin of Mexico: The effect of heat on the paleopedological record. *Catena* 137, 622–634. doi:10.1016/j.catena.2014.12.002
- Spinola, D.N., Pi-Puig, T., Solleiro-Rebolledo, E., Egli, M., Sudo, M., Sedov, S., Kühn, P., 2017a. Origin of clay minerals in Early Eocene volcanic paleosols on King George Island, Maritime Antarctica. *Sci. Rep.* doi:10.1038/s41598-017-06617-x
- Spinola, D.N., Portes, R. de C., Schaefer, C.E.G.R., Solleiro-Rebolledo, E., Pi-Puig, T., Kühn, P., 2017b. Eocene paleosols on King George Island, Maritime Antarctica: Macromorphology, micromorphology and mineralogy. *Catena*. doi:10.1016/j.catena.2017.01.004
- Srivastava, P., Sangode, S.J., Meshram, D.C., Gudadhe, S.S., Nagaraju, E., Kumar, A., Venkateshwarlu, M., 2012. Paleoweathering and depositional conditions in the inter-flow sediment units (bole beds) of Deccan Volcanic Province, India: A mineral magnetic approach. *Geoderma* 177–178, 90–109. doi:10.1016/j.geoderma.2012.01.034
- Srivastava, P., Sangode, S.J., Torrent, J., 2015. Mineral magnetic and diffuse reflectance spectroscopy characteristics of the Deccan volcanic bole beds : Implications to genesis and transformations of iron oxides. *Geoderma* 239–240, 317–330. doi:10.1016/j.geoderma.2014.11.010
- Srivastava, P., Sauer, D., 2014. Thin-section analysis of lithified paleosols from

- Dagshai Formation of the Himalayan Foreland: Identification of paleopedogenic features and diagenetic overprinting and implications for paleoenvironmental reconstruction. *Catena* 112, 86–98. doi:10.1016/j.catena.2013.08.008
- Steiger, R., Jäger, E., 1977. Subcommittee on geochronology: convention on the use of decay constants in geo- and cosmochronology. *Earth Planet. Sci. Lett.* 36, 359–362.
- Stickley, C.E., Brinkhuis, H., Schellenberg, S.A., Sluijs, A., Röhl, U., Fuller, M., Grauert, M., Huber, M., Warnaar, J., Williams, G.L., 2004. Timing and nature of the deepening of the Tasmanian Gateway. *Paleoceanography* 19, 1–18. doi:10.1029/2004PA001022
- Stoops, G., 2003. Guidelines for Analysis and Description of Soil and Regolith Thin Sections. Soil Science Society of America, Madison, Wisconsin.
- Stronck, N.A., Schmincke, H.U., 2002. Palagonite - A review. *Int. J. Earth Sci.* 91, 680–697. doi:10.1007/s00531-001-0238-7
- Torrent, J., Barrón, V., 2002. Diffuse reflectance spectroscopy of iron oxides. *Encycl. Surf. Colloid Sci.* 1438–1446.
- Torrent, J., Barrón, V., Liu, Q., 2006. Magnetic enhancement is linked to and precedes hematite formation in aerobic soil. *Geophys. Res. Lett.* 33, 4–7. doi:10.1029/2005GL024818
- Torrent, J., Liu, Q., Bloemendal, J., Barrón, V., 2007. Magnetic enhancement and iron oxides in the Upper Luochuan Loess-Paleosol sequence, Chinese Loess Plateau. *Soil Sci. Soc. Am. J.* 71, 1570–1578. doi:10.2136/sssaj2006.0328
- Torrent, J., Schwertmann, U., 1987. Influence of hematite on the colour of Red Beds. *J. Sediment. Petrol.* 57, 682–686.
- Ugolini, F.C., Dahlgren, R.A., 2002. Soil development in volcanic ash. *Glob. Environ. Res.* 6, 69–81.
- Uto, K., Ishizuka, O., Matsumoto, A., Kamioka, H., Togashi, S., 1997. Laser-heating  $^{40}\text{Ar}/^{39}\text{Ar}$  dating system of the Geological Survey of Japan: System outline and preliminary results. *Bull. Geol. Surv. Japan* 48, 23–46.
- Vacca, A., Ferrara, C., Matteucci, R., Murru, M., 2012. Ferruginous paleosols around the Cretaceous-Paleocene boundary in central-southern Sardinia (Italy) and their potential as pedostratigraphic markers. *Quat. Int.* 265, 179–190. doi:10.1016/j.quaint.2011.07.036
- Van der Gaast, S.J., Mizota, C., Jansen, J.H.F., 1986. Curved smectite in soils from

- volcanic ash in Kenya and Tanzania: a low-angle X-ray powder diffraction study. *Clays Clay Miner.* 34, 665.
- Van Houten, F., 1973. Origin of red beds - A review - 1961 - 1972. *Annu. Rev. Earth Planet. Sci.* 1, 39–61.
- Veblen, T., Alaback, P., 1996. High-Latitude Rainforests and Associated Ecosystems of the West Coast of the Americas, in: Lawford, R., Fuentes, E., Alaback, P. (Eds.), *High-Latitude Rainforest and Associated Ecosystems of the West Coast of the Americas*. Springer Verlag, New York, pp. 173–213.  
doi:10.1007/978-1-4612-3970-3
- Velde, B., Meunier, A., 2008. *The Origin of Clay Minerals in Soil and Weathered Rocks*. Springer-Verlag, Berlin Heidelberg.
- Veneman, P.L., Vepraskas, M., Bouma, J., 1976. The physical significance of soil mottling in a Wisconsin toposequence. *Geoderma* 15, 103–118.
- Weibel, R., 1999. Effects of burial on the clay assemblages in the Triassic Skagerrak Formation, Denmark. *Clay Miner.* 34, 619–635.  
doi:10.1180/claymin.1999.034.4.08
- Widdowson, M., Walsh, J.N., Subbarao, K. V., 1997. The geochemistry of Indian bole horizons: palaeoenvironmental implications of Deccan intravolcanic palaeosurfaces, in: Widdowson, M. (Ed.), *Paleosurfaces: Recognition, Reconstruction and Palaeoenvironmental Interpretation*. Geological Society Special Publication, pp. 269–281. doi:10.1144/GSL.SP.1997.120.01.17
- Wilke, F.D., O'Brien, P., Gerdes, A., Timmerman, M., Sudo, M., Khan, M.A., 2010. The multistage exhumation history of the Kaghan Valley UHP series, NW Himalaya, Pakistan from U-Pb and  $40\text{Ar}/39\text{Ar}$  ages. *Eur. J. Mineral.* 22, 703–719.
- Wilson, M.J., 1999. The origin and formation of clay minerals in soils: past, present and future perspectives. *Clay Miner.* 34, 7–25. doi:10.1180/000985599545957
- Wojdyr, M., 2010. Fityk: a general-purpose peak fitting program. *J. Appl. Crystallogr.* 43, 1126–1128. doi:10.1107/S0021889810030499
- Wright, V.P., 1992. *Paleosol recognition: A guide to early diagenesis in terrestrial settings*, *Developments in Sedimentology, Diagenesis III*. Elsevier.  
doi:10.1016/S0070-4571(08)70574-0
- Wyszecki, G., Stiles, W., 1982. *Colour science: Concepts and methods, quantitative data and formulae*. Wiley, New York.

- York, D., 1969. Least squares fitting of a straight line with correlated errors. *Earth Planet. Sci. Lett.* 5, 320–324.
- Yousefifard, M., Ayoubi, S., Poch, R.M., Jalalian, A., Khademi, H., Khormali, F., 2015. Clay transformation and pedogenic calcite formation on a lithosequence of igneous rocks in northwestern Iran. *Catena* 133, 186–197.  
doi:10.1016/j.catena.2015.05.014
- Zachos, J., Pagani, M., Sloan, L., Thomas, E., Billups, K., 2001. Trends, Rhythms, and Aberrations in Global Climate 65 Ma to Present. *Science* 292, 686–693. doi:10.1126/science.1059412
- Zachos, J.C., Quinn, T.M., Salamy, K.A., 1996. High-resolution deep-sea foraminiferal stable isotope records of the Eocene-Oligocene transition. *Paleoceanography*.

**Manuscript 3**

Geoderma: Volume 315, April 2018, Pages 149-159

10.1016/j.geoderma.2017.11.010

<https://doi.org/10.1016/j.geoderma.2017.11.010>

**Diagenetic reddening of Early Eocene paleosols on King George Island,  
Antarctica**

Diogo Noses Spinola<sup>a</sup>, Peter Kühn<sup>a</sup>, Raquel de Castro Portes<sup>b</sup>, Pankaj Srivastava<sup>c</sup>, José Torrent<sup>d</sup>, Vidal Barrón<sup>d</sup>

<sup>a</sup>Research Area Geography, Soil Science and Geomorphology, Laboratory of Soil Science and Geocology, Eberhard Karls University of Tübingen, Rümelinstraße 19-23, D-72070 Tübingen, Germany. [peter.kuehn@uni-tuebingen.de](mailto:peter.kuehn@uni-tuebingen.de)

<sup>b</sup>Department of Geography, University of Zürich, Winterthurerstrasse 190, 8057 Zürich, Switzerland. [raquel.decastroportes@geo.uzh.ch](mailto:raquel.decastroportes@geo.uzh.ch)

<sup>c</sup>Department of Geology, University of Delhi, Delhi 110 007, India. [pankajps@gmail.com](mailto:pankajps@gmail.com)

<sup>d</sup>Department of Agronomy, University of Córdoba, Edificio C4, Campus de Rabanales, 14071 Córdoba, Spain. [torrent@uco.es](mailto:torrent@uco.es); [cr1balov@uco.es](mailto:cr1balov@uco.es)

### **Abstract**

The objective of this study was to determine if the early Eocene paleosols on King George Island, Maritime Antarctica, have acquired their reddish colours during the paleopedogenesis, by burial diagenesis and/or by heating of a covering lava flow. We used micromorphology, diffuse reflectance spectroscopy, X-ray diffraction, and mineral magnetic properties to identify the iron oxides in these paleosols. These are weakly/moderately developed paleosols formed on a basaltic tephra under a cool humid paleoclimate, therefore, prone to ferrihydrite and goethite rather than hematite formation. However, the iron oxide assembly was dominated by maghemite and hematite. Nevertheless, the large grain size and high crystallinity of hematites suggested they are diagenetic, like the ones found in red beds, rather than pedogenic. The clustering, content, and distribution of hematites (finely dispersed on the groundmass; coating/replacing primary minerals and as mottles and/or nodules) rather than their crystal size were responsible for the colour differences. These properties were likely the result of past pedogenesis processes (forming originally ferrihydrite) linked with paleodrainage conditions. Heating by the covering lava flow affected the magnetic properties of two profiles but without affecting their colours. Taken together, all these results suggest that the burial reddening took place by dehydration and transformation of ferrihydrite to hematite. Our findings highlight the importance of detailed mineralogical analysis to identify iron oxides present in reddish paleosols because identification based solely on morphology (e.g. yellowish colour, gradual horizon transitions) can lead to misinterpretation of paleoenvironmental conditions.

## 1. Introduction

The colour is one of the most important soil properties because it is a reliable indicator of the pedoenvironment (Cornell and Schwertmann, 2003). Reddish pigmentation in soils is usually due to hematite ( $\alpha\text{-Fe}_2\text{O}_3$ ), which is more frequently found in well-drained soils of tropical regions undergoing seasonal droughts, whereas goethite ( $\alpha\text{-FeOOH}$ ) becomes more abundant in soils of cool temperate areas or soils that remain moist throughout the year (Cornell and Schwertmann, 2003; Schwertmann and Taylor, 1989).

Despite reddish soils being most common in warmer regions, the paleoenvironmental interpretation of reddish paleosols must be made with extreme care because of a possible diagenetic reddening that could have been caused by the dehydration of iron oxyhydroxides (e.g. goethite) to hematite (Retallack, 1991; Van Houten, 1973). This effect has to be considered in this context when a reddish paleosol (especially pre-Quaternary paleosols) has no other characteristic features of paleotropical/semi-arid and/or long-term weathering (e.g. strong chemical weathering, saprolite profiles, concretions).

Although the diagenetic reddening of paleosols is a well-known process, the persistence of goethite in Cretaceous paleosols (Porter et al., 1998; Vacca et al., 2012) and Eocene paleosols (Kraus and Hasiotis, 2006; PiPujol and Buurman, 1994) have raised some questions about the ubiquity of this process. Additionally, there is little information about the diagenetic conditions under which dehydration takes place, e.g. if there is a need for high temperatures for goethite dehydration to hematite.

Heating experiments have suggested that goethite is converted to hematite at temperatures higher than 300°C (Gialanella et al., 2010; Gualtieri and Venturelli, 1999). For some Chinese red beds, conversion of goethite to hematite required diagenetic temperatures higher than 150°C (Jiang et al., 2015) and >105°C for Triassic sandstones in Denmark (Weibel, 1999).

Another pathway for paleosol reddening, regardless of its age and climate, is due to heating by a lava flow. The heating due to the emplacement of a lava flow can result in dehydration of iron hydroxides to hematite (Lange et al., 2002; Srivastava et al., 2015). On the other hand, the effects of heating are usually limited on the top few centimeters because of the thermal isolation properties of soils (Sheldon, 2003;

Solleiro-Rebolledo et al., 2016).

Previous research described a set of three reddish weakly to moderately developed volcanic paleosols that were covered by a lava flow on King George Island (KGI), Maritime Antarctica (Spinola et al., 2017b). These paleosols were formed during the greenhouse period of the early Eocene. This was a period when Antarctica was ice-free and covered by rainforests similar to those in southern Chile, and was considered the best modern analogue environment (Francis and Poole, 2002; Poole et al., 2003). Soils formed under similar environments (i.e. cool and humid climate with volcanic parent material) are usually Andosols with brownish/yellowish colours having ferrihydrite ( $\text{Fe}_5\text{HO}_8 \cdot 4 \text{H}_2\text{O}$ ) and goethite ( $\alpha\text{-FeOOH}$ ) as the main iron hydroxides (Shoji et al., 1993; Ugolini and Dahlgren, 2002). Therefore, the reddish colour of the investigated KGI paleosols is in apparent disagreement with volcanic soils formed under a cool humid paleoenvironment.

The objective of this study was to characterize the iron oxides that impart reddish colours to the KGI paleosols and to determine their genesis: pedogenic, diagenetic, and/or heating by a lava flow. Our hypothesis was that the red colours of the KGI paleosols are the result of burial reddening because these paleosols were moderately developed under a cool humid climate, not prone to hematite formation. Our second hypothesis was that the horizons in contact with the lava flow were not substantially affected by heating because they are not redder than the deeper horizons. To test these hypotheses, we combined a set of techniques, such as X-ray diffraction (XRD), diffuse reflectance spectroscopy (DRS), magnetic susceptibility, selective iron extraction (dithionite-citrate-bicarbonate, ammonium oxalate and dissolution with  $\text{H}_2\text{SO}_4$ ), and microscopic techniques to characterize the iron oxides in KGI paleosols and understand their genesis.

## **2. Methods**

### **2.1. Site description and geological background**

The samples were collected on King George Island, South Shetland Islands, Maritime Antarctica. The specific outcrop is located at the Cytadela area of the Ezcurra Inlet in the Admiralty Bay ( $62^\circ 11.057'\text{S}$  -  $58^\circ 35.209'\text{W}$ ) (Fig. 1).

The outcrop stratigraphically belongs to the Point Thomas Formation, Ezcurra Inlet Group, which comprises a 500 m thick Paleogene (Eocene-Oligocene) volcanic

succession (Birkenmajer, 1980; Birkenmajer and Zastawniak, 1989). This formation was deposited during the Arctowski interglacial period (ca 50 to ca 32 Ma), a climostratigraphic unit introduced by Birkenmajer (1988).

Two informal units of the Point Thomas Formation are recognized at the Cytadela outcrop, the Lower Member (LM) and Upper Member (UM) (Birkenmajer, 1980). The LM is a 20–40 m thick regular high-Al flow basalt with a thickness of 1–6 m alternating with pyroclastic deposits. The UM comprises 150–450 m of irregular, lenticular basalt lavas alternating with feldspathic tuff, interbedded with coarse vent breccia and plant-bearing tuff.

13 samples were taken horizon-wise from the paleosols covered by the 6<sup>th</sup> basalt flow (from bottom to top) in the LM of the schematic field section made by Mozer (2012). Three profiles (P1, P2 and P3) were chosen, which are located with a distance of 60 m between P1 and P2 and of 90 m between P2 and P3 (Fig. 1). The basalts underlying and overlying the paleosols gave  $^{40}\text{Ar}/^{39}\text{Ar}$  ages ranging between 51 and 48 Ma, confirming their Early Eocene age (Spinola et al., 2017a).

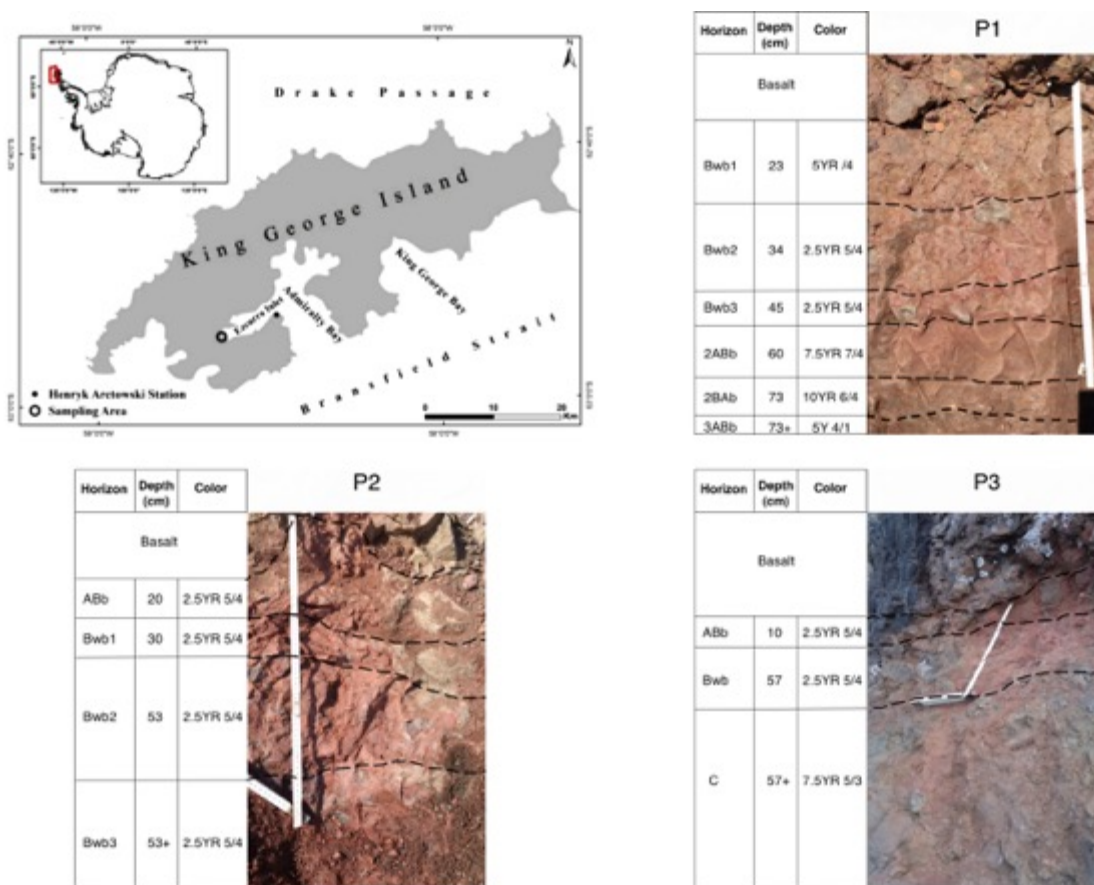


**Figure 1.** Location of the sampling site at the King George Island and photographs of the profiles with field colours.

## **2.2. Field and laboratory analyses**

The colour (dry) of the samples was measured in the field under natural light using the Munsell Colour Charts. For the subsequent laboratory analysis 13 paleosol bulk samples were ground to powder using a ball-mill with agate beakers.

## **2.3. Micromorphological and SEM-EDS analyses**

The analyses were made in 9 × 6 cm thin sections and photographed using a polarizing microscope (Zeiss Axio Imager.A2m, Software AxioVision 4.7.2) with plane polarized light (PPL) and crossed polarized light (XPL). Oblique incident light (OIL) was obtained by an external light source with a double-arm swan neckglass fiber light guide. Detailed micromorphological description can be found in Spinola et al. (2017b) mainly using the terminology of Stoops (2003).

The morphology and microchemistry of iron nodules/mottles was determined using a Hitachi TM3030 Plus Scanning electron microscope (SEM) coupled with a Bruker Quantax 70 X-ray microanalysis detector (EDS) on polished uncoated thin sections at the Institute of Mineralogy and Geodynamics, University of Tübingen.

## **2.4. Diffuse Reflectance Spectroscopy (DRS)**

The detection of goethite and hematite were performed by DRS after Torrent et al. (2007). DR spectra was recorded at a scan rate of 30 nm min<sup>-1</sup> from 380 to 770 nm in 0.5 nm steps using a Varian Cary 5000 UV-Vis-NIR spectrophotometer equipped with a diffuse reflectance attachment. The samples were heated at different temperatures in a muffle furnace for 2 hours at 300°C, 400°C, 500°C, 600°C, 700°C, 800°C and measured after each heating interval. The reason for the heating is to help the identification of goethite, which is unstable at around 300°C (Gialanella et al., 2010; Gualtieri and Venturelli, 1999) while hematite is rather stable. Thus, the goethite band should disappear after 300°C, making easier to distinguish between the most intense absorption band of goethite at ~415 nm and a less intense absorption band of hematite at ~423 nm (Scheinost et al., 1998).

The second derivative of the Kubelka–Munk (K–M) remission function within the 380–710 nm range were calculated by using a cubic spline procedure based on segments of 30 data points. The intensities of spectral bands at ~415 nm and ~535 nm are proportional to the concentration of goethite and hematite, respectively (Scheinost et

al., 1998). With this technique, it is possible to detect goethite and hematite concentrations of less than 0.1%, which is more than one order of magnitude smaller than the detection limit of ordinary X-ray diffraction (Torrent and Barrón, 2002).

The spectra measurements were converted into tristimulus values (X, Y, Z) according to the CIE colour system (Commission Internationale de L'Eclairage, 1978). Afterwards, the X, Y, Z values were converted to Munsell hue (H), value (V), and chroma (C) and to L\* a\* b\* colour systems (Wyszecki and Stiles, 1982). The L\*-axis represents “lightness-darkness”, the a\*-axis “redness-greenness”, and the b\*-axis “yellowness-blueness”.

## 2.5. Selective Iron extraction

The following extractions were made sequentially. First, the nanocrystalline Fe ( $Fe_o$ ) compounds were extracted by shaking 2.5 g of soil 100 mL 0.2M acid ammonium oxalate (pH3) for 4 h in the dark (Schwertmann, 1964). With the residuum of this treatment we carried out the selective dissolution of maghemite ( $\gamma$  -  $Fe_2O_3$ ) treating the sample with 1M  $H_2SO_4$  at 75°C for 1h ( $Fe_s$ ) (Luque, 2008 modified from Schwertmann and Fechter, 1984). The remaining residues were extracted with dithionite-citrate-bicarbonate ( $Fe_d$ ) solution, which dissolves the well-crystallized iron forms (Mehra and Jackson, 1960).

The proportion of hematite against the total amount of iron was determined using  $Fe_d/Fe_t$  ratio, where  $Fe_t$  is the total  $Fe_2O_3$ , measured by X-ray fluorescence (XRF).

## 2.6. X-ray diffraction (XRD) and Differential XRD (DXRD).

The mineralogical composition of the bulk samples was achieved by X-ray diffraction (XRD) of randomly oriented specimens using a diffractometer Bruker D-8 Advance, using CuK $\alpha$  radiation at 40 kV and 30 mA. The samples were scanned from 5° to 70° 2 $\theta$  (2h). Same procedures were repeated after removal of free-iron by DCB (Differential XRD after Schulze, 1981). The mean crystallite dimension (MCD) was calculated with the Full Width at Half Maximum (FWHM) values using the Scherrer formula.

## 2.7. Magnetic susceptibility

The magnetic susceptibility,  $\chi$ , of the fine earth fraction was measured at both low (470 Hz = Lf) and high (4700 Hz = Hf) frequencies, using a Bartington MS-2 magnetic susceptibility meter (Bartington Instruments, Witney, UK) equipped with an MS-2B

sensor. The absolute frequency-dependent susceptibility,  $\chi_{fd}$ , was defined as  $\chi_{lf} - \chi_{hf}$ . The percent frequency-dependent susceptibility,  $\chi_{fd}\%$ , was defined as  $(\chi_{fd} / \chi_{lf}) \times 100$ . Values of  $\chi_{fd}\% < 5\%$  are typical for samples in which non-superparamagnetic (SP) grains dominate the assemblage or where extremely fine grains ( $< 0.03 \mu\text{m}$ ) dominate the SP fraction. Samples dominated by SP grains (e.g. maghemite) have  $\chi_{fd}\%$  between 10 and 14% and  $\chi_{fd}$  can be used semi-quantitatively to estimate their total concentration in soils (Dearing et al., 1996).

### 3. Results

#### 3.1. Field colour

In general, the colours are similar for the three profiles, with a predominance of reddish hues with some variation in depth (Table 1). In P1, the first three horizons Bwb1, Bwb2 and Bwb3 are redder than the horizons 2ABb, 2BAb and 3ABb. Although variation in depth is a normal behavior in soils, the presence of two lithic discontinuities (LD) coincided with such a change. The first LD was identified between the Bwb3 and 2ABb horizons because of an abrupt lack of rock fragments in the 2ABb horizon. The second LD was identified between the 2BAb and 3ABb horizons because of the first appearance of dark fossil plant remains and an abrupt change to greyish being a marker of a buried A horizon.

The s in P2 are homogeneous and the horizons were separated by differences in ped size and shape. In P3, the s varied in a gradual manner, becoming less reddish with depth.

**Table 1.** Munsell s taken in field and converted DR spectra in Munsell and L\*a\*b\* s measured on powder-size samples.

| Profile | Horizon | Depth (cm) | Munsell<br>(natural<br>samples) | Munsell<br>(converted<br>from DRS<br>measurements) | L*a*b* |      |      |
|---------|---------|------------|---------------------------------|--|--------|------|------|
|         |         |            |                                 |  | L*     | a*   | b*   |
| P1      | Bwb1    | 0 – 23     | 5YR 5/4                         | 7.5YR 6/3  | 64.3   | 7.4  | 20   |
|         | Bwb2    | 23 – 34    | 2.5YR 5/4                       | 5YR 6/3  | 64.4   | 10   | 20.2 |
|         | Bwb3    | 34 – 45    | 2.5YR 5/4                       | 5YR 6/4  | 63     | 11.1 | 20.9 |
|         | 2ABb    | 45 – 60    | 7.5YR 7/4                       | 7.5YR 7/4  | 66.9   | 6.6  | 21.8 |
|         | 2BAb    | 60 – 73    | 10YR 6/4                        | 7.5YR 7/4  | 68     | 6.3  | 22.8 |
|         | 3ABb    | 73+        | 5Y 4/1                          | 0.6Y 6/3   | 63.1   | 2.6  | 17.2 |

|           |      |         |           |          |      |      |      |
|-----------|------|---------|-----------|----------|------|------|------|
| <b>P2</b> | ABb  | 0 – 20  | 2.5YR 5/4 | 5YR 6/4  | 59.7 | 11.6 | 20.5 |
|           | Bwb1 | 20 – 30 | 2.5YR 2/4 | 5YR 6/4  | 58.8 | 11.5 | 20   |
|           | Bwb2 | 30 – 53 | 2.5YR 5/4 | 5YR 6/4  | 60.4 | 13.5 | 21.3 |
|           | Bwb3 | 53+     | 2.5YR 5/4 | 5YR 6/4  | 59.6 | 11   | 18.5 |
| <b>P3</b> | ABb  | 0 – 10  | 2.5YR 5/4 | 5YR 6/4  | 62.1 | 12.2 | 23.1 |
|           | Bwb1 | 10 – 57 | 2.5YR 5/4 | 5YR 6/4  | 63   | 11.1 | 22.7 |
|           | C    | 57+     | 7.5YR 5/3 | 10YR 6/4 | 66.6 | 5    | 20.5 |

### 3.2. Micromorphology

We analyzed the thin sections to identify the possible sources and to observe the distribution of iron in these paleosols. Figure 2 illustrates the main mode of occurrence of iron oxides: finely dispersed in the groundmass, coating/replacing primary minerals and as mottles or nodules.

As a rule, the micromass of the samples were reddish under oblique incident light (OIL). The reddish micromass is likely a direct weathering product of the basaltic tephra. As can be seen in the Fig. 2a, the colour of the tephra under plane polarized light (PPL) varies from reddish yellow to dark grey and from light red to dark red under OIL. Beyond the mafic composition of the rock, the abundant presence of olivine can be considered also an important Fe source. In addition, the olivines are usually replaced by an admixture of clay and iron-rich alteromorphs (Spinola et al., 2017a) (Fig. 2h).

The concentrations of iron mottles and/or small nodules were common features. The higher the concentration of iron, either in nodules (Fig. 2c-d-e) or mottles (Fig. 2e-f), the darker were these features under PPL and reddish under OIL. The nodules/mottles were given mainly by different concentrations of Fe because no Mn was identified (Fig. 3). Even though these features were present in all horizons, they were more frequent in the horizons with finer material and generally lighter colours, i.e. P1-2ABb, P1-2BAb, and P1-3ABb.

The micromorphological observations agree with those made in the field. The micromass colours are homogeneously reddish under OIL, with few gradual changes in depth. In P1, the colour change verified between the LDs was also detected in thin sections. The colours of the horizons 2ABb and 2BAb are brown under PPL and light brown under OIL, whereas the horizon 3ABb is light brown (PPL) and olive (OIL).

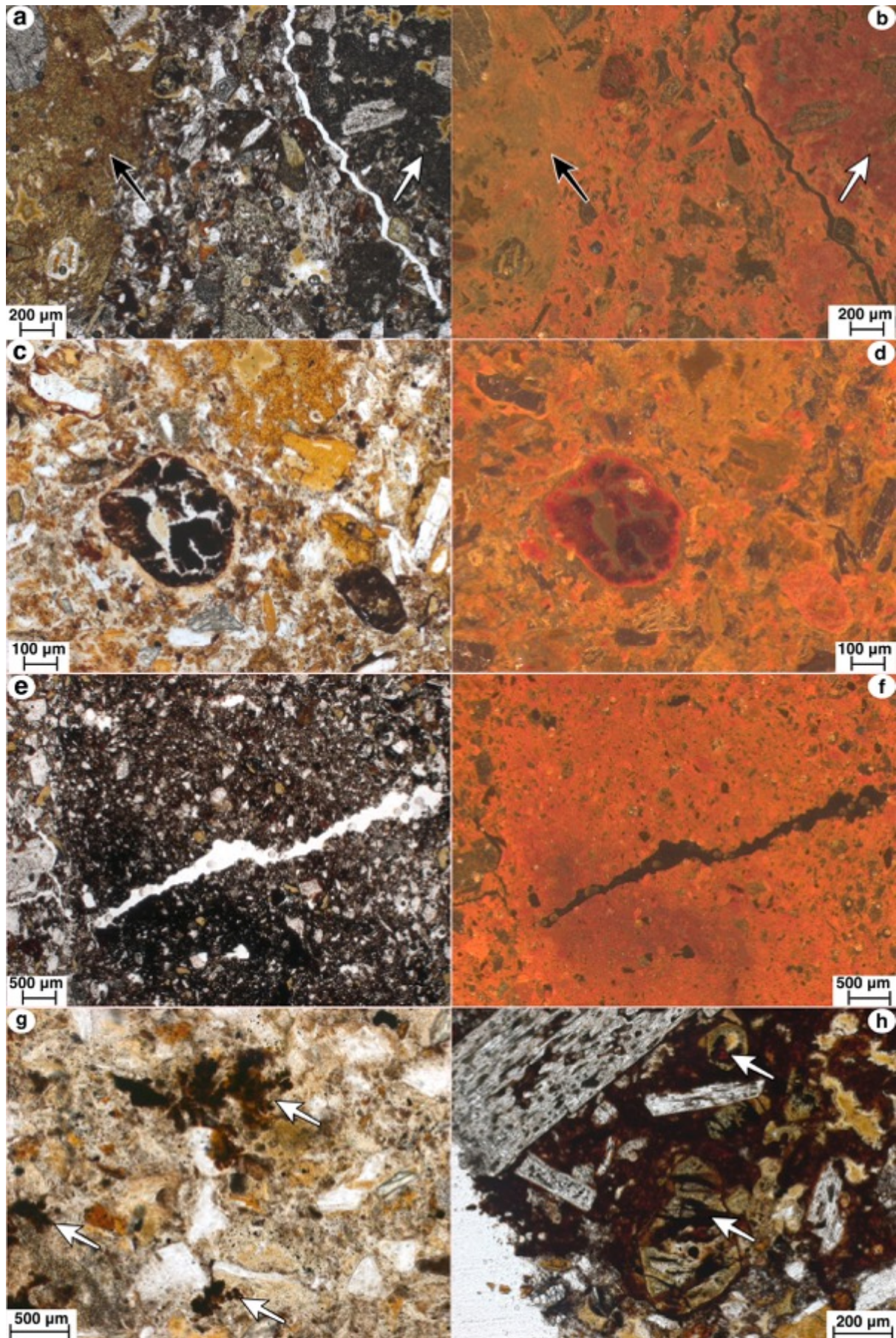


**Figure 2.** Types of iron oxide distribution in the paleosols. Photographs on the left side were taken under Plane Polarizer Light (PPL) and under Oblique Incident Light (OIL) on the right side. a-) P1-Bwb3, 34-45 cm: two different colours of rock fragments reflecting different levels of oxidation. An orange and less oxidized fragment (black arrow) and a darker, more oxidized fragment (white arrow); b-) Same under OIL. Note the strong reddish colours replacing the darker rock fragment (white arrow); c-) P1-2BAb, 60-73 cm: typical disorthic disjuncted iron nodule; d-) Same under OIL. Note the strong contrast between the iron concentration in the nodule in comparison with the surrounding groundmass; e-) P2-Bwb1, 20-30 cm: Different degrees of groundmass impregnation by iron, from strongly impregnated to moderated impregnated. Darker is the impregnation, higher is the iron concentration; f-) Same under OIL. The strongly impregnated area showed darker red colours; g-) P1-3ABb, 73+ cm: dendritic iron nodules (white arrows) in a paler groundmass; h-) P2-Bwb2, 23-34 cm: olivine phenocryst being replaced by an admixture of smectite (brownish colour) and iron oxide (white arrows), photograph taken under PPL.

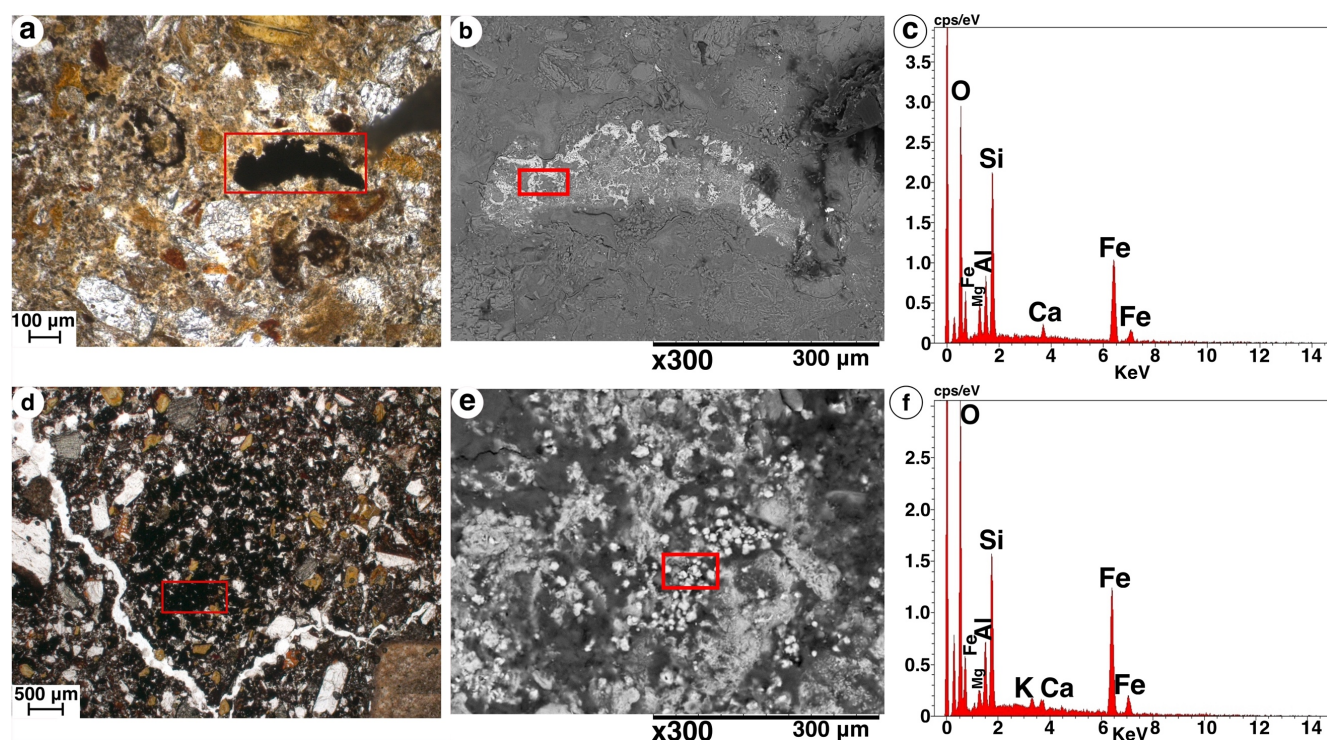


Figure 3. Iron-rich nodules and mottles under polarizing microscope and SEM/EDS. The red rectangles indicate where the analyses were performed. a-) P1-3ABb, 73+cm: an disorthic elongated digitate iron-rich nodule; b-) same under SEM in backscattered mode; c-) EDS measurements, showing intense Fe peaks and no Mn; d-) P2-Bwb1, 20-30 cm: strongly Fe impregnated area; e-) same under SEM. Brighter areas have higher Fe concentration and often showing microaggregation; f-) EDS measurements, showing intense Fe peaks and no Mn.

### 3.3. Identification of Iron oxides

#### 3.3.1. Diffuse Reflectance Spectroscopy (DRS)

The Munsell colour measured in the field is included in Table 1 for comparison with the DRS results. The colour variations of the powder-size samples (i.e. measured with DRS) were similar to those measured in the natural samples (i.e. measured in the field), with considerable homogeneity among the profiles and gradual colour changes

with depth. Nevertheless, the DRS colours were yellower in comparison with field colours in almost all samples. The exceptions were the horizons P1-2ABb and P1-2BAb; the first had the same colour whereas the second became more reddish (from 10YR to 7.5YR).

Figure 4 shows the spectra of the second derivative of the Kubelka–Munk function measured at 25°C and at 800°C for the redder and the less red horizon of each profile (see Supplementary figure 1 for other temperature measurements).

For the reddish samples (P1-Bwb3, P2-ABb and P3-ABb), there were two more intense bands at ~427 nm and ~544 nm. Both bands were also present for the less red samples (P1-3ABb and P3-C) but with lower intensity, especially for 544 nm. After heating at 800°C, the band wavelengths of the reddish samples changed a little. On the other hand, the less red samples had more pronounced changes in wavelengths and had generally sharper peaks after heating. The first band moved from 426 nm to 450 nm in P1-3ABb and from 426 nm to 448 nm in P3-C. Most important, though, is the permanence of the band at ~425 nm for all samples after heating at 800°C, indicating this band is rather related to hematite than to goethite, which is absent.

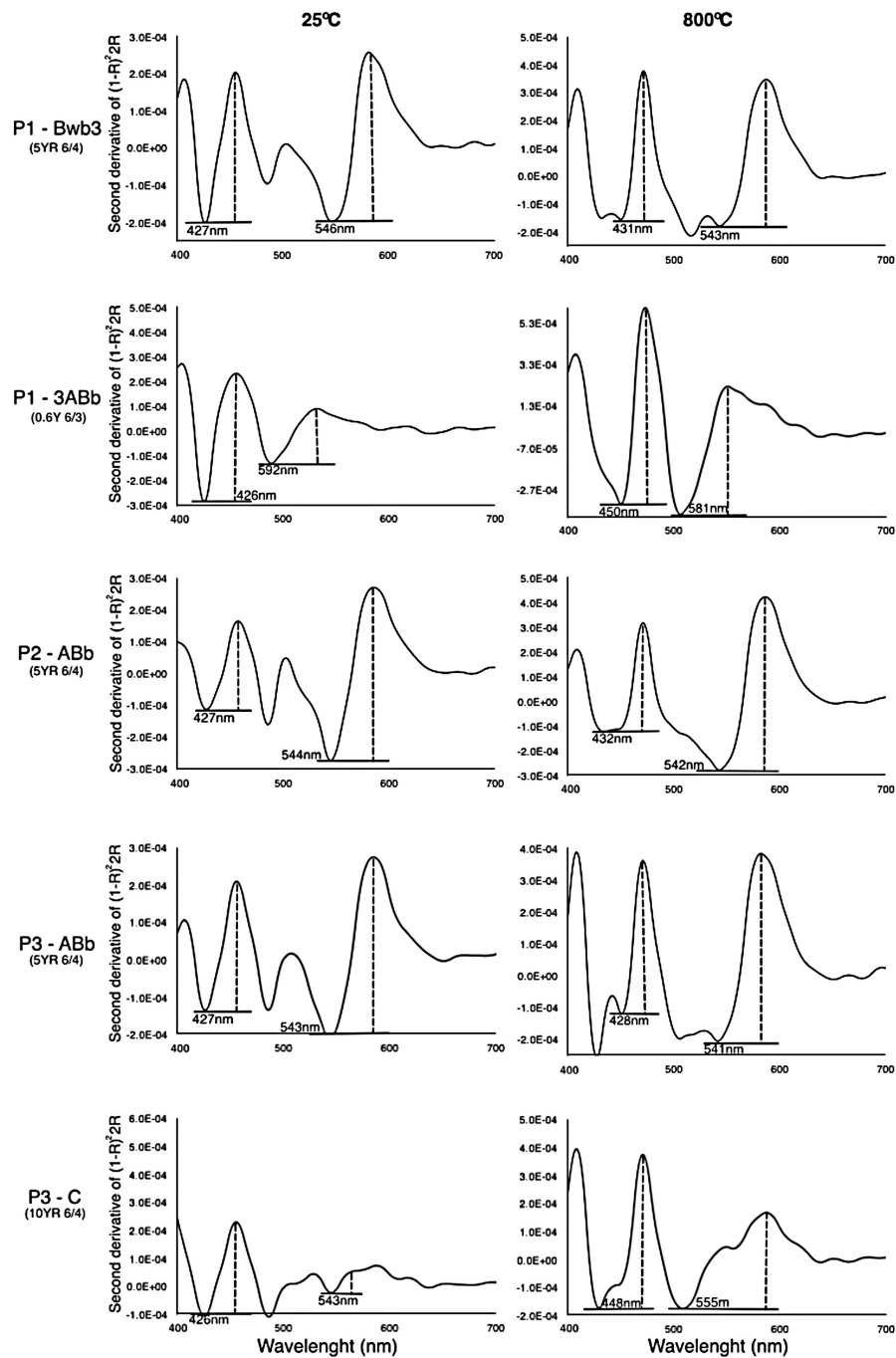


**Figure 4.** The second-derivative curves of K–M function for selected samples. Position (straight line) and amplitude (dashed line) of hematite bands. Measurements taken in air-dried samples at the left side and after heating at 800°C at the right side.

### 3.3.2. X-ray diffraction (XRD) and differential X-ray diffraction (DXRD)

The absence of goethite is supported by the XRD because its most intense peak (110) at 4.18 nm ( $21.2^\circ 2\theta$ ) was not identified in any of the samples. In the XRD, it was only possible to distinguish clearly the more intense peak (104) of hematite at 2.69 nm (Fig. 5). The peak (110) of lower intensity was more difficult to identify because of the overlap with other minerals. Hematite had a large crystallite size (between 37 nm and 62 nm) (Table 2). Another evidence of the higher crystallinity of hematite was the remaining peak (104) at 2.69 nm measured in the DRXD spectra (Fig. 5). Even though its intensity was reduced, the residue of this peak indicated that the Dithionite-Citrate-Bicarbonate (DCB) treatment did not extract all the hematite, especially the most crystalline. A weak positive correlation was found between the crystallite size and the  $L^*a^*b^*$  parameters using the Pearson correlation coefficient ( $r < 0.24$ ) (Supplementary figure 2).

**Table 2.** Hematite properties calculated from XRD. Full width at half maximum (FWHM) and crystallite size.

| Profile   | Horizon | Depth (cm) | FWHM (104) | Crystallite size (nm) |
|-----------|---------|------------|------------|-----------------------|
| <b>P1</b> | Bwb1    | 0 – 23     | 0.16       | 58                    |
|           | Bwb2    | 23 – 34    | 0.18       | 50                    |
|           | Bwb3    | 34 – 45    | 0.21       | 41                    |
|           | 2ABb    | 45 – 60    | 0.19       | 47                    |
|           | 2BAb    | 60 – 73    | 0.15       | 62                    |
|           | 3ABb    | 73+        | ND         | ND                    |
| <b>P2</b> | ABb     | 0 – 20     | 0.18       | 50                    |
|           | Bwb1    | 20 – 30    | 0.17       | 53                    |
|           | Bwb2    | 30 – 53    | 0.16       | 58                    |
|           | Bwb3    | 53+        | 0.15       | 62                    |
| <b>P3</b> | ABb     | 0 – 10     | 0.18       | 50                    |
|           | Bwb1    | 10 – 57    | 0.16       | 58                    |
|           | C       | 57+        | 0.23       | 37                    |

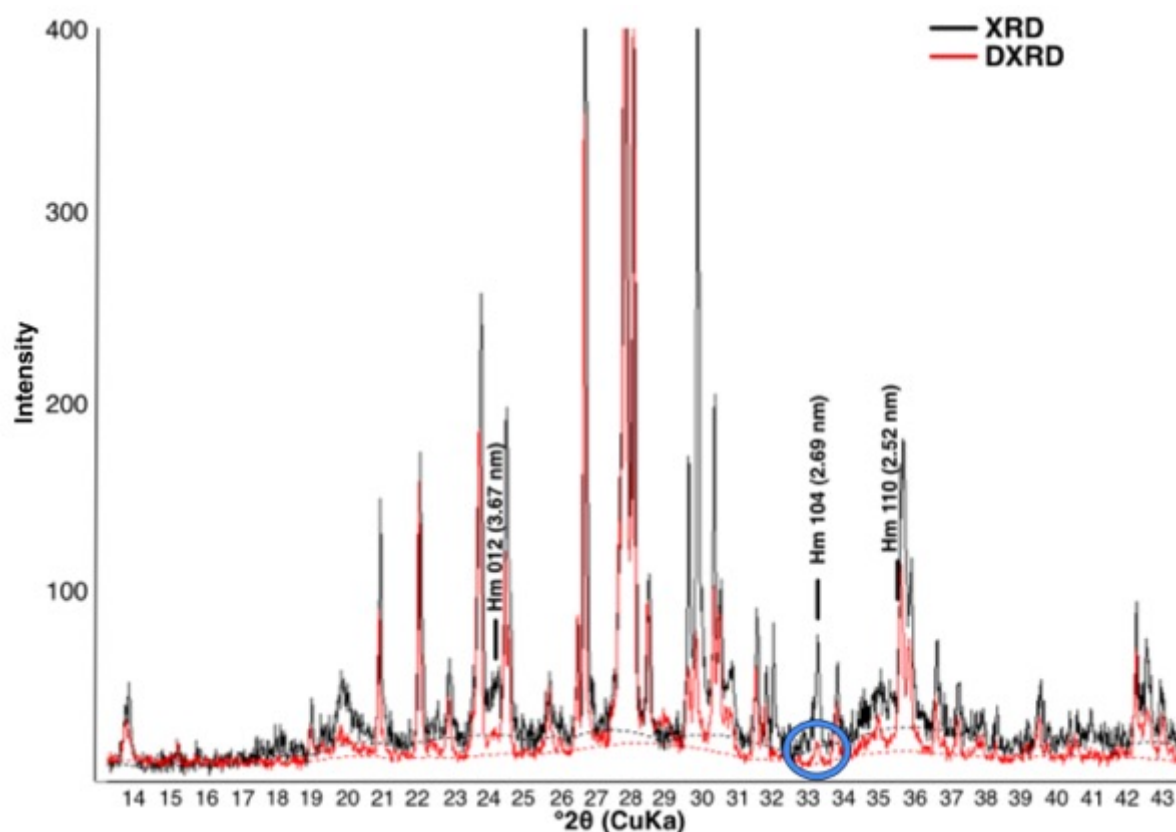


**Figure 5.** X-ray patterns of a representative sample, P1-Bwb1, 0-23 cm. XRD pattern (black) plotted against DCB treated sample (DXRD) (yellow). Note a small remnant peak of hematite peak 104 (blue circle), indicating an incomplete removal of hematite by DCB. Hm = Hematite.

### 3.3.3. Selective extraction of Iron Oxides

The previous results indicated that the paleosols colours were mostly due to hematite, even in the paleosol horizons with yellower hues. The selective extraction of iron hydroxides and oxides was carried out to provide both a quantitative and qualitative analysis of iron content and type (Table 3). The higher  $Fe_s$  values indicated that maghemite was the dominant iron oxide followed by hematite ( $Fe_d$ ) in all samples.

The proportion of hematite was higher in P2 and similar between P1 and P3. In P1, the amounts of hematite were slightly higher in the upper reddish horizons than the yellowish horizons 2ABb and 2BAb, which had much higher amounts than the greyish horizon 3ABb. Although P2 had similar colours, its hematite amounts changed weakly with depth. P3 had a slight increase in the Bwb1 horizon and distinct decrease in the C horizon reflecting the colour measurements.

**Table 3.** Selective and sequential extraction of iron oxides.

| Profile   | Horizon | Depth<br>(cm) | Fe <sub>s</sub> <sup>1</sup><br>(g/kg <sup>-1</sup> ) | Fe <sub>o</sub> <sup>2</sup><br>(g/kg <sup>-1</sup> ) | Fe <sub>d</sub> <sup>3</sup><br>(g/kg <sup>-1</sup> ) | Fe <sub>t</sub> <sup>4</sup><br>(g/kg <sup>-1</sup> ) | Fe <sub>d</sub> /Fe <sub>t</sub> *100 <sup>5</sup> |
|-----------|---------|---------------|---|---|---|---|--|
| <b>P1</b> | Bwb1    | 0 – 23        | 31  | 1.5   | 15.7  | 80.5  | 19.5   |
|           | Bwb2    | 23 – 34       | 26.7  | 0.9   | 13.5  | 79.3  | 17   |
|           | Bwb3    | 34 – 45       | 29.9  | 1   | 13.3  | 88.7  | 15   |
|           | 2ABb    | 45 – 60       | 32.4  | 0.9   | 10.5  | 79.8  | 13.2   |
|           | 2BAb    | 60 – 73       | 34  | 1   | 12.1  | 83.8  | 14.4   |
|           | 3ABb    | 73+           | 33.9  | 1.7   | 7   | 89.6  | 7.8  |
| <b>P2</b> | ABb     | 0 – 20        | 27.9  | 1   | 21.9  | 107.3   | 20.4   |
|           | Bwb1    | 20 – 30       | 25.1  | 0.8   | 21.7  | 88.3  | 24.6   |
|           | Bwb2    | 30 – 53       | 21.4  | 1.7   | 20.1  | 88.9  | 22.6   |
|           | Bwb3    | 53+           | 22.1  | 1.1   | 18.7  | 83.6  | 22.4   |
| <b>P3</b> | ABb     | 0 – 10        | 28.2  | 1.7   | 14.8  | 84.8  | 17.5   |
|           | Bwb1    | 10 – 57       | 23.9  | 1.5   | 14.7  | 80.7  | 18.2   |
|           | C       | 57+           | 24  | 2.1   | 9.6   | 80.7  | 11.9   |

<sup>1</sup>H<sub>2</sub>SO<sub>4</sub> extraction; <sup>2</sup>Ammonium oxalate extraction; <sup>3</sup>DCB extraction; <sup>4</sup>XRF analysis; <sup>5</sup>Proportion of hematite in relation to total iron (Fe).

The samples had lower chroma after the Fe<sub>d</sub> treatment because of the dissolution of hematite (Fig. 6). Furthermore, hematite showed a significant positive correlation with the a\* (redness) parameter (r = 0.82) (Supplementary figure 3). Nevertheless, as mentioned in the previous section before, hematite was not fully dissolved by DCB. This explains why the colours did not become totally grey after the DCB treatment. The treatment with oxalate caused little change in colour because the minor amounts of ferrihydrite (low Fe<sub>o</sub>) and the dissolution with H<sub>2</sub>SO<sub>4</sub> transformed the colour to reddish hue because the selective removal of brownish maghemite.

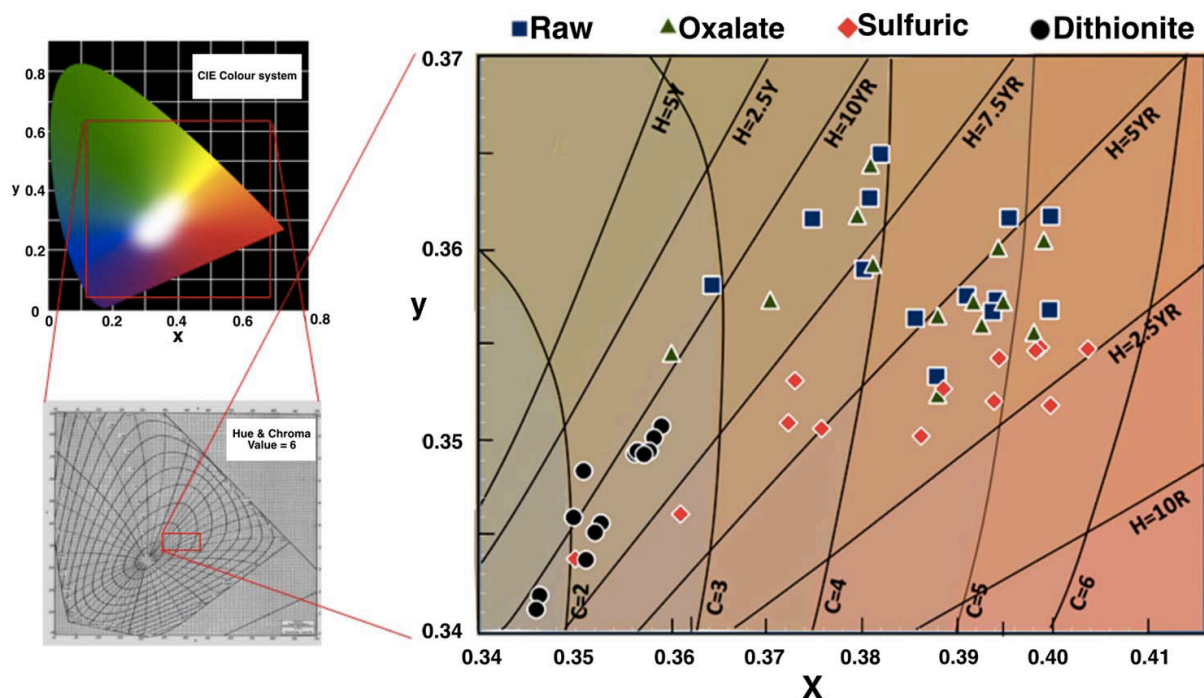


**Figure 6.** Color of the soil samples after different treatments on the CIE (x,y) chromaticity diagram showing loci of constant hue and constant chroma at value 6 of the Munsell notation system (Wysecki and Stiles, 1982)..

### 3.3.4. Magnetic susceptibility

The magnetic susceptibility provides an approximated concentration of the ferrimagnetic minerals in the soil (Fig. 7). In general, the  $\chi_{fd}\%$  of all samples (except P3-3ABb) were higher than 8%. This indicates the predominance of the superparamagnetic (SP) fraction (e.g. maghemite). Furthermore, from the Pearson correlation analysis, a significant positive correlation was found between  $\chi_{lf}$  and  $\chi_{fd}$  ( $r = 0.83$ ), reinforcing the predominance of the SP minerals over coarse-grained non-SP ferrimagnets (i.e. magnetite) (Fig. 8).

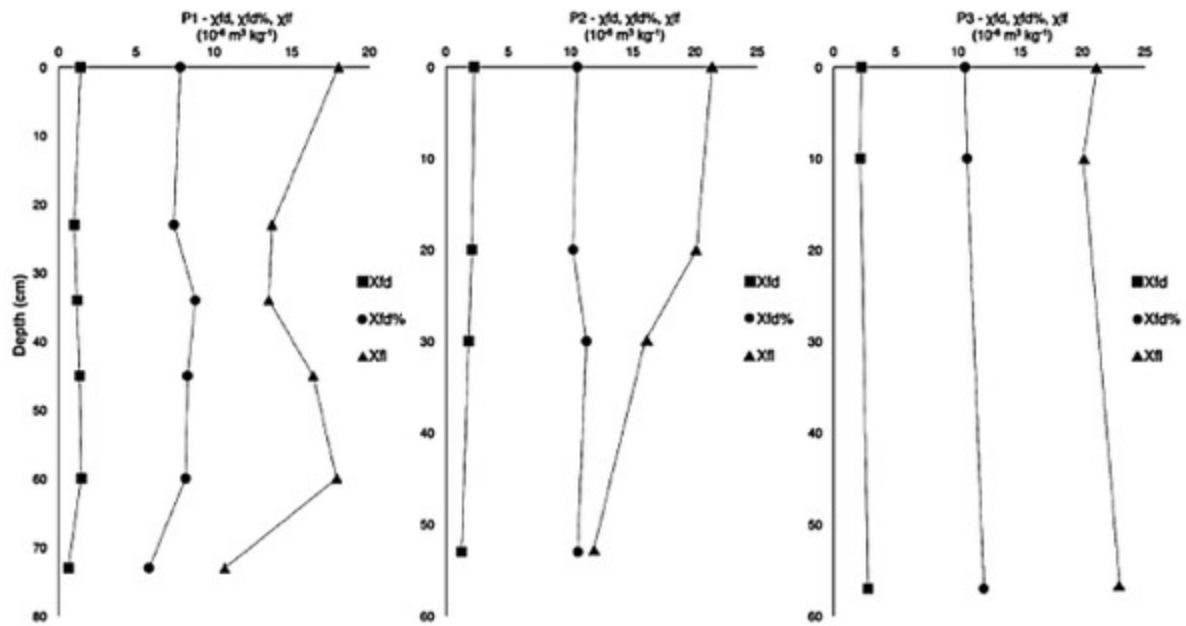


Figure 7. Depth function of mineral magnetic susceptibility parameters.

The low-frequency susceptibility ( $\chi_{lf}$ ) had much larger variations in depth than the frequency-dependent susceptibility ( $\chi_{fd}$  and  $\chi_{fd}\%$ ). The  $\chi_{lf}$  varied between 10.5 and 18  $\times 10^{-6} \text{ m}^3 \text{ kg}^{-1}$  in P1, between 11.6 and 17.8  $\times 10^{-6} \text{ m}^3 \text{ kg}^{-1}$  in P2, and between 20 and 23  $\times 10^{-6} \text{ m}^3 \text{ kg}^{-1}$  in P3.

P1 had decreasing values of  $\chi_{lf}$  with the maximum value at the uppermost horizon (18  $\times 10^{-6} \text{ m}^3 \text{ kg}^{-1}$ ) and minimum at the lowermost horizon (10.5  $\times 10^{-6} \text{ m}^3 \text{ kg}^{-1}$ ). The decreasing trend with depth is interrupted by the LD between Bwb3 and 2ABb, where  $\chi_{lf}$  has a small increase. The other LD (2BAb – 3ABb) shows a pronounced decrease of  $\chi_{lf}$ . The other parameters,  $\chi_{fd}$  and  $\chi_{fd}\%$  have less variations with lowest values in the 3ABb horizon.

The  $\chi_{lf}$  values are considerably higher in the two uppermost horizons ABb (21.5  $\times 10^{-6} \text{ m}^3 \text{ kg}^{-1}$ ) and Bwb1 (19.8  $\times 10^{-6} \text{ m}^3 \text{ kg}^{-1}$ ) of P2 in comparison with Bwb2 (15.4  $\times 10^{-6} \text{ m}^3 \text{ kg}^{-1}$ ) and Bwb3 (11.6  $\times 10^{-6} \text{ m}^3 \text{ kg}^{-1}$ ), whereas the frequency-dependent magnetic susceptibility  $\chi_{fd}$  and  $\chi_{fd}\%$  have similar values.

The magnetic properties among the horizons of P3 were similar. Contrary to the other profiles, the horizon with highest values is the lowermost C horizon with 22.4  $\times 10^{-6} \text{ m}^3 \text{ kg}^{-1}$ . The  $\chi_{fd}$  and  $\chi_{fd}\%$  had virtually the same values with depth.

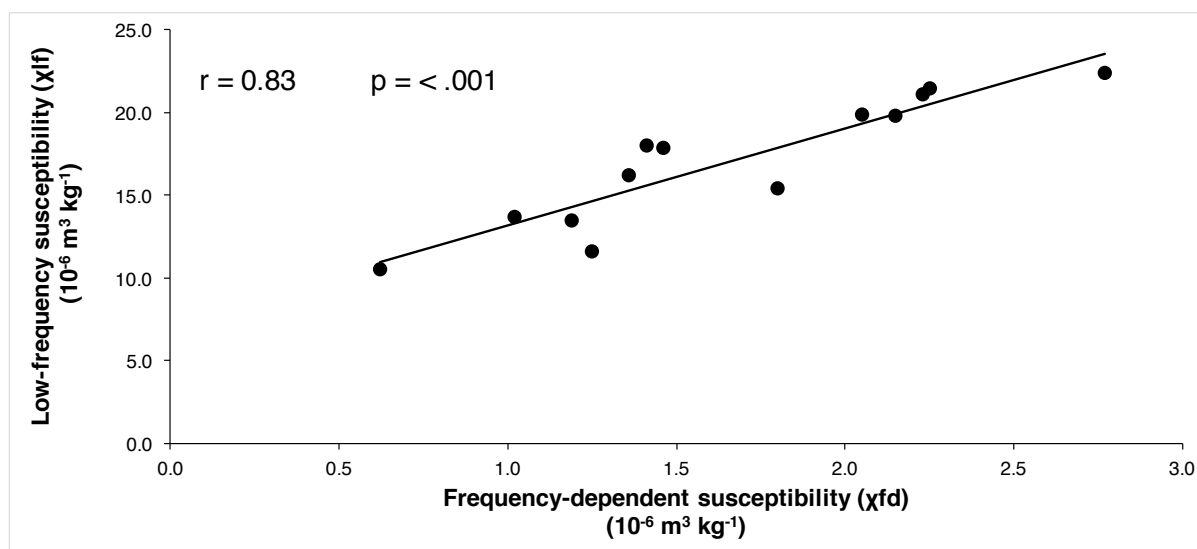


**Figure 8.** Relationship between low-frequency susceptibility ( $\chi_{lf}$ ) and frequency-dependent susceptibility ( $\chi_{fd}$ ).

## 4. Discussion

### 4.1. Morphology and distribution of hematite

The field descriptions provided a range of colours, varying from typical hematite-rich soils (2.5YR 5/4) to goethite-rich soils (5Y 4/1) colours (ref. Table 1). In addition, the colours were also reddish in thin sections, with either fine iron oxides dispersed throughout the groundmass or replacing Fe-bearing minerals and as Fe-rich mottles and nodules. The presence of iron mottles/nodules were more frequent in the less reddish horizons (P1-2ABb, P1-2BAb, and P1-3ABb) occurring as dark concentrations surrounded by a lighter coloured groundmass.

Most of the samples became yellower after mechanical grinding during sample preparation probably because of the destruction of hematite clusters (Torrent and Schwertmann, 1987). However, this behavior was not observed in horizons P1-2ABb and P1-2BAb, which had more frequently occurring mottles and nodules. While the horizon P1-2ABb had unaffected colours, the colours in P1-2BAb became redder. One hypothesis is that the paler groundmass (originally 10YR) became redder due to grinding and homogenizing with the Fe mottles/nodules.

The grain size of hematite is another property that may affect its colour (Hund, 1981). In synthetic hematite, the degree of "purpleness" ( $b^*$ ) has a positive correlation with particle size (Torrent and Schwertmann, 1987). Despite hematite in our samples had crystal size comparable with the crystal size in some red beds (e.g. Barrón and Montealegre, 1986; Torrent and Schwertmann, 1987) no relationship between crystal

size and colour was detectable. On the other hand, the amount of hematite had a significant positive correlation with the redness parameter ( $a^*$ ). Therefore, the red colour in these paleosols was mainly caused by clustering, content, and the mode of occurrence of hematite, i.e. finely dispersed in the groundmass; coating/replacing primary minerals and as mottles or nodules, rather than its crystal size.

Despite the differences in colour among the samples, only hematite was detected on DRS and XRD-DXRD. The absence of goethite was confirmed after heating at 800°C because of the permanence of the band at ~425 nm, which can be associated to hematite rather than goethite (Scheinost et al., 1998). Some experimental studies have demonstrated that goethite should dehydrate to hematite at about 300°C (Gialanella et al., 2010; Gualtieri and Venturelli, 1999). In Chinese red beds a conversion of goethite to hematite was identified at diagenetic temperatures >150°C (Jiang et al., 2015) and >105°C for Triassic sandstones in Denmark (Weibel, 1999). In reddish pre-Quaternary paleosols, goethite was detected in those not affected by deep-burial or high diagenetic temperatures (Dawit, 2016; Kraus and Hasiotis, 2006; Srivastava et al., 2015; Srivastava and Sauer, 2014; Vacca et al., 2012). Therefore, the conversion of goethite into hematite in buried paleosols or sediments needs a heating source produced by deep-burial.

The KGI paleosols were shallowly buried at a maximum thickness of 160 m of new basalt flows (Mozer, 2012). Therefore, diagenetic heating seems unlikely under such shallow burial. The presence of higher amounts of maghemite ( $Fe_s$ ) compared to hematite can be taken as a further evidence of no burial diagenetic heating, otherwise maghemite would have transformed to hematite under hydrothermal conditions between 150°C ±180°C (Blesa and Matijević, 1989). Another evidence in favor of little or no burial heating is the presence of plant residues with preservation of the distinct plant cell structure (Spinola et al., 2017b).

#### **4.2. Heating by lava flow**

Neoformation and enrichment of ferrimagnetic compounds in the uppermost horizons of P1 and P2 suggest thermal transformation of other iron oxy-hydroxides at temperatures >250°C in combination with organic matter and lower  $O_2$  supply (Maher, 1986).

An enhancement of low-frequency ( $\chi_{lf}$ ) magnetic susceptibility was detected in P1

from 0 to 23 cm (Bwb1 horizon) and in P2 from 0 to 30 cm. Nevertheless, the frequency-dependent susceptibility,  $\chi_{fd}$  and  $\chi_{fd}\%$ , were similar for all horizons. In soils formed in non-mafic parent materials (e.g. loess, mudstone), enhancement of  $\chi_{lf}$  occurs simultaneously with  $\chi_{fd}$  and  $\chi_{fd}\%$  caused by the neoformation of nano-sized magnetite and/or maghemite (Dearing et al., 1996; Torrent et al., 2006). On the other hand, soils formed from volcanic parent material show an opposite behavior: they have high initial  $\chi_{lf}$  values because of inherited magnetite and lower  $\chi_{fd}$  and  $\chi_{fd}\%$ . With the progressive weathering of magnetite and other Fe-bearing minerals, the  $\chi_{lf}$  values decrease and  $\chi_{fd}$  and  $\chi_{fd}\%$  increase due to neoformation of maghemite (Lu et al., 2008; Preetz et al., 2017; Rivas et al., 2006). Thus, enhanced  $\chi_{lf}$  values with homogeneous  $\chi_{fd}$  and  $\chi_{fd}\%$  in the uppermost horizons of P1 and P2 indicate enrichment in magnetite.

#### **4.3. Hematite formation and paleoenvironmental implications**

The strong red colours of KGI paleosols given by the predominance of maghemite and hematite is not compatible with their weak to moderate pedogenic development. Although these iron oxides could have been inherited from more intense and/or longer weathering periods and the erosion such more weathered horizons could have occurred prior or during the lava deposition, there are no other evidences of deep weathering (e.g. presence of kaolinite). Furthermore, at least partial preservation of surficial horizons is demonstrated by the presence of former A horizons (discussed below). The presence of nodules/mottles also points to a lack of significant former erosion because they suggest weak hydromorphic conditions (probably related to rainwater rather than groundwater), which are usually associated to a flat topography. Even though more field work would be necessary, the abrupt contact between lava and paleosol seems to be more related to the fast emplacement of the basaltic lava rather than to erosion and truncation of the paleosols. In summary, it is unlikely that a predominance of hematite would have been achieved during past pedogenic processes (Retallack, 1991).

Weakly to moderately developed volcanic soils are usually brownish/yellowish with ferrihydrite as the main iron hydroxide. With time and under a cool humid climate, ferrihydrite usually converts to goethite rather than hematite (Shoji et al., 1993; Ugolini and Dahlgren, 2002). The formation of ferrihydrite in soils depends upon a combination of factors, such as a high rate of Fe<sup>II</sup> release, presence of silicate, and organic matter

(Shoji et al., 1993). Some of these conditions count for the investigated soils, such as considerably high amounts of  $Fe_d$ , and widespread iron pigmentation found in thin sections. Although organic matter was not detected because of the burial oxidation (Retallack, 1991), there are preserved evidences suggesting former A horizons, such as plant residues, bioturbation voids (e.g. channels) and granular/crumb microstructure (Spinola et al., 2017b). Nonetheless, ferrihydrite would hardly be preserved in Eocene paleosols because of its metastable nature (Cornell and Schwertmann, 2003). For instance, air-dry storage of ferrihydrite containing  $100 \pm 150 g H_2O \cdot kg^{-1}$  of water (found by weight loss) at room temperature for 20.4 years in closed vessels led to partial transformation of ferrihydrite to well crystalline hematite with a little goethite (Schwertmann et al., 1999).

Both hematite and goethite are common stable end-products of ferrihydrite. Their relative portions are controlled by climate (as mentioned before) and specific soil chemical conditions: the transformation of ferrihydrite to hematite involves a dehydration step, whereas transformation to goethite involves dissolution and recrystallization. Furthermore, a pH around 7 – 8 will favor hematite (Schwertmann et al., 1999). Although it is not possible to assess the pH of the paleosol prior to burial, some characteristics of these paleosols are indicative of basic pH, such as base-rich parent material (basaltic tephra) and presence of smectite (Spinola et al., 2017a). Hence, we assume that goethite was probably never formed in these paleosols and ferrihydrite was the main iron hydroxide, which later converted to hematite by dehydration after the burial because of a lack of further moisture and favorable soil chemistry, without relationship with the paleoclimate. Therefore, it seems that there was not sufficient pedogenesis time for ferrihydrite convert to goethite, otherwise, goethite would likely be detected.

The presence of grey and yellowish horizons in P1 were the result of changes in paleodrainage. Despite this, it is not possible to make direct associations of changes in colour with specific paleoclimate conditions (Sheldon, 2005). The main chemical evidences for different soil drainage was the lower contents of iron and reduced magnetic susceptibility in the grey horizon P1-3ABb. Reduced magnetic susceptibility is a common feature of waterlogged soils (Maher, 1986). This horizon and the yellower ones, P1-2ABb and P1-2BAb, were also those with finer texture, less rock fragments, and more abundance of nodules/mottles and plant fragments (Spinola et al., 2017b).

Therefore, the two LDs indicate also changes in the past soil hydrological conditions, from greyish (partially impeded drainage) to yellowish and finally to the reddish horizons (free drainage).

## 5. Conclusions

We verified the hypothesis that the red colour of the investigated paleosols was formed by diagenesis, because 1) the iron oxide assemblage was composed only by maghemite and hematite. This iron oxide assemblage is not common in weakly to moderately developed volcanic soils. Considering the lack of evidences for inheritance of these iron oxides from more weathered horizons, diagenesis after burial seems the best explanation; 2) the high crystallinity of hematites, having a large grain size, is more rather known from diagenetically altered red beds than from soils. Since hematite and goethite have similar thermodynamic stabilities and no diagenetic heating took place, our results indicate the formation of hematite in these paleosols was formed rather by the transformation of ferrihydrite after burial than by the dehydration of goethite.

The differences in colour throughout the horizons were mainly given by the clustering, content and the distribution of hematite (finely dispersed in the groundmass; coating/replacing primary minerals and as mottles or nodules). These properties were the result of paleopedogenic processes originally forming ferrihydrite linked rather with paleodrainage than with paleoclimate conditions. The colour differences among the lithic discontinuities in P1 is an important issue for future research. A quantitative approach using stable isotope geochemistry and/or lipid biomarkers should provide more detailed information regarding potential paleoclimatic changes.

Our second hypothesis was that the paleosols were not affected by the heating of lava flow because it had no colour differences on uppermost horizons. In fact, there were no colour differences. However, the enhancement of magnetic susceptibility, with magnetite neoformation, in the upper horizons of P1 and P2, indicate that these horizons were exposed to high temperatures (250°C – 400°C) with organic matter under a low O<sub>2</sub> supply. Nevertheless, lost of information due to erosion of upper layers, which could have recorded better the effects of heating, should not be excluded.

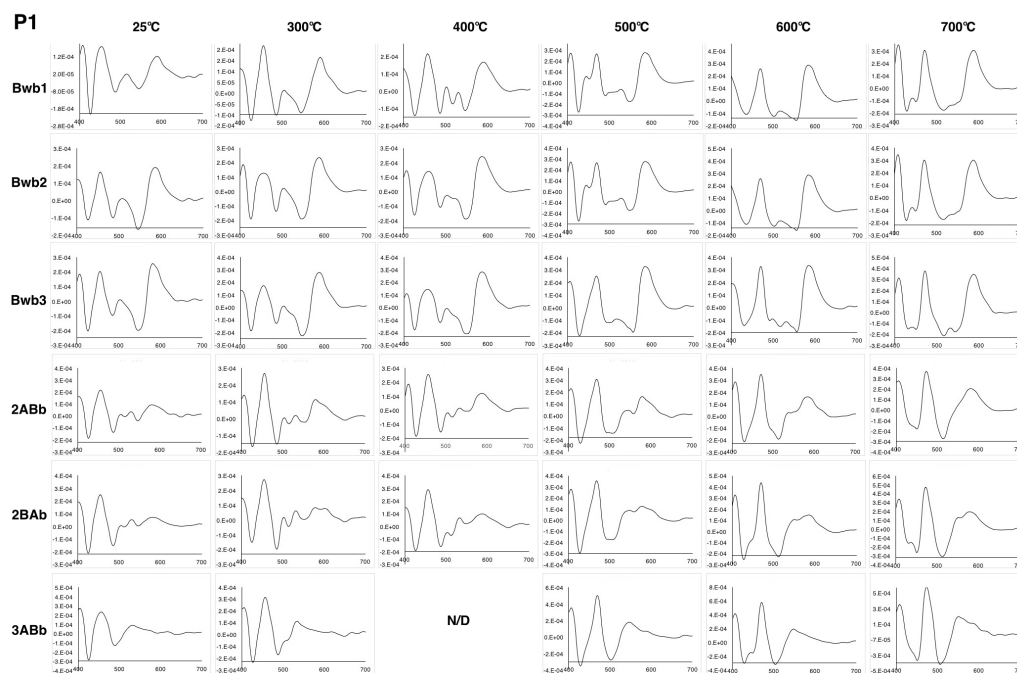
Our findings highlight the importance of detailed mineralogical analysis to identify iron oxides present in reddish paleosols because identification based solely on morphology

(e.g. yellowish colour, gradual horizon transitions) can lead to a misinterpretation of paleoenvironment.

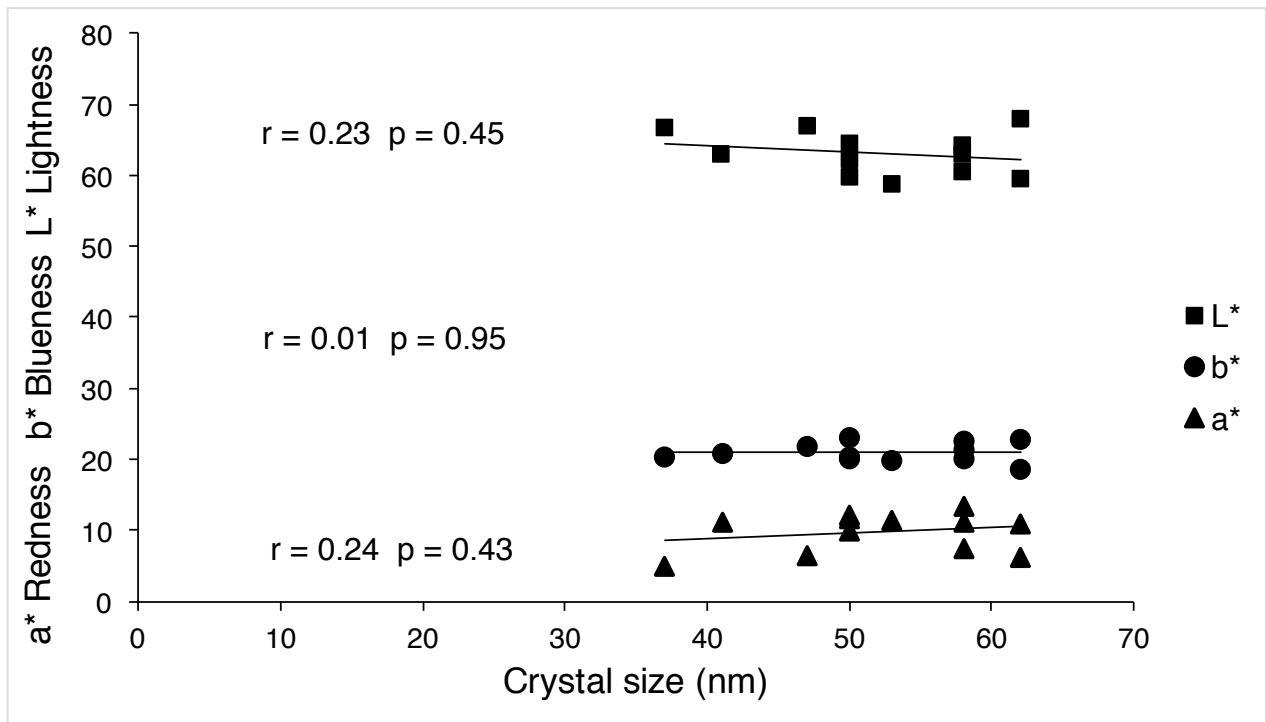
**Acknowledgements:**

The present work was possible with financial support of the National Counsel of Technological and Scientific Development (CNPq), Brazil. This study was also supported by the German Research Foundation (DFG KU 1946/9-1). We thank the Brazilian Navy and the colleagues (38. Polska Wyprawa Antarktyczna) from the Henry Arctowski Station for all logistics and much additional support to realize the successful field work during the Antarctic expedition in the summer of 2013/2014. We also thank José María Méndez Álvarez (University of Córdoba) for carrying out the DCB and oxalate analyses and Simon Degler (University of Tübingen) for helping with the sample preparation.

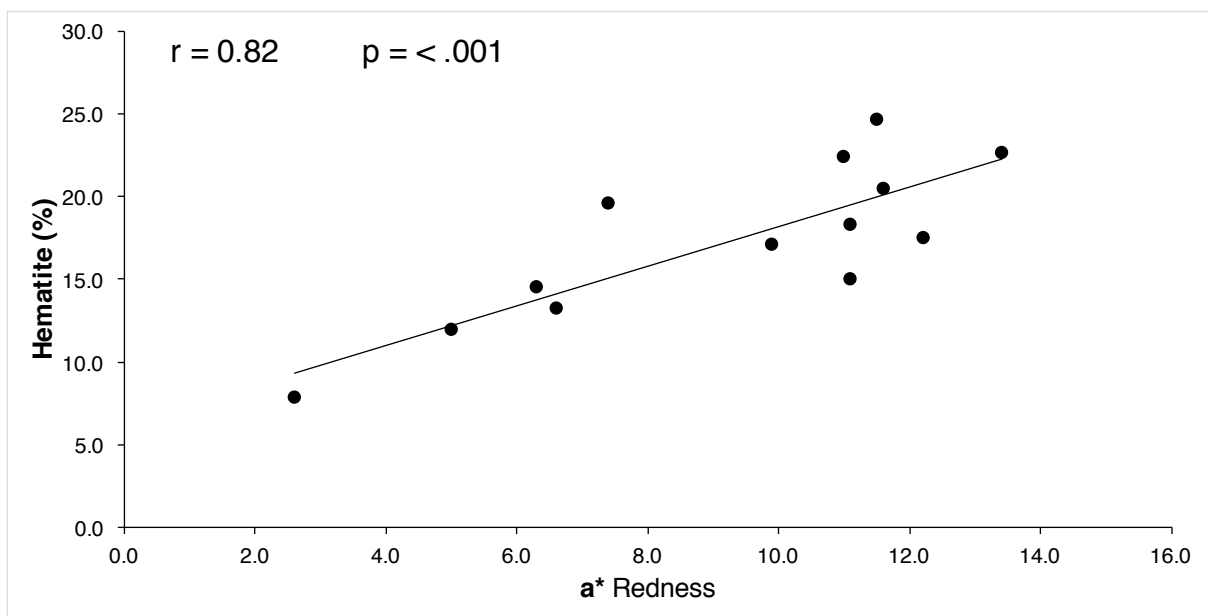
Supplementary data



Supplementary Figure 1. Diffuse Reflectance Spectra (DRS) of all samples after heating intervals.



**Supplementary Figure 2.** Relationship between L\*a\*b\* colour system with hematite crystallite size (nm).



**Supplementary Figure 3.** Relationship between hematite and redness parameter (a\*).

## References

- Arduino, E., Barberis, E., Carraro, F., Forno, M.G., 1984. Estimating relative ages from Iron-oxide/Total-Iron ratio of soils in the Western Po Valley, Italy. *Geoderma* 33, 39–52.
- Askin, R.A., 1991. Late Cretaceous-Early Tertiary Antarctic outcrop evidence for past vegetation and climates, in: Kennett, J.P., Warnke, D.. (Eds.), *The Antarctic Paleoenvironment: A Perspective on Global Change*. Antarctic Research Series. American Geophysical Union, Washington D.C, pp. 61–73.
- Bakker, L., Lowe, D.J., Jongmans, A.G., 1996. A micromorphological study of pedogenic processes in an evolutionary soil sequence formed on Late Quaternary rhyolitic tephra deposits, North Island, New Zealand. *Quat. Int.* 34–36, 249–261. doi:10.1016/1040-6182(95)00090-9
- Barrett, P., 2008. A History of Antarctic Cenozoic Glaciation - View from the Margin. *Dev. Earth Environ. Sci.* 8, 33–83. doi:10.1016/S1571-9197(08)00003-7
- Barrón, V., Montealegre, L., 1986. Iron Oxides and Colour of Triassic Sediments: Application of the Kubelka-Munk Theory. *Am. J. Sci.* doi:10.2475/ajs.286.10.792
- Berggaut, V., Singer, A., Stahr, K., 1994. Palagonite reconsidered: Paracrystalline illite-smectites from regoliths on basic pyroclastics. *Clays Clay Miner.* 42, 582–592. doi:10.1346/CCMN.1994.0420511
- Bijl, P.K., Schouten, S., Sluijs, A., Reichert, G.-J., Zachos, J.C., Brinkhuis, H., 2009. Early Palaeogene temperature evolution of the southwest Pacific Ocean. *Nature* 461, 776–779. doi:10.1038/nature08399
- Birkenmajer, K., 1988. Tertiary glacial and interglacial deposits, South Shetland Islands, Antarctica: geochronology versus biostratigraphy. *Bull. Polish Acad. Sci. Earth Sci.* 36, 133–145.
- Birkenmajer, K., 1980a. Tertiary volcanic-sedimentary succession at Admiralty Bay, King George Island (South Shetland Islands, Antarctica). *Stud. Geol. Pol.* 64, 7–65.
- Birkenmajer, K., 1980b. Geology of Admiralty Bay, King George Island (South Shetland Islands) — An outline. *Polish Polar Res.* 1, 29–54.
- Birkenmajer, K., Gaździcki, A., Krajewski, K.P., Przybycin, A., Solecki, A., Tatur, A., Yoon, H.I., 2005. First Cenozoic glaciers in West Antarctica. *Polish Polar Res.* 26, 3–12.

- Birkenmajer, K., Łydka, K., 1990. Mineralogical evidence for warm Palaeogene climate from the Ezcurra Inlet Group, King George Island, West Antarctica. *Bull. Polish Acad. Sci. Earth Sci.* 38, 25–38.
- Birkenmajer, K., Zastawniak, E., 1989. Late Cretaceous-early Tertiary floras of King George Island, West Antarctica: their stratigraphic distribution and palaeoclimatic significance. *Geol. Soc. London, Spec. Publ.* 47, 227–240. doi:10.1144/GSL.SP.1989.047.01.17
- Blesa, M., Matijević, E., 1989. Phase transformations of iron oxides, oxohydroxides, and hydrous oxides in aqueous media. *Adv. Colloid Interface Sci.* 29, 173–221. doi:10.1016/0001-8686(89)80009-0
- Blodgett, R., Crabaugh, J., McBride, E.F., 1993. The colour of red beds: a geologic perspective, in: Bigham, J.H., Ciolkosz, E. (Eds.), *Soil Colour*. Soil Science Society of America Special Publication, pp. 127–159.
- Borchardt, G., 1989. Smectites, in: Dixon, J., Weed, S. (Eds.), *Minerals in Soil Environments*. Soil Science Society of America, Madison, Wisconsin, pp. 675–727.
- Bouma, J., Fox, C., Miedma, R., 1990. Micromorphology of hydromorphic soils: applications for soil genesis and land evaluation, in: Douglas, L. (Ed.), *Soil Micromorphology: A Basic and Applied Science*. Elsevier, Amsterdam, pp. 257–278.
- Bronger, A., Heinkele, T., 1990. Mineralogical and clay mineralogical aspects of loess research. *Quat. Int.* 7/8, 37–51.
- Buurman, P., 1975. Possibilities of paleopedology. *Sedimentology* 22, 289–298.
- Canile, F.M., 2010. Evidências geológicas de mudanças climáticas (greenhouse-icehouse) na Antártica Ocidental durante a passagem Eoceno-Oligoceno. Universidade Federal de São Paulo.
- Churchman, G.J., Lowe, D., 2012. Alteration, formation, and occurrence of minerals in soils. *Handb. Soil Sci. Prop. Process.* 1, 20–72. doi:doi:10.1201/b11267-24
- Colman, S.M., 1982. Clay mineralogy of weathering rinds and possible implications concerning the sources of clay minerals in soils. *Geology* 10, 370–375.
- Commission Internationale de L'Eclairage, 1978. Recommendations on uniform colour spaces colour difference equations psychometric colour terms, Supplement 2. CIE Publ. 15 (E-1.3.1) 1971/(TC-1.3). Bur. Centrale de la CIE. Paris. Paris.

- Cornell, R.M., Schwertmann, U., 2003. *The Iron Oxides - Structure, properties, reactions, occurrences and uses*, 2nd ed. Wiley-VCH Verlag, Weinheim.
- Coxall, H.K., Wilson, P.A., Pälike, H., Lear, C.H., Backman, J., 2005. Rapid stepwise onset of Antarctic glaciation and deeper calcite compensation in the Pacific Ocean. *Nature* 433, 53–57. doi:10.1038/nature03135
- Craig, P., Chevrier, V., Sayyed, M.R.G., Islam, R., 2017. Spectral analysis of Deccan intrabasaltic bole beds: Implications for the formation and alteration of phyllosilicates on Mars. *Planet. Space Sci.* 135, 55–63. doi:10.1016/j.pss.2016.11.008
- D'Amore, D. V., Stewart, S.R., Huddleston, J.H., 2004. Saturation, Reduction, and the Formation of Iron–Manganese Concretions in the Jackson-Frazier Wetland, Oregon. *Soil Sci. Soc. Am. J.* 68, 1012. doi:10.2136/sssaj2004.1012
- Dahms, D., 1994. Mid-holocene erosion of soil catenas on moraines near the type pinedale till, wind river range, Wyoming. *Quat. Res.* 42, 41–48.
- Dalrymple, J.B., Jim, C.Y., 1984. Experimental study of soil microfabrics induced by isotropic stresses of wetting and drying. *Geoderma* 34, 43–68. doi:10.1016/0016-7061(84)90005-3
- Dawit, E.L., 2016. Paleoclimatic records of Late Triassic paleosols from Central Ethiopia. *Palaeogeogr. Palaeoclimatol. Palaeoecol.* 449, 127–140. doi:10.1016/j.palaeo.2016.02.011
- Dearing, J.A., 1999. Environmental Magnetic Susceptibility Using the Bartington MS2 System. *Interpret. A J. Bible Theol.* 52.
- Dearing, J.A., Hay, K.L., Baban, S.M.J., Huddleston, A.S., Wellington, E.M.H., Loveland, P.J., 1996. Magnetic susceptibility of soil: An evaluation of conflicting theories using a national data set. *Geophys. J. Int.* 127, 728–734. doi:10.1111/j.1365-246X.1996.tb04051.x
- DeConto, R.M., Pollard, D., 2003. Rapid Cenozoic glaciation of Antarctica induced by declining atmospheric CO<sub>2</sub>. *Nature* 421, 245–249. doi:10.1038/nature01290
- Delvigne, J., 1998. *Atlas of Micromorphology of Mineral Alteration and Weathering*, ORSTOM. ed. Mineralogical Association of Canada, Ottawa.
- Delvigne, J., 1990. Hypogene and supergene alteration of orthopyroxene in the Koua Bocca ultra mafic intrusion, Ivory Coast. *Chem. Geol.* 84, 49–53.
- Delvigne, J., Bisdorf, E.B., Sleeman, J., Stoops, G., 1979. Olivines, their pseudomorphs and secondary products. *Pedologie* 3, 247–309.

- DIN ISO 10693, 1995. Bodenbeschaffenheit Bestimmung des Carbonatgehaltes e Volumetrisches Verfahren. Beuth, Berlin.
- DIN ISO 10694, 1995. Bodenbeschaffenheit Bestimmung von organischem Kohlenstoff und Gesamtkohlenstoff nach trockener Verbrennung (Elementaranalyse). Beuth, Berlin.
- Dingle, R.V., Lavelle, M., 2000. Antarctic Peninsula Late Cretaceous-Early Cenozoic paleoenvironments and Gondwana paleogeographies. *J. African Earth Sci.* 31, 91–105. doi:10.1016/S0899-5362(00)00075-0
- Dingle, R. V., Lavelle, M., 1998a. Antarctic Peninsular cryosphere: Early Oligocene (c. 30 Ma) initiation and a revised glacial chronology. *J. Geol. Soc. London.* 155, 433–437. doi:10.1144/gsjgs.155.3.0433
- Dingle, R. V., Lavelle, M., 1998b. Late Cretaceous-Cenozoic climatic variations of the northern Antarctic Peninsula: New geochemical evidence and review. *Palaeogeogr. Palaeoclimatol. Palaeoecol.* 141, 215–232. doi:10.1016/S0031-0182(98)00056-X
- Dudas, M.J., Harward, M.E., 1975. Inherited and detrital 2:1 type phyllosilicates in soils developed from Mazama ash. *Soil Sci. Soc. Am. J.* 39, 571–577. doi:10.2136/sssaj1975.03615995003900030050x
- Eberl, D.D., 1984. Clay mineral formation and transformation in rocks and soils. *Philos. Trans. R. Soc. London* 311, 241–257.
- Ehrmann, W.U., Melles, M., Kuhn, G., Grobe, H., 1992. Significance of clay mineral assemblages in the Antarctic Ocean. *Mar. Geol.* 107, 249–273. doi:10.1016/0025-3227(92)90075-S
- Elliot, D.H., Askin, R.A., Kyte, F.T., Zinsmeister, W.J., 1994. Iridium and dinocysts at the Cretaceous-Tertiary boundary on Seymour Island, Antarctica: implications for the K-T event. *Geology* 22, 675–678. doi:10.1130/0091-7613
- Emeleus, C.H., Allwright, E.A., Kerr, A.C., Williamson, I.T., 1996. Red tuffs in the Palaeocene lava successions of the Inner Hebrides. *Scottish J. Geol.* 32, 83–90. doi:10.1144/sjg32010083
- FAO, 2006. Guidelines for soil description, 4th ed. Rome.
- Fedoroff, N., Courty, M.-A., Guo, Z., 2010. Paleosoils and Relict Soils, in: Stoops, G. Marcelino, V. Mees, F. (Ed.), *Interpretation of Micromorphological Features of Soils and Regoliths*. Elsevier, Amsterdam, pp. 623–662. doi:10.1016/B978-0-444-53156-8.00027-1

- Feldmann, R., Woodburne, M., 1988. Geology and paleontology of Seymour Island, Antarctic Peninsula. Geological Society of America, Memoir 169.
- Fenwick, I., M., 1985. Paleosols: problems of recognition and interpretation, in: Boardman, J. (Ed.), Soils and Quaternary Landscape Evolution. John Wiley and Sons, Norwich, p. 391.
- Fiore, S., 1993. The occurrences of smectite and illite in a pyroclastic deposit prior to weathering: implications on the genesis of 2:1 clay minerals in volcanic soils. *Appl. Clay Sci.* 8, 249–259. doi:10.1016/0169-1317(93)90007-N
- Fiore, S., Huertas, F., Linares, J., 1992. Mineralogy and geochemistry of some “so-called” paleosols from Mt. Vulture volcano (southern Italy). *Chem. Geol.* 99, 237–252. doi:10.1016/0009-2541(92)90179-9
- Fleck, R., Sutter, J., Elliot, D., 1977. Interpretation of discordant  $^{40}\text{Ar}/^{39}\text{Ar}$  age-spectra of Mesozoic tholeiites from Antarctica. *Geochim. Cosmochim. Acta* 41, 15–32.
- Francis, J., Poole, I., 2002. Cretaceous and early Tertiary climates of Antarctica: evidence from fossil wood. *Palaeogeogr. Palaeoclimatol. Palaeoecol.* 182, 47–64.
- Francis, J.E., Ashworth, A., Cantrill, D.J., Crame, J.A., Howe, J., Stephens, R., Tosolini, A.-M., Thorn, V., 2007. 100 Million Years of Antarctic Climate Evolution: Evidence from Fossil Plants. *Proc. 10th Int. Symp. Antarct. Earth Sci.* 19–27. doi:10.3133/of2007-1047.kp03
- Francis, J.E., Marenssi, S., Levy, R., Hambrey, M., Thorn, V.C., Mohr, B., Brinkhuis, H., Warnaar, J., Zachos, J., Bohaty, S., DeConto, R., 2009. From Greenhouse to Icehouse - The Eocene/Oligocene in Antarctica. *Dev. Earth Environ. Sci.* 8, 309–368. doi:10.1016/S1571-9197(08)00008-6
- Galán, E., 2006. Genesis of Clay Minerals, in: *Developments in Clay Science*. pp. 1129–1162. doi:10.1016/S1572-4352(05)01042-1
- García-Romero, E., Vegas, J., Baldonado, J.L., Marfil, R., 2005. Clay minerals as alteration products in basaltic volcanoclastic deposits of La Palma (Canary Islands, Spain). *Sediment. Geol.* 174, 237–253. doi:10.1016/j.sedgeo.2004.12.007
- Gérard, M., Caquineau, S., Chenet, A., Fluteau, F., Courtillot, V., Subbarao, K. V., 2006. Red boles in the Deccan traps: time constraints from alteration processes, in: *Geophysical Research Abstracts*. p. 7092.

- Gérard, M., Caquineau, S., Pinheiro, J., Stoops, G., 2007. Weathering and allophane neoformation in soils developed on volcanic ash in the Azores. *Eur. J. Soil Sci.* 58, 496–515. doi:10.1111/j.1365-2389.2007.00910.x
- Ghosh, P., Sayeed, M.R.G., Islam, R., Hundekari, S.M., 2006. Inter-basaltic clay (bole bed) horizons from Deccan traps of India: Implications for palaeo-weathering and palaeo-climate during Deccan volcanism. *Palaeogeogr. Palaeoclimatol. Palaeoecol.* 242, 90–109. doi:10.1016/j.palaeo.2006.05.018
- Gialanella, S., Girardi, F., Ischia, G., Lonardelli, I., Mattarelli, M., Montagna, M., 2010. On the goethite to hematite phase transformation. *J. Therm. Anal. Calorim.* 102, 867–873. doi:10.1007/s10973-010-0756-2
- Graef, F., Singer, A., Stahr, K., Jahn, R., 1997. Genesis and diagenesis of paleosols from Pliocene volcanics on the Golan Heights. *Catena* 30, 149–167. doi:10.1016/S0341-8162(97)00026-X
- Greenwood, D.R., Wing, S.L., 1995. Eocene continental climates and latitudinal temperature gradients. *Geology* 23, 1044–1048.
- Griener, K.W., Nelson, D.M., Warny, S., 2013. Declining moisture availability on the Antarctic Peninsula during the Late Eocene. *Palaeogeogr. Palaeoclimatol. Palaeoecol.* 383–384, 72–78. doi:10.1016/j.palaeo.2013.05.004
- Gualtieri, A.F., Venturelli, P., 1999. In situ study of the goethite-hematite phase transformation by real time synchrotron powder diffraction. *Am. Mineral.* 84, 895–904. doi:10.2138/am-1999-5-624
- Halama, R., Konrad-Schmolke, M., Sudo, M., Marschall, H., Wiedenbeck, M., 2014. Effects of fluid-rock interaction on  $^{40}\text{Ar}/^{39}\text{Ar}$  geochronology in high-pressure rocks (Sesia-Lanzo Zone, Western Alps). *Geochim. Cosmochim. Acta* 126, 475–494.
- Heidari, A., Mahmoodi, S., Stoops, G., Mees, F., 2004. Micromorphological Characteristics of Vertisols of Iran, Including Nonsmectitic Soils. *Arid L. Res. Manag.* 19, 29–46. doi:10.1080/15324980590887164
- Hekinian, R., 1982. *Petrology of the Ocean Floor*, Elsevier O. ed. Elsevier, Amsterdam-Oxford-New York. doi:10.1016/S0422-9894(08)70937-1
- Holliday, V., 1988. Genesis of a late-holocene soil chronosequence at the Lubbock lake archeological site, Texas. *Ann. Assoc. Am. Geogr.* 78, 594–610.
- Huber, M., Brinkhuis, H., Stickley, C.E., Döös, K., Sluijs, A., Warnaar, J., Schellenberg, S.A., Williams, G.L., 2004. Eocene circulation of the Southern

- Ocean: Was Antarctica kept warm by subtropical waters? *Paleoceanography* 19, 1–12. doi:10.1029/2004PA001014
- Hund, F., 1981. Inorganic Pigments: Bases for Coloured, Uncoloured, and Transparent Products. *Angew. Chemie Int. Ed. English* 20, 723–730. doi:10.1002/anie.198107231
- Hunt, R.J., Poole, I., 2003. Paleogene West Antarctic climate and vegetation history in light of new data from King George Island. *Geol. Soc. Am. Spec. Pap.* 369, 395–412. doi:10.1130/0-8137-2369-8.395
- IREN, 1978. Estudio de suelos de la provincia de Valdivia.
- Ishizuka, O., 1998. Vertical and horizontal variation of the fast neutron flux in a single irradiation capsule and their significance in the laser-heating  $^{40}\text{Ar}/^{39}\text{Ar}$  analysis: Case study for the hydraulic rabbit facility of the JMTR reactor, Japan. *Geochem. J* 32, 243–252.
- IUSS Working Group WRB, 2014. World reference base for soil resources 2014. International soil classification system for naming soils and creating legends for soil maps, World Soil Resources Reports No. 106. doi:10.1017/S0014479706394902
- Jeong, G.Y., Yoon, H. II, Lee, S.Y., 2004. Chemistry and microstructures of clay particles in smectite-rich shelf sediments, South Shetland Islands, Antarctica. *Mar. Geol.* 209, 19–30. doi:10.1016/j.margeo.2004.05.027
- Jiang, L., Chen, G., Grapes, R., Peng, Z., 2015. Journal of Asian Earth Sciences Thermal origin of continental red beds in SE China : An experiment study. *J. Asian Earth Sci.* 101, 14–19. doi:10.1016/j.jseaes.2015.01.019
- Jongmans, A.G., Nieuwenhuysse, A., Buurman, P., van Doesburg, J.D.J., van Oort, F., Jaunet, A.M., 1994. Inheritance of 2:1 phyllosilicates in Costa Rican Andisols. *Soil Sci. Soc. Am. J.* 58, 494–501. doi:10.2136/sssaj1994.03615995005800020035x
- Jongmans, a. G., Nieuwenhuysse, a., Buurman, P., van Doesburg, J.D.J., van Oort, F., Jaunet, a. M., 1994. Inheritance of 2:1 Phyllosilicates in Costa Rican Andisols. *Soil Sci. Soc. Am. J.* 58, 494. doi:10.2136/sssaj1994.03615995005800020035x
- Kovda, I., Mermut, A.R., 2010. Vertic Features, in: Stoops, G., Marcelino, V., Mees, F. (Eds.), *Interpretation of Micromorphological Features of Soils and Regoliths*. Elsevier, Amsterdam, pp. 109–122. doi:10.1016/B978-0-444-53156-8.00013-1

- Kraus, M.J., 1997. Lower Eocene alluvial paleosols: Pedogenic development, stratigraphic relationships, and paleosol/landscape associations. *Palaeogeogr. Palaeoclimatol. Palaeoecol.* 129, 387–406. doi:10.1016/S0031-0182(96)00056-9
- Kraus, M.J., Hasiotis, S.T., 2006. Significance of different modes of rhizolith preservation to interpreting paleoenvironmental and paleohydrologic settings: Examples from Paleogene paleosols, Birghorn Basin, Wyoming, U.S.A. *J. Sediment. Res.* 76, 633–646. doi:10.2110/jsr.2006.052
- Kristmannsdottir, H., Tomasson, J., 1978. Zeolite zones in geothermal areas of Iceland, in: Sand, L.B., Mumpton, F.M. (Eds.), *Natural Zeolite Occurrence, Properties and Use*. Pergamon Press, Oxford, pp. 277–284.
- Kühn, P., Aguilar, J., Miedma, R., 2010. Textural features and their related horizons, in: Stoops, G., Marcelino, V., Mees, F. (Ed.), *Micromorphological Features of Soils and Regoliths. Their Relevance for Pedogenic Studies and Classifications*. Elsevier B.V., pp. 217–250. doi:10.1016/B978-0-444-53156-8.00011-8
- Kühn, P., Pietsch, D., 2013. Soil micromorphogenesis and Early Holocene paleoclimate at the desert margin of Southern Arabia 3, 59–77. doi:10.3232/SJSS.2013.V3.N2.04
- Kühn, P., Techmer, A., Weidenfeller, M., 2013. Lower to middle Weichselian pedogenesis and palaeoclimate in Central Europe using combined micromorphology and geochemistry: The loess-paleosol sequence of Alsheim (Mainz Basin, Germany). *Quat. Sci. Rev.* 75, 43–58. doi:10.1016/j.quascirev.2013.05.019
- Lange, F.M., Frick, C., Stahr, K., Graef, F., Singer, A., 2002a. Fritted Paleosols as Indicators for the Local Paleoclimate - Examples from the Golan Heights. *Die Erde* 133, 259–274.
- Lange, F.M., Frick, C., Stahr, K., Graef, F., Singer, A., 2002b. Fritted paleosols as indicators for the local paleoclimate - examples from the Golan Heights. *Die Erde* 133, 259–274.
- Lanson, B., 1997. Decomposition of experimental x-ray diffraction patterns (profile fitting): A convenient way to study clay minerals. *Clays Clay Miner.* 45, 132–146. doi:10.1346/CCMN.1997.0450202
- Lee, Y. II, Lim, H.S., Yoon, H. II, 2004. Geochemistry of soils of King George Island, South Shetland Islands, West Antarctica: Implications for pedogenesis in cold

polar regions. *Geochim. Cosmochim. Acta* 68, 4319–4333.

doi:10.1016/j.gca.2004.01.020

Lessovaia, S.N., Plötze, M., Inozemzev, S., Goryachkin, S., 2016. Traprock transformation into clayey materials in soil environments of the central Siberian plateau, Russia. *Clays Clay Miner.* 64, 668–676.

doi:10.1346/CCMN.2016.064042

Lowe, D.J., 2000. Upbuilding pedogenesis in multisequal tephra- derived soils in the Waikato region, in: Adams, J., Metherell, A. (Eds.), *Soil 200: New Horizons for a New Century*. Australian and New Zealand Second Joint Soils Conference Volume 2: Lincoln University. New Zealand Society of Soil Science, pp. 183–184.

Lowe, D.J., Tonkin, P.J., 2010. Unravelling upbuilding pedogenesis in tephra and loess sequences in New Zealand using tephrochronology, in: Gilkes, R.J., Prakongkep, N. (Eds.), *Proceedings of the 19th World Congress of Soil Science “Soil Solutions for a Changing World”* (1–6 Aug., 2010, Brisbane), Symposium 1.3.2 Geochronological Techniques and Soil Formation. Brisbane, pp. 34–37.

Lu, S.G., Xue, Q.F., Zhu, L., Yu, J.Y., 2008. Mineral magnetic properties of a weathering sequence of soils derived from basalt in Eastern China. *Catena* 73, 23–33. doi:10.1016/j.catena.2007.08.004

Luque, E., 2008. *Propiedades magnéticas de los óxidos de hierro en suelos mediterráneos*. Universidad de Córdoba.

Mackensen, A., Ehrmann, W.U., 1992. Middle Eocene through Early Oligocene climate history and paleoceanography in the Southern Ocean: Stable oxygen and carbon isotopes from ODP Sites on Maud Rise and Kerguelen Plateau. *Mar. Geol.* 108, 1–27. doi:10.1016/0025-3227(92)90210-9

Maher, B., 1986. Characterisation of soils by mineralmagnetic measurements. *Phys. Earth Planet. Inter.* 42, 76–92. doi:10.1016/S0031-9201(86)80010-3

Mansilla, H.G., De Valais, S., Stinnesbeck, W., Varela, N.A., Leppe, M.A., 2012. New Avian tracks from the lower to middle Eocene at Fossil Hill, King George Island, Antarctica. *Antarct. Sci.* 24, 500–506. doi:10.1017/S0954102012000260

Mansilla, H.G., Stinnesbeck, W., Varela, N., Leppe, M., 2013. Eocene fossil feather from King George Island, South Shetland Islands, Antarctica. *Antarct. Sci.* 26, 384–388. doi:10.1017/S0954102013000771

Marques, R., Prudêncio, M.I., Waerenborgh, J.C., Rocha, F., Dias, M.I., Ruiz, F.,

- Ferreira, E.S., Abad, M., Muñoz, A.M., 2014. Origin of reddening in a paleosol buried by lava flows in Fogo island (Cape Verde). *J. African Earth Sci.* 96, 60–70. doi:10.1016/j.jafrearsci.2014.03.019
- Materechera, S.A., Dexter, A.R., Alston, A.M., 1992. Formation of aggregates by plant roots in homogenised soils. *Plant Soil* 142, 69–79. doi:10.1007/BF00010176
- Maynard, J.B., 1992. Chemistry of modern soils as a guide to interpreting Precambrian paleosols. *J. Geol.* 100, 279–289.
- McDaniel, P.A., Falen, A.L., Tice, K.R., Graham, R.C., Fendorf, S.E., 1995. Beidellite in e horizons of Northern Idaho spodosols formed in Volcanic ash. *Clays Clay Miner.* 43, 525–532. doi:10.1346/CCMN.1995.0430502
- McPherson, J., 1980. Genesis of variegated redbeds in the fluvial Aztec siltstone (Late Devonian), Southern Victoria Land, Antarctica. *Sediment. Geol.* 27.
- Mehra, O.P., Jackson, M.L., 1960. Iron Oxide Removal from Soils and Clays by a Dithionite-Citrate System Buffered with Sodium Bicarbonate. *Clays Clay Miner.* 7, 317–327. doi:10.1346/CCMN.1958.0070122
- Ming, D.W., Boettinger, J.L., 2001. Zeolites in Soil Environments. *Rev. Mineral. Geochemistry* 45, 323–345. doi:10.2138/rmg.2001.45.11
- Mirabella, A., Egli, M., Raimondi, S., Giaccari, D., 2005. Origin of clay minerals in soils on pyroclastic deposits in the Island of Lipari (Italy). *Clays Clay Miner.* 53, 409–421. doi:10.1346/CCMN.2005.0530409
- Mizota, C., Takahashi, Y., 1982. Eolian origin of quartz and mica in soils developed on basalts in northwestern Kyushu and San-in, Japan. *Soil Sci. Plant Nutr.* 28, 369–378. doi:10.1080/00380768.1982.10433652
- Mokma, D., Syers, J., Jackson, M., Clayton, R., Rex, R., 1972. Eolian additions to soils and sediments in the South Pacific area. *J. Soil Sci.* 23, 147–162.
- Moore, D., Reynolds Jr, R., 1997. X-ray Diffraction and the Identification of Clay Minerals, 2nd ed. Oxford University.
- Mozer, A., 2012. Pre-glacial sedimentary facies of the Point Thomas Formation (Eocene) at Cytadela, Admiralty Bay, King George Island, West Antarctica. *Polish Polar Res.* 33, 41–62. doi:10.2478/v10183-012-0002-7
- Müller, H., Schwaighofer, B., 1979. Frittung oder tertiäre Verwitterung — Zur Frage der Rotfärbung in den tertiären Liegendsedimenten des Basalts von Stoob (Burgenland, Österreich). *Verh.Geol.B.-A* 2, 133–160.

- Nahon, D., Colin, F., Tardy, Y., 1982. Formation and distribution of Mg,Fe,Mn-smectites in the first stages of the lateritic weathering of forsterite and tephroite. *Clay Miner.* 17, 339–348. doi:10.1180/claymin.1982.017.3.06
- Nawrocki, J., Pańczyk, M., Williams, I.S., 2011. Isotopic ages of selected magmatic rocks from King George Island (West Antarctica) controlled by magnetostratigraphy. *Geol. Q.* 55, 301–322.
- NRCS, 1996. Soil Survey Laboratory Methods Manual 716. doi:10.1021/ol049448I
- Ollier, C., 1965. Some features of granite weathering in Australia. *Zeitschrift für Geomorphol.* 9, 285–304.
- Pagani, M., Zachos, J.C., Freeman, K.H., Tripple, B., Bohaty, S., 2005. Marked decline in Atmospheric Carbon Dioxide Concentrations during the Paleocene. *Science* (80-. ). 309, 600–603. doi:10.1126/science.1110063
- Parra, M., Delmont, P., Dumon, J.C., Ferragne, A., Pons, J.C., 1987. Mineralogy and origin of Tertiary interbasaltic clays from the Faeroe island, Northeastern Atlantic. *Clay Miner.* 22, 63–82.
- Pearson, P.N., Foster, G.L., Wade, B.S., 2009. Atmospheric carbon dioxide through the Eocene–Oligocene climate transition. *Nature* 461, 1110–1113. doi:10.1038/nature08447
- Pearson, P.N., Palmer, M.R., 2000. Atmospheric carbon dioxide concentrations over the past 60 million years. *Nature* 406, 695–699. doi:10.1038/35021000
- Pevear, D., Dethier, D., Frank, D., 1982. Clay minerals in the 1980 deposits from Mount St. Helens. *Clays Clay Miner.* 30, 241–252. doi:10.1346/CCMN.1982.0300401
- Pietsch, D., Kühn, P., 2012. Early Holocene paleosols at the southwestern Ramlat As-Sab'atayn desert margin: New climate proxies for southern Arabia. *Palaeogeogr. Palaeoclimatol. Palaeoecol.* 365–366, 154–165. doi:10.1016/j.palaeo.2012.09.023
- PiPujol, M.D., Buurman, P., 1994. The distinction between ground-water gley and surface-water gley phenomena in Tertiary paleosols of the Ebro basin, NE Spain. *Palaeogeogr. Palaeoclimatol. Palaeoecol.* 110, 103–113. doi:10.1016/0031-0182(94)90112-0
- Poole, I., Cantrill, D., Utescher, T., 2005. A multi-proxy approach to determine Antarctic terrestrial palaeoclimate during the Late Cretaceous and Early Tertiary. *Palaeogeogr. Palaeoclimatol. Palaeoecol.* 222, 95–121.

doi:10.1016/j.palaeo.2005.03.011

- Poole, I., Hunt, R.J., Cantrill, D.J., 2001. A fossil wood flora from King George Island: ecological implications for an Antarctic Eocene vegetation. *Ann. Bot.* 88, 33–54. doi:10.1006/anbo.2001.1425
- Poole, I., Mennega, A.M.W., Cantrill, D.J., 2003. Valdivian ecosystems in the Late Cretaceous and Early Tertiary of Antarctica: Further evidence from myrtaceous and eucryphiaceous fossil wood. *Rev. Palaeobot. Palynol.* 124, 9–27. doi:10.1016/S0034-6667(02)00244-0
- Porter, D.A., McCahont, T., Ransom, M.D., 1998. Differentiating pedogenic and diagenetic properties in a Cretaceous paleosol in Kansas. *Quat. Int.* 51/52, 35–54.
- Preetz, H., Igel, J., Hannam, J.A., Stadler, S., 2017. Relationship between magnetic properties and reddening of tropical soils as indicators of weathering. *Geoderma* 303, 143–149. doi:10.1016/j.geoderma.2017.05.007
- Pross, J., Contreras, L., Bijl, P.K., Greenwood, D.R., Bohaty, S.M., Schouten, S., Bendle, J. a, Röhl, U., Tauxe, L., Raine, J.I., Huck, C.E., van de Flierdt, T., Jamieson, S.S.R., Stickley, C.E., van de Schootbrugge, B., Escutia, C., Brinkhuis, H., 2012. Persistent near-tropical warmth on the Antarctic continent during the early Eocene epoch. *Nature* 488, 73–7. doi:10.1038/nature11300
- Prudencio, M.I., Sequeira Braga, M.A., Paquet, H., Waerenborgh, J.C., Pereira, L.C.J., Gouveia, M.A., 2002. Clay mineral assemblages in weathered basalt profiles from central and southern Portugal: Climatic significance. *Catena* 49, 77–89. doi:10.1016/S0341-8162(02)00018-8
- Rasmussen, C., Dahlgren, R. a., Southard, R.J., 2010. Basalt weathering and pedogenesis across an environmental gradient in the southern Cascade Range, California, USA. *Geoderma* 154, 473–485. doi:10.1016/j.geoderma.2009.05.019
- Rasmussen, C., Matsuyama, N., Dahlgren, R.A., Southard, R.J., Brauer, N., 2007. Soil genesis and mineral transformation across an environmental gradient on andesitic lahar. *Soil Sci. Soc. Am.* 71, 225–237.
- Reguero, M.A., Marensi, S.A., Santillana, S.N., 2002. Antarctic Peninsula and South America (Patagonia)\nPaleogene terrestrial faunas and environments: biogeographic\nrelationships. *Palaeogeogr. Palaeoclimatol. Palaeoecol.* 2776, 1–22.
- Retallack, G.J., 2001. *Soils of the Past: An Introduction to Paleopedology*, second.

- ed. Blackwell Science, United Kingdom. doi:10.1002/9780470698716
- Retallack, G.J., 1991. Untangling the effects of burial alteration and ancient soil formation. *Annu. Rev. Earth Planet. Sci.* 19, 183–206.  
doi:10.1146/annurev.earth.19.1.183
- Retallack, G.J., 1988. Field recognition of paleosols. *Geol. Soc. Am. Spec. Pap.* 1–20. doi:10.1130/SPE216-p1
- Righi, D., Terribile, F., Petit, S., 1998. Pedogenic formation of high-charge beidellite in a Vertisol of Sardinia (Italy). *Clays Clay Miner.* 46, 167–177.  
doi:10.1346/CCMN.1998.0460207
- Rivas, J., Ortega, B., Sedov, S., Solleiro, E., Sychera, S., 2006. Rock magnetism and pedogenetic processes in Luvisol profiles: Examples from Central Russia and Central Mexico. *Quat. Int.* 156–157, 212–223.  
doi:10.1016/j.quaint.2006.05.007
- Robert, C., Kennett, J.P., 1997. Antarctic continental weathering changes during Eocene-Oligocene cryosphere expansion: Clay mineral and oxygen isotope evidence. *Geology* 25, 587–590. doi:10.1130/0091-7613
- Sánchez, S., 2015. Los paleosuelos “negros” como indicadores de cambios ambientales naturales e inducidos por el hombre en el periodo de ocupacion teotihuacano. UNAM.
- Sayed, M.R.G., Pardeshi, R.G., Islam, R., 2014. Palaeoweathering characteristics of an intrabasaltic red bole of the Deccan Flood Basalts near Shrivardhan of western coast of India. *J. Earth Syst. Sci.* 1717–1728. doi:10.1007/s12040-014-0481-5
- Schatz, A.-K., Scholten, T., Kühn, P., 2015. Paleoclimate and weathering of the Tokaj (Hungary) loess–paleosol sequence. *Palaeogeogr. Palaeoclimatol. Palaeoecol.* 426, 170–182. doi:10.1016/j.palaeo.2015.03.016
- Scheinost, A., Chavernas, A., Barrón, V., Torrent, J., 1998. Use and limitations of second-derivative diffuse reflectance spectroscopy in the visible to near-infrared range to identify and quantify Fe oxide minerals in soils. *Clays Clay Miner.* 46, 528–536.
- Schulze, D., 1981. Identification of soil iron oxide minerals by Differential X-ray Diffraction. *Soil Sci. Soc. Am. J.* 45, 437–440.
- Schwertmann, U., 1964. Differenzierung der Eisenoxide des Bodens durch Extraktion mit Ammoniumoxalat-Lösung. *J. Plant Nutr. Soil Sci.* 105, 194–202.

- Schwertmann, U., Fechter, H., 1984. The Influence of aluminum on iron oxides: XI. Aluminum-substituted maghemite in soils and its formation. *Soil Sci. Soc. Am.* 48, 1462–1463. doi:10.2136/sssaj1984.03615995004800060054x
- Schwertmann, U., Friedl, J., Stanjek, H., 1999. From Fe(III) Ions to Ferrihydrite and then to Hematite. *J. Colloid Interface Sci.* 209, 215–223. doi:10.1006/jcis.1998.5899
- Schwertmann, U., Murad, E., Schulze, D.G., 1982. Is there Holocene reddening (hematite formation) in soils of axeric temperate areas? *Geoderma* 27, 209–223.
- Schwertmann, U., Taylor, R., 1989. Iron Oxides, in: Dixon, J., Weed, S. (Eds.), *Minerals in Soil Environments*. Soil Science Society of America, Madison, Wisconsin, pp. 379–438.
- Sedov, S., Solleiro-Rebolledo, E., Morales-Puente, P., Arias-Herreia, A., Vallejo-Gomez, E., Jasso-Castaneda, C., 2003. Mineral and organic components of the buried paleosols of the Nevado de Toluca, Central Mexico as indicators of paleoenvironments and soil evolution. *Quat. Int.* 106–107, 169–184. doi:10.1016/S1040-6182(02)00171-4
- Sedov, S., Stoops, G., Shoba, S., 2010. Regoliths and Soils on Volcanic Ash, in: Stoops, G., Marcelino, V., Mees, F. (Ed.), *Interpretation of Micromorphological Features of Soils and Regoliths*. Elsevier, Amsterdam, pp. 275–303. doi:10.1016/B978-0-444-53156-8.00013-1
- Sheldon, N.D., 2005. Do red beds indicate paleoclimatic conditions? A Permian case study. *Palaeogeogr. Palaeoclimatol. Palaeoecol.* 228, 305–319. doi:10.1016/j.palaeo.2005.06.009
- Sheldon, N.D., 2003. Pedogenesis and geochemical alteration of the Pacific Gorge subgroup Columbia River basalt, Oregon. *Bull. Geol. Soc. Am.* 115, 1377–1387. doi:10.1130/B25223.1
- Sheldon, N.D., Retallack, G.J., 2004. Regional paleoprecipitation records from the Late Eocene and Oligocene of North America. *J. Geol.* 112, 487–494. doi:10.1086/421076
- Sheldon, N.D., Tabor, N.J., 2009. Quantitative paleoenvironmental and paleoclimatic reconstruction using paleosols. *Earth-Science Rev.* 95, 1–52. doi:10.1016/j.earscirev.2009.03.004
- Shoji, S., Nanzyo, M., Dahlgren, R.A., 1993. *Volcanic ash soils - Genesis, properties and utilization*, Statewide Agricultural Land Use Baseline 2015. Elsevier

Science, Amsterdam.

- Shukla, A.D., Ray, D., Pande, K., Shukla, P.N., 2014. Formation of paleosol (fossil soil) in Deccan continental flood basalt: alteration style and implications towards aqueous environments of early mars, in: Eighth International Conference on Mars. Pasadena, California, p. 1194.
- Singer, A., 1980. The palaeoclimate interpretation of clay minerals in soil and weathering profiles. *Earth-Science Rev.* 15, 303–326.
- Singer, A., 1970. Edaphoids and paleosols of basaltic origin in The Galilee, Israel. *J. Soil Sci.* 21.
- Singer, A., Ben-Dor, E., 1987. Origin of red clay layers interbedded with basalts of the Golan Heights. *Geoderma* 39, 293–306. doi:10.1016/0016-7061(87)90049-8
- Singer, A., Navrot, J., 1977. Clay formation from basic volcanic rocks in a humid Mediterranean climate. *Soil Sci. Soc. Am. J.* 41, 645–650.
- Solleiro-Rebolledo, E., Straubinger, M., Terhorst, B., Sedov, S., Ibarra, G., Sánchez-Alaniz, J.I., Solanes, M.C., Marmolejo, E., 2016. Paleosols beneath a lava flow in the southern basin of Mexico: The effect of heat on the paleopedological record. *Catena* 137, 622–634. doi:10.1016/j.catena.2014.12.002
- Spinola, D.N., Pi-Puig, T., Solleiro-Rebolledo, E., Egli, M., Sudo, M., Sedov, S., Kühn, P., 2017a. Origin of clay minerals in Early Eocene volcanic paleosols on King George Island, Maritime Antarctica. *Sci. Rep.* doi:10.1038/s41598-017-06617-x
- Spinola, D.N., Portes, R. de C., Schaefer, C.E.G.R., Solleiro-Rebolledo, E., Pi-Puig, T., Kühn, P., 2017b. Eocene paleosols on King George Island, Maritime Antarctica: Macromorphology, micromorphology and mineralogy. *Catena*. doi:10.1016/j.catena.2017.01.004
- Srivastava, P., Sangode, S.J., Meshram, D.C., Gudadhe, S.S., Nagaraju, E., Kumar, A., Venkateshwarlu, M., 2012. Paleoweathering and depositional conditions in the inter-flow sediment units (bole beds) of Deccan Volcanic Province, India: A mineral magnetic approach. *Geoderma* 177–178, 90–109. doi:10.1016/j.geoderma.2012.01.034
- Srivastava, P., Sangode, S.J., Torrent, J., 2015. Mineral magnetic and diffuse reflectance spectroscopy characteristics of the Deccan volcanic bole beds : Implications to genesis and transformations of iron oxides. *Geoderma* 239–240, 317–330. doi:10.1016/j.geoderma.2014.11.010

- Srivastava, P., Sauer, D., 2014. Thin-section analysis of lithified paleosols from Dagshai Formation of the Himalayan Foreland: Identification of paleopedogenic features and diagenetic overprinting and implications for paleoenvironmental reconstruction. *Catena* 112, 86–98. doi:10.1016/j.catena.2013.08.008
- Steiger, R., Jäger, E., 1977. Subcommission on geochronology: convention on the use of decay constants in geo- and cosmochronology. *Earth Planet. Sci. Lett.* 36, 359–362.
- Stickley, C.E., Brinkhuis, H., Schellenberg, S.A., Sluijs, A., Röhl, U., Fuller, M., Grauert, M., Huber, M., Warnaar, J., Williams, G.L., 2004. Timing and nature of the deepening of the Tasmanian Gateway. *Paleoceanography* 19, 1–18. doi:10.1029/2004PA001022
- Stoops, G., 2003. Guidelines for Analysis and Description of Soil and Regolith Thin Sections. Soil Science Society of America, Madison, Wisconsin.
- Stroncik, N.A., Schmincke, H.U., 2002. Palagonite - A review. *Int. J. Earth Sci.* 91, 680–697. doi:10.1007/s00531-001-0238-7
- Torrent, J., Barrón, V., 2002. Diffuse reflectance spectroscopy of iron oxides. *Encycl. Surf. Colloid Sci.* 1438–1446.
- Torrent, J., Barrón, V., Liu, Q., 2006. Magnetic enhancement is linked to and precedes hematite formation in aerobic soil. *Geophys. Res. Lett.* 33, 4–7. doi:10.1029/2005GL024818
- Torrent, J., Liu, Q., Bloemendal, J., Barrón, V., 2007. Magnetic enhancement and iron oxides in the Upper Luochuan Loess-Paleosol sequence, Chinese Loess Plateau. *Soil Sci. Soc. Am. J.* 71, 1570–1578. doi:10.2136/sssaj2006.0328
- Torrent, J., Schwertmann, U., 1987. Influence of hematite on the colour of Red Beds. *J. Sediment. Petrol.* 57, 682–686.
- Ugolini, F.C., Dahlgren, R.A., 2002. Soil development in volcanic ash. *Glob. Environ. Res.* 6, 69–81.
- Uto, K., Ishizuka, O., Matsumoto, A., Kamioka, H., Togashi, S., 1997. Laser-heating  $^{40}\text{Ar}/^{39}\text{Ar}$  dating system of the Geological Survey of Japan: System outline and preliminary results. *Bull. Geol. Surv. Japan* 48, 23–46.
- Vacca, A., Ferrara, C., Matteucci, R., Murru, M., 2012. Ferruginous paleosols around the Cretaceous-Paleocene boundary in central-southern Sardinia (Italy) and their potential as pedostratigraphic markers. *Quat. Int.* 265, 179–190. doi:10.1016/j.quaint.2011.07.036

- Van der Gaast, S.J., Mizota, C., Jansen, J.H.F., 1986. Curved smectite in soils from volcanic ash in Kenya and Tanzania: a low-angle X-ray powder diffraction study. *Clays Clay Miner.* 34, 665.
- Van Houten, F., 1973. Origin of red beds - A review - 1961 - 1972. *Annu. Rev. Earth Planet. Sci.* 1, 39–61.
- Veblen, T., Alaback, P., 1996. High-Latitude Rainforests and Associated Ecosystems of the West Coast of the Americas, in: Lawford, R., Fuentes, E., Alaback, P. (Eds.), *High-Latitude Rainforest and Associated Ecosystems of the West Coast of the Americas*. Springer Verlag, New York, pp. 173–213.  
doi:10.1007/978-1-4612-3970-3
- Velde, B., Meunier, A., 2008. *The Origin of Clay Minerals in Soil and Weathered Rocks*. Springer-Verlag, Berlin Heidelberg.
- Veneman, P.L., Vepraskas, M., Bouma, J., 1976. The physical significance of soil mottling in a Wisconsin toposequence. *Geoderma* 15, 103–118.
- Weibel, R., 1999. Effects of burial on the clay assemblages in the Triassic Skagerrak Formation, Denmark. *Clay Miner.* 34, 619–635.  
doi:10.1180/claymin.1999.034.4.08
- Widdowson, M., Walsh, J.N., Subbarao, K. V., 1997. The geochemistry of Indian bole horizons: palaeoenvironmental implications of Deccan intravolcanic palaeosurfaces, in: Widdowson, M. (Ed.), *Paleosurfaces: Recognition, Reconstruction and Palaeoenvironmental Interpretation*. Geological Society Special Publication, pp. 269–281. doi:10.1144/GSL.SP.1997.120.01.17
- Wilke, F.D., O'Brien, P., Gerdes, A., Timmerman, M., Sudo, M., Khan, M.A., 2010. The multistage exhumation history of the Kaghan Valley UHP series, NW Himalaya, Pakistan from U-Pb and  $^{40}\text{Ar}/^{39}\text{Ar}$  ages. *Eur. J. Mineral.* 22, 703–719.
- Wilson, M.J., 1999. The origin and formation of clay minerals in soils: past, present and future perspectives. *Clay Miner.* 34, 7–25. doi:10.1180/000985599545957
- Wojdyr, M., 2010. Fityk: a general-purpose peak fitting program. *J. Appl. Crystallogr.* 43, 1126–1128. doi:10.1107/S0021889810030499
- Wright, V.P., 1992. *Paleosol recognition: A guide to early diagenesis in terrestrial settings*, *Developments in Sedimentology, Diagenesis III*. Elsevier.  
doi:10.1016/S0070-4571(08)70574-0
- Wyszecki, G., Stiles, W., 1982. *Colour science: Concepts and methods, quantitative*

data and formulae. Wiley, New York.

York, D., 1969. Least squares fitting of a straight line with correlated errors. *Earth Planet. Sci. Lett.* 5, 320–324.

Yousefifard, M., Ayoubi, S., Poch, R.M., Jalalian, A., Khademi, H., Khormali, F., 2015. Clay transformation and pedogenic calcite formation on a lithosequence of igneous rocks in northwestern Iran. *Catena* 133, 186–197.  
doi:10.1016/j.catena.2015.05.014

Zachos, J., Pagani, M., Sloan, L., Thomas, E., Billups, K., 2001. Trends, Rhythms, and Aberrations in Global Climate 65 Ma to Present. *Science* 292, 686–693. doi:10.1126/science.1059412

Zachos, J.C., Quinn, T.M., Salamy, K.A., 1996. High-resolution deep-sea foraminiferal stable isotope records of the Eocene-Oligocene transition. *Paleoceanography*.

**Scientific publications and conference contributions****Peer reviewed publications**

Spinola, D.N., Portes, R. de C., Srivastava, P., Torrent, J., Barrón, V., Kühn, P., 2017. Diagenetic reddening of Early Eocene paleosols on King George Island, Antarctica. *Geoderma* 315, 149–159. doi:10.1016/j.geoderma.2017.11.010

Spinola, D.N., Portes, R.C., Schaefer, C.E.G.R., Solleiro-Rebolledo, E., Pi-Puig, T., Kühn, P., 2017. Eocene paleosols on King George Island, Maritime Antarctica: Macromorphology, micromorphology and mineralogy. *Catena* 152, 69–81. doi:10.1016/j.catena.2017.01.004

Spinola, D.N., Portes, R. C., Schaefer, C.E.G.R., Solleiro-Rebolledo, E., Pi-Puig, T., Kühn, P., 2017. Eocene paleosols on King George Island, Maritime Antarctica: Macromorphology, micromorphology and mineralogy. *Catena*. doi:10.1016/j.catena.2017.01.004

**Conference contributions**

Spinola, D.N., Pi-Puig, T., Solleiro-Rebolledo, E., Egli, M., Sudo, M., Sedov, S., Kühn, P. 2017. Origin of clay minerals in Early Eocene volcanic paleosols on King George Island, Maritime Antarctica, in: GSA Annual Meeting 2017, Seattle, USA.

Spinola, D.N., Portes, R., Schaefer, C.E.G.R., Solleiro-Rebolledo, E, Pi-Puig, T, Kühn, P., 2016. Eocene Paleosols on King George Island, Maritime Antarctica: Macromorphology, Micromorphology and Mineralogy, in: 15<sup>th</sup> International Conference on Soil Micromorphology. Mexico City, Mexico.

Spinola, D.N., Portes, R. de C., Schaefer, C.E.G.R., Kühn, P., 2016. Eocene paleosols of King George Island, Maritime Antarctica, in: EGU General Assembly. Vienna, Austria.

**Acknowledgments**

This thesis was carried out with the financial support of the National Council of Technological and Scientific Development (CNPq), Brazil. I thank the Brazilian Navy and my colleagues (38. Polska Wyprawa Antarktyczna) from the Henry Arctowski Station for all logistics and considerable additional support to realize the successful fieldwork during the Antarctic expedition in the summer of 2013–2014.

I would like to thank my supervisor Dr. Peter Kühn for giving me the opportunity to join his research group. Furthermore, I would like to express my gratitude for his unconditional support, friendship and patience during the last years. Our long hours of discussion had transformed “problems” into “challenges”. I have learned much more than paleopedology with Peter.

I also thank Prof. Thomas Scholten, Prof. Yvonne Oelmann and Prof. Karl Stahr for kindly refereeing this thesis.

This research was only made possible with the assistance of the technical staff of the Institute of Geography: Margaretha Bauer, Sabine Flaiz, Panos Kritikakis, Lisa-Marie Funke, Rita Mögenburg, and Christian Bick. Furthermore, the colleagues of the research group also made my work and adaptation in Tübingen smoother: Ann-Kathrin Schatz, Steffen Seitz, Jessica Henkner, Felix Stumpf, Zhengshan Song, Mona Morsi, Lars-Arne Meier, Phillipp Gries, Sandra Teuber, Nadine Bernhard, and Karla Dietrich. Also, I thank my friends from Human Geography: Vicente Fernandes and Cesar Leal Soto.

Throughout this research, I had the opportunity to work in collaboration with great researchers: Elizabeth Solleiro Rebolledo Teresa Pi-Puig, Sergey Sedov, Vidal Barrón, José Torrent, Masafumi Sudo, Markus Egli, and Pankaj Srivastava. I would like to thank them all for their openness to this research.

A deep thanks to my family in Brazil. Their support in all matters made the distance bearable.

Finally, special thanks to my wife and scientific partner, Raquel Portes. Her wisdom, care, support and love (for me and soils) makes everything easier.